TU/e EINDHOVEN UNIVERSITY OF TECHNOLOGY

Systems biology of Metabolic Syndrome development and treatment

Citation for published version (APA):
Rozendaal, Y. J. W. (2018). *Systems biology of Metabolic Syndrome development and treatment*. [Phd Thesis 1 (Research TU/e / Graduation TU/e), Biomedical Engineering]. Technische Universiteit Eindhoven.

Document status and date:
Published: 21/12/2018

Document Version:
Publisher's PDF, also known as Version of Record (includes final page, issue and volume numbers)

Please check the document version of this publication:

• A submitted manuscript is the version of the article upon submission and before peer-review. There can be important differences between the submitted version and the official published version of record. People interested in the research are advised to contact the author for the final version of the publication, or visit the DOI to the publisher's website.
• The final author version and the galley proof are versions of the publication after peer review.
• The final published version features the final layout of the paper including the volume, issue and page numbers.

Link to publication

General rights
Copyright and moral rights for the publications made accessible in the public portal are retained by the authors and/or other copyright owners and it is a condition of accessing publications that users recognise and abide by the legal requirements associated with these rights.

• Users may download and print one copy of any publication from the public portal for the purpose of private study or research.
• You may not further distribute the material or use it for any profit-making activity or commercial gain
• You may freely distribute the URL identifying the publication in the public portal.

If the publication is distributed under the terms of Article 25fa of the Dutch Copyright Act, indicated by the "Taverne" license above, please follow below link for the End User Agreement:

www.tue.nl/taverne

Take down policy
If you believe that this document breaches copyright please contact us at:

openaccess@tue.nl

providing details and we will investigate your claim.

Download date: 16. Nov. 2023

SYSTEMS BIOLOGY of METABOLIC SYNDROME DEVELOPMENT and TREATMENT

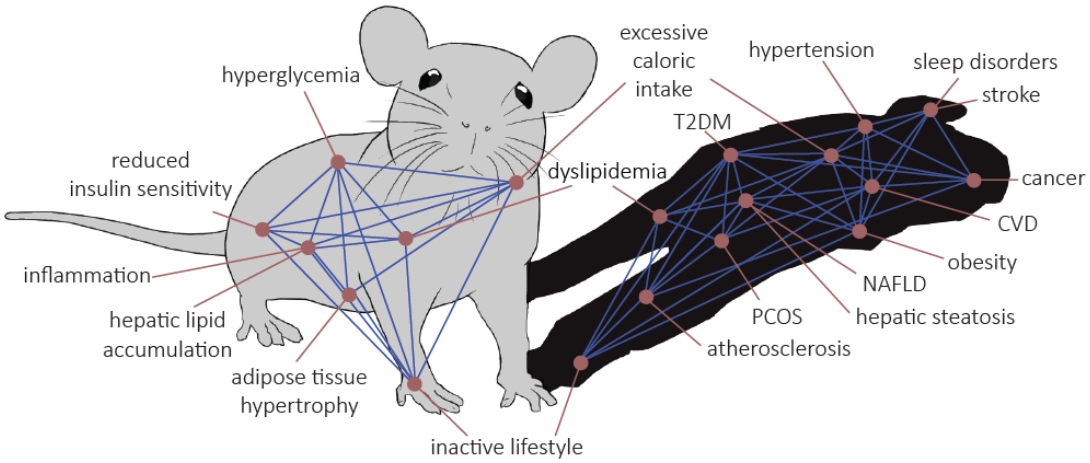

Yvonne Rozendaal

A catalogue record is available from the Eindhoven University of Technology Library.

ISBN 978-90-386-4641-1

Copyright © 2018 by Yvonne J.W. Rozendaal

All rights reserved. No part of this publication may be reproduced, stored in a database or retrieval system, or transmitted, in any form or by any means, electronically, mechanically, by print, photo print, microfilm, or any other means without the prior written permission of the author.

Cover design by Stijn Verhagen & Yvonne Rozendaal

Printed by Ipskamp Printing, Enschede

The work in this thesis was supported by the European Union's Seventh Framework Programme for research, technological development and demonstration under grant agreement no. 305707 (RESOLVE).

Systems biology of Metabolic Syndrome development and treatment

PROEFSCHRIFT

ter verkrijging van de graad van doctor aan de Technische Universiteit Eindhoven,
op gezag van de rector magnificus prof.dr.ir. F.P.T. Baaijens,
voor een commissie aangewezen door het College voor Promoties,
in het openbaar te verdedigen op vrijdag 21 december 2018 om 13:30 uur

door

Yvonne Jeanette Wilhelmina Rozendaal

geboren te Eindhoven

Dit proefschrift is goedgekeurd door de promotoren en de samenstelling van de promotiecommissie is als volgt:

voorzitter:	prof.dr.ir. C.W.J. Oomens
1e promotor:	prof.dr.ir. N.A.W. van Riel
2e promotor:	prof.dr. P.A.J. Hilbers
leden:	prof.dr. B.M. Bakker (Rijksuniversiteit Groningen; Universitair Medisch Centrum Groningen)
	prof.dr.ir. I.C.W. Arts (Maastricht University)
	prof.dr.ir. U. Kaymak
adviseur(s):	prof.dr. A.K. Groen (Academisch Medisch Centrum; Universiteit van Amsterdam)

Het onderzoek of ontwerp dat in dit proefschrift wordt beschreven is uitgevoerd in overeenstemming met de TU/e Gedragscode Wetenschapsbeoefening.

Contents

1	General introduction	1
2	The need for a generic model predicting dynamic adaptations of chronic metabolic disorders *Interface Focus 2016;6(2):20150075*	11
3	A model of the integration of glucose and lipid dynamics (MINGLeD) *PLoS Comput Biol 2018;14(6):e1006145*	29
4	*In vivo* and *in silico* dynamics of the development of Metabolic Syndrome *PLoS Comput Biol 2018;14(6):e1006145*	41
5	Heterogeneity and variability in the long-term development of Metabolic Syndrome	67
6	Computational modelling of energy balance in individuals with Metabolic Syndrome *BMC Syst Biol (submitted)*	85
7	Summarizing discussion and future perspectives	105
	Bibliography	116
	Ethical paragraph	126
	Summary	128
	Samenvatting	130
	List of publications	132
	Dankwoord	135
	Curriculum Vitae	138

1

General introduction

1.1 Obesity: a global pandemic

The global prevalence of obesity has nearly doubled in the last four decades [World Health Organization, 2014, 2016], and the incidence of childhood obesity has even increased ten-fold since 1975. [NCD Risk Factor Collaboration, 2017] It is estimated that 39% of the worldwide adult population suffers from overweight and 13% is estimated as being obese. Obesity is a growing problem that is now reaching pandemic proportions, as shown in Figure 1.1. It is projected that in 2030 over half of the worldwide population could have become obese. [Finkelstein *et al.*, 2012]

The most prominent cause of weight gain is a positive energy imbalance induced by lifestyle. The Western-style diet is typically high in sugar, (saturated) fat, and cholesterol. [Turnbaugh *et al.*, 2009] Since these diets are high in energy and are often accompanied by a sedentary lifestyle with little physical activity, the surplus of energy is stored as fat. A prolonged state of a positive energy balance will result in weight gain. In addition, the development of obesity may be enhanced by possible genetic defects, use of medication, and hormonal imbalance. [Goldstone and Beales, 2008; Loos and Bouchard, 2003; Ness-Abramof and Apovian, 2005]

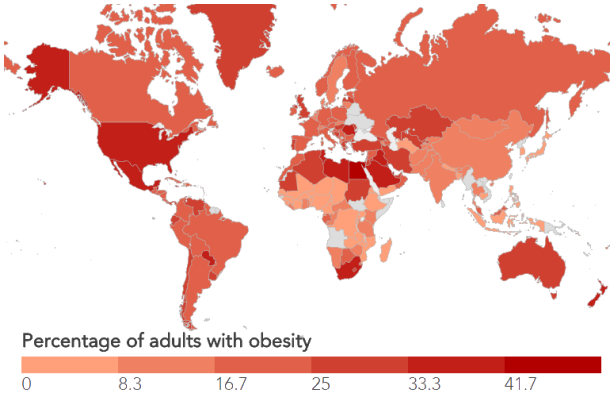

Figure 1.1

Global prevalence of obesity in adults according to the World Obesity Federation.

Obesity was defined as ≥30 kg/m² (in China the Asia specific cut-off of 27 kg/m² was applied). Downloaded from worldobesity.org/data/map/overview-adults (accessed January 19th, 2018)

1.1.1 Severe health implications

Recent evidence indicates that obesity does not always lead to adverse metabolic effects. A subgroup of approximately 10-30% of obese individuals is considered metabolically healthy despite having an excessive accumulation of body fat. [Denis and Obin, 2013] However, being overweight or obese is often accompanied by other (metabolic) abnormalities. Many studies have demonstrated that obesity imposes severe health risks and complications and increases the risk to develop other diseases, i.e. comorbidities. These range from cardiovascular diseases (CVD), type 2 diabetes mellitus (T2DM), sleep disorders, polycystic ovary syndrome (PCOS), non-alcoholic fatty liver disease (NAFLD), to some types of cancer. [Beltrán-Sánchez *et al.*, 2013; Font-Burgada *et al.*, 2016; Vanita and Jhansi, 2011]

1.1.2 Metabolic Syndrome

To objectively consider these comorbidities, a number of specific risk factors have been identified, including obesity, hypertension, hyperglycemia, hypertriglyceridemia (HTG), and hypoalphalipoproteinemia (HALP; low high-density lipoprotein (HDL)-cholesterol levels). These metabolic derailments may affect each other and are possibly linked to the development of other abnormalities. The co-occurrence of these symptoms is referred to as the Metabolic

Syndrome (MetS). [Grundy *et al.*, 2004; International Diabetes Federation, 2006; Kassi *et al.*, 2011; Parikh and Mohan, 2012; World Health Organization, 2014] The term "syndrome" refers to MetS being a clustering or constellation of health markers – i.e. a health/disease status – that together predispose a drastically increased risk of the development of the aforementioned comorbidities.

We should also consider that obesity and MetS may manifest themselves in different clinical presentations. The terms "obesity" and "MetS" inevitably refer to a highly diverse population. However, the pathophysiology and etiology underlying MetS are incompletely understood. This impedes the design of adequate and patient-specific treatment options, but also that of preventive measures. Given that the prevalence of MetS is growing at an alarming rate, and the severe risks associated with MetS, we need to invest in studies to elucidate this syndrome.

1.1.3 Systems biology approach

The challenge central in this thesis is obtaining an integrative understanding of longitudinal MetS development. We believe that a systems biology approach offers the best prospects towards this objective. The research described in this thesis was hereto funded by the European FP7 Research Program "RESOLVE" (FP7-HEALTH-305707). This consortium aims at resolving the disturbed dynamics in patients with the Metabolic Syndrome by combining basic pre-clinical and clinical research, network analysis, and computational modelling.

1.2 Metabolic Syndrome

The decision to adopt a systems biology approach is closely related to the complexity of MetS. This complexity lies in several aspects, but the majority of obstacles and challenges in MetS research are associated with its slowly progressive behaviour, its multi-factorial nature, and its heterogeneous clinical presentation.

1.2.1 Clinical definition

The constellation of metabolic risk factors was initially named "Syndrome X". [Reaven, 1993] In subsequent years, the definition shifted from a glucocentric ("insulin resistance syndrome") towards a more flexible and obesity-centric definition, as described in Table 1.1. However, there is no unique or unifying definition as different healthcare organizations have defined different classification systems. These classifications differ both in specific criteria and in used cut-off points, but there is a general consensus as the different definitions do comprise the same common features: obesity, insulin resistance/hyperglycemia, high triglyceride levels, low HDL-cholesterol levels, and hypertension. [Kassi *et al.*, 2011; Parikh and Mohan, 2012] As a consequence of the often used "three out of five" criterion, many different phenotypes can be classified under the terminology of MetS. [Agyemang *et al.*, 2012; Lee *et al.*, 2008]

Table 1.1

Definitions for clinical diagnosis of Metabolic Syndrome according to different healthcare organizations.

1998	WHO	World Health Organization [Alberti and Zimmet, 1998]	☑ insulin resistance [T2DM or IFG] *plus any two of the following:* ☐ abdominal obesity [waist:hip ratio man≥0.9; women≥0.85, or BMI≥30 kg/m²] ☐ HTG [≥150 mg/dL] and/or HALP [men≤40; women≤50 mg/dL] ☐ hypertension [≥140/90 mmHg] ☐ microalbuminuria [urinary albumin secretion rate≥20 µg/min, or albumin:creatinine ratio≥30 mg/g]
1999	EGIR	European Group for the study of Insulin Resistance [Balkau and Charles, 1999] ⍟ "insulin resistance syndrome"	☑ insulin resistance [≥75 percentile] *plus any two of the following:* ☐ obesity [waist circumference men≥94; women≥80cm] ☐ HTG [≥150 mg/dL] and/or HALP [≤39 mg/dL] ☐ hypertension [≥150 mmHg, or on antihypertensive drugs] ☐ IFG [≥110 mg/dL]
2001	NCEP:ATPIII	National Cholesterol Education Program Adult Treatment Panel III [Expert Panel on Detection, Evaluation, and Treatment of High Blood Cholesterol in Adults, 2001]	*any three of the following:* ☐ obesity [waist circumference men≥102; women≥88cm] ☐ HTG [≥150 mg/dL] ☐ HALP [men≤40; women≤50 mg/dL] ☐ hypertension [≥100 mg/dL] ☛ NB: IR is not considered as necessary diagnostic component!
2003	AACE	American Association of Clinical Endocrinologists [Einhorn *et al.*, 2003]	☑ IGT *plus any of the following:* ☐ obesity [BMI≥25 kg/m²] ☐ HTG [≥150 mg/dL] and/or HALP [men≤40; women≤50 mg/dL] ☐ hypertension [≥130/85 mmHg]
2004	AHA/NHLBI	American Heart Association/National Heart, Lung, and Blood Institute [Grundy *et al.*, 2004]	*any three of the following:* ☐ obesity [waist circumference men≥102; women≥88 cm] ☐ HTG [≥150 mg/dL] ☐ HALP [men≤40; women≤50 mg/dL] ☐ hypertension [≥130/85 mmHg] ☐ IFG [≥100 mg/dL]
2005	IDF	International Diabetes Federation [International Diabetes Federation, 2006]	☑ central obesity [waist circumference* or BMI≥30 kg/m²] *plus two of the following:* ☐ HTG [≥150 mg/dL] ☐ HALP [men≤40; women≤50 mg/dL] ☐ hypertension [≥130/85 mmHg] ☐ IFG [≥100 mg/dL]

* According to population and country-specific definitions

BMI, body mass index; HALP, hypoalphalipoproteinemia (low HDL-C); HTG: hypertriglyceridemia; IFG, impaired fasting glucose; IGT, impaired glucose tolerance; IR, insulin resistance; T2DM, type 2 diabetes mellitus

1.2.2 Epidemiology

Due to the differences in clinical definitions, it is difficult to assess the worldwide prevalence of MetS. However, estimates are available for different continents and ethnic groups. It has been extrapolated that almost 40% of the adult worldwide population would meet the MetS criteria [Kassi *et al.*, 2011; Cameron *et al.*, 2004], but depending on the population studied and definition criteria, the prevalence may range between <10% to as much as 84%! [Moore, 2017; Moreira *et al.*, 2014; van Vliet-Ostaptchouk *et al.*, 2014; Desroches and Lamarche, 2007; Kaur, 2014; Kolovou *et al.*, 2007]

It has also been shown that MetS prevalence increases with age. [Dominguez and Barbagallo, 2016; Bonomini *et al.*, 2015; Nunn *et al.*, 2009]

However, MetS manifests itself differently among different ethnic groups (that are in the same geographical area). [DeBoer, 2011; Abate and Chandalia, 2011; Tillin and Forouhi, 2011] African-Americans and Hispanics are more likely to exhibit obesity and insulin resistance. These groups are at higher risk of T2DM, but due to lower dyslipidemia rates, these groups are much less likely to be diagnosed with MetS. Although ethnic-specific cut-off values for obesity have been identified (as included in Figure 1.1 and Table 1.1), these are not yet available for the other MetS criteria. However, these ethnic differences strongly suggest a genetic component in the pathogenesis of MetS. [Song *et al.*, 2006]

The incidence of MetS has been growing at an alarming rate and is rising to pandemic proportions. MetS in itself is not merely the problem; the danger lies within the associated comorbidities. Alberti *et al.* reported that "*MetS confers a five-fold increase in the risk of T2DM and two-fold the risk of developing CVD over the next five to ten years. Patients with MetS are at two- to four-fold increased risk of stroke, a three- to four-fold increased risk of myocardial infarction, and two-fold the risk of dying from such an event compared with those without the syndrome regardless of a previous history of cardiovascular events*". [Alberti *et al.*, 2009] Since also metabolically healthy [Denis and Obin, 2013], but overweight, people have a 20% increased risk of CVD, this proves that obesity is an independent risk factor – regardless of other metabolic risk factors – for cardiovascular complications. [Eckel *et al.*, 2018]

1.2.3 Pathophysiology

But what mechanisms cause obesity to predispose such an increased disease risk? It is evident that MetS is a lifestyle-related disorder that has a strong multi-factorial and multi-scale nature. The complex interplay and crosstalk between adipose tissue, (skeletal) muscle, liver, pancreas, the cardiovascular system, and the brain [Symonds *et al.*, 2009] includes a role for both genetic and environmental factors contributing to MetS development.

However, its pathophysiology and etiology go beyond overeating and an inactive lifestyle. There is an evident imbalance in the mechanisms controlling dietary intake, physical activity, glucose handling, lipid homeostasis, and autonomic control. [Rask-Madsen and Kahn, 2012]

Whereas on an epidemiological level there is a clear link between obesity and T2DM, its underlying mechanisms are not fully understood yet. However, the most commonly accepted pathogenic scheme comprises the adipose tissue expandability hypothesis to explain the obesity-driven development of MetS. Adipose tissue (AT) is the dedicated depot for storage of (excess) energy in the form of triglycerides. A positive energy balance and metabolic overload demand plasticity of the AT. This involves both the formation of new adipocytes and hypertrophy of existing cells; the latter leading to increased production and secretion of pro-inflammatory cytokines. This indicates dysfunctional AT. [Goossens and Blaak, 2015]

AT can take up excess energy, but only up until a certain threshold. Consequently, dysfunctional AT causes lipid spillover into the circulation. Ectopic lipid accumulation in non-adipocyte cells leads to lipotoxicity and promotes systemic inflammation. [Virtue and Vidal-Puig, 2010] Macrophage infiltration of AT [Neels and Olefsky, 2006], excess reactive oxygen species, and mitochondrial oxidative stress [Bonomini *et al.*, 2015; Frisard and Ravussin, 2006] also play a role in this inflammatory response. In addition, ectopic fat and increasing levels of circulating free fatty

acids lead to a decrease of insulin sensitivity in various tissues and organs. Insulin sensitivity is further exacerbated by cytokines that are released from AT. [Grundy *et al.*, 2004; Rask-Madsen and Kahn, 2012]

1.2.4 Heterogeneity

However, these proposed mechanisms remain debatable and inconclusive to explain in detail the metabolic derailments during MetS development. This lack of knowledge of the underlying pathophysiology may be precluded by the heterogeneous clinical presentation of MetS. [Lee *et al.*, 2008; Agyemang *et al.*, 2012] On the one hand, this variability is inherent to the definition of MetS, where different combinations of features may be included. Whereas on the other hand, metabolic profiling seems to depend on sex and ethnicity. Nevertheless, even within specific cohorts, the heterogeneity in MetS presentation remains apparent. We presume that particular combinations of MetS components may have different underlying mechanisms of derailment. It is important to recognize this heterogeneity in the design of adequate treatment strategies for different MetS patients. [Matfin, 2010]

1.2.5 Treatment strategies

Lifestyle modification (involving nutritional management and exercise programmes) still remains the fundamental treatment strategy for MetS. [Bassi *et al.*, 2014; Grave *et al.*, 2010] Although this generic approach may be the most economical method, it may not be the most effective in combating disease risk. The first line of treatment of MetS is dietary and lifestyle modification, but it only has the potential to succeed if executed in an early stage of MetS. [Kataria *et al.*, 2013] Treatment may also be combined with pharmacotherapy of singular MetS aspects. Metformin is often used as an anti-diabetic drug, statins as lipid-lowering drugs, and fibrates as cholesterol-lowering agents. These are also often prescribed in combination therapy. [van Stee *et al.*, 2018] Although several pharmacotherapeutic options for weight loss are available that may contribute to lose more weight and maintain weight loss, these also have many adverse side-effects. [Apovian *et al.*, 2015]

Whereas intensive lifestyle intervention is considered appropriate for all obese patients, pharmacotherapy and bariatric surgery are generally reserved for patients with a more severe phenotype. Roux-en-Y gastric bypass (RYGB) [Wittgrove *et al.*, 1994] has been shown very effective for weight loss and improving glucose metabolism in MetS patients. [Nassour *et al.*, 2017; Batsis *et al.*, 2008; Cazzo *et al.*, 2014] It causes weight loss by restricting the amount of food the stomach can hold, and, moreover, causes malabsorption of nutrients. However, surgery is highly invasive and does not fill the gap of current treatment strategies being inadequate to deal with the growing rate of metabolic disorders.

Recently there has been tremendous interest in Brown Adipose Tissue (BAT) as potential anti-obesity target, owing to the vast capacity of BAT for burning energy in the process of thermogenesis. [Bartelt and Heeren, 2014; Chechi *et al.*, 2014; Yoneshiro *et al.*, 2013; Mukherjee *et al.*, 2016; Nedergaard and Cannon, 2010; Lidell *et al.*, 2014] Activation of BAT could contribute to (partially) solving the positive energy imbalance that is central to obesity and MetS development. Studies targeting BAT have demonstrated its beneficial effects for improving glucose metabolism, lipid handling, and inducing weight loss. [Wang *et al.*, 2015; Gao *et al.*, 2009; Berbée *et al.*, 2015; Seale and Lazar, 2009] This indicates

that BAT could play a significant role in the design of new therapeutic interventions and prevention strategies.

1.2.6 Challenges associated with MetS research

As of yet, no patient-specific treatment can be provided for the MetS population. This would require a deeper understanding of the complex interplay of the mechanisms underlying MetS onset and development. The main challenges in MetS research remain its multi-factorial complexity (simultaneous derailment of various physiological processes), heterogeneity, and progressive yet slowly changing behaviour over inherently long timescales. It has been shown to be challenging to monitor the longitudinal aspects of such metabolic diseases. [Enrique Caballero, 2017; Muzio *et al.*, 2005; Karas *et al.*, 2008] Because of its complexity, *in vivo* studies alone will not provide the quantitative and mechanistic insight we are looking for. The many challenges associated with the complexity of MetS make it, therefore, a strong case for the adoption of a systems biology approach.

1.3 Systems biology

Systems biology is a holistic approach that aims to improve understanding of complex biological systems as a whole. [Sauer *et al.*, 2007] It explores how the overall system's behaviour emerges from the collective behaviour of individual components. Systems biology is highly interdisciplinary: it is on the interface between engineering and biology and combines techniques from, amongst others, mathematics, computer science, control theory, and biostatistics with fundamentals from biology and medicine.

Models are essential in systems biology. A model is an abstraction of a complex system intended to gain a deeper understanding of biological phenomena. This terminology applies to experimental, conceptual, mathematical, and computational models. In view of this thesis, the experimental model consists of an *in vivo* preclinical animal model that embodies MetS development. The conceptual model can be regarded as a "thought experiment" to delineate the most important concepts from prior knowledge on metabolic regulation. The key challenge is to determine consistent and physiologically realistic mathematical descriptions of these processes for translation into a mathematical model. [Brodland, 2015] A computational model is obtained by combining the mathematical representation of the system with observations (data) from the experimental model. This computational model can subsequently be used to generate quantitative simulations of the system.

1.3.1 Computational models

A long history of computational models has provided extensive knowledge on the regulatory networks that compose the metabolic system. [Nyman *et al.*, 2016] Model development is continuously evolving, as can for example be seen in the Biomodels Database. [Chelliah *et al.*, 2013] Such modelling approaches can roughly be divided into network-based and constraint-based modelling. [van Riel, 2006] The first category comprises genome-scale metabolic models (GSMM), such as Recon2 (and the more recently updated Recon2.2 and Recon3D) being a "consensus metabolic reconstruction" and allegedly the most comprehensive representation available of

the human metabolic system. [Thiele *et al.*, 2013; Swainston *et al.*, 2016; Brunk *et al.*, 2018] On the other hand, constraint-based models adopt a more data-driven approach. Dedicated dynamic and "minimal" models have contributed to a deeper understanding of the regulatory mechanisms involved in the metabolic system. Recent advances have for example proven insightful for the glucose-insulin system [Ajmera *et al.*, 2013; Dalla Man *et al.*, 2007; Rozendaal *et al.*, 2018a] and for systemic lipid metabolism. [Jelic *et al.*, 2009; Roy and Parker, 2006; de Graaf *et al.*, 2009; Sips *et al.*, 2015]

1.3.2 Metabolic Syndrome models

Although these models are relevant to study isolated aspects of MetS, the underlying pathways are cross-linked and especially the interplay between the MetS components is highly important. [Hallgreen, 2009] Therefore, increasing emphasis is being put on system-based approaches to further understanding of MetS as a whole. [Orešič and Vidal-Puig, 2014; Dumas *et al.*, 2014; Lusis *et al.*, 2008] The big data community has contributed with a data-driven approach using genome-wide association studies (GWAS), showing different "metabolic signatures" in MetS. [Karns *et al.*, 2013; Khoo *et al.*, 2013] However, we do not follow this approach. We are specifically interested in the phenotypic and pathophysiological consequence of lifestyle and genetic factors, i.e. the dynamics of longitudinal disease progression of MetS. Since a cohesive model describing the multitude of MetS abnormalities was not available, in this thesis, we develop a comprehensive model describing the full metabolic complexity of MetS during disease progression.

1.3.3 Modelling methodology

In contrast to steady state modelling describing time-stationary processes, dynamic modelling approaches describe nonstationary processes and express the kinetic behaviour of a system over time. The evolution of a dynamic system over time can be described using differential equations. From a mathematical point of view, differential equations describe the relationship between a function and the function's derivative; i.e. represent the rate of change. In the context of MetS, we are interested in how species involved in both carbohydrate and lipid regulation behave over time. The change in concentration of these metabolites can be expressed in ordinary differential equations (ODEs) based on the underlying metabolic fluxes. These fluxes describe processes involved in the regulation, transformation, and transport of these species among different compartments (organs and tissues). The model comprises a system of *coupled* nonlinear ODEs, allowing for interaction between the different pathways and metabolites.

The actual mathematical expressions composing the ODEs can be based on different kinetics, such as mass action [Guldberg and Waage, 1864; Voit *et al.*, 2015] (used for chemical reactions in which the reaction speed depends on the concentration of reactants) or Michaelis-Menten kinetics [Michaelis and Menten, 1913; Johnson and Goody, 2011] (often used for simple enzymatic reactions). These techniques may be combined with compartmentalized modelling to take spatial distribution into account (e.g. transport between organs). On the other hand, pharmacokinetic-pharmacodynamic (PK-PD) models [Sheiner *et al.*, 1972, 1977] are designed to study exposure-response relationships, i.e. the immediate effects of a drug after administration and for dose response analysis. Chapter 3 outlines the development of a comprehensive, macroscopic and systemic (whole-body level) MetS model.

To apply this model to generate quantitative simulations, information on parameters and initial conditions (starting point of the model simulations; i.e. the situation of the variables at t=0) of the ODE system is required. However, the parameter vector is typically unknown. To parameterize the model, quantitative information is presented in the form of experimentally measured data that can (directly) be linked to specific states or fluxes in the network. Typically, this data provides only a partial observation of the system: measurements are performed on a subset of the states described in the model. Moreover, these differential equations are too complex to be solved exactly and analytically. Therefore, these are approximated via numerical integration. Parameter estimation is a technique to calibrate a model using such experimental data. Subsequent simulation of the model yields predictions of the unknown and unobserved processes (fluxes, species, and time points). However, since the system is only partially observed and biological measurements are hampered by noise, the solution of the system will be non-unique: simulations using different parameter vectors may represent the observed data equally well. We therefore perform simulations and optimizations iteratively, yielding not a single, unique model simulation as output, but a large set (distribution) of results. This *in silico* set can be regarded as a virtual population, i.e. a set of model simulations representing different phenotypic presentations of MetS. [Kononowicz *et al.*, 2015]

1.3.4 Data acquisition: essential yet challenging

Longitudinal, quantitative data is essential in order to parameterize the model. Biomarker data is often used for model calibration. A biomarker is an objective measure that gives an indication of the medical state of the patient. Commonly used biomarkers are for example metabolite concentrations measured from blood plasma or urine. However, a key issue at hand is determining the relationship between measurable biomarkers and relevant clinical endpoints. [Strimbu and Tavel, 2010] Computational models provide an objective way to do this. By integration with these data, the model provides insight into the dynamics of the underlying, unobserved processes, i.e. of which no data is or can experimentally be measured.

When studying chronic and progressive diseases such as MetS, longitudinal data is required. However, acquiring longitudinal data during disease development is complicated. It would involve a timespan of at least a couple of years, but possibly (much) longer. Moreover, there is no clear point of disease onset to be identified.

Although such longitudinal experiments are not feasible for the human situation, dedicated preclinical disease models in the form of genetically engineered animals offer a solution. [Softic *et al.*, 2017] The APOE*3-Leiden(E3L).CETP mouse has been shown to be a good experimental surrogate to study diet-induced MetS development. [van den Hoek *et al.*, 2014; Westerterp *et al.*, 2006] Upon feeding a high-fat, high-cholesterol diet, the healthy phenotype evolves into a fully developed MetS phenotype within several months. This much faster timeline accommodates measurement of biomarkers at regular intervals in time and thereby provides insight into the progressive adaptations during disease development.

1.4 Thesis outline

The aim of this thesis is to study how MetS develops over time using *in vivo* and *in silico* modelling. The work is divided into the following chapters as outlined in Figure 1.2. In chapter 2 we explore methodologies for long-term disease progression modelling and how to deal with challenges associated with integrating biomarker data in computational models. In chapter 3 we develop a mathematical model which network topology describes the metabolic system for both healthy and MetS phenotypes. Chapter 4 first describes a preclinical *in vivo* study of diet-induced MetS. The mathematical model of chapter 3 is then integrated with this *in vivo* data. An *in silico* database is yielded that comprises different virtual populations, i.e. sets of model simulations representing different MetS phenotypes.

In chapter 5 the *in vivo* experiment was repeated using a set-up with longer timespans and a larger population to verify the MetS phenotypes found in the previous chapter. Differences among these *in vivo* studies are outlined in terms of heterogeneity in the degree of dyslipidemia (DLP) attained during MetS development.

The large *in silico* population obtained in chapter 4 is further stratified in chapter 6 based on energy handling. Also, short-term perturbations of energy expenditure are applied to test the robustness of the metabolic system to changes in energy balance – providing a possible target for therapeutic interventions. Chapter 7 concludes this thesis and discusses the main contributions and provides an outlook on the possible future perspectives of this line of research.

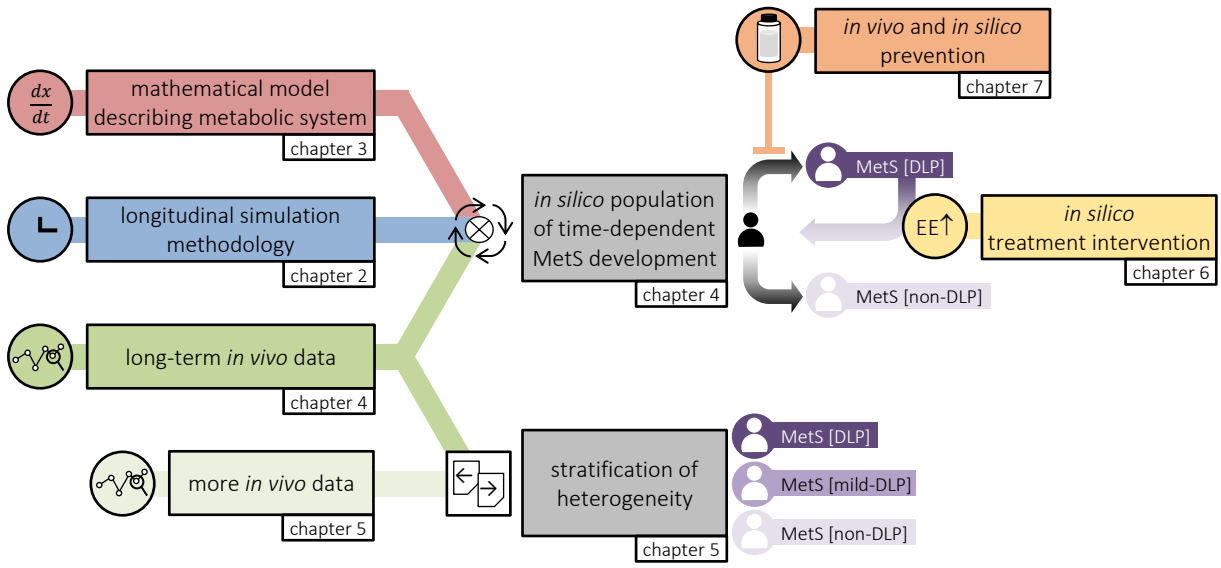

Figure 1.2

Graphical guide through the chapters of this thesis.

Different MetS phenotypes (highlighted in purple) are denoted in terms of the degree of dyslipidemia (DLP).

2

The need for a generic model predicting dynamic adaptations of chronic metabolic disorders

The case study described in this chapter is published in:

Nyman E, Rozendaal YJW, Helmlinger G, Hamrén B, Kjellsson MC, Strålfors P, van Riel NAW, Gennemark P, Cedersund G. Requirements for multi-level systems pharmacology models to reach end-usage: the case of type 2 diabetes. *Interface Focus*, 2016, 6(2):20150075 doi.org/10.1098/rsfs.2015.0075

Progression of chronic diseases is a complex, multifactorial phenomenon that occurs slowly over long timescales. Computational modelling can provide insight into the dynamics with which phenotypes change over time and identify which underlying processes are adapting simultaneously. We discuss several existing longitudinal models describing metabolic changes involved in ageing, disease progression, and treatment interventions. However, these models all have a very specific application and make *a priori* assumptions on the dynamics with which the disease progresses. We suggest ADAPT as a generic computational, data-driven technique to describe the long-term timespan using time-dependent model parameters. We highlight its use by comparing its predictions with a mechanism-based disease progression model for type 2 diabetes.

2.1 Studying long-term dynamics of phenotype transition

Computational models are widely used to study the underlying mechanisms of (patho)physiological phenomena. In the field of metabolic research, most kinetic models describe either glucose [Ajmera *et al.*, 2013; Bergman *et al.*, 1979; Cobelli *et al.*, 2014; Dalla Man *et al.*, 2007; Kim *et al.*, 2007; König *et al.*, 2012; Maas *et al.*, 2015; Palumbo *et al.*, 2013; Salinari *et al.*, 2011; Xu *et al.*, 2011; Rozendaal *et al.*, 2018a] or lipid [Jelic *et al.*, 2009; Lu *et al.*, 2014; Paalvast *et al.*, 2015; van de Pas *et al.*, 2012] regulation. Some models include interactions between carbohydrate and lipid metabolism [Chalhoub *et al.*, 2007a, 2007b; Roy and Parker, 2006; Sips *et al.*, 2015], in either specific organs [Micheloni *et al.*, 2014; Orsi *et al.*, 2011] or in a whole-body perspective. [Nyman *et al.*, 2011; Xu *et al.*, 2011] These models generally focus on short-term behaviour, e.g. in response to a meal or challenge test, and integrate observed time course data with a timescale ranging from minutes to hours. Depending on which data and which assumptions are used, the model can describe different conditions and provides a comparison between healthy and diseased phenotype, or diseased versus treated individuals.

2.1.1 Phenotype transition is a dynamic process

However, the difference between a healthy and a diseased state is not static. Usually, there is not a single healthy phenotype and not only one single diseased phenotype. A clear tipping point cannot be identified. Disease development, especially of chronic cardiometabolic diseases, is a dynamic process and computational analysis should also treat it as such. Phenotypes change slowly in time and go through different degrees or stages of disease development as depicted in Figure 2.1.

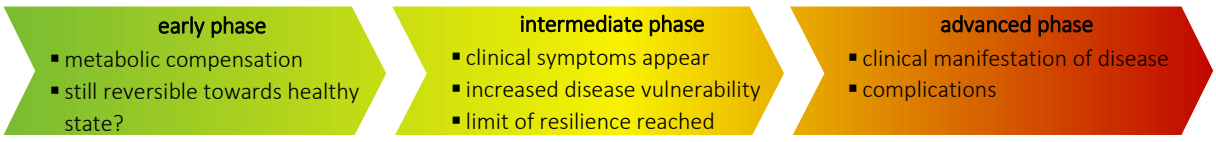

Figure 2.1
Phenotype transition over time: from onset to fully matured chronic metabolic disease.

2.1.2 Phenotype transition involves multiple timescales

Moreover, the timescales on which these adaptations take place shift towards the long-term perspective when studying the effects of ageing, natural or induced disease progression, or the effects of treatment interventions. For example in the development of cardiovascular diseases (CVD): people may suffer from elevated lipid levels in the plasma for years, but it may take decades before an actual cardiovascular event takes place. Monitoring of intermediate stages in time may attribute to early identification and adequate treatment planning to reduce the risk of CVD.

2.1.3 Multiple spatial levels are involved in phenotype transition

These progressive changes occur slowly over a long period of time and involve a complex network of regulatory processes. Phenotype transition is typically monitored using a snapshot read-out of circulating (plasma) biomarkers that reflect the metabolic status at that current point in time. However, the concentrations of plasma metabolites naturally fluctuate during the course of a day, e.g. upon fasting/feeding and hormonal control. These read-outs should, therefore, be standardized to provide an accurate, comparable, and representative snapshot of the metabolic status. This also allows separation of daily fluctuations from the slow changes in body composition and physiology that occur over longer timescales. Furthermore, whereas the disease manifests itself on organ and tissue level, the underlying adaptations that are responsible for the observed macroscopic changes occur on a molecular level. Although data is mostly acquired at plasma level, disease-modulating mechanisms are presumed to occur in the underlying proteome and transcriptome. [Dunn *et al.*, 2011]

2.1.4 Longitudinal data should be quantitative and time course

In order to get insight into the complex, multi-scale, and multi-factorial nature of disease progression using computational approaches, it is important to acquire quantitative, time course data from different tissues and spatial levels. This data should at least comprise (plasma) biomarkers, and – if possible – additional measurements in tissues, flux measurements, or transcriptomics (gene expression).

The timing with which these data are measured should be chosen carefully. Prospective studies only consist of a pre/post set-up and comprise a collection of single baseline measurements, followed by an intervention and a single follow-up measurement. However, data should be observed at multiple points in time to gain information about the actual dynamical behaviour and to enable ranking of observed effects in time.

2.2 Longitudinal modelling approaches

Literature reports on a considerable amount of disease progression models, but these mainly focus on the effects of ageing in fields such as cardiovascular diseases [Weinberg *et al.*, 2009], chronic obstructive pulmonary disease [Wang *et al.*, 2014b] and neurological disorders such as Alzheimer. [Cook and Bies, 2016; Fonteijn *et al.*, 2011; Samtani *et al.*, 2013] However, studying the long-term process of disease progression in chronic metabolic disorders requires a different approach that should

provide quantitative and dynamic predictions. Since metabolic disorders are often multi-factorial, the longitudinal modelling approach should be able to comprise multiple types of data and should not focus on only one isolated aspect of the disorder since we aim at analysing it from a systems perspective.

2.2.1 Long-term model of beta-cell deterioration

There are only a few computational disease progression models available in the literature that focus on metabolic (dys)regulation. Bagust *et al.* studied long-term beta-cell deterioration in type 2 diabetics. [Bagust and Beale, 2003] They make use of both a simple exponential model and a more sophisticated model consisting of time-displacement parameters and two exponential decaying functions to describe the trend in HOMA (Homeostatic Model Assessment) [Wallace *et al.*, 2004] beta-cell function over a time course of six years. However, this approach only tests the fit of pre-defined, hypothetical profiles based on the HOMA index.

2.2.2 Long-term model of anti-diabetic treatment

In the field of type 2 diabetes, a long-term model addressing multiple metabolic read-out parameters (biomarkers) is presented by de Winter *et al.* [de Winter *et al.*, 2006] This mechanism-based disease progression model aims to compare long-term treatment effects among different anti-diabetic compounds. Longitudinal data on plasma glucose, insulin, and glycosylated hemoglobin A1c (HbA_{1c}) have been integrated into a simple ODE-based model that is driven by asymptotically declining functions that represent decreasing beta-cell function and increasing insulin resistance upon natural disease progression, whilst taking into account the effect of the anti-diabetic treatment on these factors. This model is explored and evaluated in detail in section 2.4. However, the time-dependent profiles are imposed on both beta-cell function and insulin resistance, although these are not *a priori* known.

2.2.3 Long-term model of cholesterol metabolism during ageing

Efforts of long-term modelling have also been accomplished in the field of cholesterol metabolism. Mc Auley *et al.* developed a whole-body mathematical model of the complex interplay of cholesterol metabolism and its age-associated dysregulation on a timescale between 20 and 65 years of age. [Mc Auley *et al.*, 2012] The model considers different classes of lipoproteins carrying cholesterol in the plasma, intestine, liver, and periphery, but mainly evaluates the effects of ageing based on low-density lipoprotein cholesterol (LDL-C) levels in the plasma. They have shown to reproduce elevated LDL-C levels with ageing due to an increasing rate of intestinal cholesterol absorption whilst gradually decreasing the rate of hepatic clearance of LDL-C.

In contrast to the above-mentioned models, the Mc Auley *et al.* model integrates long-term data from different sources as well as uses a whole-body perspective since it considers metabolic status in different metabolically active tissues. Although some parameters are estimated based on observed LDL-C data, many of the parameter values are taken directly from literature. However, uncertainty on these assumptions is not taken into account.

2.2.4 The need for a generic approach for long-term modelling

Although the discussed long-term models have proven their functionality, these are only applicable in the limited area directly related to the scope of that specific research field. We pursue a more generic approach to study long-term metabolic adaptations using computational modelling.

A fundamental framework offering a longitudinal modelling approach is provided by the method for Analysis of Dynamic Adaptations in Parameter Trajectories (ADAPT). [Tiemann *et al.*, 2011, 2013; van Riel *et al.*, 2013] In contrast to the above-mentioned studies, ADAPT is a universally applicable method and does not limit its use to one specific ODE model. It is based on the time-dependency of the model parameters to study the long-term behaviour of the biological system, but does not require *a priori* assumptions on how the parameters change with time. Moreover, the ADAPT methodology accounts for experimental and methodological variability in its predictions, as is explained in detail in the following section.

2.3 Analysis of Dynamic Adaptations in Parameter Trajectories (ADAPT)

Analysis of Dynamic Adaptations in Parameter Trajectories (ADAPT) is a generic computational approach to study long-term adaptations in a biological system. [Tiemann *et al.*, 2011, 2013; van Riel *et al.*, 2013] Whereas classical modelling approaches assume that the parameters are constant in time, this is typically not the case in long-term studies following phenotype transition due to (a combination of) disease progression or (pharmacological) treatment interventions. Typically, measurements are performed on a macroscopic level, whereas adaptations usually occur on lower levels. [Dunn *et al.*, 2011] ADAPT integrates experimental data on metabolic pools and fluxes obtained at different points in time with a mathematical model of choice of the biological system that is studied. ADAPT is a highly data-driven approach and requires large amounts of data to span the model. In general, the majority of metabolic states in the model should be observed throughout time, and the more fluxes that have been measured, the more constrained the model becomes. [van Diepen, 2014]

Although mathematical models alone can describe the mechanisms that we already know, these models will not discover any new biology. Since ADAPT is highly data-driven, it offers a method to make new discoveries embedded in existing knowledge. The mathematical model itself will describe the known network topology, whereas the time-dependent parameters capture the dynamics of disease progression and phenotype transition. The time-dependent evolution of the model parameters is referred to as parameter trajectories. To describe phenotype transition, ADAPT identifies trajectories of parameter adaptations that are essential for the phenotypic changes observed in the experimental data. Unobserved fluxes and metabolite concentrations are inferred, whereby the ADAPT framework provides additional insight into the affected underlying biological system.

ADAPT was originally conceived from the fields of model learning, parameter identification, and (non-)identifiability. [Gábor and Banga, 2015] ADAPT combines concepts from maximum likelihood estimation (MLE), Bayesian inference, and (prediction) uncertainty analysis. [Vanlier *et al.*, 2013] Hence, the ADAPT pipeline (Figure 2.2) comprises different algorithms arising from each of

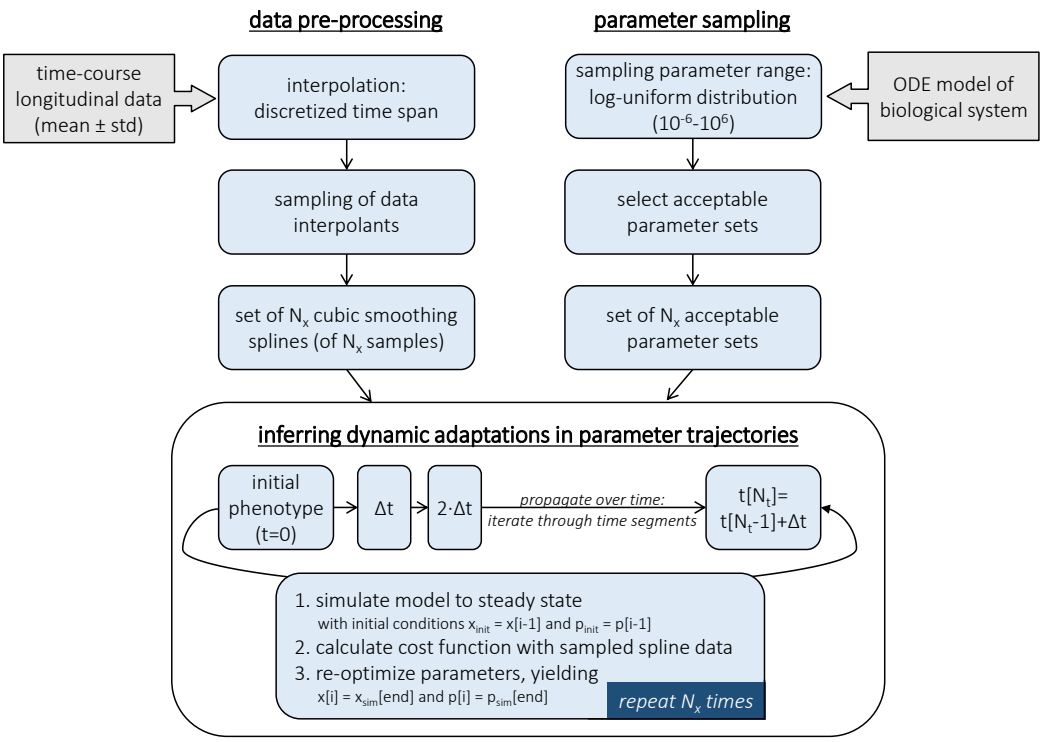

Figure 2.2
Schematic workflow of the ADAPT methodology.

these fields. The data pre-processing and parameter sampling branches consecutively converge towards the heart of ADAPT: the repeated simulation and optimization in the parameter estimation protocol, yielding a collection of N_x parameter trajectories.

ADAPT is particularly useful to study biological systems from which the network topology is relatively well-known, such as the mass fluxes in metabolic pathways. The modulating effects on these pathways via interactions with the proteome and transcriptome – which are less well understood – are captured by the time-dependent descriptions of the parameters. Hence, pathway adaptations can be described without the necessity to develop detailed kinetic models of the modulating mechanisms.

2.3.1 Pre-processing of experimental data

During the long-term dynamics of phenotype transition, quantitative data should hereto be measured at multiple points in time. These data typically contain information about changes in metabolite concentration in plasma and tissue compartments, but could also comprise metabolic flux measurements. These data describe phenotypic snapshots that are linked in time. Some data pre-processing is required to describe the metabolic status at any given point in the studied timeframe. This is approximated by discretization of the timespan using a finite amount of time segments. Piecewise polynomial (cubic smoothing) splines are used to describe the dynamic trend of the experimental data, as illustrated in Figure 2.3B. This is regarded the preferred interpolation scheme in cases of noisy observations. [Craven and Wahba, 1978]

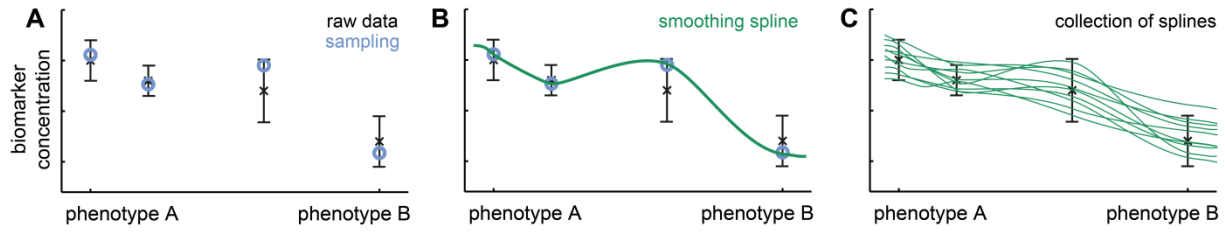

Figure 2.3

Pre-processing of experimental data for ADAPT.

The experimental data generally consists of time course, longitudinal data obtained at multiple points in time, describing the transition from phenotype A (e.g. untreated or healthy phenotype) to phenotype B (e.g. diseased or treated phenotype). In panel A, the black error bars represent mean and standard deviation at each point in time. To account for experimental and biological uncertainties, a Monte Carlo approach is employed. Hereto the data is randomly sampled (A; blue circles) and a cubic smoothing spline (B; green line) is fitted through these samples to obtain a continuous description over time. This process is iteratively repeated, obtaining a collection of splines (C).

To account for experimental and biological uncertainty, and to determine the propagation of data uncertainty through model predictions [Vanlier *et al.*, 2012], ADAPT employs a Monte Carlo approach. Given that the experimental data comprise multiple measurements at each point in time (either obtained from different individuals or from repeated measurements from the same person), random samples (replicates) can be generated from the experimental data. The data is sampled assuming that the data is Gaussian distributed with mean and standard deviation of the data (Figure 2.3A). Consecutively these samples are interpolated, yielding a collection of data spline interpolants (Figure 2.3C) as input data for the parameter estimation protocol. This collection is the same size N_x as the desired amount of parameter trajectories to be calculated. The sampling of replicates of experimental data and their subsequent utilization in parameter estimation is a common approach to assess prediction uncertainty, and is also referred to as "bootstrapping". [Cedersund and Roll, 2009]

2.3.2 Mathematical model description of the biological system

Since ADAPT is a generic computational approach, it can be used with a mathematical model of choice, depending on the studied biological system and amount and type of observed data. *A priori* information is combined into a network topology with reaction kinetics, which is translated into an ordinary differential equation (ODE) model (2.1) with kinetic parameters $\vec{\theta}$ that describe how the fluxes are related to metabolite concentrations:

$$\frac{d\vec{x}}{dt} = N\vec{f}\left(\vec{x}(t),\vec{\theta}\right) \tag{2.1}$$

$$\vec{y}(t) = \vec{g}\left(\vec{x}(t),\vec{\theta}\right) \tag{2.2}$$

$$\vec{x}(t_0) = \overrightarrow{x_0} \tag{2.3}$$

in which $\frac{d\vec{x}}{dt}$ represents the vector of first derivatives of modelled species (states) $\vec{x}$, given by the topology of the network (matrix N), and a set of functions $\vec{f}$. The model parameters typically represent reaction rate constants but could be any other quantity expressible in a mathematical model. The vector $\vec{g}$ maps the model components (e.g. states or fluxes) to the desired output quantities $\vec{y}$, given initial conditions $\overrightarrow{x_0}$.

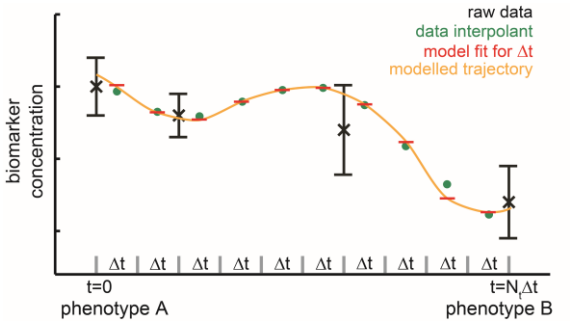

Discretization of the timespan.
The original raw experimental data are depicted by black error bars. For each of the time segments, one example of a data interpolant (see Figure 2.3B) is depicted by green dots. The model (red) is fitted to these data interpolants per time segment. These piecewise model trajectories (red) become a fully continuous, smooth curve (orange) through ODE integration.

Figure 2.4

2.3.3 Discretization: new equations with time-dependent parameters

Discretization of the system is applied as follows:

$$\vec{X}[n] = \vec{x}(\Delta t, \vec{\theta}[n]) \quad (2.4)$$

$$\vec{Y}[n] = \vec{g}(\vec{X}[n], \vec{\theta}[n]) \quad (2.5)$$

$$\vec{X}[0] = \overrightarrow{x_{ss}}(\vec{\theta}[0]) \quad (2.6)$$

in which $\vec{X}$ and $\vec{Y}$ are the discretized quantities of $\vec{x}$ (2.1) and $\vec{y}$ (2.2) respectively. The total simulated timespan $N_t \cdot \Delta t$ is represented by $0<n<N_t$.

Hereto, the total simulation is divided into N_t segments with time step Δt, which is graphically illustrated in Figure 2.4 using hypothetical data and a model simulation with n=10 segments in time. Note that in real cases, the Δt is chosen much smaller than in this hypothetical example, such that the obtained model trajectory is much smoother than the one illustrated in Figure 2.4.

2.3.4 Parameter sampling

Prior to entering the simulation and optimization branch – the data now having been pre-processed – the last initialization step involves the sampling of initial model parameters from a log-uniform distribution ranging twelve orders of magnitude (10^{-6} - 10^{6}). This yields a widely dispersed range of parameter sets that are used to calculate the initial conditions of the model with. From this initial run, N_x acceptable sets are selected to be optimized to the t=0 conditions of the system.

2.3.5 Model optimization

For each acceptable parameter set θ_x, a parameter adaptation trajectory is identified according to the following protocol.

The initial phenotype (t=0 state) is simulated with the initial parameter set θ_x provided by the previous step. This parameter set is optimized to the interpolated spline data (sample x) by simulating the model with parameters θ_x, and comparing the steady-state values with the data sample. In a classical optimization approach, this objective function would be:

$$\chi_t^2(\vec{\theta}) = \sum_{i=1}^{N_y} \left(\frac{y_{ss,i}(\vec{\theta}) - d_i(t)}{\sigma_i(t)} \right)^2 \quad (2.7)$$

$$\widehat{\vec{\theta}_t} = \arg\min_{\vec{\theta}} \chi_t^2(\vec{\theta}) \quad (2.8)$$

To fit the model to the observed data, the difference between the model observables y (2.2) and corresponding data is evaluated. The model parameters are estimated using Maximum Likelihood Estimation (MLE) during which the weighted squared error (2.7) is minimized (2.8). The objective function is repeatedly evaluated over N_y model-data pairs, in which $d_i(t)$ represents the data interpolant of the experimental data at time t, and $\sigma_i(t)$ the corresponding standard deviation at time t. The optimized set of parameters $\overrightarrow{\hat{\theta}_t}$ is obtained when the weighted least squared error χ^2_t is minimized.

With the discretized timespan, the objective function becomes:

$$\chi^2_d(\vec{\theta}[n]) = \sum_{i=1}^{N_y} \left(\frac{Y_i[n]-d_i(n\Delta t)}{\sigma_i(n\Delta t)} \right)^2 \tag{2.9}$$

Subsequently, the full trajectory (t>0) can be determined, which yields a distribution of piecewise constant parameter trajectories. ADAPT iterates over the time segments (t=Δt; t=2·Δt; … ; t=N_t·Δt). The simulation is initiated with the steady-state values $\overrightarrow{x_{ss}}$ obtained with the parameter set $\vec{\theta}[0]$ for the initial (untreated or healthy) phenotype.

For each step n>0, the model is simulated for a time period of Δt using the final steady-state values of the model states of the previous step (n-1) as initial conditions. The parameter set $\theta_x[n]$ is optimized according to the squared differences of the data interpolant and the model at the corresponding time segment (i.e. objective function (2.9)).

This parameter estimation protocol is performed iteratively over the N_x initial parameter sets and N_x data interpolants, yielding a collection of N_x parameter trajectories as well as N_x corresponding trajectories describing metabolite concentrations and metabolic fluxes.

2.3.6 Regularisation: minimizing fluctuations in parameter trajectories

ADAPT identifies necessary dynamic changes in the model parameters to describe the phenotypic changes in the observed data, whilst being constraint by the network topology and kinetic equations of the biological system. It is assumed that the induced adaptations are minimal and proceed progressively in time. Moreover, it is *a priori* not known which parameters need to change with time to induce phenotype transition. Highly fluctuating parameter trajectories are considered to be non-physiological. To prevent the occurrence of such behaviour, to ensure smooth curves, and to minimize the occurrence of unnecessary changes of parameters with time, regularisation of the parameter trajectories is imposed during the optimization procedure. The derivatives of the parameter trajectories are regulated by extending the objective function with a regularisation term:

$$\vec{\theta}[n] = \arg\min_{\vec{\theta}[n]} \left(\chi^2_d(\vec{\theta}[n]) + \lambda_r \cdot \chi^2_r(\vec{\theta}[n]) \right) \tag{2.10}$$

in which χ^2_d represents the weighted squared difference between data interpolant and model entities (2.9), and χ^2_r the regularisation objective function given by the sum of squared derivatives of the normalized parameter values:

$$\chi^2_r(\vec{\theta}[n]) = \sum_{i=1}^{N_p} \left(\frac{\theta_i[n]-\theta_i[n-1]}{\Delta t} \cdot \frac{1}{\theta_i[0]} \right)^2 \tag{2.11}$$

in which N_p represents the number of parameters and λ_r the regularisation strength. Hence, changing a parameter is costly, and is, therefore, avoided if this is not required to describe the data. The regularisation strength λ_r should be chosen carefully. It is preferred to bias data fitting as little as possible and therefore a minimal value for λ_r, while still being effective, should be selected. Figure 2.5 illustrates that if too large a value for λ_r (to the right on the horizontal axis) is chosen, the regularisation term becomes dominant and the model will not describe the data accurately anymore (χ^2_d increases drastically). The priority in the optimization algorithm should always be at fitting the data (i.e. low χ^2_d). A small value for λ_r should already be sufficient to minimize parameter changes and fluctuations (reduced χ^2_r), whilst still describing the experimental data accurately (trade-off being a small increase in χ^2_d). It should be noted that the tuning of λ_r highly depends on the model and data at hand, and therefore will vary on a case-by-case basis.

2.3.7 Implementation details

The ADAPT methodology is implemented in MATLAB (2013b, The Mathworks, Natick, Massachusetts). Ordinary differential equations are solved with compiled MEX files using numerical integrators from the SUNDIALS CVode package (2.6.0, Lawrence Livermore National Laboratory, Livermore, California). [Hindmarsh *et al.*, 2005] An absolute and relative tolerance of 10^{-6} is used. The MATLAB nonlinear least-squares solver *lsqnonlin* (from the Optimization Toolbox), which uses an inferior reflective Newton method, is used to estimate model parameters. [Coleman and Li, 1996] The termination tolerances for the objective function and the parameter estimates were set to 10^{-8}, the maximum number of iterations allowed is set to 10^3 and the maximum number of function evaluations allowed to 10^5. The MATLAB *csaps* function (from the Curve Fitting Toolbox) is used to calculate cubic smoothing splines using the default smoothness setting (=1) and the roughness dependent on the variation in the data: $(1/\text{std})^2$.

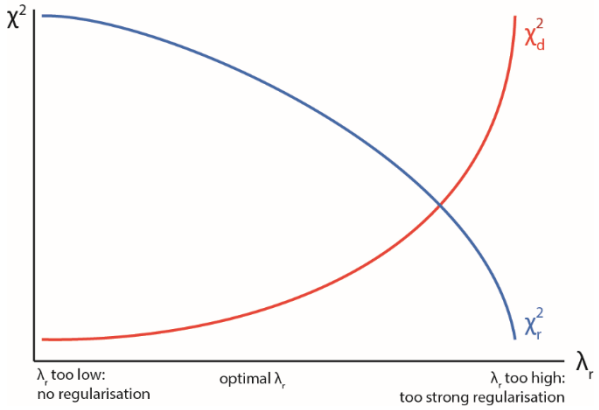

Determination of regularisation strength coefficient λ_r.
Trade-off between fitting the data as closely as possible (red line; to the left on the horizontal axis) and enforcing smooth parameters (red line; to the right on the horizontal axis).

Figure 2.5

2.4 *Case study* Long-term prediction of beta-cell function and insulin sensitivity – a mechanism-based approach compared to ADAPT

We demonstrate the use of ADAPT by comparing it to a mechanistic model description of disease progression of type 2 diabetes. De Winter *et al.* [de Winter *et al.*, 2006] published a mechanism-based population pharmacodynamic (PD) disease progression approach in type 2 diabetes mellitus (T2DM) patients undergoing different anti-diabetic treatments over the time course of a year. PD modelling can quantitatively interpret disease progression and assess drug effects in a mechanistic manner. [Atkinson and Lalonde, 2007] The de Winter *et al.* model is a descriptive model to simulate the impact of chronic loss of glycemic control on the initial improvement of glucose control induced by pharmacotherapy over one year. It quantifies the time course effects of different pharmacological agents on plasma glucose, insulin, and HbA_{1c} levels over time using mechanistic descriptions for the beta-cell function and hepatic insulin sensitivity.

2.4.1 Biomarker data

Glycosylated hemoglobin A1c (HbA_{1c}) is the primary glycemic biomarker for measuring long-term glycemic control since it provides an estimate of overall control of blood glucose levels in the preceding eight to twelve weeks. [Nathan *et al.*, 2007] Secondary biomarkers include fasting plasma glucose (FPG) and fasting serum insulin (FSI), which are more responsive to changes in glycemic control in the short-term.

Over the time course of one year of anti-hyperglycemic treatment, these biomarkers were repeatedly assessed at ten observations in time (nine for insulin). Data originates from two multi-centre, randomized, double-blind, double-dummy, parallel-group studies that compared the long-term effects of pioglitazone, metformin, and gliclazide monotherapy on FSI, FPG, and HbA_{1c}. [Charbonnel *et al.*, 2005; Schernthaner *et al.*, 2004] The population comprised in total 2,408 newly diagnosed T2DM patients that were naïve to antidiabetic medication and were inadequately controlled by diet alone.

The included pharmacological agents achieve their anti-hyperglycemic effects through different physiological mechanisms. Pioglitazone and metformin are classified as insulin-sensitizing agents [Inzucchi, 2002], whereas gliclazide acts as an insulin secretagogue. Pioglitazone affects insulin resistance by increasing insulin sensitivity in the liver, muscle, and adipose tissue [Aronoff *et al.*, 2000; Olefsky, 2000] and thereby enhances peripheral glucose uptake as well as reduces hepatic glucose production. Metformin acts primarily by decreasing hepatic glucose production. [DeFronzo, 1999; Inzucchi, 2002; Matthaei *et al.*, 2000] Gliclazide stimulates insulin secretion by the pancreatic beta-cells. [DeFronzo, 1999; Inzucchi, 2002; Matthaei *et al.*, 2000]

2.4.2 Mechanism-based disease progression model describing the progression of T2DM

The mechanism-based population PD disease progression model by de Winter *et al.* aims to integrate information on the time course of the disease available in data on FPG, FSI, and HbA_{1c} into a single comprehensive, physiologically meaningful model structure. It incorporates mechanism-based representations of the homeostatic feedback relationships between FPG

and FSI, and the physiological feed-forward relationship between FPG and HbA_{1c}, which are implemented as two linked turn-over models. [Dayneka *et al.*, 1993] The mechanism-based representation of the glucose-insulin homeostasis should allow the model to describe T2DM progression in terms of loss of beta-cell function and insulin sensitivity over time, and to represent the effects of different treatments at their specific sites of action. The model aims to differentiate the immediate effects of a treatment on glycemic control from its long-term, disease-modifying effects on the chronic loss of beta-cell function and insulin sensitivity.

The de Winter *et al.* model (Figure 2.6) consists of a system of three Ordinary Differential Equations (ODEs), six model parameters, two treatment-specific factors, and two coefficients representing disease status. These coefficients represent disease status in terms of the fraction of remaining beta-cell function (B) and of hepatic insulin sensitivity (S) relative to, respectively, normal functionality and sensitivity in healthy persons. Since disease progression in T2DM is caused by a chronic loss of both beta-cell function and decreased insulin sensitivity, the coefficients B and S should be allowed to decrease as a function of time, whilst taking into account the disease history of patients at baseline. Hereto, the coefficients B and S are implemented to decline as asymptotic functions over time and range between one (full, normal functionality) and zero (complete loss of functionality). The model equations and parameter values are given in Appendix 2.6. It should be noted that the implied trend in time course of the coefficients B and S are biologically unknown and may vary among patients, and that the asymptotic equations for B and S are hypothetically imposed in the original paper.

2.4.3 Simulating the effects of different anti-diabetic treatments over the time course of a year in terms of biomarkers and disease progression curves

Figures 2.7A-C presents the simulated profiles for FSI, FPG, and HbA_{1c} over time by the de Winter *et al.* model, including the mean observed data on these biomarkers for treatment with gliclazide (red), pioglitazone (green), and metformin (blue). The trend in fasting plasma glucose (Figure 2.7B) and HbA_{1c} (Figure 2.7C) are adequately described by the simulated profiles. Although the model was developed and calibrated onto these biomarker data, the trend in fasting serum insulin (Figure 2.7A) is only described adequately for pioglitazone treatment, but not for gliclazide and metformin treatments.

The model equations are driven by disease progression (chronic loss of both beta-cell function and insulin sensitivity), but also by the stimulatory effect on the beta-cell function by

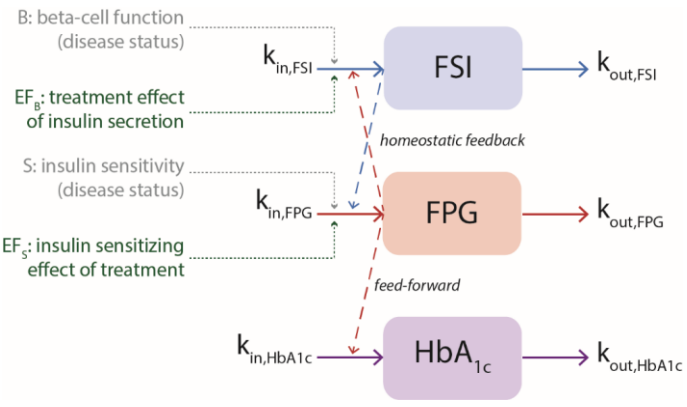

Schematic overview of the mechanism-based population PD disease progression model proposed by de Winter *et al.*

FSI: fasting serum insulin; FPG: fasting plasma glucose; HBA_{1c}: glycosylated hemoglobin A1c

Figure 2.6

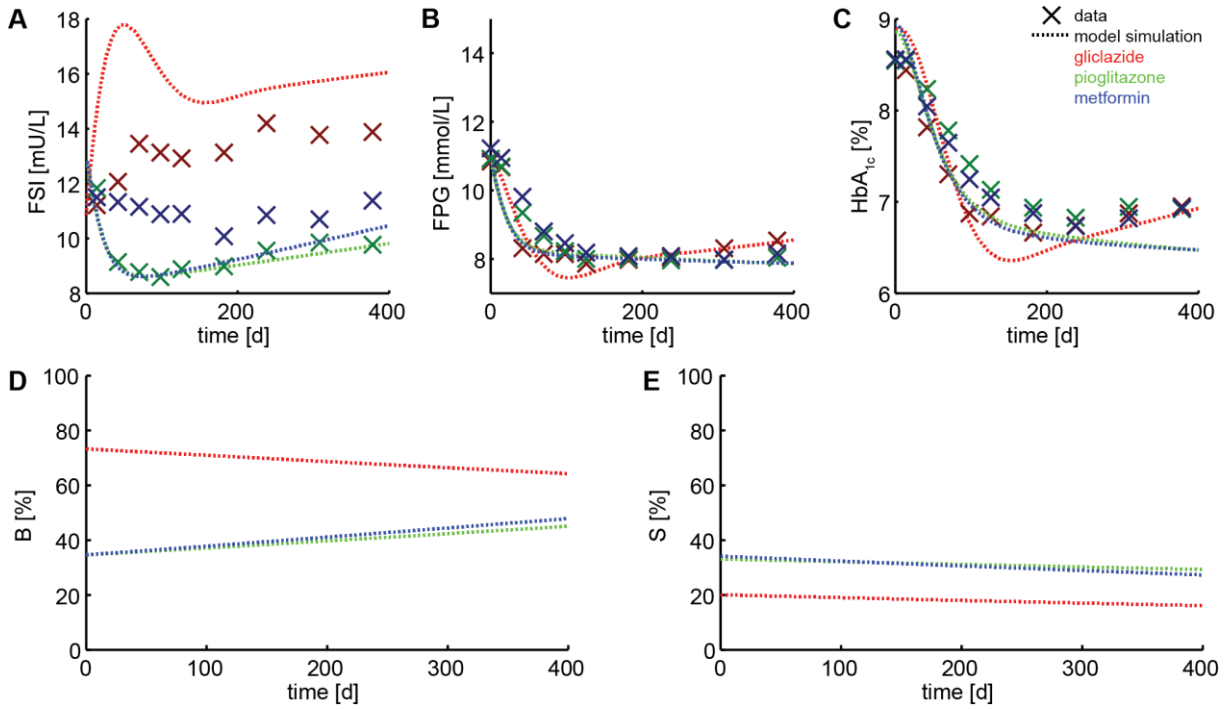

Figure 2.7

Experimental observations (crosses representing the mean value of 2,408 subjects) and simulated profiles (dotted lines) by the de Winter *et al.* model in plasma biomarkers (A-C).

Plasma markers are assessed given the changes in beta-cell function B (D) and insulin sensitivity S (E) imposed by the de Winter *et al.* model for treatment with either gliclazide (red), pioglitazone (green), or metformin (blue).

gliclazide treatment or by enhanced insulin sensitizing upon pioglitazone and metformin biomarker profiles in panels A-C. Although B and S are defined as asymptotically declining functions, the model reveals linear functions over a timespan of one year. Note that the disease history has been taken into account: baseline disease status is reflected by a lower residual functionality and sensitivity at t=0. This shows that the "classical" approach of fitting all model parameters (Table 2.1 in Appendix 2.6) as being constant over the complete time period (one year) is insufficient to yield an adequate model fit of all biomarkers over time.

2.4.4 Inferring beta-cell function and insulin sensitivity using ADAPT

Since the trend in disease progression is not *a priori* known, these pre-defined decaying profiles for how beta-cell function and insulin sensitivity change over time may not be physiologically correct. Although these entities could indirectly be assessed using demanding clamp studies [DeFronzo *et al.*, 1979; Matsuda and DeFronzo, 1999], we use a different approach in which we pair the basic ODEs from the de Winter *et al.* model with our ADAPT approach to infer B and S from the available biomarker data. In this way, the model could serve as an "observer system" that integrates and translates biological data into clinically relevant information. The beta-cell function and insulin sensitivity are treated as time-dependent parameters and fitted to the time course data on the observed FSI, FPG, and HbA_{1c} levels. These parameters represent natural disease progression simultaneously with the effect of the anti-diabetic treatment. Figure 2.8 shows that without predefining how the beta-cell function and insulin sensitivity are expected to change over time, the ADAPT predictions resemble the clinical read-out parameters (FSI,

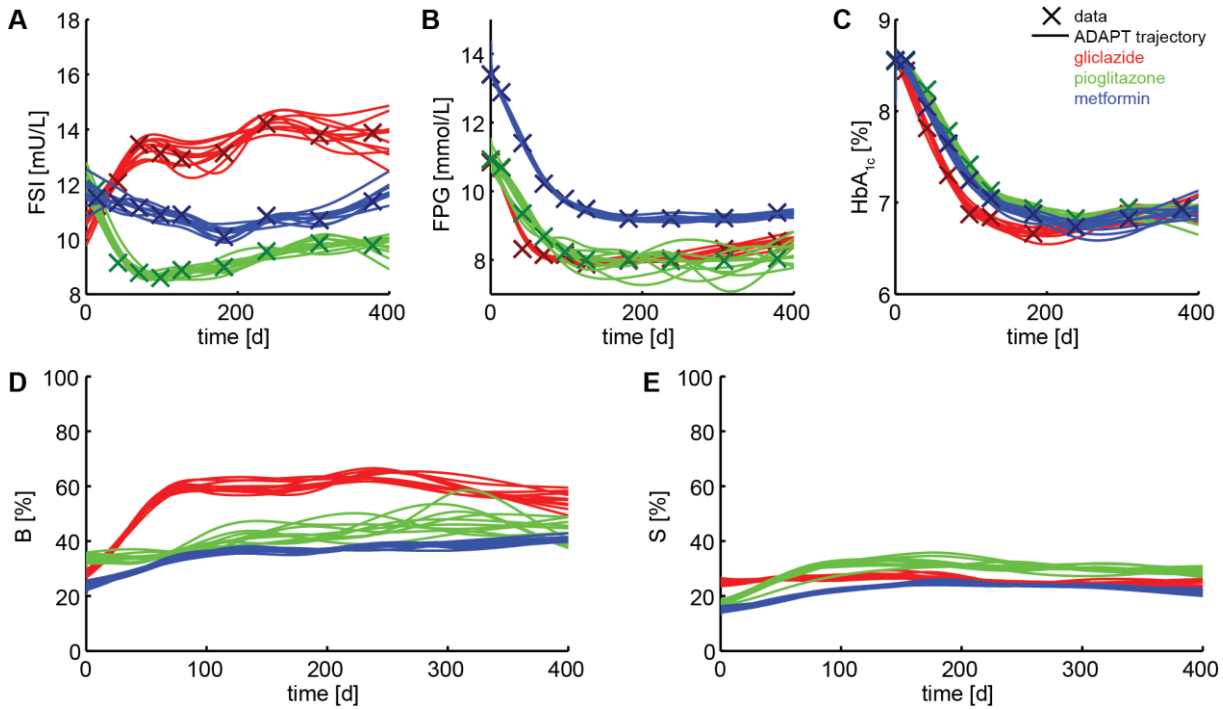

Figure 2.8

Predicted trajectories for the plasma biomarkers (A-C, solid lines) with beta-cell function (D) and insulin sensitivity (E) inferred using ADAPT.

In each panel, ten of the best-found trajectories are depicted (solid lines) with respect to the experimental observations (crosses) during treatment with gliclazide (red), pioglitazone (green), and metformin (blue).

FPG, and HbA_{1c}) more closely than the original model. Furthermore, whereas the changes over time in B and S as proposed for the original model (Figures 2.7D-E) are linear over time (despite the assumption that they should decrease in an asymptotic manner), the parameter trajectories inferred by ADAPT (Figures 2.8D-E) show more dynamic behaviour. The clinically observed biomarker data suggest changes in the underlying physiology to occur mostly at the beginning of the study, reaching a plateau after around 200 days. This hypothesis matches the predicted trend in beta-cell function and insulin sensitivity by ADAPT. Presumably, this dynamic behaviour inferred by ADAPT reflects the physiological changes to different anti-diabetic treatments better than the original mechanism-based disease progression model.

Furthermore, ADAPT infers an increase in both B and S for virtually all treatment arms when comparing one-year treatment effect with baseline values. As expected, gliclazide being an insulin secretagogue yields the largest improvement in B. However, gliclazide appears to have a strong effect in the first ~80 days but reaches a plateau after that. It has little to no effect on S. The insulin sensitizers pioglitazone and metformin do improve S, but according to different trends in time. Both these insulin sensitizers beneficially affect B, which is in line with previous observations. [Rasouli *et al.*, 2007]

2.5 Discussion

2.5.1 Requirements for modelling long-term dynamics

Disease progression and phenotype transition involve longitudinal timescales. The complex long-term phenomena involved introduce an inherent complexity. Computational modelling offers a quantitative approach to model long-term dynamics, but should consider to:

- describe phenotype transition over time;
- handle longitudinal data;
- integrate different (types of) data;
- deal with heterogeneity and variability in data;
- provide quantitative predictions;
- account for different spatial levels;
- not require any *a priori* assumptions about adaptations (which processes do change and how).

The limited availability of longitudinal computational models describing metabolic regulation has also shown to be very specifical in scope. [Mc Auley and Mooney, 2014] In contrast to such models, ADAPT is not a hypothesis-driven but a data-driven approach and enables discovery. Moreover, ADAPT is a generic approach that incorporates the time-dependency and does not limit itself to one specific model or study objective. Uncertainty in data, e.g. due to imperfect data, missing data, or a more heterogeneous response than expected, may bias model predictions. ADAPT, on the other hand, improves identifiability by taking both experimental and methodological variability into account by employing its Monte Carlo approach in both data handling and parameter sampling. [Vanlier *et al.*, 2013]

2.5.2 ADAPT applications

ADAPT has shown to be applicable to models of different sizes, using data from different organisms, considering models with different metabolic pathways, and simulating different timespans. Regardless of what type of phenotype transition (natural/induced disease development versus treatment intervention) takes place, ADAPT has proven its functionality.

ADAPT was initially used with a murine lipid metabolism model and has shown to identify dynamic adaptations induced by a three-week pharmacological treatment intervention of the liver X receptor in C57BL/6J mice. [Tiemann *et al.*, 2013]

Using a much smaller toy model, ADAPT has proven its ability to identify and reproduce the single, underlying cause of phenotype adaptation upon an externally applied intervention to a toy model. [van Riel *et al.*, 2013]

Switching to models of carbohydrate metabolism rather than lipid metabolism, we have shown here that ADAPT can be applied using datasets measured in human subjects. [Nyman *et al.*, 2016] In addition, not all model parameters have to become time-dependent in order to show ADAPT's functionality. Using a minimal glucose model with the rate of appearance being time-dependent has shown to explain the implications of the Roux-en-Y gastric bypass on glucose homeostasis and T2DM. [Snel, 2015]

2.5.3 Extending the ADAPT methodology

ADAPT can be extended such that while inferring parameter trajectories, these can be regulated by time course data on gene expression. This extended version of ADAPT has shown to provide more constraint predictions. [Hijmans *et al.*, 2015]

The dynamic parameters predicted by ADAPT can also be applied to identify missing regulations, as shown by identifying modulation points of the insulin signalling pathway. [Çölmekçi, 2015]

2.5.4 Conclusion

ADAPT is a generic approach that accommodates both modelling of the dynamics of phenotype transition in response to treatment interventions, but also to long-term disease development and progression.

2.6 Appendix: Model description of the mechanism-based disease progression model for T2DM by de Winter *et al.*

The change in biomarker levels for fasting serum insulin (FSI), fasting plasma glucose (FPG), and glycosylated hemoglobin (HbA_{1c}) is modelled as:

$$\frac{dFSI}{dt} = EF_B \cdot B \cdot (FPG\text{-}th) \cdot k_{in,FSI} - FSI \cdot k_{out,FSI} \quad (2.12)$$

$$\frac{dFPG}{dt} = \frac{k_{in,FPG}}{EF_S \cdot S \cdot FSI} - FPG \cdot k_{out,FPG} \quad (2.13)$$

$$\frac{dHbA_{1c}}{dt} = FPG \cdot k_{in,HbA_{1c}} - HbA_{1c} \cdot k_{out,HbA_{1c}} \quad (2.14)$$

in which EF_B and EF_S represent the treatment effect on either beta-cell function (B) or insulin sensitivity (S) respectively. See Table 2.1 for a description of the model parameters and their corresponding values.

In the original de Winter *et al.* model, the disease status (progression) in terms of beta-cell function (B) and insulin sensitivity (S) is described as:

$$B = \frac{1}{1+\exp(b_0 + r_B \cdot t)} \quad (2.15)$$

$$S = \frac{1}{1+\exp(s_0 + r_s \cdot t)} \quad (2.16)$$

in which b_0 and s_0 represent the shift of the disease progression curves over the time axis, and r_B and r_S represent the slope of the disease progression curves (and hence the rate of change over time in B and S respectively).

Note that for ADAPT, both B and S are converted to time-dependent model parameters; equations (2.15) and (2.16) are omitted.

Table 2.1

Values of all model coefficients in the de Winter *et al.* model.

coefficient		value	unit	description
$k_{out,FSI}$		1	day^{-1}	efflux rate constant of FSI
$k_{out,FPG}$		0.021	day^{-1}	efflux rate constant of FPG
$k_{out,HbA_{1c}}$		0.0272	day^{-1}	efflux rate constant of HbA_{1c}
$k_{in,FSI}$		$= 5 \cdot k_{out,FSI}$	day^{-1}	influx rate constant of FSI
$k_{in,FPG}$		$= 22.5 \cdot k_{out,FPG}$	day^{-1}	influx rate constant of FPG
$k_{in,HbA_{1c}}$		$= fr_{HbA_0} \cdot k_{out,HbA_0}$	day^{-1}	influx rate constant of HbA_{1c}
b_0		0.635	-	shift of disease progression curve over time
s_0		1.38	-	shift of disease progression curve over time
th		3.5	mmol/L	threshold of FPG stimulated FSI production
fr_{HbA_0}		0.82	-	fraction HbA_0/FPG_0
EF_B	*gliclazide*	2.115 (111.5% increase)	day^{-1}	treatment effect on beta-cell function: ▪ =1 untreated ▪ 0-1 loss of beta-cell function ▪ >1 stimulatory effect of insulin secretagogues on beta-cells
	metformin	1		
	pioglitazone	1		
EF_S	*gliclazide*	1	day^{-1}	treatment effect on insulin sensitivity: ▪ =1 untreated ▪ 0-1 loss of hepatic insulin sensitivity ▪ >1 increased insulin sensitivity upon suppressing effect of EGP by insulin sensitizers
	metformin	1.699 (69.9% increase)		
	pioglitazone	1.649 (64.9% increase)		
r_B	*gliclazide*	0.178/365	day^{-1}	slope of disease progression curve/rate of change over time
	metformin	=-2.82·(0.178/365) (-282% of gliclazide reference)		
	pioglitazone	=-2.24·(0.178/365) (-224% of gliclazide reference)		
r_S	*gliclazide*	0.245/365	day^{-1}	slope of disease progression curve/rate of change over time
	metformin	=1.01·(0.245/365) (101% of gliclazide reference)		
	pioglitazone	=0.567·(0.245/365) (56.7% of gliclazide reference)		

3

A model of the integration of glucose and lipid dynamics (MINGLeD)

This chapter is published in:

Rozendaal YJW, Wang Y, Paalvast Y, Tambyrajah LL, Li Z, Willems van Dijk K, Rensen PCN, Kuivenhoven JA, Groen AK, Hilbers PAJ, van Riel NAW. *In vivo* and *in silico* dynamics of the development of Metabolic Syndrome. *PLoS Comput. Biol.*, 2018, 14(6):e1006145 doi.org/10.1371/journal.pcbi.1006145

The Model INtegrating Glucose and Lipid Dynamics (MINGLeD) is a novel dynamic and computational model describing whole-body carbohydrate and lipid metabolism. It is composed of a system of coupled, nonlinear ordinary differential equations (ODEs). The steady state of the ODE model represents a snapshot of the metabolic state and describes the mass balance of the metabolite pools and flux rates for carbohydrate, lipid, and cholesterol species in the plasma, liver, intestinal lumen, and periphery. The model aims to describe the metabolic system in a whole-body perspective under healthy conditions as well as at different stages during Metabolic Syndrome development.

MINGLeD describes metabolite pools originating from carbohydrate substrates (glucose, glucose-6-phosphate, acetyl-Coenzyme A), lipid species (free fatty acids, triglycerides, various lipoproteins), and cholesterol (free cholesterol, cholesteryl esters, bile acids). The metabolic pathways that define the interactions between these metabolites include the uptake of dietary macronutrients, glycolysis, hepatic gluconeogenesis, lipoprotein assembly and (remnant) uptake, cholesteryl ester transfer between lipoproteins (CETP action), transintestinal cholesterol excretion (TICE), exchange between free cholesterol and cholesteryl esters (via ACAT and CEH) in hepatic tissue, hepatic fatty acid uptake, peripheral lipolysis, β-oxidation, *de novo* lipogenesis (DNL), cholesterol biosynthesis, bile acid synthesis, biliary bile acid and cholesterol excretion, enterohepatic reuptake, fecal excretion of bile acids and cholesterol, and respiration of acetyl-Coenzyme A in hepatic and peripheral tissues.

3.1 Introducing MINGLeD

MINGLeD (Model Integrating Glucose and Lipid Dynamics) is a physiology-based computational model that describes the metabolic status on a systemic level for both healthy and metabolically derailed phenotypes. It comprises the pathways that are necessary to describe energy metabolism from dietary intake to storage and exchange between tissues. Metabolite pools have been lumped to obtain a comprehensive model that has sufficient level of detail to describe the interactions and regulations occurring in a healthy metabolic system, but also in different Metabolic Syndrome phenotypes. A conceptual scheme of the metabolite pools and fluxes is given in Figure 3.1. MINGLeD uses a whole body approach and includes metabolically active tissues. The multi-compartmental design comprises the plasma, liver, intestinal lumen, and peripheral tissues. The main contributors to the metabolic pathways in the periphery are considered to be adipose tissue and skeletal muscle.

MINGLeD includes pathways for carbohydrate, lipid, and cholesterol metabolism, and computes pool sizes (concentrations) of various metabolites present in these systems. Table 3.1 in Appendix 3.4.1 lists which metabolites are included in MINGLeD in each of the metabolically active tissues. Acetyl-Coenzyme A (ACoA) is the central intermediate metabolite interconnecting the carbohydrate and lipid metabolic pathways. The metabolic fluxes are based on first order mass action kinetics and listed in Table 3.2 in Appendix 3.4.2. This type of equations is similar to those used in previous ADAPT studies. [Tiemann *et al.*, 2013, 2011; van Riel *et al.*, 2013; Hijmans *et al.*, 2015]

These lumped flux and reaction equations were derived using previous (biological) knowledge about the processes we are modelling. Since the underlying regulation is often

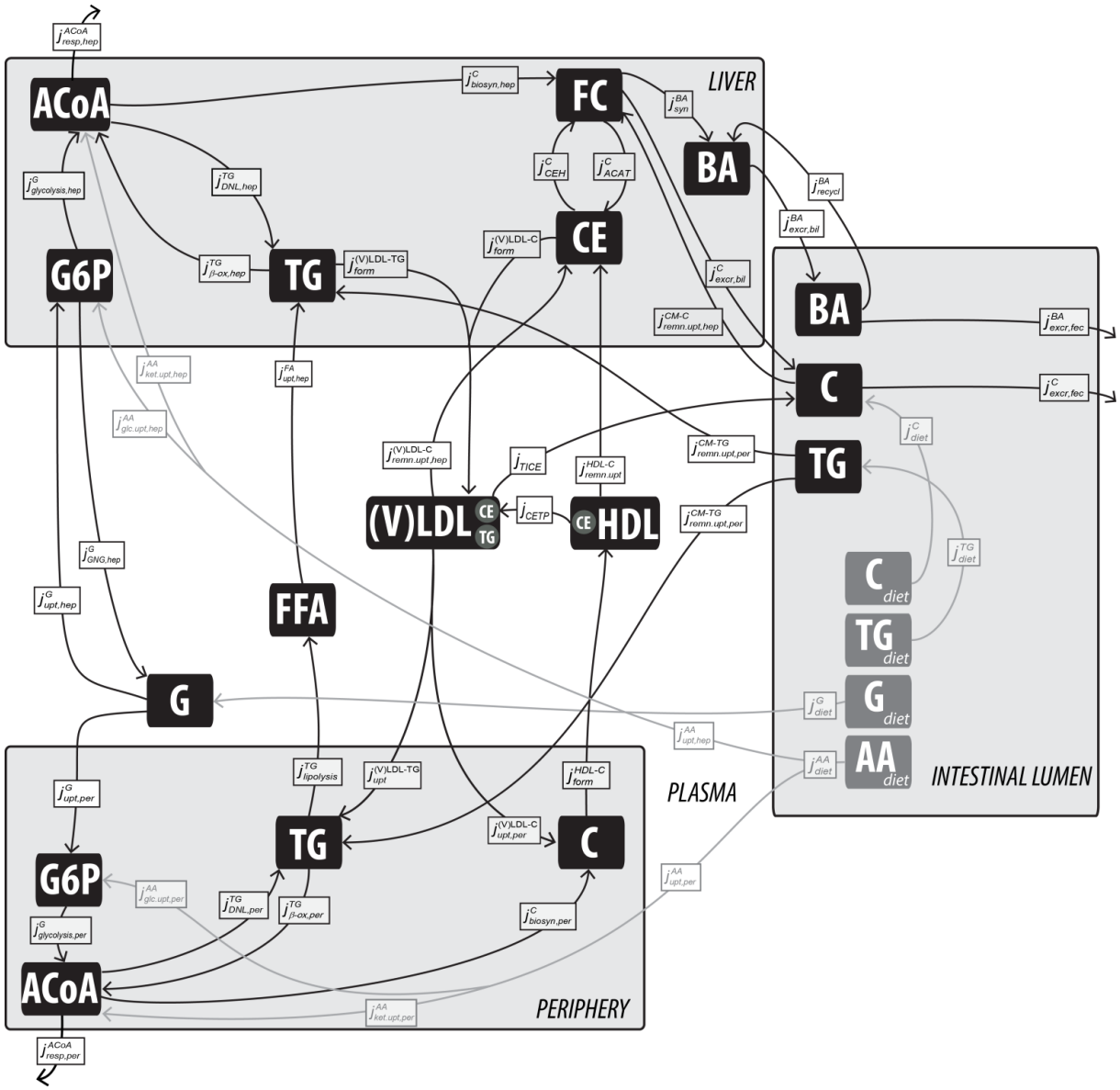

Figure 3.1

Schematic overview of the computational model MINGLeD.

This multi-compartment framework encompasses pathways in dietary absorption, hepatic, peripheral, and intestinal lipid metabolism, hepatic, and plasma lipoprotein metabolism and plasma, hepatic, and peripheral carbohydrate metabolism. The metabolite pools in the different tissue compartments are displayed in the black frames; the corresponding metabolic fluxes are represented using the arrows. The grey fluxes represent the dietary inflow in terms of the different macronutrients derived from the experimental data. See Tables 3.1 and 3.2 for a description of the metabolic states and fluxes: AA, amino acid; ACAT, Acyl-coenzyme A:cholesterol acyltransferase; ACoA, acetyl-Coenzyme A; BA, bile acid; C, cholesterol; CE, cholesteryl ester; CEH, cholesterol ester hydrolase; CETP, cholesteryl ester transfer protein; CM, chylomicron; DNL, de novo lipogenesis; (F)C, (free) cholesterol; (F)FA, (free) fatty acid; G, glucose; G6P, glucose-6-phosphate; GNG, gluconeogenesis; HDL, high density lipoprotein; TG, triglyceride; TICE, transintestinal cholesterol absorption; (V)LDL, (very) low density lipoprotein.

unknown (especially for lipid species), we refrained from composing our flux equations using stoichiometry coefficients. Therefore the underlying regulation is not explicatively modelled but is inferred by the time-dependent parameters using ADAPT.

MINGLeD aims to describe the metabolic pathways of the day's average; a metabolic snapshot. Therefore, specific (detailed) pathways for neither the postprandial phase nor the fasting state have been included. The overall metabolic fluxes are able to describe the day's

average in a consistent manner and describe both healthy metabolic states and various stages of metabolic derailment of the system as is present in the Metabolic Syndrome. Note that insulin has not been included since insulin synthesis, secretion, and action are on a much shorter timescale (minutes) than we use the model for (day's average).

3.2 Model derivation

Below we provide a detailed description of the modelled metabolites, how they are biologically regulated, the motivation to include these in the computational model, and how these interactions and pathways have been implemented in a system of Ordinary Differential Equations (ODEs) to describe mass balance during steady state.

3.2.1 Macronutrient intake

Dietary intake is specified in the form of carbohydrates (in MINGLeD referred to as glucose substrates), fat (in MINGLeD referred to as triglycerides substrates), cholesterol, and proteins. All these macronutrients are included such that the energy intake of the complete diet is taken into account.

In the model, glucose is taken up into the plasma from the dietary glucose directly. Fat and cholesterol are packed into chylomicrons (CM). These undergo triglyceride hydrolysis and are delivered to the hepatic and peripheral tissues; the chylomicron remnants that contain cholesterol are delivered to the liver. Note that chylomicrons are not explicitly included in MINGLeD since we do not aim to create a specific model describing the postprandial phase. Including the chylomicron particles would not improve the ability of the model to describe the available experimental data.

Although the metabolic pathways of amino acid metabolism have not been included in MINGLeD, we do take dietary protein intake into account since 20% of the energy of the diet is derived from protein sources. The amino acids (AA) are taken up by the liver and the periphery, and in each of these tissues, they can undergo either glucogenic or ketogenic uptake.

3.2.2 Glucose metabolism

Plasma glucose metabolism is controlled by glucose inflow from the diet, consecutive glucose uptake by liver and periphery, and gluconeogenesis (GNG) in the liver (3.1). Insulin-independent, glucose-concentration-independent glucose uptake by the brain and erythrocytes was not taken into account since these tissues were not explicitly specified, and no experimental data on these fluxes is available. Instead, the brain and erythrocytes can be considered part of the periphery since this compartment comprises all other tissues apart from the liver, intestine, and plasma.

Glucose is trapped in the form of glucose-6-phosphate (G6P) and can be retrieved in the plasma through GNG in the liver. Glycogen pools were omitted since glycogenolysis and glycogenesis would both be connected to G6P, and on a day's average basis would not be separable (only the net effect is modelled).

The amino acids (AA) of which the dietary protein is composed of are converted to G6P via the glucogenic pathway and to acetyl-Coenzyme A (ACoA) via the ketogenic pathway in both liver and periphery. We impose that both pathways contribute equally to the metabolism of the dietary protein uptake (j_{10}-j_{13}).

$$\frac{dG_{pl}}{dt} = j^{G}_{diet} + j^{G}_{GNG,hep} - j^{G}_{upt,hep} - j^{G}_{upt,per} \qquad \left(\frac{dx_1}{dt}\right) \qquad (3.1)$$

$$\frac{dG6P_{hep}}{dt} = j^{G}_{upt,hep} + j^{AA}_{glc.upt,hep} - j^{G}_{glycolysis,hep} - j^{G}_{GNG,hep} \qquad \left(\frac{dx_9}{dt}\right) \qquad (3.2)$$

$$\frac{dG6P_{per}}{dt} = j^{G}_{upt,per} + j^{AA}_{glc.upt,per} - j^{G}_{glycolysis,per} \qquad \left(\frac{dx_{14}}{dt}\right) \qquad (3.3)$$

It is worth mentioning that all these pathways have been lumped and therefore no intermediates in e.g. the glycolysis pathway have been included. This yields a compact model of which the majority of the modelled variables can be estimated from the data with accuracy. If we would include detailed pathways with many intermediates (which cannot be coupled to experimental data) an identifiable model cannot be obtained, i.e. these intermediate metabolites and fluxes do not provide accurate predictions and may present non-physiological behaviour.

3.2.3 Plasma lipid metabolism

Free fatty acids (FFA) – also called non-esterified fatty acids – are carboxylic acids with long hydrocarbon chains. These FFAs differ by length and saturation, ranging from short-chain (≤5 carbons) up to very long chain fatty acids (≥22 carbons). We do not consider these different chain lengths as different species; we have lumped the fatty acids to be one pool that inherently comprises all these different types of fatty acids.

Circulating free fatty acids originate after lipolysis of peripheral triglycerides through lipoprotein lipase (LPL) activity. Fatty acids are taken up from the plasma by the liver, where they are stored in the form of triglycerides (TG).

$$\frac{dFFA_{pl}}{dt} = 3 \cdot j^{TG}_{lipolysis} - j^{FA}_{upt,hep} \qquad \left(\frac{dx_2}{dt}\right) \qquad (3.4)$$

3.2.4 Plasma lipoprotein metabolism

Lipoproteins are particles that have a hydrophobic core with a surrounding hydrophilic layer. This makes them ideal for the transport of triglycerides and cholesterol through the circulation. They are traditionally classified based on density, size, apolipoprotein composition, and origin of synthesis. The density of a lipoprotein is determined by the amount of protein and lipid the particle contains. A higher density indicates that the lipoprotein has a higher ratio of protein to lipid content. High-density lipoproteins (HDL) are the smallest and most dense particles.

Commonly, a distinction into five classes is made: chylomicrons (CM), very low-density lipoproteins (VLDL), intermediate-density lipoproteins (IDL), low-density lipoproteins (LDL), and high-density lipoproteins (HDL). In MINGLeD we distinguish between high-density lipoproteins that carry cholesterol (HDL-C) and (very) low-density lipoproteins that carry both cholesterol ((V)LDL-C) and triglycerides ((V)LDL-TG). All endogenously derived triglyceride-rich lipoproteins (TRL) have been packed under the name of (V)LDL, but inherently comprise VLDL, IDL, and LDL.

Note that HDL-TG has not been included since it is generally known that the majority of the molecules within HDL can be contributed to cholesterol particles and the TG content is negligible. Furthermore, the ratio between TG and cholesterol in HDL is not known.

HDL-C is formed from pre-HDL which originates from the periphery and is packed with cholesterol that has been esterified through lecithin-cholesterol acyltransferase (LCAT). Plasma HDL-C is subjected to plasma lipid transfer upon the action of the cholesteryl ester transfer protein (CETP), and the remaining remnant particles are taken up by the liver via scavenger receptor class B1 (SR-B1). CETP collects triglycerides from TRL in exchange for cholesteryl esters from HDL and vice versa. However, since we did not include HDL-TG, MINGLeD only considers the cholesterol transfer from HDL-C to (V)LDL-C. Note that the rate equation for CETP (j_{27}) was chosen to be dependent on plasma TG pools since this is generally considered to be the driver behind CETP action.

HDL-C also plays an important role in the reverse cholesterol transport (RCT) pathway: the transport of cholesterol from the peripheral tissues back to the liver, after which cholesterol can be secreted via the bile into the feces. The pathways in MINGLeD allow for this reverse cholesterol transport to take place.

$$\frac{dHDL\text{-}C_{pl}}{dt} = j_{form}^{HDL\text{-}C} - j_{CETP} - j_{remn.upt}^{HDL\text{-}C} \qquad \left(\frac{dx_3}{dt}\right) \qquad (3.5)$$

(V)LDL is assembled in the liver from the hepatic triglyceride and cholesteryl ester pool and then secreted into the plasma. Circulating (V)LDL is being lipolyzed and thereby delivers triglycerides and cholesterol to peripheral tissues. The remaining remnant particles are TG depleted and are taken up by LDL receptor-mediated uptake by the liver, where they are recycled into the cholesteryl ester pool.

(V)LDL can also undergo transport to the intestinal lumen through transintestinal cholesterol excretion (TICE). The TICE rate equation (j_{26}) was chosen to be dependent on the VLDL-C pool. The plasma compartments contributing to TICE are not completely known and may be coming from both ApoB-containing lipoproteins and erythrocytes. It was therefore decided to make it dependent on VLDL-C only since erythrocytes are not included in the model.

$$\frac{d(V)LDL\text{-}C_{pl}}{dt} = j_{form}^{(V)LDL\text{-}C} + j_{CETP} - j_{remn.upt,hep}^{(V)LDL\text{-}C} - j_{upt,per}^{(V)LDL\text{-}C} - j_{TICE} \qquad \left(\frac{dx_4}{dt}\right) \qquad (3.6)$$

$$\frac{d(V)LDL\text{-}TG_{pl}}{dt} = j_{form}^{(V)LDL\text{-}TG} - j_{upt}^{(V)LDL\text{-}TG} \qquad \left(\frac{dx_5}{dt}\right) \qquad (3.7)$$

3.2.5 Hepatic lipid metabolism

The hepatic triglyceride pool is supplied by chylomicron remnant uptake, fatty acid uptake from the plasma, and *de novo* lipogenesis (DNL; synthesis of triglycerides from ACoA substrates). Details about the reaction stoichiometry can be found in Table 3.2. The triglyceride pool is drained by β-oxidation and for the assembly of (V)LDL particles.

Acetyl-Coenzyme A is a species that participates in many different metabolic processes. It plays a role in carbohydrate, lipid, and cholesterol metabolism. It originates from the breakdown of carbohydrate substrates (glycolysis) and from the breakdown of fatty acids (β-oxidation). It is used as a substrate for *de novo* lipogenesis of triglycerides and for the biosynthesis of

cholesterol (through the mevalonate pathway). It can also be oxidized via the citric acid cycle, yielding ATP.

$$\frac{dTG_{hep}}{dt} = j^{CM\text{-}TG}_{remn.upt,hep} + \frac{j^{FA}_{upt,hep}}{3} + \frac{j^{TG}_{DNL,hep}}{21.4} - j^{TG}_{\beta\text{-}ox,hep} - j^{(V)LDL\text{-}TG}_{form} \qquad \left(\frac{dx_6}{dt}\right) \quad (3.8)$$

$$\frac{dACoA_{hep}}{dt} = j^{AA}_{ket.upt,hep} + 2 \cdot j^{G}_{glycolysis,hep} + 21.4 \cdot j^{TG}_{\beta\text{-}ox,hep} - j^{TG}_{DNL,hep} - j^{C}_{biosyn,hep} - j^{ACoA}_{resp,hep} \qquad \left(\frac{dx_{10}}{dt}\right) \quad (3.9)$$

3.2.6 Hepatic cholesterol metabolism

We distinguish between free cholesterol (FC) and cholesteryl ester (CE) as pools of cholesterol present in the liver. The hepatic free cholesterol pool is supplied by chylomicron remnant uptake, cholesterol biosynthesis, and cholesteryl ester hydrolase (CEH; hydrolysis of CE to FC). The FC pool is drained by Acyl-coenzyme A:cholesterol acyltransferase (ACAT; esterification of FC to CE) and biliary cholesterol excretion. Hepatic free cholesterol is also a precursor for bile acid synthesis.

$$\frac{dFC_{hep}}{dt} = j^{CM\text{-}C}_{remn.upt} + \frac{j^{C}_{biosyn,hep}}{13.5} + j^{C}_{CEH} - j^{C}_{ACAT} - j^{BA}_{syn} - j^{C}_{excr,bil} \qquad \left(\frac{dx_7}{dt}\right) \quad (3.10)$$

The hepatic cholesteryl ester pool is supplied by (V)LDL-C and HDL-C remnant uptake and esterification of free cholesterol through ACAT. Cholesteryl esters are drained from the liver for (V)LDL-C assembly and by hydrolysis through CEH.

$$\frac{dCE_{hep}}{dt} = j^{(V)LDL\text{-}C}_{remn.upt,hep} + j^{HDL\text{-}C}_{remn.upt,hep} + j^{C}_{ACAT} - j^{(V)LDL\text{-}C}_{form} - j^{C}_{CEH} \qquad \left(\frac{dx_8}{dt}\right) \quad (3.11)$$

3.2.7 Hepatic bile acid metabolism

Bile acids are synthesized in the liver from endogenous cholesterol and can be secreted into the lumen of the intestine. Because of their amphipathic properties, they are able to emulsify dietary lipids and they thereby facilitate lipid absorption. The majority of the intestinal bile acids are recycled by the enterohepatic circulation. The bile acids can be taken up into the circulation, return to the liver, and be re-secreted.

$$\frac{dBA_{hep}}{dt} = j^{BA}_{synt,hep} + j^{BA}_{recycl} - j^{BA}_{excr,bil} \qquad \left(\frac{dx_{11}}{dt}\right) \quad (3.12)$$

3.2.8 Peripheral lipid metabolism

Many pathways in peripheral lipid metabolism resemble those of hepatic lipid metabolism. Triglycerides enter the peripheral compartment by chylomicron remnant uptake, TG uptake resulting from lipolyzed (V)LDL and *de novo* lipogenesis. When triglycerides undergo lipolysis – by the activity of lipoprotein lipase (LPL) – they are released into the plasma in the form of free fatty acids. Triglycerides are also removed from the peripheral TG pool by β-oxidation.

$$\frac{dTG_{per}}{dt} = j^{CM\text{-}TG}_{remn.upt,per} + j^{(V)LDL\text{-}TG}_{upt} + \frac{j^{TG}_{DNL,per}}{21.4} - j^{TG}_{lipolysis} - j^{TG}_{\beta\text{-}ox,per} \qquad \left(\frac{dx_{12}}{dt}\right) \quad (3.13)$$

The peripheral ACoA pool is determined by many processes that yield ACoA particles: the ketogenic uptake of dietary proteins, from carbohydrate substrates originating after glycolysis,

and from lipid substrates originating after the β-oxidation of triglycerides. ACoA is a substrate for both lipid production (DNL) and for cholesterol production (biosynthesis). It can also be oxidized to generate energy.

$$\frac{dACoA_{per}}{dt} = j^{AA}_{ket.upt,per} + 2 \cdot j^{G}_{glycolysis,per} + 21.4 \cdot j^{TG}_{\beta\text{-}ox,per} - j^{TG}_{DNL,per} - j^{C}_{biosyn,per} - j^{ACoA}_{resp,per} \qquad \left(\frac{dx_{15}}{dt}\right) \qquad (3.14)$$

3.2.9 Peripheral cholesterol metabolism

In the peripheral compartment, MINGLeD does not discriminate between free cholesterol and cholesteryl ester particles as no experimental data on the cholesterol pools in these tissues is available. Therefore we consider the peripheral cholesterol pool to be referred to as the total cholesterol content present in the periphery.

The cholesterol present in the HDL-C particles is retrieved from the peripheral cholesterol pool. The cholesterol pool is replenished by (V)LDL-C uptake and cholesterol biosynthesis from ACoA. ACoA is the common precursor that links TG and cholesterol synthesis and exists not only in the liver but in every tissue (adipose tissue also expresses HMG-CoA reductase, which is the limiting step in cholesterol biosynthesis).

$$\frac{dC_{per}}{dt} = j^{(V)LDL\text{-}C}_{upt,per} + \frac{j^{C}_{biosyn,per}}{13.5} - j^{HDL\text{-}C}_{form} \qquad \left(\frac{dx_{13}}{dt}\right) \qquad (3.15)$$

3.2.10 Intestinal metabolism

In the intestinal lumen, MINGLeD distinguishes between triglycerides, cholesterol, and bile acids. Triglycerides and cholesterol originating from the diet are packed into chylomicrons that deliver these species to the liver and peripheral tissues. Biliary excretion from the liver delivers cholesterol and bile acids to the luminal compartment. Bile acids can be re-absorbed into the liver. Additional cholesterol originating from (V)LDL enters the intestine through transintestinal cholesterol excretion (TICE). Both bile acids and cholesterol can be eliminated from the system through fecal excretion.

$$\frac{dTG_{int}}{dt} = j^{TG}_{diet} - j^{CM\text{-}TG}_{remn.upt,hep} - j^{CM\text{-}TG}_{remn.upt,per} \qquad \left(\frac{dx_{16}}{dt}\right) \qquad (3.16)$$

$$\frac{dC_{int}}{dt} = j^{C}_{diet} + j^{C}_{excr,bil} + j_{TICE} - j^{CM\text{-}C}_{remn.upt} - j^{C}_{excr,fec} \qquad \left(\frac{dx_{17}}{dt}\right) \qquad (3.17)$$

$$\frac{dBA_{int}}{dt} = j^{BA}_{excr,bil} - j^{BA}_{excr,fec} - j^{BA}_{recycl} \qquad \left(\frac{dx_{18}}{dt}\right) \qquad (3.18)$$

3.3 Implementation details

The mathematical model and optimization procedures are implemented in MATLAB (2013b, The Mathworks, Natick, Massachusetts). The ordinary differential equations are solved with compiled MEX files using numerical integrators from the SUNDIALS CVode package (2.6.0, Lawrence Livermore National Laboratory, Livermore, California). [Hindmarsh *et al.*, 2005] An absolute and relative tolerance of 10^{-6} is used. The MATLAB nonlinear least-squares solver *lsqnonlin* (from the Optimization Toolbox), which uses an inferior reflective Newton method, is used to estimate model parameters. [Coleman and Li, 1996] The termination tolerances for the objective function and the parameter estimates are set to 10^{-8}, the maximum number of iterations allowed is set to 10^3 and the maximum number of function evaluations allowed to 10^5.

3.4 Appendix

3.4.1 Metabolite pools in MINGLeD

Table 3.1

Metabolite pools as modelled states described in MINGLeD.

All metabolite pools in MINGLeD are expressed in µmol.

G_{pl}	plasma glucose	(x_1)
FFA_{pl}	plasma free fatty acids	(x_2)
HDL-C_{pl}	plasma HDL-C	(x_3)
(V)LDL-C_{pl}	plasma (V)LDL-C	(x_4)
(V)LDL-TG_{pl}	plasma (V)LDL-TG	(x_5)
TG_{hep}	hepatic triglycerides	(x_6)
FC_{hep}	hepatic free cholesterol	(x_7)
CE_{hep}	hepatic cholesterol ester	(x_8)
$G6P_{hep}$	hepatic glucose-6-phosphate	(x_9)
$ACoA_{hep}$	hepatic acetyl-Coenzyme A	(x_{10})
BA_{hep}	hepatic bile acids	(x_{11})
TG_{per}	peripheral triglycerides	(x_{12})
C_{per}	peripheral cholesterol	(x_{13})
$G6P_{per}$	peripheral glucose-6-phosphate	(x_{14})
$ACoA_{per}$	peripheral acetyl-Coenzyme A	(x_{15})
TG_{int}	intestinal triglycerides	(x_{16})
C_{int}	intestinal cholesterol	(x_{17})
BA_{int}	intestinal bile acids	(x_{18})

3.4.2 Flux pathways in MINGLeD

Table 3.2

List of included flux pathways in MINGLeD.

All fluxes in MINGLeD are expressed in µmol/day.

Dietary fluxes			
j^{G}_{diet}	$G_{diet} \rightarrow G_{pl}$	dietary glucose intake flux *	(j_1)
j^{TG}_{diet}	$TG_{diet} \rightarrow TG_{int}$	dietary triglyceride intake flux *	(j_2)
j^{C}_{diet}	$C_{diet} \rightarrow C_{int}$	dietary cholesterol intake flux *	(j_3)
j^{AA}_{diet}	$AA_{diet} \rightarrow AA_{hep} + AA_{per}$	dietary protein intake flux *	(j_4)
Macronutrient uptake fluxes			
$j^{CM\text{-}TG}_{remn.upt,hep} = k^{CM\text{-}TG}_{remn.upt,hep} \cdot TG_{int}$	$TG_{int} \rightarrow TG_{hep}$	hepatic chylomicron remnant uptake	(j_5)
$j^{CM\text{-}TG}_{remn.upt,per} = k^{CM\text{-}TG}_{remn.upt,per} \cdot TG_{int}$	$TG_{int} \rightarrow TG_{per}$	peripheral chylomicron remnant uptake	(j_6)
$j^{CM\text{-}C}_{remn.upt,hep} = k^{CM\text{-}C}_{remn.upt,hep} \cdot C_{int}$	$C_{int} \rightarrow FC_{hep}$	hepatic chylomicron remnant uptake	(j_7)
$j^{AA}_{upt,hep} = k^{AA}_{upt,hep} \cdot j^{AA}_{diet}$	$AA_{diet} \rightarrow AA_{hep}$	hepatic protein uptake	(j_8)
$j^{AA}_{upt,per} = k^{AA}_{upt,per} \cdot j^{AA}_{diet}$	$AA_{diet} \rightarrow AA_{per}$	peripheral protein uptake	(j_9)
$j^{AA}_{glc.upt,hep} = 0.5 \cdot j^{AA}_{upt,hep}$ #	$AA_{hep} \rightarrow G6P_{hep}$	hepatic glucogenic protein uptake	(j_{10})
$j^{AA}_{glc.upt,per} = 0.5 \cdot j^{AA}_{upt,per}$ #	$AA_{per} \rightarrow G6P_{per}$	peripheral glucogenic protein uptake	(j_{11})
$j^{AA}_{ket.upt,hep} = 0.5 \cdot j^{AA}_{upt,hep}$ #	$AA_{hep} \rightarrow ACoA_{hep}$	hepatic ketogenic protein uptake	(j_{12})
$j^{AA}_{ket.upt,per} = 0.5 \cdot j^{AA}_{upt,per}$ #	$AA_{per} \rightarrow ACoA_{per}$	peripheral ketogenic protein uptake	(j_{13})
$j^{G}_{upt,hep} = k^{G}_{upt,hep} \cdot G_{pl}$	$G_{pl} \rightarrow G6P_{hep}$	hepatic glucose uptake	(j_{14})
$j^{G}_{upt,per} = k^{G}_{upt,per} \cdot G_{pl}$	$G_{pl} \rightarrow G6P_{per}$	peripheral glucose uptake	(j_{15})
Carbohydrate fluxes			
$j^{G}_{glycolysis,hep} = k^{G}_{glycolysis,hep} \cdot G6P_{hep}$	$1 \cdot G6P_{hep} \rightarrow 2 \cdot ACoA_{hep}$ (a)	hepatic glycolysis	(j_{16})
$j^{G}_{GNG,hep} = k^{G}_{GNG,hep} \cdot G6P_{hep}$	$G6P_{hep} \rightarrow G_{pl}$	gluconeogenesis	(j_{17})
$j^{G}_{glycolysis,per} = k^{G}_{glycolysis,per} \cdot G6P_{per}$	$1 \cdot G6P_{per} \rightarrow 2 \cdot ACoA_{per}$ (a)	peripheral glycolysis	(j_{18})
Lipoprotein fluxes			
$j^{(V)LDL\text{-}TG}_{upt} = k^{(V)LDL\text{-}TG}_{upt} \cdot (V)LDL\text{-}TG_{pl}$	$(V)LDL\text{-}TG_{pl} \rightarrow TG_{per}$	peripheral (V)LDL-TG uptake	(j_{19})
$j^{(V)LDL\text{-}C}_{upt,per} = k^{(V)LDL\text{-}C}_{upt,per} \cdot (V)LDL\text{-}C_{pl}$	$(V)LDL\text{-}C_{pl} \rightarrow C_{per}$	peripheral (V)LDL-C uptake	(j_{20})
$j^{(V)LDL\text{-}C}_{remn.upt,per} = k^{(V)LDL\text{-}C}_{remn.upt,per} \cdot (V)LDL\text{-}C_{pl}$	$(V)LDL\text{-}C_{pl} \rightarrow CE_{hep}$	hepatic (V)LDL-C remnant uptake	(j_{21})
$j^{(V)LDL\text{-}TG}_{form} = k^{(V)LDL\text{-}TG}_{form} \cdot TG_{hep}$	$TG_{hep} \rightarrow (V)LDL\text{-}TG_{pl}$	recruitment of triglycerides for (V)LDL assembly	(j_{22})
$j^{(V)LDL\text{-}C}_{form} = k^{(V)LDL\text{-}C}_{form} \cdot CE_{hep}$	$CE_{hep} \rightarrow (V)LDL\text{-}C_{pl}$	recruitment of cholesterol particles for (V)LDL assembly	(j_{23})
$j^{HDL\text{-}C}_{form} = k^{HDL\text{-}C}_{form} \cdot CE_{per}$	$C_{per} \rightarrow HDL\text{-}C_{pl}$	HDL-C formation	(j_{24})
$j^{HDL\text{-}C}_{remn.upt} = k^{HDL\text{-}C}_{remn.upt} \cdot HDL\text{-}C_{pl}$	$HDL\text{-}C_{pl} \rightarrow CE_{hep}$	hepatic HDL-C remnant uptake	(j_{25})
$j_{TICE} = k_{TICE} \cdot (V)LDL\text{-}TG_{pl}$	$(V)LDL\text{-}C_{pl} \rightarrow C_{int}$	transintestinal cholesterol excretion	(j_{26})
$j_{CETP} = k_{CETP} \cdot (V)LDL\text{-}TG_{pl}$	$HDL\text{-}C_{pl} \rightarrow (V)LDL\text{-}C_{pl}$	cholesterol ester transfer protein flux: exchange of cholesterol derived from HDL to (V)LDL	(j_{27})

Lipid fluxes			
$j^{FA}_{upt,hep} = k^{FA}_{upt,hep} \cdot FFA_{pl}$	$3 \cdot FFA_{pl} \rightarrow 1 \cdot TG_{hep}$ [(b)]	hepatic fatty acid uptake	(j_{28})
$j^{TG}_{\beta\text{-}ox,hep} = k_{\beta\text{-}ox,hep} \cdot TG_{hep}$	$1 \cdot TG_{hep} \rightarrow 21.4 \cdot ACoA_{hep}$ [(c)]	hepatic β-oxidation	(j_{29})
$j^{C}_{biosyn,hep} = k_{biosyn,hep} \cdot ACoA_{hep}$	$13.5 \cdot ACoA_{hep} \rightarrow 1 \cdot FC_{hep}$ [(d)]	hepatic cholesterol biosynthesis	(j_{30})
$j^{TG}_{DNL,hep} = k_{DNL,hep} \cdot ACoA_{hep}$	$21.4 \cdot ACoA_{hep} \rightarrow 1 \cdot TG_{hep}$ [(c)]	hepatic *de novo* lipogenesis	(j_{31})
$j^{TG}_{lipolysis} = k_{LPL} \cdot TG_{per}$	$1 \cdot TG_{per} \rightarrow 3 \cdot FFA_{pl}$ [(b)]	peripheral lipolysis	(j_{32})
$j^{TG}_{\beta\text{-}ox,per} = k_{\beta\text{-}ox,per} \cdot TG_{per}$	$1 \cdot TG_{per} \rightarrow 21.4 \cdot ACoA_{per}$ [(c)]	peripheral β-oxidation	(j_{33})
$j^{C}_{biosyn,per} = k_{biosyn,per} \cdot ACoA_{per}$	$13.5 \cdot ACoA_{per} \rightarrow 1 \cdot C_{per}$ [(d)]	peripheral cholesterol biosynthesis	(j_{34})
$j^{TG}_{DNL,per} = k_{DNL,per} \cdot ACoA_{per}$	$21.4 \cdot ACoA_{per} \rightarrow 1 \cdot TG_{per}$ [(c)]	peripheral *de novo* lipogenesis	(j_{35})
Cholesterol fluxes			
$j^{C}_{ACAT} = k_{ACAT} \cdot FC_{hep}$	$FC_{hep} \rightarrow CE_{hep}$	hepatic cholesterol storage	(j_{36})
$j^{C}_{CEH} = k_{CEH} \cdot CE_{hep}$	$CE_{hep} \rightarrow FC_{hep}$	hepatic cholesterol release	(j_{37})
$j^{BA}_{syn} = k^{BA}_{syn} \cdot FC_{hep}$	$FC_{hep} \rightarrow BA_{hep}$	bile acid synthesis	(j_{38})
$j^{BA}_{excr,bil} = k^{BA}_{excr,bil} \cdot BA_{hep}$	$BA_{hep} \rightarrow BA_{int}$	biliary bile acid excretion	(j_{39})
$j^{BA}_{recycl} = k^{BA}_{recycl} \cdot BA_{int}$	$BA_{int} \rightarrow BA_{hep}$	bile acid recycling	(j_{40})
$j^{C}_{excr,bil} = k^{C}_{excr,bil} \cdot FC_{hep}$	$FC_{hep} \rightarrow C_{int}$	biliary cholesterol excretion	(j_{41})
Removal fluxes			
$j^{C}_{excr,fec} = k^{C}_{excr,fec} \cdot C_{int}$	$C_{int} \rightarrow \emptyset$	fecal cholesterol excretion	(j_{42})
$j^{BA}_{excr,fec} = k^{BA}_{excr,fec} \cdot BA_{int}$	$BA_{int} \rightarrow \emptyset$	fecal bile acid excretion	(j_{43})
$j^{ACoA}_{resp,hep} = k_{resp,hep} \cdot ACoA_{hep}$	$ACoA_{hep} \rightarrow \emptyset$	hepatic ACoA respiration	(j_{44})
$j^{ACoA}_{resp,per} = k_{resp,per} \cdot ACoA_{per}$	$ACoA_{per} \rightarrow \emptyset$	peripheral ACoA respiration	(j_{45})

* The dietary fluxes are considered as inputs from the experimental dataset.

The factor 0.5 originates from our assumption that both the glucogenic and ketogenic pathway contribute equally to the metabolism of the dietary protein uptake.

The flux equations are derived using stoichiometry rules:

(a) The breakdown of one molecule of glucose results in two molecules of ACoA: $2 \cdot G6P \leftrightarrow 1 \cdot ACoA$

(b) Triglycerides are esters derived from glycerol and three fatty acids per particle: $3 \cdot FFA \leftrightarrow 1 \cdot TG$

(c) The composition of triglycerides depends on the length and saturation of the fatty acid chains of which it is composed. The conversion of TG to ACoA is therefore derived based on energy content. We adjust the number of ACoA molecules derived from TG assuming that the energy density of body fat equals the energy density of the consumed food. This results in: $1 \cdot TG \leftrightarrow 21.4 \cdot ACoA$

(d) ACoA ($CH_3COSCoa$) is a two-carbon compound; cholesterol ($C_{27}H_{46}O$) has 27 carbon units: $1 \cdot (F)C \leftrightarrow 13.5 \cdot ACoA$

4

In vivo and *in silico* dynamics of the development of Metabolic Syndrome

This chapter is published as:

Rozendaal YJW, Wang Y, Paalvast Y, Tambyrajah LL, Li Z, Willems van Dijk K, Rensen PCN, Kuivenhoven JA, Groen AK, Hilbers PAJ, van Riel NAW. *In vivo* and *in silico* dynamics of the development of Metabolic Syndrome. *PLoS Comput. Biol.*, 2018, 14(6):e1006145 doi.org/10.1371/journal.pcbi.1006145

The Metabolic Syndrome (MetS) is a complex, multi-factorial disorder that develops slowly over time presenting itself with large differences among MetS patients. We applied a systems biology approach to describe and predict the onset and progressive development of MetS, in a study that combined *in vivo* and *in silico* models. The new data-driven, physiological model (MINGLeD: Model INtegrating Glucose and Lipid Dynamics) was developed, describing glucose, lipid, and cholesterol metabolism. Since classic kinetic models cannot describe slowly progressing disorders, the simulation method ADAPT was used to describe longitudinal dynamics and to predict metabolic concentrations and fluxes. This approach yielded a novel model that can describe long-term MetS development and progression. This model was integrated with longitudinal *in vivo* data that was obtained from male APOE*3-Leiden.CETP mice fed a high-fat, high-cholesterol diet for three months and that developed MetS as reflected by classical symptoms including obesity and glucose intolerance. Two distinct subgroups were identified: those who developed dyslipidemia, and those who did not. The combination of MINGLeD with ADAPT could correctly predict both phenotypes, without making any prior assumptions about changes in kinetic rates or metabolic regulation. Modelling and flux trajectory analysis revealed that differences in liver fluxes and dietary cholesterol absorption could explain this occurrence of the two different phenotypes. In individual mice with dyslipidemia, dietary cholesterol absorption and hepatic turnover of metabolites, including lipid fluxes, were higher compared to those without dyslipidemia. Predicted differences were also observed in gene expression data, and consistent with the emergence of insulin resistance and hepatic steatosis, two well-known MetS comorbidities. Whereas MINGLeD specifically models the metabolic derangements underlying MetS, the simulation method ADAPT is generic and can be applied to other diseases where dynamic modelling and longitudinal data are available.

4.1 Introduction

The simultaneous presentation of obesity, dyslipidemia, insulin resistance, and hypertension is generally referred to as the Metabolic Syndrome (MetS). [Grundy *et al.*, 2004; International Diabetes Federation, 2006; Kassi *et al.*, 2011; World Health Organization, 2014; Parikh and Mohan, 2012] Together, these factors impose an increased risk of the development of comorbidities including cardiovascular diseases, type 2 diabetes, and non-alcoholic fatty liver disease. [Beltrán-Sánchez *et al.*, 2013; Vanita and Jhansi, 2011] MetS is considered to be the result of an imbalance in the mechanisms controlling dietary intake, energy expenditure, glucose handling, and lipid homeostasis. [Rask-Madsen and Kahn, 2012; Han and Lean, 2016; Kaur, 2014] The high prevalence of obesity and MetS [Finkelstein *et al.*, 2012; NCD Risk Factor Collaboration, 2017; van Vliet-Ostaptchouk *et al.*, 2014; Moore, 2017; Moreira *et al.*, 2014], in combination with the heterogeneous presentation of MetS patients [Agyemang *et al.*, 2012; Lee *et al.*, 2008], asks for the design of adequate treatment and prevention strategies. Clinical research on MetS is mostly cross-sectional in nature and tends to focus on either lipid or glucose metabolism, while both makeup MetS. Knowledge on the interplay between these different metabolic components during the relatively slow progression into disease is therefore limited, but which a systems biology approach could provide.

Modelling efforts in the past have shown that systems biology can be a powerful approach to gain both qualitative and quantitative insight into the inherently complex systems that drive the development of MetS. For example, Lu *et al*. [Lu *et al.*, 2014] demonstrated how HDL raising modulators fail to reduce cardiovascular diseases by elucidating the effects on the reverse cholesterol transport pathway. Likewise, Topp *et al.* [Topp *et al.*, 2000] have identified different response pathways and physiological outcomes during prolonged hyperglycemia.

However, these computational models were designed to model the healthy [Cobelli *et al.*, 2014; Dalla Man *et al.*, 2006; Jelic *et al.*, 2009; Kim *et al.*, 2007; König *et al.*, 2012; Lu *et al.*, 2014; Nyman *et al.*, 2011; Roy and Parker, 2006; Sips *et al.*, 2015; Xu *et al.*, 2011; Chalhoub *et al.*, 2007b] or diseased state exclusively. [Toghaw *et al.*, 2012; Topp *et al.*, 2000] Furthermore, these models only describe short-term dynamics (e.g. the postprandial response period) and do not take into account long-term dynamics that may be expected to occur in progressive diseases such as MetS. Moreover, models that do explicitly study the gradual phenotype transition into a diseased state, have only considered either the lipid component [Mc Auley *et al.*, 2012] or the glucose component [Bagust and Beale, 2003; de Winter *et al.*, 2006; Ha *et al.*, 2016; Sarkar *et al.*, 2018] of MetS.

The long-term simulation method "Analysis of Dynamic Adaptations in Parameter Trajectories" (ADAPT; chapter 2) [Tiemann *et al.*, 2011, 2013; van Riel *et al.*, 2013] provides a method to describe long-term dynamics. It infers time-varying parameters that gradually change over time, reflecting the slow change in the regulation of metabolic processes during disease development. Therefore, ADAPT is a very powerful approach to study the longitudinal development of diseases and therapeutic interventions and uses experimental data to infer adaptations in the system. [Hijmans *et al.*, 2015; Nyman *et al.*, 2016; Tiemann *et al.*, 2011, 2013] In previous studies, ADAPT has been applied to study hepatic steatosis [Hijmans *et al.*, 2015; Tiemann *et al.*, 2013], and treatment of T2DM [Nyman *et al.*, 2016] (chapter 2), but has not yet been applied to study the full metabolic complexity of MetS.

Therefore, we aimed to design a computational, data-driven approach to study the longitudinal and progressive dynamics of the majority of metabolic alterations of MetS, i.e. obesity, glucose intolerance, insulin resistance, and dyslipidemia. We employed a systems biology methodology that integrates three main concepts to infer metabolic adaptations during MetS development: 1) the long-term simulation method ADAPT, combined with 2) the newly developed *in silico* MetS model (from chapter 3) that describes the metabolic processes involved in whole-body carbohydrate and lipid metabolism, and integrated with 3) time-series data obtained from an *in vivo* MetS model. The APOE*3-Leiden(E3L).CETP mouse [Westerterp *et al.*, 2006; Leiden Metabolic Research Services, 2016] is a preclinical animal model for human MetS that develops diet-induced dyslipidemia and is prone to develop obesity and insulin resistance. It has been used in cross-sectional studies addressing different metabolic facets of MetS. [Auvinen *et al.*, 2013; de Haan *et al.*, 2008; Kleemann *et al.*, 2003; Kooistra *et al.*, 2006; Li *et al.*, 2012; van den Hoek *et al.*, 2014; van der Hoorn *et al.*, 2009; Wang *et al.*, 2014a; Zadelaar *et al.*, 2007; Westerterp *et al.*, 2006] We made use of this *in vivo* model to study the development of diet-induced MetS in a longitudinal setting [van den Hoek *et al.*, 2014; van Dam *et al.*, 2015] by collecting measurements in the same animals within a three-month period and at multiple intermediate time points.

Our *in silico* modelling quantitatively analyses and integrates the experimental data and provides estimates of metabolite concentrations and fluxes that were experimentally not measured. With this modelling approach, we demonstrate when and how the onset and development of MetS occurs. Although we expected to find a homogeneous population, our modelling approach shows the emergence of different phenotypes of MetS. This heterogeneity is associated with differences in intestinal and hepatic metabolic fluxes.

4.2 E3L.CETP mice on a high-fat diet with cholesterol develop obesity, glucose intolerance, and dyslipidemia

We combined data-driven and physiology-based modelling. Hereto we integrated prior knowledge on the complex metabolic systems that underlie the pathophysiology of MetS with experimental observations on the actual metabolic status over time: *in vivo* data on the onset and progressive development of MetS have been collected from eleven-week-old male E3L.CETP mice that were fed diets differing in fat and cholesterol content and were followed for three months. These diets comprised a low-fat diet (LFD; 20% of energy from fat; n=8), high-fat diet (HFD; 60% of energy from fat; n=12), and a high-fat diet with additional dietary cholesterol (HFD+C; 0.25% cholesterol; n=8). For each diet group, longitudinal data was obtained throughout the time course of the study: body weight was monitored weekly, plasma markers were measured monthly, and liver lipids were assessed after three months. Appendix 4.10 provides a detailed overview of the experimental set-up and measurement details.

Figure 4.1 presents the results of feeding LFD, HFD, and HFD+C as average (left) and individually (right) for HFD+C feeding; the latter is discussed in the next section. As compared with LFD feeding, increased fat intake (HFD) resulted in increased weight gain (Figure 4.1A) reflected by a marked increase in fat mass (Figure 4.1B) with no changes in lean mass (Figure 4.1C). HFD feeding also significantly increased fasting plasma glucose (Figure 4.1D) and insulin (Figure 4.1E) levels. Although HFD did not affect the plasma total cholesterol level (TC; Figure 4.1G), a shift in the lipoprotein ratio was observed, reflected by increased plasma HDL-cholesterol (HDL-C) levels (Figure 4.1H) upon feeding a high-fat diet.

As compared to the HFD alone, obesity development was slightly increased by cholesterol feeding (Figures 4.1A-B), as monitored by increased fat mass at three months after starting the diet, even though the daily food intake did not increase (data not shown). Although the additional dietary cholesterol did not affect plasma glucose and insulin levels (Figures 4.1D-E), it did impair glucose tolerance in the oral glucose tolerance test (Figure 4.6 in Appendix 4.10.9), indicating that dietary cholesterol increased insulin resistance.

As compared to HFD, plasma triglyceride (TG) levels were significantly increased after three months of feeding HFD with cholesterol (Figure 4.1F). Cholesterol feeding did not seem to have an effect on circulating TC levels until the second month of the dietary induction (Figure 4.1G). Plasma HDL-C level (Figure 4.1H), on the other hand, was increased after starting the diet (HFD and HFD+C) over the first two months.

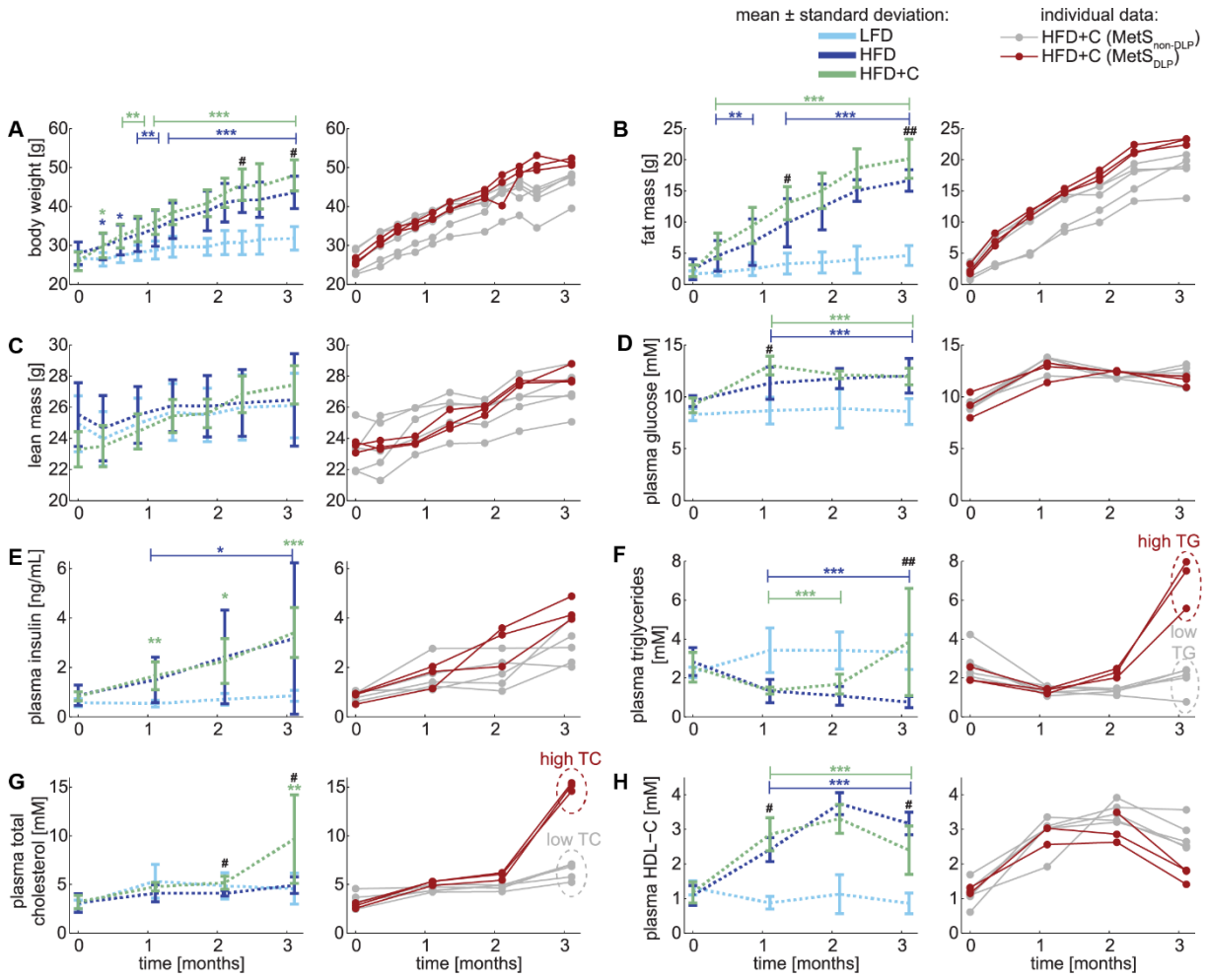

Figure 4.1

In vivo development of the Metabolic Syndrome results in different phenotypes.

Experimentally observed metabolic parameters upon dietary induction in male E3L.CETP mice over the time course of three months is displayed in two ways: in the left panels the data are expressed as mean ± standard deviation (error bars) for the low-fat diet (LFD; n=8; light blue), high-fat diet (HFD; n=12 (pooled from two groups n=7 for the full time period, n=5 until two months of dietary induction; dark blue) and high-fat diet with 0.25% cholesterol (HFD+C; n=8; green) groups, whereas in the right panels the data of the animals on HFD+C are depicted for each animal individually. Individuals in this cohort were subdivided into two groups based on the plasma triglyceride (TG; panel F) and plasma total cholesterol (TC; panel G) levels. The dyslipidemic Metabolic Syndrome phenotypes are depicted in red ($MetS_{DLP}$; mice with high plasma TG and simultaneous high plasma TC at three months) and the non-dyslipidemic Metabolic Syndrome phenotypes in grey ($MetS_{non\text{-}DLP}$; mice with low plasma TG and simultaneous low plasma TC at three months).

Differences between groups were determined using a one-way ANOVA test. When significant differences were found, Fisher's LSD test was used as a post hoc test to determine the differences between two independent groups:

* P<0.05; ** P<0.01; *** P<0.001 HFD as compared to LFD

# P<0.05; ## P<0.01; ### P<0.001 HFD+C as compared to HFD

4.3 E3L.CETP mice respond bimodally to cholesterol feeding suggesting the presence of two distinct Metabolic Syndrome phenotypes

Male E3L.CETP mice developed HFD-induced obesity, glucose intolerance, and dyslipidemia, mimicking the classical symptoms seen in human MetS. However, the high variability in both triglyceride and cholesterol levels complicated the interpretation of the dyslipidemic component. Therefore, we also presented the data of mice fed with the HFD+C individually in

the right-hand side panels of Figure 4.1. When inspecting the levels of plasma TG (Figure 4.1F) and plasma TC (Figure 4.1G) at the three months' time point, the data reveal clear differences among the individual mice: while some develop dyslipidemia upon feeding HFD+C (shown in red), others do not (shown in grey), suggesting a bimodal distribution. With this insight, we divided the HFD+C cohort into two subgroups: the mode with high plasma TG and high plasma TC levels after three months of HFD+C is referred to as the dyslipidemic Metabolic Syndrome phenotypes ($MetS_{DLP}$; n=3) and the other mode as the non-dyslipidemic Metabolic Syndrome phenotypes ($MetS_{non\text{-}DLP}$; n=5). This subdivision shows a consistent pattern in both TG and TC at the three months' time point but is already present earlier in time. In fact, the onset of dyslipidemia is already noticeable after two months of the diet and progresses further towards the three months' time period. Note that the subdivision in phenotype development is a result of the HFD+C diet; no baseline differences are observed (t=0 months in this dataset), and these observations are limited to the HFD+C group and not present in HFD.

This separation into two phenotypes is clearly present in the lipid trait, but it is also reflected in markers of carbohydrate metabolism. Although the individual mice cannot be separated based on the fasting plasma glucose (Figure 4.1D) data, the fasting plasma insulin (Figure 4.1E) indicates that the $MetS_{DLP}$ individuals are significantly more insulin resistant than the $MetS_{non\text{-}DLP}$ individuals at the three months' time point. This trend is even more profound in the insulin dynamics in response to a glucose challenge test (Figure 4.6 in Appendix 4.10.9): $MetS_{DLP}$ individuals show a markedly higher insulin peak that also lasts longer than the $MetS_{non\text{-}DLP}$ individuals. This indicates that dyslipidemia and glucose intolerance develop in parallel, but it is unclear how these are causally related.

4.4 MINGLeD describes metabolic snapshots accurately

MINGLeD was integrated with the *in vivo* data whilst considering four subgroups: the LFD group, HFD group, $MetS_{non\text{-}DLP}$ phenotypes, and $MetS_{DLP}$ phenotypes. For each subgroup, MINGLeD was fitted to the data of each of the four snapshots in time separately. The resulting sixteen models differ in the values for their estimated parameters. For each model, the parameter estimation procedure was repeated with 500 different initial parameter sets using multi-start optimization. Figure 4.2 displays that MINGLeD accurately fits the metabolic snapshots over time for each of these groups. This shows that MINGLeD is capable of describing different metabolic phenotypes upon varying dietary intake and at different metabolic stages in time.

4.5 MINGLeD with ADAPT describes dyslipidemic and non-dyslipidemic Metabolic Syndrome progression

Calibration of MINGLeD yielded separate models for each subgroup (LFD, HFD, $MetS_{non\text{-}DLP}$, and $MetS_{DLP}$). However, this ignores the fact that the phenotypes represented by each of those four models are causally connected in time. MINGLeD describes metabolic fluxes and concentrations but does not explicitly include the multiple pathways that regulate and

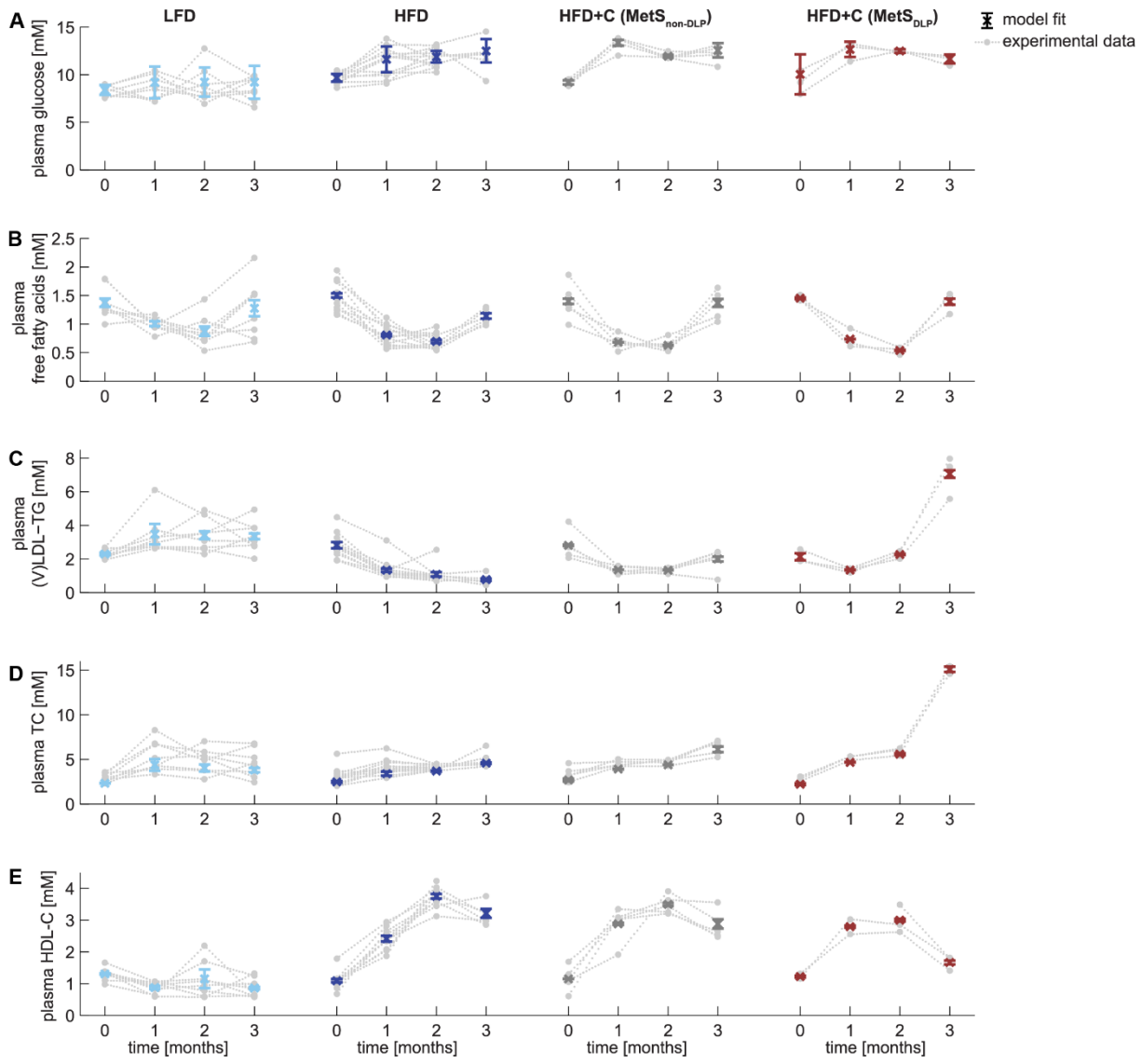

Figure 4.2

MINGLeD describes metabolic phenotypes of male E3L.CETP mice on different diets and time points.

The metabolic phenotypes are depicted for three different diets (with HFD+C composed of two subgroups that emerged after two months of dietary induction) at four different time points. Model fits (coloured error bars: mean ± standard deviation) of MINGLeD calibrated to the phenotype snapshots (raw, individual mouse data shown in grey) separately. Only acceptable model simulations were included, which was classified as having a weighted sum of squared errors (see equation (4.1) in Appendix 4.11) below 100.

modulate metabolism over a three months' time period (such as changes in gene expression and protein activity). Both limitations were overcome by combining MINGLeD with a dedicated approach for longitudinal modelling of biological systems: "Analysis of Dynamic Adaptations of Parameter Trajectories" (ADAPT). [Tiemann *et al.*, 2011, 2013; van Riel *et al.*, 2013] ADAPT uses the experimental data to infer adaptations in the system, which is implemented by introducing time-varying model parameters. Model parameters are iteratively re-estimated over the time course of the simulation, yielding parameter trajectories that govern the time-dependent evolution of the modelled state variables and fluxes. Combining MINGLeD with ADAPT and the experimental data resulted in a dynamic, continuous model of MetS development and progression. ADAPT uses ensemble-based simulation to account for both methodological and

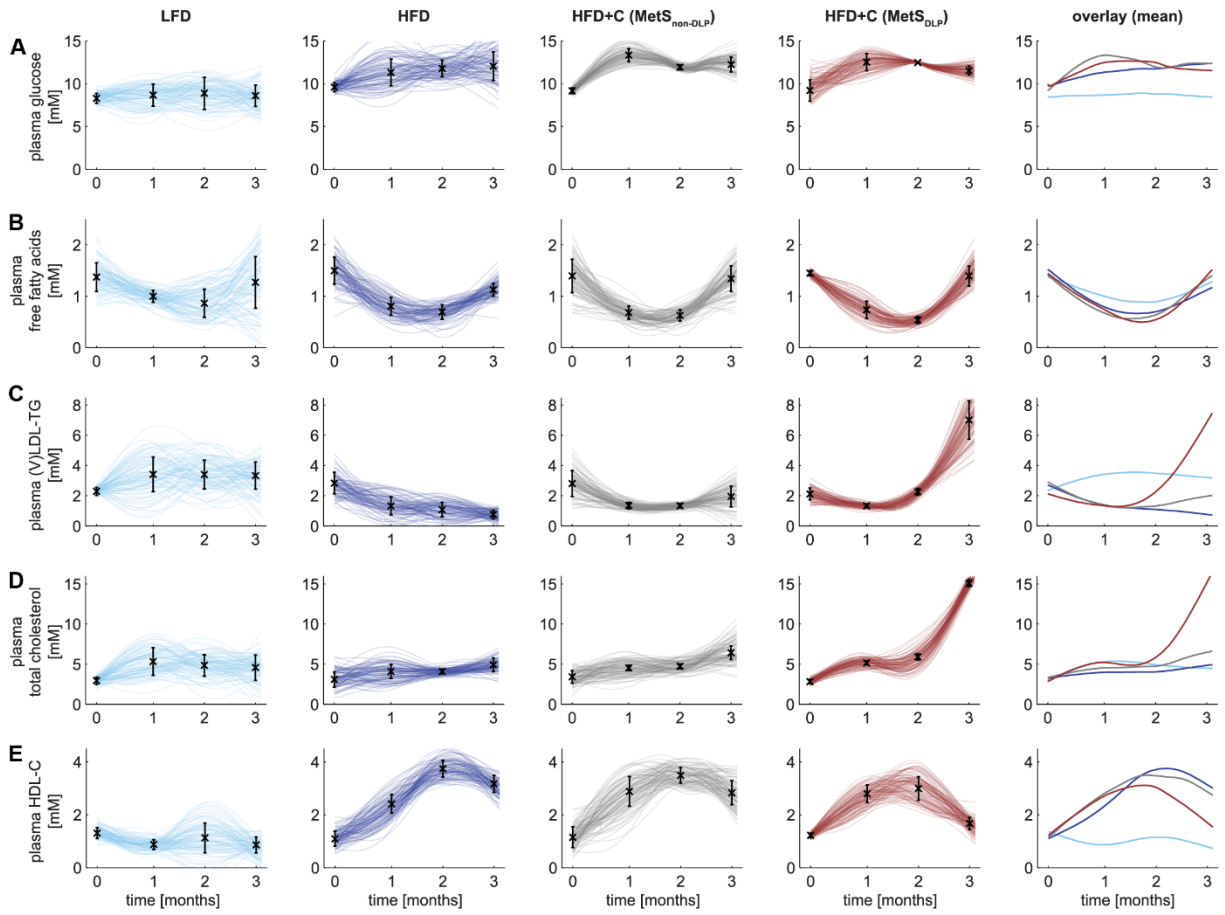

Figure 4.3

Onset and development of the Metabolic Syndrome reveal two distinct phenotypes of dyslipidemic status.

The classical hallmarks of MetS are depicted by simulations of the individual trajectories (the top 10% best were selected from n=1,000) for the low-fat diet (LFD) are shown in light blue; high-fat diet (HFD) in dark blue, the non-dyslipidemic Metabolic Syndrome phenotypes ($MetS_{non\text{-}DLP}$) in grey and the dyslipidemic Metabolic Syndrome phenotypes ($MetS_{DLP}$) in red. The colour intensity reflects the density of the trajectories: the darker, the more probable the simulated solution. Experimental *in vivo* data are shown as black error bars that represent the mean ± standard deviation. The 5th column shows an overlay of the mean of the trajectories for each of the subgroups showing the development of increased triglycerides and cholesterol levels in the plasma in the dyslipidemic MetS phenotypes between two and three months.

and experimental uncertainty resulting from biological variability and relatively low power in the HFD+C subgroups. By repeated Monte Carlo sampling of the *in vivo* data, sampled datasets are generated and for each sampled dataset a parameter trajectory was estimated. This was repeated resulting in a set of 1,000 simulated models yielding a database comprising of *in silico* populations of 1,000 virtual individuals for each subgroup. Each simulation describes the experimental data adequately, though with variation in parameter trajectories yielding differences in fluxes and concentrations, especially for model variables that are not experimentally observed.

Figure 4.3 shows that the simulated trajectories for the plasma metabolites fit the *in vivo* data points accurately and provide a continuous description of the dynamics with which the system behaves over time, illustrating the different trajectories for the different subgroups. Note that ADAPT did not yield one single simulation but provided ensembles of state and flux trajectories. Each line in Figure 4.3 is one trajectory solution, where a darker colour represents more overlap (higher density) of trajectory solutions in that region. These density plots cover

the solution space for each of the modelled components. To aid visual analysis, the mean of the trajectory distributions for each of the subgroups is depicted in the panels to the far-right. These trajectories illustrate the clear distinction that can be made between the dyslipidemic (in red) and non-dyslipidemic (in grey) MetS phenotypes.

4.6 Flux trajectory analysis identifies distinct differences in dietary cholesterol absorption and hepatic metabolism during dyslipidemia

We showed that the *in silico* model accurately captures the trends as observed in the *in vivo* data. The ensembles of simulated concentration and flux trajectories provide insight into how the underlying metabolic network is affected by the emergence of the two different MetS phenotypes. Figure 4.4 displays the median with 10% range of the collection of trajectories for several metabolic fluxes. Clear differences between the dyslipidemic and non-dyslipidemic MetS phenotypes can be observed. A complete overview of all model state trajectories and metabolic flux trajectories is documented in Appendix 4.12.

Despite equal intake of food and thus cholesterol, dietary cholesterol absorption from the intestinal lumen was markedly higher in the dyslipidemic compared to the non-dyslipidemic MetS group (Figure 4.4A), which may have promoted the development of dyslipidemia. The modelling also predicted that within the dyslipidemic phenotype, rates of lipid shuttling towards (V)LDL-TG uptake (Figure 4.4B; see also Figures 4.8K-L in Appendix 4.12) were increased, as higher rates of hepatic fatty acid uptake (Figure 4.4C) and lipogenesis (Figure 4.4E) were observed accompanied by a lower rate of hepatic β-oxidation (Figure 4.4F).

We observed similar changes if we analyse the gene expression data (Table 4.3 in Appendix 4.10.10) from the same animals: we could qualitatively relate our flux predictions with the gene expression profiles of the fully developed MetS phenotype after three months of dietary induction. We found, as compared to LFD, an upregulation of hepatic fatty acid uptake in the HFD, HFD+C ($MetS_{non\text{-}DLP}$) and HFD+C ($MetS_{DLP}$) groups (Figure 4.4C).

Figure 4.4D shows that hepatic bile acid synthesis is predicted to be higher in the $MetS_{DLP}$ phenotype. This aspect could also be observed in the gene expression data: the expression of bile acid synthesis genes nuclear farnesoid X receptor (*Fxr*) and cholesterol 7 alpha-hydroxylase (*Cyp7a1*) was largely upregulated, as compared to HFD alone. Hepatic *de novo* lipogenesis (Figure 4.4E; DNL) is predicted to be higher in the dyslipidemic phenotype, for which data at the three months' time point was available and was used in the model fitting. Genes related to DNL, including fatty acid synthase (*Fasn*), acetyl-CoA carboxylase 2 (*Acc2*), acyl-CoA:diacylglycerol acyltransferase 2 (*Dgat2*), and sterol regulatory element binding protein 1c (*Srebp1c*) were all largely downregulated probably as a compensatory mechanism.

In addition, the hepatic β-oxidation (Figure 4.4F) is predicted to be lower in the dyslipidemic group. This could be linked to a compensatory upregulation of genes related to fatty acid β-oxidation such as peroxisome proliferator-activated receptor α (*Pparα*), peroxisomal acyl-coenzyme A oxidase 1 (*Acox1*), and carnitine palmitoyltransferase 1a (*Cpt1a*). Collectively, these predictions suggest more lipid accumulation in the liver of the dyslipidemic mice.

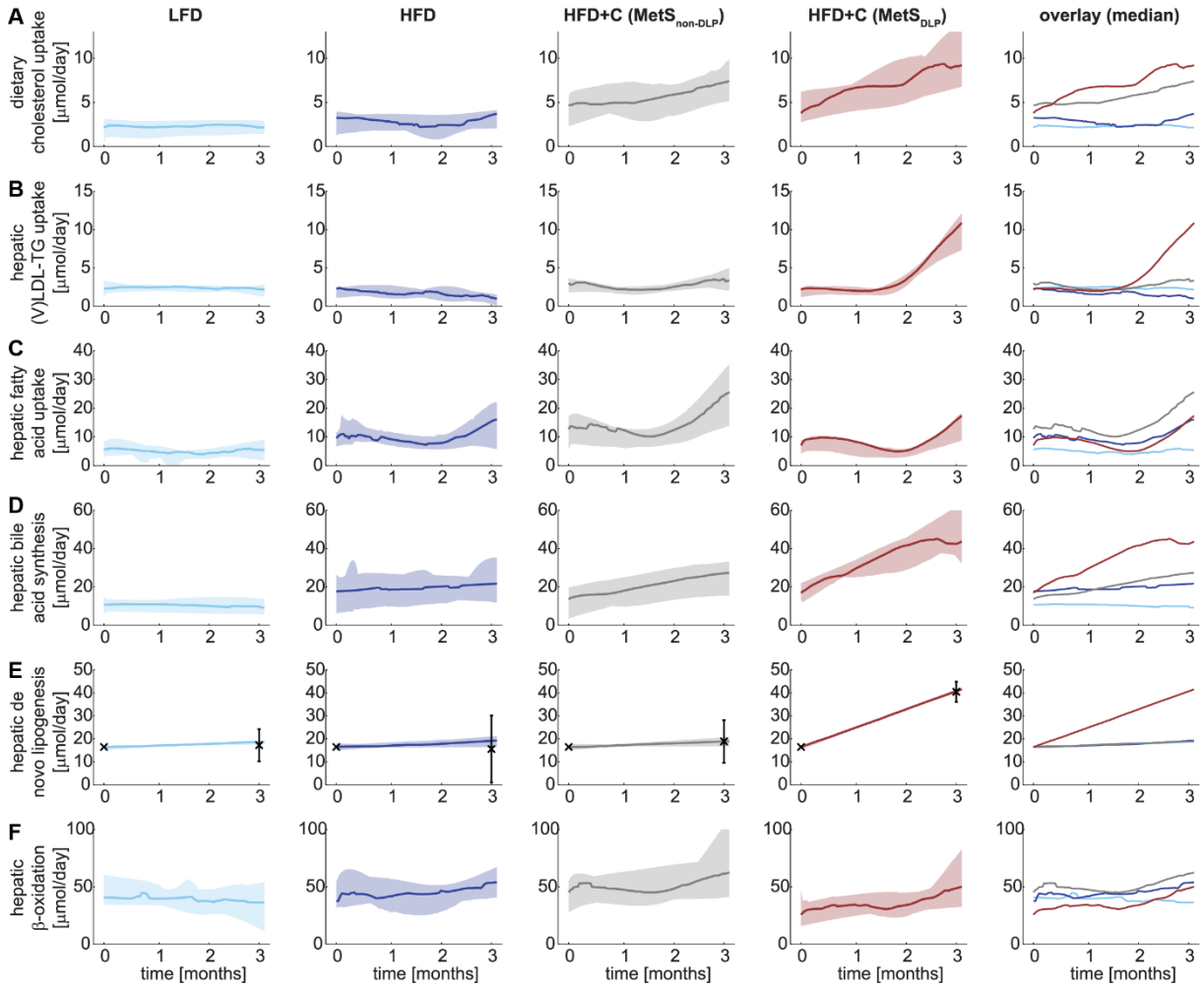

Figure 4.4

Metabolic flux trajectory analysis depicts differences among phenotypes and dyslipidemia development.

Trajectory analysis reveals decreased dietary cholesterol absorption from the intestinal lumen in the non-dyslipidemic Metabolic Syndrome phenotype (A) and increased hepatic activity in the dyslipidemia Metabolic Syndrome phenotype (B-F). The median metabolic flux trajectories (calculated from the top 10% best trajectories from n=1,000) are depicted with a solid line for the hepatic dietary cholesterol absorption from the intestinal lumen (A), hepatic (V)LDL-TG uptake from the plasma (B), hepatic fatty acid uptake from the plasma (C), hepatic bile acid synthesis from cholesterol (D), hepatic *de novo* lipogenesis (E), and hepatic β-oxidation (F). The shaded area depicts the 10% range of trajectories around the median. The low-fat diet cohort is depicted in light blue; the high-fat cohort in dark blue; the non-dyslipidemic Metabolic Syndrome phenotype in grey and the dyslipidemic Metabolic Syndrome phenotype in red. The experimental hepatic *de novo* lipogenesis (E) data are shown as black error bars that represent the mean ± standard deviation.

4.7 Both Metabolic Syndrome phenotypes develop hepatic steatosis

MINGLeD with ADAPT predicted the trajectories of the liver lipid profiles and calculated the hepatic lipid pool sizes over the entire time course of three months. Next, we measured lipid turnover and the lipid content in livers from individual mice after three months of dietary induction to verify these *in silico* predictions at the last time point. Indeed, the addition of cholesterol did lead to an increase in lipid turnover and the hepatic lipid pool sizes as compared to the high-fat diet without cholesterol, both in the dyslipidemic and non- dyslipidemic phenotype (Figure 4.5). Moreover, this accumulation of lipids in the liver – in particular that of cholesterol components – was more profound in $MetS_{DLP}$ mice.

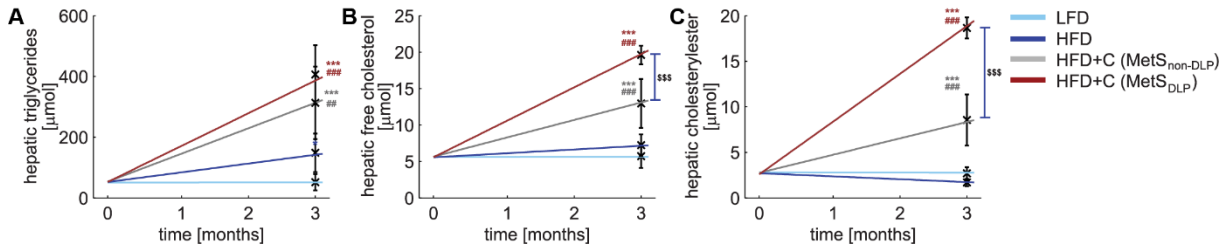

Figure 4.5

Metabolic Syndrome development is associated with hepatic steatosis in both dyslipidemic and non-dyslipidemic phenotypes.

The mean trajectories of the liver lipid profiles (calculated from the top 10% best trajectories from n=1,000) are depicted for the hepatic triglyceride pool (A), hepatic free cholesterol pool (B) and the hepatic cholesteryl ester pool (C). Experimental data was obtained at the end of the study and is depicted by the black error bars representing the mean ± standard deviation for each of the groups. The data from the LFD cohort is used as the initial value, assuming no hepatic lipid accumulation to have occurred in this control group.

Differences between groups were determined using a one-way ANOVA test. When significant differences were found, Fisher's LSD test was used as a post hoc test to determine the differences between two independent groups:

* P<0.05; ** P<0.01; *** P<0.001 as compared to LFD

# P<0.05; ## P<0.01; ### P<0.001 as compared to HFD

$ P<0.05; $$ P<0.01; $$$ P<0.001 as compared to HFD+C ($MetS_{non-DLP}$)

Flux trajectory analysis revealed substantial differences in hepatic fluxes between the non-dyslipidemic and the dyslipidemic MetS phenotypes. In terms of plasma metabolite levels (see Figures 4.3A-E), $MetS_{non-DLP}$ mice closely resemble the mouse population fed the HFD without cholesterol, and intriguingly, appears not to be affected by the additional dietary cholesterol load. MINGLeD with ADAPT predicted that this may be due to reduced dietary cholesterol absorption (Figure 4.4A) in the non-dyslipidemic phenotype.

Furthermore, the predicted lipid pool sizes were in agreement with liver histology data (Figure 4.7 in Appendix 4.10.8), which showed the establishment of microvesicular steatosis upon HFD feeding. In contrast, steatosis was exacerbated in $MetS_{DLP}$ mice, as was revealed by a more severe type of macrovesicular steatosis.

4.8 Discussion

Our goal was to design an approach to study the longitudinal and progressive dynamics of metabolic alterations of MetS. Not only do the results show that our systems biology approach successfully describes the multitude of the metabolic changes, our modelling approach also describes the development of clinically relevant pathophysiological symptoms, including liver lipid accumulation (hepatic steatosis) and reduced insulin sensitivity (pre-diabetes). This demonstrates that our modelling approach can be used to study the onset and progression of MetS as well as its comorbidities. From the heterogeneous dataset, our model identified differences among tested individual mice. Unexpectedly, the existence of two different phenotypes in MetS development was predicted.

4.8.1 Heterogeneity in phenotype development

The clinical presentation of MetS in humans is highly heterogeneous and spans over decades. Male E3L.CETP mice fed a high-fat diet supplemented with cholesterol develop MetS within a

timescale of several months. Although all of these animals have the same genetic background, received the same diet, and were kept and monitored in a controlled, standardized environment, this *in vivo* model did show heterogeneity in its phenotypic presentation. In addition, the manifestation of the full repertoire of metabolic alterations associated with MetS makes this a useful *in vivo* model, whereas other animal models only describe one or partial metabolic aspects of MetS. [Roberts *et al.*, 2013; Yanai *et al.*, 2008; Mendizábal *et al.*, 2013; Adiels *et al.*, 2008; Kolovou *et al.*, 2005; Redinger, 2007; Lutz and Woods, 2012]

Using a traditional statistical approach, both this heterogeneity and limited datasets comprising of a low number of animals are problematic. Moreover, the time-dependency of the data – i.e. individual data of consecutive points in time are interrelated and therefore not independent samples – would further complicate analysis. Our computational modelling approach tackles these problems by combining MINGLeD with ADAPT. Contrary to other computational models, MINGLeD integrates both glucose and lipid species at a whole-body level. Both carbohydrates and fat are of importance in MetS and MINGLeD allows for a simultaneous description of these key components in terms of both metabolite pool sizes (concentrations) and metabolic fluxes.

Complexity and detail in model equations were considered in close relation to what is experimentally feasible to measure throughout long-term MetS development. Therefore, MINGLeD's data-driven and physiological design allows for describing both flux and concentration data on a whole-body level. MINGLeD per se can be simulated to describe metabolic snapshots, whereas the long-term dynamics are captured by using MINGLeD in conjunction with ADAPT. ADAPT has been designed to work with this kind of data and makes use of the time-dependent observations and simultaneously assesses uncertainty based on the variability in the data. The strength of the ADAPT methodology in dealing with heterogeneity became evident with the identification of two distinctly different phenotypes despite the limited number of animals that were studied. These two phenotypes mainly differ in terms of dyslipidemia, and flux trajectory analysis pinpointed differences in 1) hepatic turnover of metabolites, including lipid fluxes and 2) the intestinal cholesterol absorption. This appears to mimic the observation in humans showing that levels of cholesterol absorption efficiency can vary greatly among individuals. [Bosner *et al.*, 1999; Kesäniemi and Miettinen, 1987] These model predictions are open for further experimental validation.

4.8.2 Future perspectives

The methodology of integrating *in vivo* and *in silico* information allows to combine pre-existing knowledge with experimental quantitative data and can, therefore, be applied to study other multi-factorial, progressive diseases where longitudinal data are available. A future application of the model is to quantify energy intake and energy expenditure and analyse the energy balance over time for the development of obesity and MetS.

4.8.3 Conclusion

In conclusion, we combined data from animal experiments with a computer model and computer simulations to study the development of MetS. The new model predicted which changes in the underlying metabolic processes could explain the MetS symptoms. Two different

subgroups were identified: those with high cholesterol and high triglycerides, and those without. The computer model found that in those who develop lipid abnormalities, both dietary cholesterol absorption and hepatic liver fluxes were higher.

4.9 Methods

4.9.1 Ethics statement

All animal experiments were performed in accordance with the regulations of Dutch law on animal welfare, and the Animal Ethics Committee of the Leiden University Medical Centre, Leiden, The Netherlands. Animals were sacrificed by CO_2 inhalation.

4.9.2 *In vivo* model of Metabolic Syndrome development

The first step of our systems approach involved the gathering of *in vivo* data at different stages during the development of the Metabolic Syndrome. To this end, we used male APOE*3-Leiden(E3L).CETP transgenic mice as diet-induced *in vivo* model to study the metabolic adaptations that occur over time.

Male E3L.CETP transgenic mice were housed under standard conditions with a twelve-hour light/dark cycle (7AM-7PM), housed with one to two animals per conventional cage with free access to chow diet and water; unless indicated otherwise. At the age of eleven weeks, randomized according to body weight and plasma lipids (total cholesterol and triglycerides) and glucose, mice were divided into three groups: mice were fed either a low-fat diet (LFD; n=8), high-fat diet (HFD; n=12), or an HFD with additional cholesterol (HFD+C; 0.25%, w/w; Sigma) (HFD+C; n=8) for three months. The LFD has a 20% energy content derived from lard and contains 3.8 kcal/g diet; the HFD and HFD+C have a 60% energy content derived from lard and contain 5.2 kcal/g diet (OpenSource Diets, Research Diets, Inc. New Brunswick, USA). The specific composition of each diet is listed in Table 4.1 in Appendix 4.10.3.

During the study, body weight and food intake were measured weekly, body composition (lean and fat mass) every other week. Blood samples were taken monthly and analysed for glucose, insulin, free fatty acids, total cholesterol, HDL-cholesterol, and triglycerides. At the end of the three months dietary induction experiment, animals were sacrificed. Livers were isolated for measuring lipid metabolites and gene expression, and the hepatic *de novo* lipogenesis was determined by using an isotope tracer. For further details on the experimental set-up, the reader is referred to Appendix 4.10.

4.9.3 Modelling metabolic snapshots of different phenotypes

To validate the proposed structure of the *in silico* model, we calibrate MINGLeD to the *in vivo* data of the different metabolic snapshots. The experimentally measured metabolites are closely related to many of the variables in the computational model, such that an identifiable model is achieved of which the model parameters can be determined using parameter estimation. For each of the diet cohorts, MINGLeD is fitted separately to the phenotype snapshot determined at each month during the dietary induction period. For each snapshot, we compute the average and standard deviation of the measured data at this time point and

use this data to fit the model to using maximum likelihood estimation. Appendix 4.11 describes how we relate the experimentally observed data to the specific model outputs and equations using the weighted sum of squares as the error measure to be minimized. A Monte Carlo approach is employed to account for methodological and experimental uncertainties. The optimization procedure is repeated 500 times using a widely dispersed range of initial parameter values (10^{-1} - 10^{1}) to accommodate multi-start optimization. The implementation details can be found in section 3.3. Once optimized, MINGLeD predicts unobserved species and fluxes and is used to make predictions on the underlying differences between phenotype snapshots.

4.9.4 Modelling phenotype transition: modelling the onset and progressive behaviour over time

The next step in our systems approach is to couple the phenotype snapshots in time. Hereto we make use of the computational technique entitled "Analysis of Dynamic Adaptations of Parameter Trajectories" (ADAPT). [Tiemann *et al.*, 2011, 2013; van Riel *et al.*, 2013] By employing this concept of the time-dependent evolution of model parameters (see section 2.3), dynamic disease trajectories are obtained from which the onset and progression of MetS symptoms and comorbidities can be studied. The progression of these adaptations is predicted by identifying necessary dynamic changes in the model parameters to describe the transition between experimental data observed at different points in time during the dietary induction.

Since it is *a priori* unknown which model parameters change with time, it is not possible to perform a dynamic simulation of the entire timespan in one go. Therefore we discretize the timespan into 90 segments, each representing one day. ADAPT interpolates between the individual snapshots in time (at which experimental data was obtained) and simulates every day in between these time points. To facilitate this, some pre-processing steps are required. Since the quantitative experimental data is discrete and only available at four points in time, the data is interpolated using cubic smoothing splines to obtain continuous dynamic descriptions of the experimentally observed metabolite pools and fluxes. To account for experimental and biological uncertainties, a collection of 1,000 splines is calculated using a Monte Carlo approach: different random samples of the experimental data are generated assuming Gaussian distributions with means and standard deviations of the data. Subsequently, for each generated sample, a cubic smoothing spline is calculated. This bootstrapping approach yields samples of data replicates which are subsequently utilized in parameter estimation. [Vanlier *et al.*, 2013] By combining bootstrapping of data, sampling of parameters, and a robust optimization of model simulations, ADAPT provides feedback about uncertainty in model predictions accounting for uncertainty in both experimental measurements and fitting procedures.

The system is first simulated for the phenotype prior to the dietary induction by optimization to the t=0 data. For each step in time, the system is simulated using the final values of the model states of the previous time step as initial conditions. Since we consider the parameters to be time-varying, the model parameters are re-optimized for each time step by minimizing the difference between the (sampled and interpolated) experimental data and the corresponding model outputs. The estimated parameter set from the previous time point is

used as the initial set for the optimization procedure. It is assumed that the induced adaptations are minimal and proceed progressively in time. Therefore, highly fluctuating parameter trajectories are considered to be non-physiological. To prevent the occurrence of such behaviour, the parameter estimation protocol is extended to prevent unnecessary change of parameters and to identify minimal parameter adaptations that are required to describe phenotype transition. The cost function is extended with a regularisation term (see (4.2) in Appendix 4.11), given by the sum of squared derivatives of the normalized parameter values. Hence, changing a parameter is costly, and is, therefore, avoided if this is not required to describe the experimental data. The constant λ that determines the strength of this regularisation term, should be chosen carefully such that the data fitting is biased as little as possible. If too large a value for λ is chosen, the regularisation term becomes dominant and the model will not describe the experimental data accurately anymore. Since a small λ is already sufficient to minimize parameter changes and fluctuations, whilst still describing the experimental data accurately, λ was set to 0.1 in this study.

All simulation code and *in silico* data files are available on GitHub (via github.com/yvonnerozendaal/MINGLeD).

ADAPT yields a collection of parameter sets that describe the dynamics of the onset and development of MetS over time. The obtained trajectories for the model parameters, but also for the fluxes and pool sizes provide insight into the affected underlying biological system. This provides information about the adaptations that have taken place during the dietary induction, and these model-based predictions are compared to the gene expression data that is measured at the end of the dietary induction study.

4.10 Appendix: Experimental set-up

In this study, we used male APOE*3-Leiden.CETP mice on a high-fat, cholesterol-containing diet to study the onset and development of diet-induced Metabolic Syndrome.

4.10.1 Choice of animal model

The APOE*3-Leiden.CETP mouse is a double transgenic animal. Through the genetic APOE*3-Leiden (E3L) mutation, E3L mice have a defective triglyceride-rich lipoprotein (TRL) clearance, which mimics the lower TRL clearance in humans. The E3L mice display an elevated basal cholesterol level and exhibit a human-like lipoprotein profile, develop atherosclerosis upon saturated fat and cholesterol feeding [Westerterp *et al.*, 2006; Zadelaar *et al.*, 2007] and also respond in a human-like manner to drugs used in the treatment of cardiovascular diseases. [Delsing *et al.*, 2001; van der Hoorn *et al.*, 2007; Kleemann *et al.*, 2003; Kooistra *et al.*, 2006]

Another important difference between the murine and human lipoprotein metabolic system is the exchange and transfer of cholesteryl esters (CE) and triglycerides (TG) between HDL and (V)LDL particles through the cholesteryl ester transfer protein (CETP). Mice do not naturally possess the CETP gene and do therefore not respond to HDL-modulating interventions. By cross-breeding the E3L mice to mice expressing the human CETP gene [Jiang *et al.*, 1992], E3L.CETP mice show an even more human-like lipoprotein metabolism. The expression of the human

CETP gene shifts the distribution of cholesterol from HDL towards (V)LDL. [Rensen and Havekes, 2006; Westerterp *et al.*, 2006] E3L.CETP mice have the ability to reproduce obesity, diabetes, dyslipidemia, and atherosclerosis and they respond to both lipid-lowering and HDL-raising interventions. [de Haan *et al.*, 2008; van den Hoek *et al.*, 2014; van der Hoogt *et al.*, 2007; van der Hoorn *et al.*, 2008]

Previous studies using E3L.CETP mice revealed that male E3L.CETP mice upon feeding a high-fat diet develop obesity and diabetes. [van den Hoek *et al.*, 2014; van Dam *et al.*, 2015] Female E3L.CETP mice that are fed with a high-fat, high-cholesterol diet (the so-called "Western-type diet") develop dyslipidemia and atherosclerosis. [Auvinen *et al.*, 2013; Berbée *et al.*, 2015; de Haan *et al.*, 2008; van der Hoorn *et al.*, 2008, 2009; Kühnast *et al.*, 2015; Li *et al.*, 2012; Wang *et al.*, 2011, 2014a; Westerterp *et al.*, 2006; van der Tuin *et al.*, 2013]

The E3L.CETP mouse model can be used to study the associated processes in MetS in more depth. We expected this animal model to develop obesity, diabetes, and dyslipidemia upon feeding male E3L.CETP mice a high-fat, high-cholesterol diet.

4.10.2 Study outline

All animal experiments were performed in accordance with the regulations of Dutch law on animal welfare, and the Animal Ethics Committee of the Leiden University Medical Centre, Leiden, The Netherlands. Homozygous CETP transgenic mice expressing the human CETP gene under the control of its natural flanking regions (Jackson Laboratory, Bar Harbor, Maine, USA) [Jiang *et al.*, 1992] were crossbred with heterozygous APOE*3-Leiden (E3L) mice [van den Maagdenberg *et al.*, 1993] to obtain E3L.CETP mice in our own animal facility.

4.10.3 Dietary induction protocol

In this study, we used male E3L.CETP transgenic mice that were housed under standard conditions with a twelve-hour light/dark cycle (7AM-7PM), co-housed with one to four animals in conventional cages with free access to food and water, unless indicated otherwise. Animals were housed in a temperature-controlled environment (21 °C). At the age of 10.8 ± 2.2 weeks, randomized according to body weight and plasma lipids (total cholesterol and triglyceride) and glucose level, mice were divided into three groups: mice were fed a low-fat diet (LFD; n=8), high-fat diet (HFD; n=12) or a high-fat diet with supplemental cholesterol (Sigma, 0.25 gm%) (HFD+C; n=8) for twelve weeks. The low-fat diet has a 20% energy content derived from lard and contains 3.8 kcal/g diet; the high-fat diets have a 60% energy content derived from lard and contains 5.2 kcal/g diet (OpenSource Diets, Research Diets, Inc. New Brunswick, USA). The specific composition of each diet is listed in Table 4.1.

Table 4.1

Composition of the low-fat, high-fat and high-fat with cholesterol diets.

	LFD		HFD		HFD+C	
	gm%	kcal%	gm%	kcal%	gm%	kcal%
protein	19	20	26	20	26	20
carbohydrates	67	70	26	20	26	20
fat	4	10	35	60	35	60
cholesterol	0	0	0.028	0	0.25	0
kcal/g	3.8		5.2		5.2	

4.10.4 Responders and non-responders

Only animals correctly expressing the genotype and responding to the high-fat diet (if applicable) were included in this study. We used the following selection criteria: 1) correct animal genotype (expressing the APOE*3-Leiden and CETP genes) and phenotype: baseline measurement (animals on chow-diet, hence before the start of the dietary induction) of plasma triglycerides ≥1 mM and plasma total cholesterol ≥2 mM; and 2) responding to dietary induction: bodyweight ≥35 g after eight weeks of HFD.

4.10.5 Experimental details of the measurement protocol

During the study, body weight and food intake were measured weekly (Figures 4.1A-C). Body composition (lean and fat mass) was determined in conscious mice using an EchoMRI-100 (EchoMRI, Houston, Texas, USA) every other week.

Before (0) and four, eight, and twelve weeks after dietary induction, blood samples were taken by tail vein bleeding into heparin and paraoxon (to inhibit lipase activity) coated capillary tubes, after five hours of fasting with food withdrawn at 8AM. The tubes were placed on ice and centrifuged, and the obtained plasma was snap frozen in liquid nitrogen and stored at -20°C until further measurements. Plasma was analysed for cholesterol, triglycerides, lipoproteins, glucose, and insulin (Figures 4.1D-H).

4.10.6 Plasma metabolites

Blood plasma was assessed for glucose using Glucose reagent 1 and 2 (start reagent) (Instruchemie, Delfzijl, The Netherlands) with a 1 mg/mL glucose standard (Sigma-Aldrich, Saint Louis, Missouri, USA). Insulin was measured using the Ultra Sensitive Mouse Insulin ELISA Kit (Crystal Chem, Downers Grove, Illinois, USA).

Besides the monthly five-hour fasting values, also oral glucose tolerance tests (OGTT) have been performed before (0) and after six and eleven weeks of dietary induction in overnight fasted mice (7PM-9AM). The glucose (Figures 4.6A-C) and insulin (Figures 4.6D-F) responses were measured at 0, 5, 18, 35, 60 and 120 minutes after oral gavage (1 g glucose per kg body

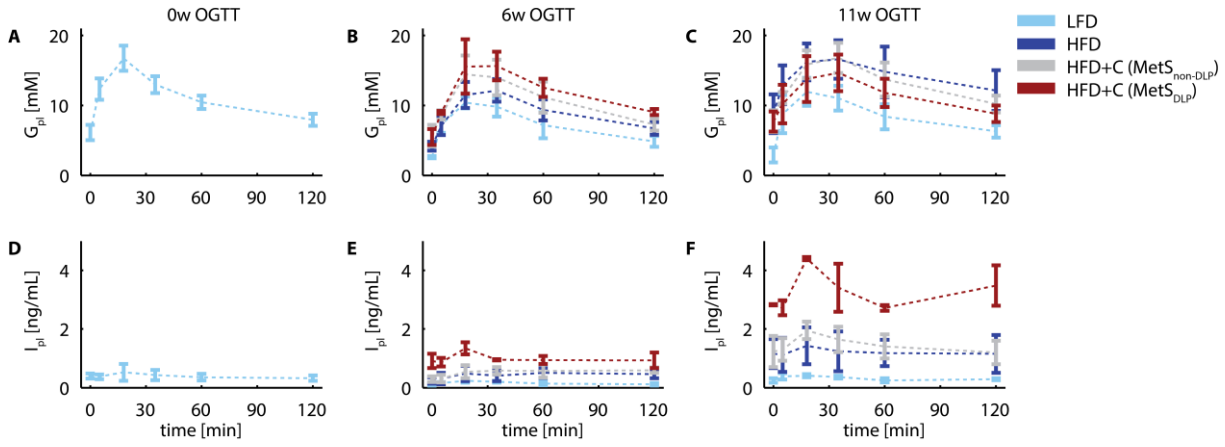

Figure 4.6

Glucose (A-C) and insulin (D-F) response profiles to an Oral Glucose Tolerance Test (OGTT) after zero (A;D), six (B;E) and eleven (C;F) weeks of dietary induction.

The data are depicted using error bars representing the mean ± standard deviation for each subgroup separately.

weight). Blood glucose is determined by tail bleeding using a portable glucometer (2 µL) and a half of capillary of blood (30 µL) is collected by tail bleeding for insulin measurements.

Circulating lipid species were also assessed monthly after five hours of fasting. Plasma triglycerides (TG) were measured using a total triglyceride set (Roche Diagnostics) using precimat glycerol of 2.29 mM. Plasma free fatty acids were measured using the NEFA-HR(2) kit from Wako Diagnostics (Instruchemie, Delfzijl, The Netherlands). Plasma total cholesterol (TC) was measured using a total cholesterol set (Roche Diagnostics) using a cholesterol calibrator of 200 mg/dL (Instruchemie, Delfzijl, The Netherlands). Plasma HDL cholesterol was measured using precipitation of ApoB-containing lipoproteins with PEG 6000#.

4.10.7 Hepatic de novo lipogenesis

Hepatic *de novo* lipogenesis (DNL) was assessed at the three months' time point using a labelled acetate tracer experiment (Figure 4.4D). Animals receive drinking water containing sodium-1-^{13}C-acetate (2%) during the final 24 hours of the study (started at 8AM). To subject the animals to a postprandial fast, food was removed the next morning at 8AM while the acetate containing drinking water remained available. At 10AM the animals were sacrificed by CO_2 inhalation and livers were quickly exercised and stored for further lipid analysis.

4.10.8 Liver histology score

Paraffin-embedded liver sections were stained with hematoxylin and eosin (H&E). According to the histological NAFLD (non-alcoholic fatty liver disease) scoring system for rodent models of Liang *et al.* [Liang *et al.*, 2014] the two key features of NASH (non-alcoholic steatotic hepatitis) – steatosis and inflammation – were determined. Briefly, steatosis was scored by hepatocellular vesicular steatosis, i.e. macrovesicular steatosis and microvesicular steatosis fractions separately. Inflammation was scored by analysing the number of inflammatory cell aggregates per field using a 100x magnification (view size of 1.46 mm^2) (Figure 4.7).

4.10.9 Liver metabolites

At the end of the three months' dietary induction experiment, mice were sacrificed and perfused with ice-cold saline via the heart. The livers were isolated and the liver weight was assessed. Liver lipids were extracted according to a modified protocol from Bligh and Dyer. [Bligh and Dyer, 1959] Briefly, small liver pieces were homogenized in ice-cold methanol. After centrifugation, lipids were extracted after addition of 1800 µl CH_3OH:$CHCl_3$ (1:3 v/v) to 45 µl homogenate, followed by vigorous vortexing and phase separation by centrifugation (5 minutes at 2,000 rpm). The $CHCl_3$ phase was dried and dissolved in 2% Triton X-100. TG and TC concentrations were measured as described above. Free cholesterol (FC) and cholesteryl ester (CE) concentrations were measured using a commercial kit (Cholesterol/Cholesteryl Ester Quantitation Kit, BioVision, USA). Liver lipids (Figure 4.5) were expressed as nmol/mg liver tissue.

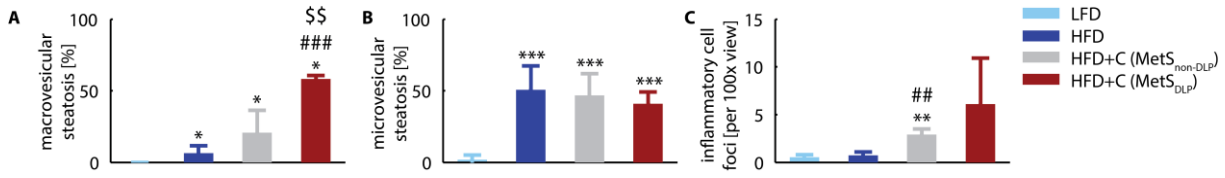

Figure 4.7

Liver histology data on steatosis (A-B) and inflammation markers (C).

The data are depicted using error bars representing the mean ± standard deviation for each subgroup separately. Differences between groups were determined using a one-way ANOVA test. When significant differences were found, Fisher's LSD test was used as a post hoc test to determine the differences between two independent groups:

* P<0.05; ** P<0.01; *** P<0.001 as compared to LFD

# P<0.05; ## P<0.01; ### P<0.001 as compared to HFD

$ P<0.05; $$ P<0.01; $$$ P<0.001 as compared to HFD+C ($MetS_{non\text{-}DLP}$)

4.10.10 Hepatic gene expression analysis

Total RNA was extracted from liver pieces using TriPure isolation reagent (Roche Applied Science, Indianapolis, IN, USA) according to the manufacturer's instructions. RNA quality was examined by the lab-on-a-chip method using Experion Std Sens analysis kit (Biorad, Hercules, CA, USA) and RNA concentration was determined by Nanodrop 1000 spectrophotometer (Thermo-Fischer Scientific). Subsequently, total RNA was reverse-transcribed with RevertAid™ M-MuLV Reverse Transcriptase (Promega, Madison, WI, USA). Quantitative real-time PCR was performed on a CFX96 machine (Bio-Rad, California), the reaction mixture consisting of SYBR-Green Sensimix (QT615, GC Biotech), cDNA, primers (Biolegio, Nijmegen, The Netherlands; see Table 4.2 for primer sequences), and nuclease-free water in a total reaction volume of 10 µl. Expression of the selected transcripts was normalized to mRNA levels of hypoxanthine ribosyltransferase (*Hprt*) and cyclophilin (*Cyclo*). Data were calculated as fold difference as compared with the LFD group and are presented in Table 4.3.

Table 4.2

Primer sequences used for RT-qPCR.

gene	forward primer	reverse primer
Acc2	AGATGGCCGATCAGTACGTC	GGGGACCTAGGAAAGCAATC
Acox1	TATGGGATCAGCCAGAAAGG	ACAGAGCCAAGGGTCACATC
Ctp1a	GAGACTTCCAACGCATGACA	ATGGGTTGGGGTGATGTAGA
Cyclo	*CAAATGCTGGACCAAACACAA*	GCCATCCAGCCATTCAGTCT
Cyp7a1	CAGGGAGATGCTCTGTGTTCA	AGGCATACATCCCTTCCGTGA
Cyp27a1	TCTGGCTACCTGCACTTCCT	CTGGATCTCTGGGCTCTTTG
Dgat2	TCGCGAGTACCTGATGTCTG	CTTCAGGGTGACTGCGTTCT
Fasn	GCGCTCCTCGCTTGTCGTCT	TAGAGCCCAGCCTTCCATCTCCTG
Fxr	GGCCTCTGGGTACCACTACA	ACATCCCCATCTCTTTGCAC
Hprt	*TTGCTCGAGATGTCATGAAGGA*	*AGCAGGTCAGCAAAGAACTTATAG*
Pparα	ATGCCAGTACTGCCGTTTTC	GGCCTTGACCTTGTTCATGT
Srebp1c	AGCCGTGGTGAGAAGCGCAC	ACACCAGGTCCTTCAGTGATTTGCT

Table 4.3

Relative mRNA expression.

Values are presented as the mean value ± standard deviation and have been calculated as fold difference with respect to the mean expression value of the LFD group.

Differences between groups were determined using a one-way ANOVA test. When significant differences were found, Fisher's LSD test was used as a post hoc test to determine the differences between two independent groups:

* P<0.05; ** P<0.01; *** P<0.001 as compared to LFD

# P<0.05; ## P<0.01; ### P<0.001 as compared to HFD

$ P<0.05; $$ P<0.01; $$$ P<0.001 as compared to HFD+C ($MetS_{non-DLP}$)

Processes/fluxes	genes	LFD	HFD	HFD+C ($MetS_{non-DLP}$)	HFD+C ($MetS_{DLP}$)
bile acid synthesis	*Cyp7a1*	1 ± 0.50	4.41 ± 2.07*	6.08 ± 2.76**	8.20 ± 5.25***,#
	Cyp27a1	1 ± 0.20	1.19 ± 0.11	1.07 ± 0.24	0.80 ± 0.23#
de novo lipogenesis	*Fasn*	1 ± 0.62	0.49 ± 0.13	0.46 ± 0.36*	0.76 ± 0.36
	Acc2	1 ± 0.42	0.80 ± 0.22	0.52 ± 0.23*	0.81 ± 0.21
	Dgat2	1 ± 0.09	1.21 ± 0.37	0.23 ± 0.05***,###	0.20 ± 0.08***,###
fatty acid β-oxidation	*Acox1*	1 ± 0.20	1.24 ± 0.39	1.43 ± 0.48*	1.41 ± 0.39
	Cpt1a	1 ± 0.29	2.16 ± 0.67**	2.24 ± 0.94**	2.19 ± 0.69*
nuclear transcript factors	*FXR*	1 ± 0.21	1.48 ± 0.39*	1.62 ± 0.41**	1.67 ± 0.46*
	Srebp1c	1 ± 0.29	0.99 ± 0.30	1.11 ± 0.48	0.84 ± 0.03
	Pparα	1 ± 0.21	1.95 ± 0.37***	2.05 ± 0.39***	2.30 ± 0.70***

4.11 Appendix: Model fitting to experimental data

Parameters for MINGLeD are estimated to calibrate the model by fitting to experimentally observed data. Maximum likelihood estimation is used to minimize the difference between model output and data. This error is referred to as the cost function and consists of the weighted sum of squared errors (WSSE) between model outputs and data. Table 4.4 describes which model outputs are constraint to which data. When fitting MINGLeD to separate phenotype snapshots, the cost function is as follows:

$$\chi_j^2 = \sum_{i=1}^{N_i} \left(\frac{y_i(\theta, t_j) - \mu_{i,j}}{\sigma_{i,j}} \right)^2 \quad (4.1)$$

with χ_j^2 representing the WSSE at time point j. It evaluates model outputs y_i (listed in Table 4.4) as predicted by the parameter set θ in comparison to the mean ($\mu_{i,j}$) and standard deviation ($\sigma_{i,j}$) of the corresponding experimentally observed data on metabolite i at time j.

When MINGLeD is fitted over the complete timespan using the ADAPT methodology, the cost function is as follows:

$$\chi^2_{ADAPT} = \chi^2 + \chi^2_{reg}$$
$$\sum_{i=1}^{N_i} \sum_{j=1}^{N_t} \left(\frac{y_i(\theta, t_j) - \mu_{i,j}}{\sigma_{i,j}} \right)^2 + \lambda \cdot \sum_{k=1}^{N_p} \left(\frac{\theta_{j,k} - \theta_{j,k-1}}{\theta_{0,k}} \right)^2 \quad (4.2)$$

The WSSE (χ^2) was extended and is now evaluated over the complete timespan. Note that the cost function was also extended with a regularisation term, weighted by the regularisation coefficient λ (which was set to 0.1 in this study) in which N_p is the number of parameters and $\theta_{j,k}$ the parameter k at time j and $\theta_{0,k}$ the initial value of parameter k.

Table 4.4

List of SSE components.

observable	model output		respective data component	unit
y_1	x_1	G_{pl}	plasma glucose [mM] · estimated plasma volume [mL] [(a)]	µmol
y_2	x_2	FFA_{pl}	plasma FFA data [mM] · estimated plasma volume [mL] [(a)]	µmol
y_3	x_3	$HDLC_{pl}$	plasma HDL-C data [mM] · estimated plasma volume [mL] [(a)]	µmol
y_4	x_5	$(V)LDL\text{-}TG_{pl}$	plasma TG data [mM] · estimated plasma volume [mL] [(a)]	µmol
y_5	x_4	$(V)LDL\text{-}C_{pl}$	(plasma total cholesterol data [mM] - plasma HDL-C data [mM]) · estimated plasma volume [mL] [(a)]	µmol
y_6	x_6	TG_{hep}	hepatic TG data [µmol]	µmol
y_7	x_7	FC_{hep}	hepatic FC data [µmol]	µmol
y_8	x_8	CE_{hep}	hepatic TC data [µmol] - hepatic FC data [µmol]	µmol
y_9	j_{31}	$j^{TG}_{DNL,hep}$	$DNL_{C16:0}$ data + $DNL_{C18:0}$ data + $DNL_{C18:1}$ data + $^1/_9 \cdot CE_{C18:0}$ data + $^1/_9 \cdot CE_{C18:1}$ data [µmol/g liver] · liver weight data [g] [(b)]	µmol/day
y_{10}	x_{12}	TG_{per}	(fat mass data [mg] / molar mass of TG[(c)]) $\cdot 10^6$	µmol
y_{11}	$j_8 + j_9$	$j^{AA}_{upt,hep} + j^{AA}_{upt,per}$	dietary protein intake data[(d)]	µmol/day

[(a)] the plasma volume is approximated by $V_{pl} = 0.7704 + 0.0117 \cdot BW$ [Yen *et al.*, 1970]

[(b)] chain elongation is accounted for as $^1/_9{}^{th}$ of a newly synthesized fatty acid

[(c)] the molar mass of an average triglyceride molecule was assumed to be 853 g/mol [Desilva, 2007]

[(d)] the daily dietary protein intake was calculated in terms of glucose equivalent particles, taking into account the 20% of the energy content of the diet is derived from protein, and glucose having an energy density of 4.18 kcal/g and a molar mass of 180 g/mol [Desilva, 2007]

4.12 Appendix: Predicted metabolite pools and flux trajectories

A – Plasma metabolite pools

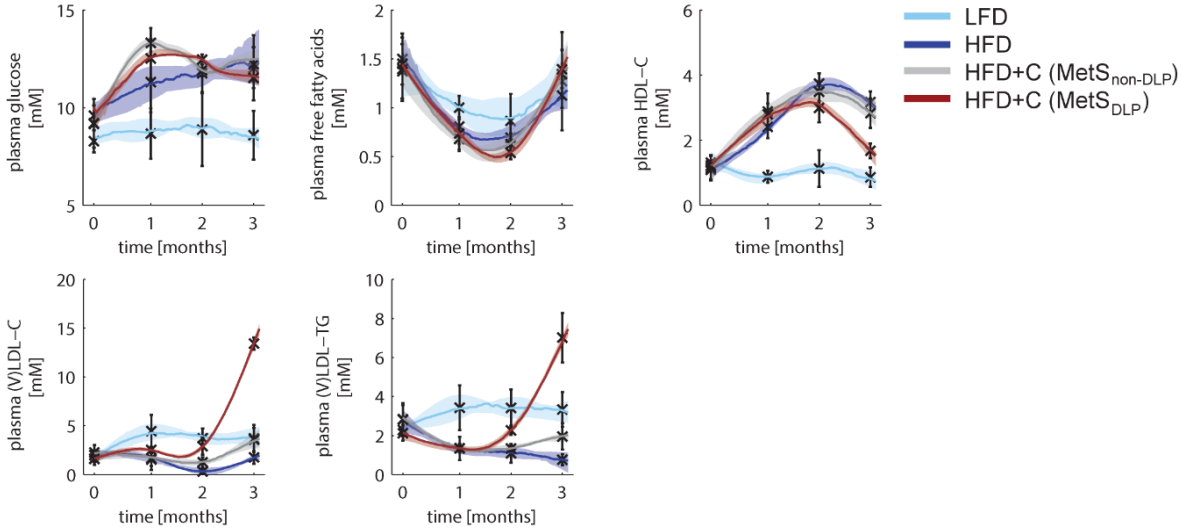

B – Hepatic metabolite pools

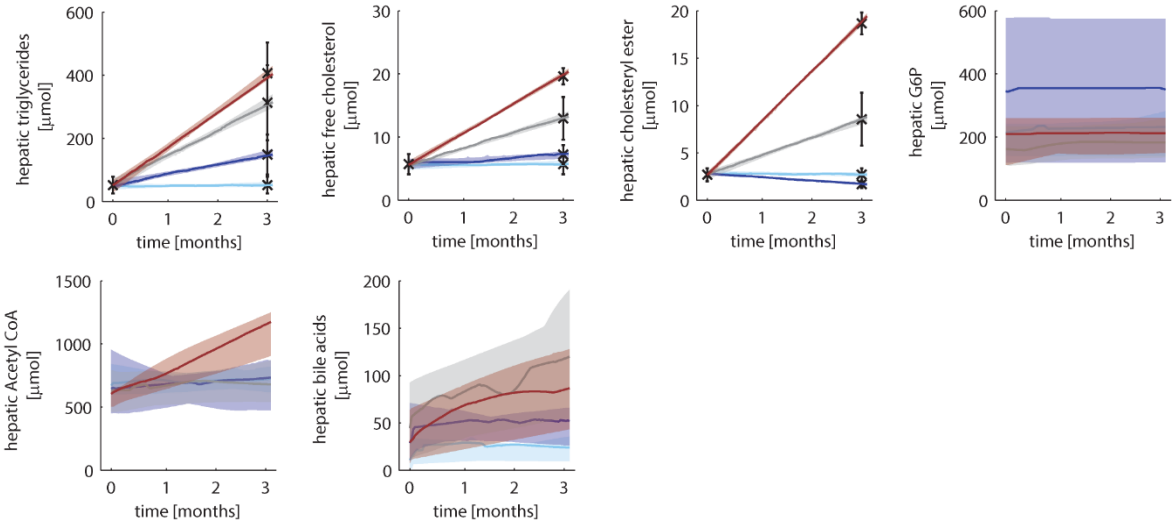

C – Peripheral metabolite pools

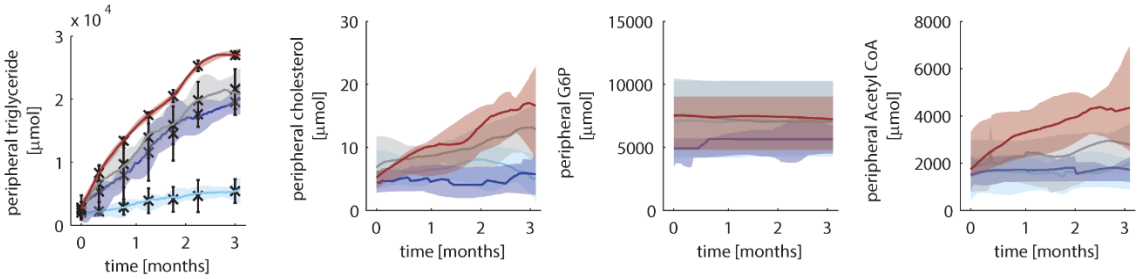

D – Metabolite pools in the intestinal lumen

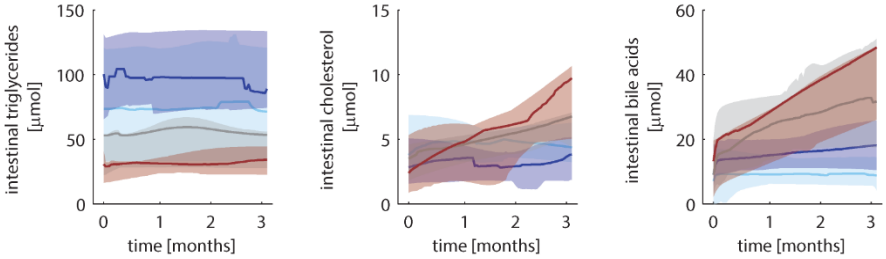

E – Dietary intake in terms of macronutrients

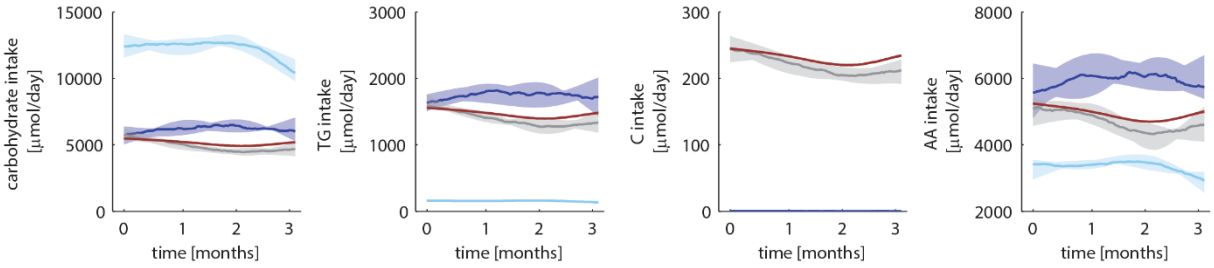

F – Dietary triglyceride and cholesterol uptake

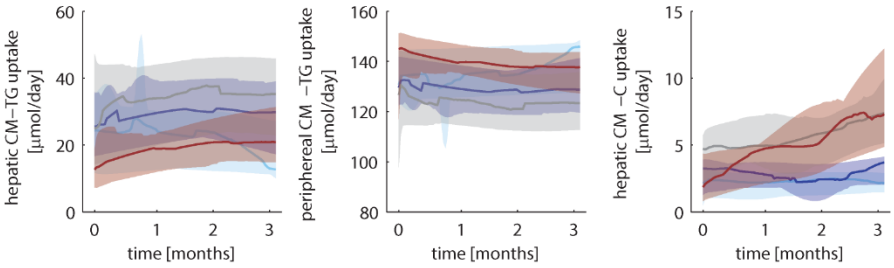

G – Dietary amino acid uptake fluxes

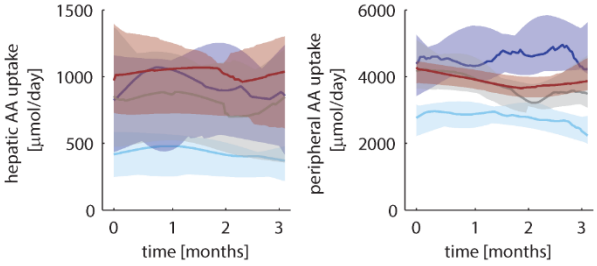

H – Amino acid uptake via the glucogenic (50%) and ketogenic (50%) pathway in liver and periphery

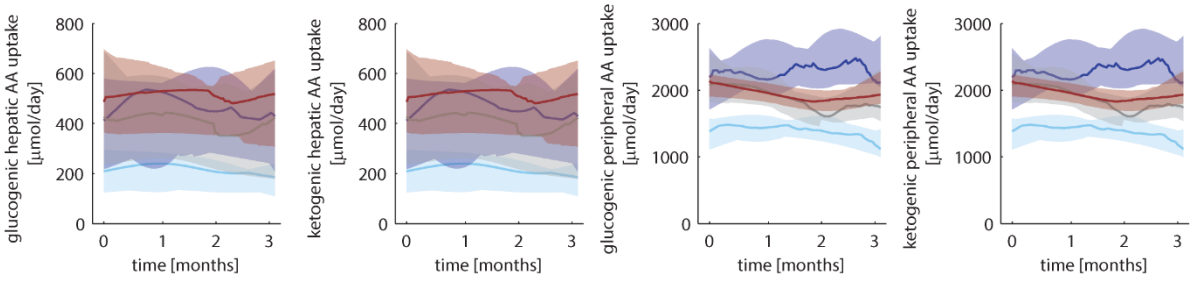

I – Dietary carbohydrate uptake fluxes

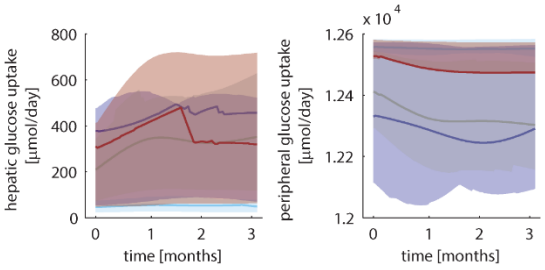

J – Carbohydrate metabolic fluxes

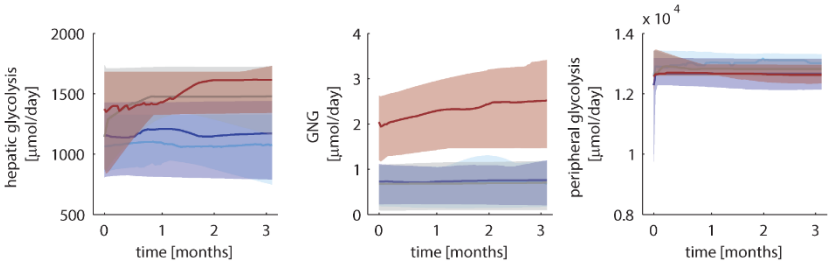

K – Lipoprotein formation fluxes

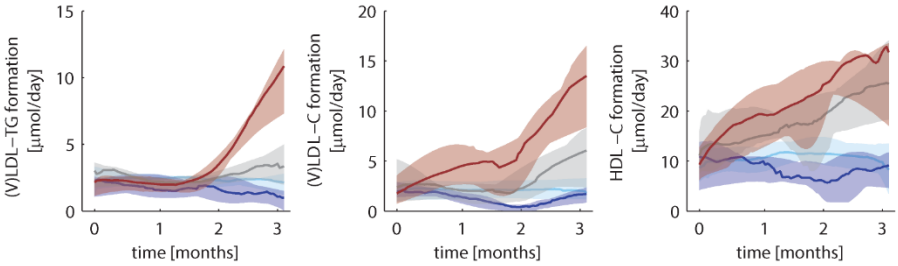

L – Lipoprotein (remnant) uptake fluxes

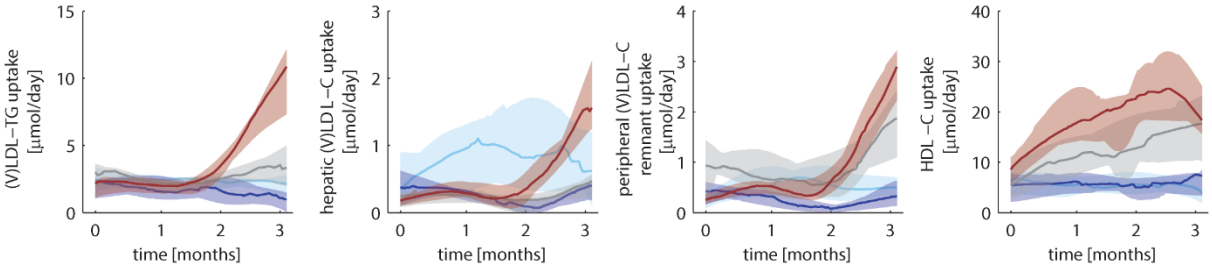

M – Lipoprotein metabolism fluxes

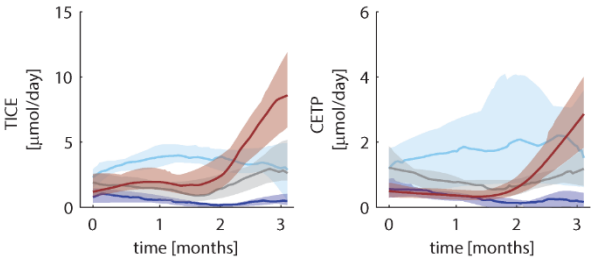

N – Fatty acid uptake flux

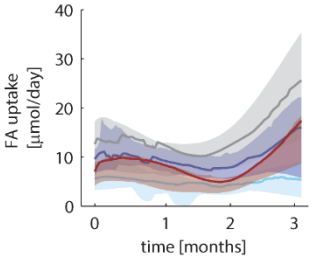

O – Hepatic metabolic fluxes

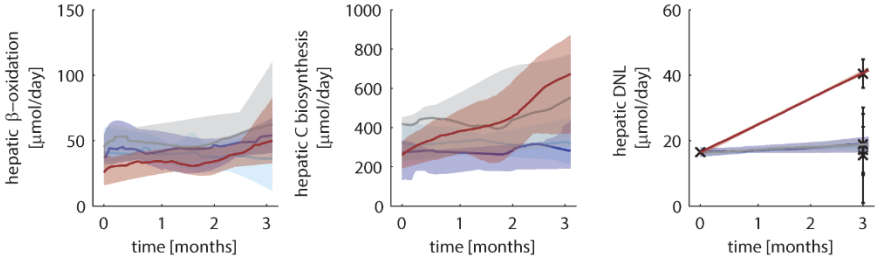

P– Peripheral metabolic fluxes

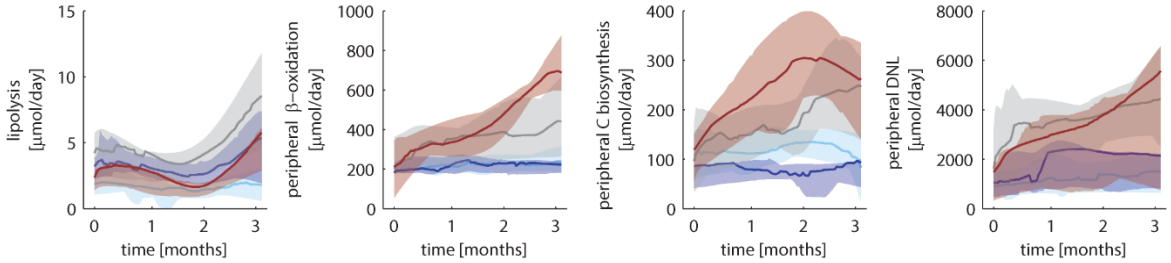

Q – Hepatic cholesterol storage and release fluxes

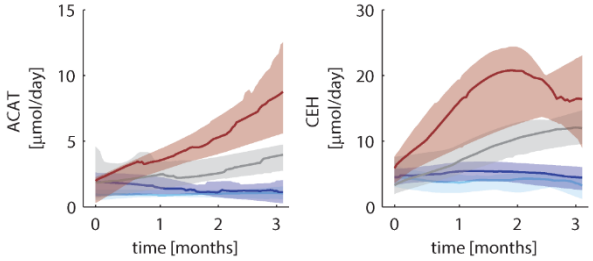

R – Bile acid fluxes

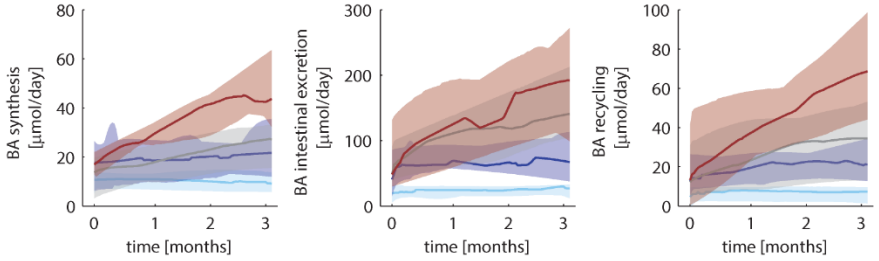

S – Intestinal metabolic fluxes

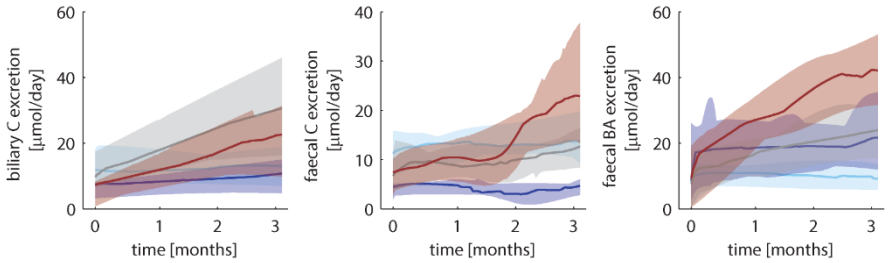

T – Respiratory fluxes

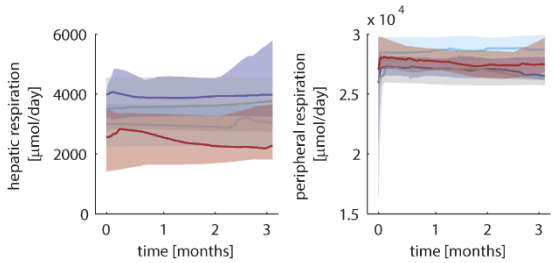

Figure 4.8

Predicted metabolite pools and flux trajectories.

Panels A-B display the dynamics in metabolite pools over time and panels E-T display the corresponding flux trajectories. We selected the n=100 best trajectories (top 10% based on WSSE). The 10% range around the median trajectory is depicted by the shaded area and the median trajectory for each model component is depicted by the solid line for the low-fat diet group (light blue), high-fat diet group (dark blue), non-dyslipidemic Metabolic Syndrome phenotype (grey) and the dyslipidemic Metabolic Syndrome phenotype (red) respectively. Experimental data is represented by the black error bars (mean ± standard deviation).

5

Heterogeneity and variability in the long-term development of Metabolic Syndrome

Male E3L.CETP mice develop Metabolic Syndrome after being fed with a high-fat, high-cholesterol diet for at least three months. Here we repeated this diet induction study using a larger population and for up to six months and found that the development of Metabolic Syndrome symptoms occurs mainly in the first three months of the diet induction and stabilizes in the later months in a time window up to six months. The degree to which these animals develop dyslipidemia is highly heterogeneous. Hereto we have identified three different subpopulations that develop dyslipidemia to different degrees (relatively low, intermediate, and relatively high) using *k*-means clustering based on the three-month plasma triglyceride and plasma total cholesterol levels.

5.1 Introduction

In the previous chapter, we have shown that male E3L.CETP mice develop Metabolic Syndrome (MetS) symptoms after feeding a high-fat, high-cholesterol diet for three months. [Rozendaal *et al.*, 2018b] In addition, we identified two different phenotypic outcomes: dyslipidemic ($MetS_{DLP}$) and non-dyslipidemic ($MetS_{non\text{-}DLP}$) Metabolic Syndrome. Due to the limited population size ($MetS_{DLP}$, n=3; $MetS_{non\text{-}DLP}$, n=5), a follow-up study was required and performed using a much larger cohort of animals that were followed for a longer period of time. [Paalvast *et al.*, 2017]

Isolated diet-induced MetS aspects have been shown to be reproducible in male E3L.CETP mice. [Auvinen *et al.*, 2013; de Haan *et al.*, 2008; Kleemann *et al.*, 2003; Kooistra *et al.*, 2006; Li *et al.*, 2012; van den Hoek *et al.*, 2014; van der Hoorn *et al.*, 2009; Wang *et al.*, 2014a; Zadelaar *et al.*, 2007; Westerterp *et al.*, 2006] In this chapter, we investigate whether the previously found multitude of MetS symptoms is reproducible, and more precisely, whether the distinct dyslipidemic phenotypes are a coherent feature of MetS.

The multi-laboratory set-up of RESOLVE is centred around different partners conducting experiments on the same preclinical animal model (male E3L.CETP fed an HFD+C). Since the E3L.CETP transgenic mouse model was originally constructed by the group of prof. Havekes (TNO; Leiden University Medical Centre), all mice were bred in the Leiden facilities and subsequently distributed to the RESOLVE partners. Animals were held in established and approved animal housing facilities of each of the respective partners. In order to obtain comparable data, pre-defined standard operation procedures (SOPs) were established which include standardized protocols for the acquisition, storage, and shipment of plasma and tissue samples.

However, prior to study design and analysis, we have to consider that the multi-laboratory set-up may induce uncontrollable variation. [Crabbe *et al.*, 1999; Wahlsten *et al.*, 2003] Inference from environmental factors, such as the location of a mouse's cage within the lab that may introduce additional light, noise, or odours, can cause behaviour-changing anxiety. Especially stress is known to have confounding metabolic consequences. [Bartolomucci *et al.*, 2009; Ghosal *et al.*, 2015] We, therefore, tried to standardize the set-up of this follow-up study [Paalvast *et al.*, 2017] to resemble the set-up as described in the previous chapter [Rozendaal *et al.*, 2018b] as closely as possible. We investigate whether on the long-term male E3L.CETP mice on a high-fat, high-cholesterol diet develop MetS consistently. Also, we explore the heterogeneity and variability involved in the

long-term development of MetS. Lastly, we study the subdivision of the population in subgroups describing different degrees of dyslipidemia development.

5.2 Study design

The six-month diet induction study was performed at the University Medical Centre Groningen (UMCG) and was set up similarly as the three-month diet induction study that was performed at the Leiden University Medical Centre (LUMC). Male E3L.CETP mice were housed under standard conditions with a twelve-hour light/dark cycle (7AM-7PM) and housed individually. At the age of four months, mice were divided into five separate cohorts (see Table 5.1) and all fed a high-fat (60% energy), high-cholesterol (0.25% w/w; Sigma) diet (OpenSource Diets, Research Diets, Inc. New Brunswick, USA) for up to four (n=20), ten (n=19), thirteen (n=20), and 28 (n=30 and n=16) weeks.

Body weight and food intake were measured weekly throughout the experiment. Blood samples were taken monthly (after four-hour fasting) and analysed for glucose, insulin, triglycerides (TG), total cholesterol (TC), and HDL-cholesterol. At the end of the study, mice in the respective cohorts were distributed evenly in two groups, where one group underwent VLDL-TG production measurement and the other hepatic *de novo* lipogenesis (DNL) measurement (data reported in [Paalvast *et al.*, 2017]).

Animals were classified as responders (see Table 5.1 and section 4.10.4) to the genetic intervention when showing a plasma triglyceride (TG) level ≥1 mM and plasma total cholesterol (TC) level ≥2 mM prior to start of the diet induction scheme (i.e. t=0 in this experiment). Responders to the high-fat, high-cholesterol diet were identified as having a body weight of at least 35 grams after eight weeks of the diet. This yielded a total population of 84 animals being classified as responders.

Table 5.1

Cohort sizes in the six-month diet induction study.

			#total	#responders
6M cohort	cohort 1	28w	30	23
	cohort 2	28w	16	13
	cohort 3	13w	20	18
	cohort 4	10w	19	15
	cohort 5	4w	20	15
		total	105	84

The experimental data presented in this chapter are courtesy of our RESOLVE partners at the University Medical Centre Groningen and have been published in:

Paalvast Y, Gerding A, Wang Y, Bloks VW, van Dijk TH, Havinga R, Willems van Dijk K, Rensen PCN, Bakker BM, Kuivenhoven JA, Groen AK. Male APOE*3-Leiden.CETP mice on high-fat high-cholesterol diet exhibit a biphasic dyslipidemic response, mimicking the changes in plasma lipids observed through life in men. *Physiol. Rep.*, 2017, 5(19):e13376 doi.org/10.14814/phy2.13376

5.3 The effects of long-term feeding of a high-fat, high-cholesterol diet

We first performed explorative data analysis and compared the data obtained in the six-month diet induction study [Paalvast *et al.*, 2017] to the data obtained in the three-month diet induction study. [Rozendaal *et al.*, 2018b]

5.3.1 Obesity development

Body weight (Figure 5.1A) rapidly increases in response to the high-fat, high-cholesterol diet, following the same trend as the three-month study and plateaus after around three months. Baseline body weight is generally higher in the six-month study, which could be attributed to the fact that these animals are roughly one month older at the start of the diet induction than those in the three-month study. More importantly, the weight gain (Figure 5.1B) is comparable to that in the three-month study, as is the variability in weight gain.

Information about change in body weight provides important information on the overall health status of the animal. A sudden decrease in body weight may indicate that the health of the animal is impaired. Cases of tumour development have shown to coincide with large drops in body weight, and these animals were sacrificed prematurely.

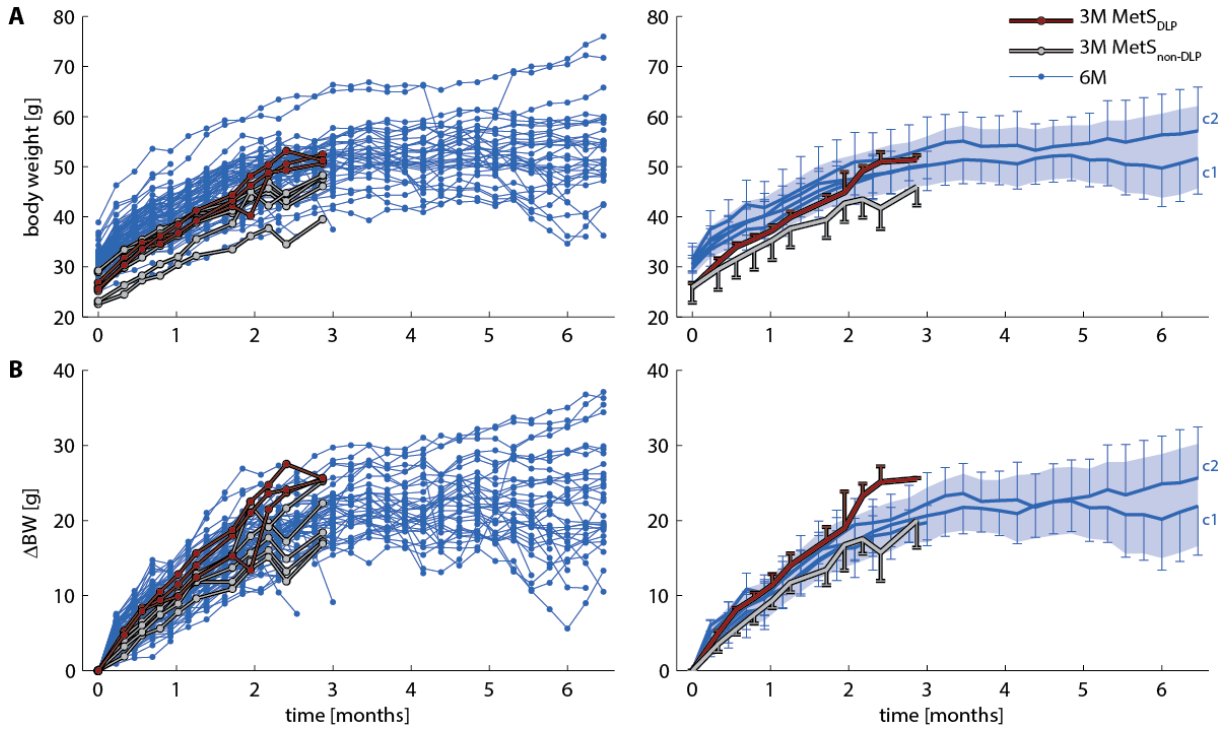

Figure 5.1

Body weight (A) and weight gain (B) in male E3L.CETP mice on a high-fat, high-cholesterol diet over time.

The left panels display individual data (dots connected with lines originate from the same individual), the right panels display the average longitudinal trend with the mean ± standard deviation for each point in time per cohort; the light blue shaded area depicts the mean ± standard deviation for when the cohorts are pooled. Data are colour-coded per study: cohorts from the six-month diet induction study are depicted in blue; dyslipidemic mice from the three-month diet induction study in red and the non-dyslipidemic mice in grey.

5.3.2 Plasma glucose and insulin

Whole blood glucose (Figure 5.2A) initially increases in response to the high-fat, high-cholesterol diet and then decreases after around three months to the baseline level in the six-month study. This is not found in the three-month study which shows a plateauing of plasma glucose after two months.

Although the plasma insulin (Figure 5.2B) profiles are a bit more difficult to interpret due to the large variation, glucose appears to peaks earlier (around one month after diet induction) than insulin (between two and three months after diet induction).

The right-hand side panels of Figure 5.2 depict the average glucose and insulin levels over time. For all five cohorts, the glucose profiles are quite similar overall. However, for insulin, this is not the case. Especially cohort 3 (with a follow-up to thirteen weeks) shows a major increase in insulin that is not reflected in the other cohorts. This explains the unexpected peak in insulin when considering all cohorts of this study at the same time (blue shaded area). If we would leave out this point in time, we can still agree that the average, overall insulin profile peaks later than seen in the glucose profile.

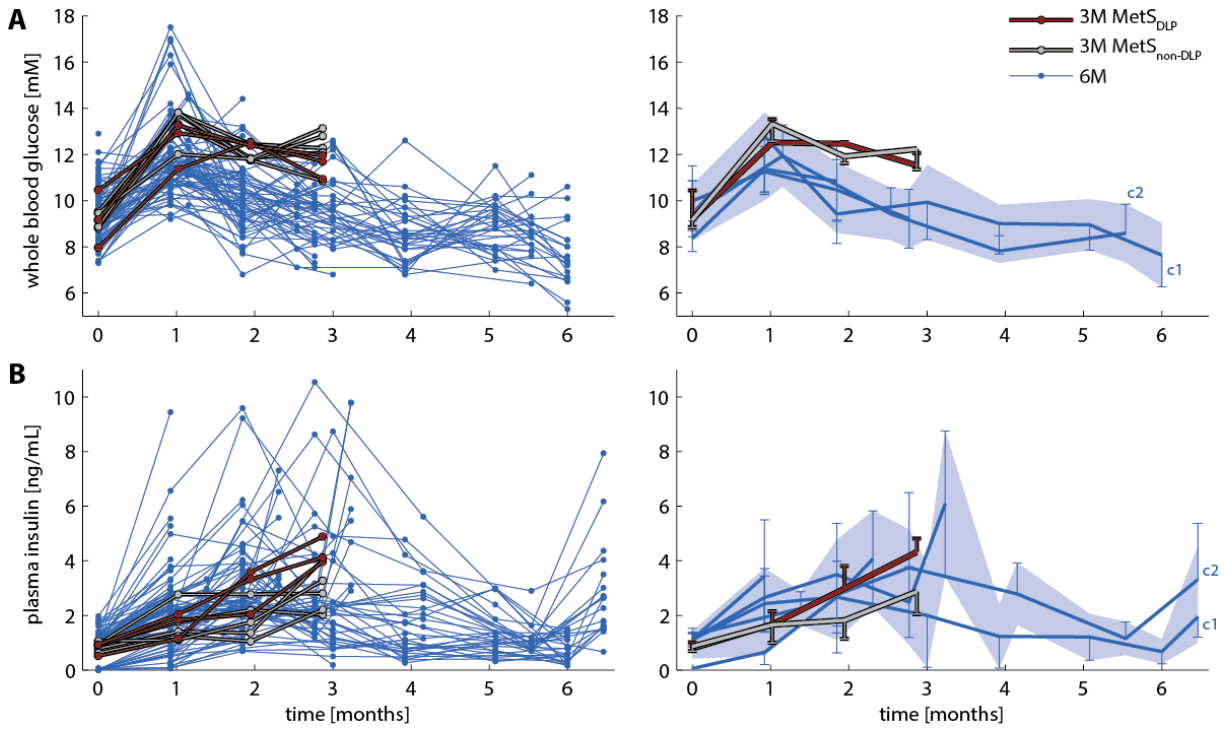

Figure 5.2

Whole blood glucose (A) and plasma insulin (B) levels in male E3L.CETP mice on a high-fat, high-cholesterol diet over time.

The left panels display individual data (dots connected with lines originate from the same individual), the right panels display the average longitudinal trend with the mean ± standard deviation for each point in time per cohort; the light blue shaded area depicts the mean ± standard deviation for when the cohorts are pooled. Data are colour-coded per study: cohorts from the six-month diet induction study are depicted in blue; dyslipidemic mice from the three-month diet induction study in red and the non-dyslipidemic mice in grey.

5.3.3 Plasma lipid pools

Whereas changes in the glucose and insulin domain are already apparent after one month of HFD+C, the response in circulating lipids appears later (Figure 5.3A) and plasma total cholesterol (TC; Figure 5.3B) increases drastically after three months of high-fat, high-cholesterol feeding. Plasma HDL-cholesterol (Figure 5.3C) fluctuates more and lacks a coherent pattern among the separate cohorts due to its large variability.

Interestingly, the variation in plasma lipid measurements is largest after four months of diet. If we would omit the variance when analysing the overall trend (light blue shaded area in the right-hand side panels of Figure 5.3), the concentrations of TG, TC, and HDL-C in the plasma appear to plateau after around three months up and remain at the same level up to six months.

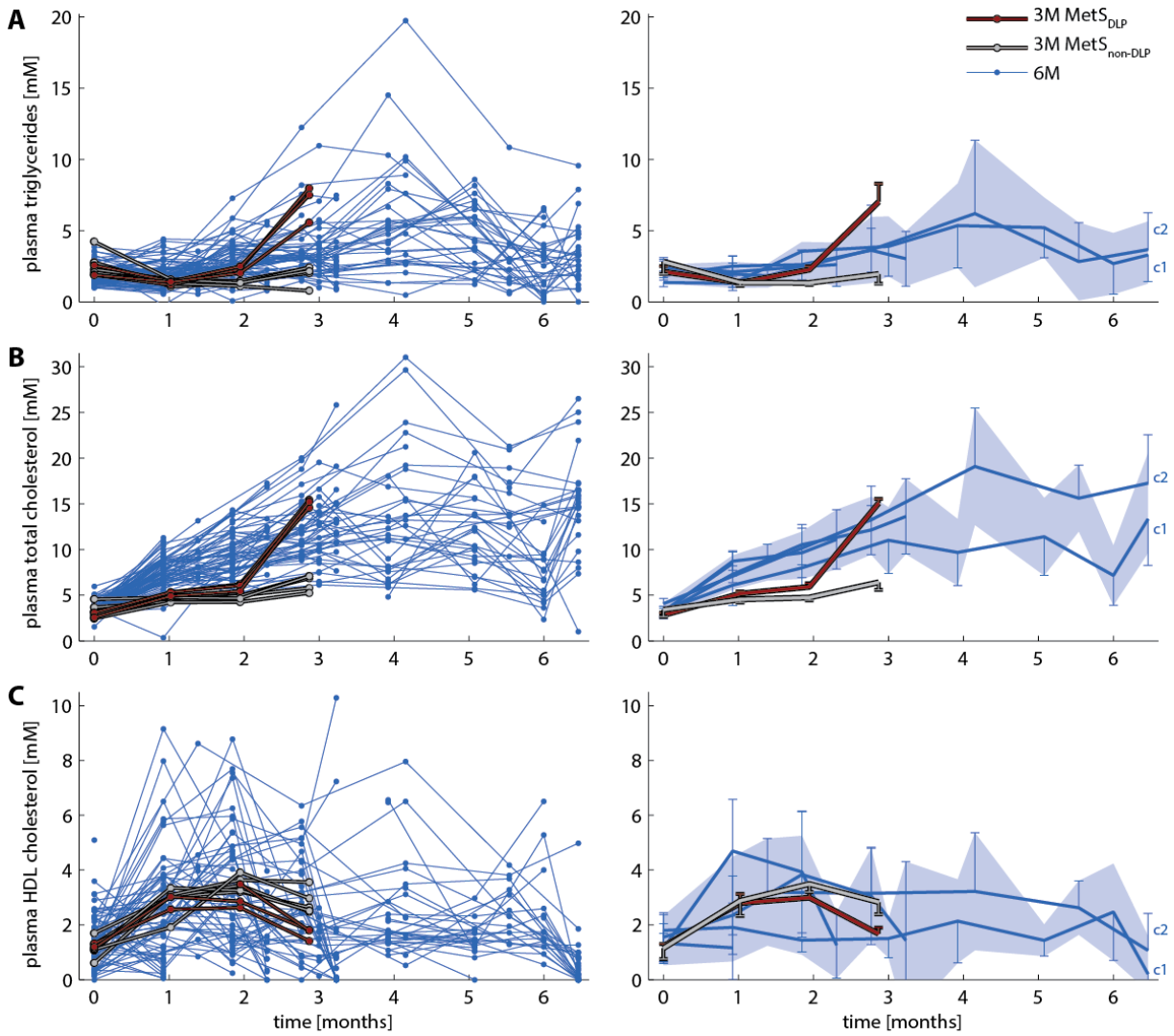

Figure 5.3

Plasma triglycerides (A), plasma total cholesterol (B) and plasma HDL-cholesterol (C) in male E3L.CETP mice on a high-fat, high-cholesterol diet over time.

The left panels display individual data (dots connected with lines originate from the same individual), the right panels display the average longitudinal trend with the mean ± standard deviation for each point in time per cohort; the light blue shaded area depicts the mean ± standard deviation for when the cohorts are pooled. Data are colour-coded per study: cohorts from the six-month diet induction study are depicted in blue; dyslipidemic mice from the three-month diet induction study in red and the non-dyslipidemic mice in grey.

5.3.4 Hepatic lipid pools

In contrast to plasma pools which could be assessed throughout the experiment, hepatic lipids were only available at the end of each respective cohort as depicted in Figure 5.4. A consistent incremental trend in the accumulation of both total (Figure 5.4B) and free cholesterol (FC; Figure 5.4C) is observed. On the contrary, considering the large variation, the hepatic TG pool (Figure 5.4A) remains stable over time.

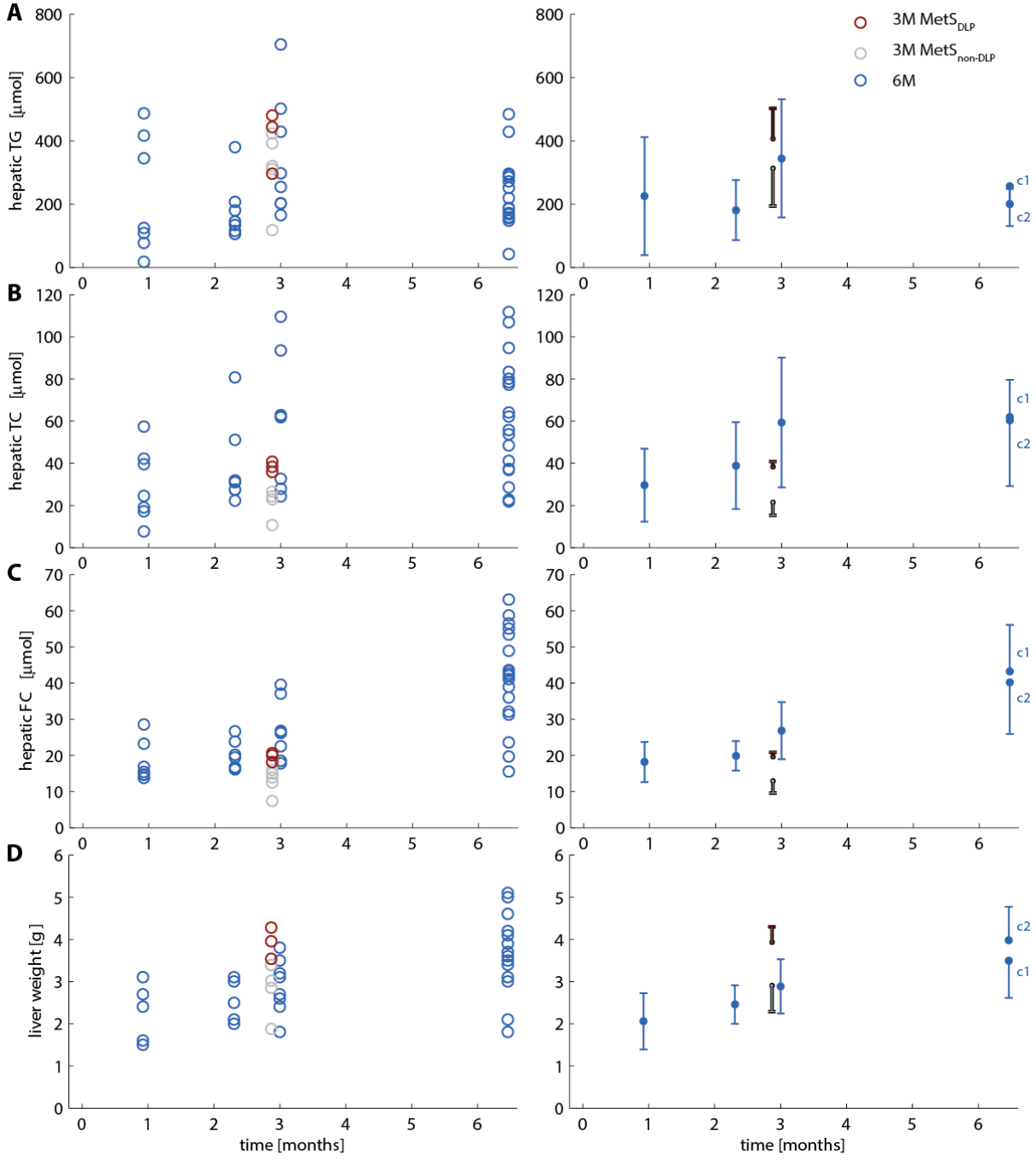

Figure 5.4

Hepatic triglycerides (A), hepatic total cholesterol (B), hepatic free cholesterol (C) and liver weight (D) in male E3L.CETP mice on a high-fat, high-cholesterol diet over time.

The left panels display individual data, the right panels display the average longitudinal trend with the mean ± standard deviation for each point in time per cohort. Data are colour-coded per study: cohorts from the six-month diet induction study are depicted in blue; dyslipidemic mice from the three-month diet induction study in red and the non-dyslipidemic mice in grey.

5.4 Phenotypic outcome in terms of dyslipidemic status after three months of diet induction

In the previous chapter, we have shown the identification and classification of (non)dyslipidemic status after three months of diet induction. The three-month study suggested a bimodal distribution in plasma TG versus plasma TC levels after three months of diet induction, whereby we classified the dyslipidemic ($MetS_{DLP}$) and non-dyslipidemic ($MetS_{non\text{-}DLP}$) phenotypes. Since the distinction in both plasma TG and plasma TC was very clear, and possibly as a result of the small population size, we could separate the animals manually into dyslipidemic (high TG and high TC) and non-dyslipidemic individuals (low TG and low TC).

Here we examine the distribution in plasma TG and plasma TC levels obtained from the six-month diet induction study. We assess whether the data from the six-month study can be classified using the $MetS_{DLP}$ and $MetS_{non\text{-}DLP}$ definitions. Figure 5.5 demonstrates that the much larger population of the six-month study shows a more continuous distribution than the bimodal outcome suggested by the three-month study. While appreciating the measurement accuracy of 1.5 CV% (coefficient of variation) for plasma TG and 0.8 CV% for cholesterol, it can be observed that the plasma TG levels are significantly lower than those in the three-month $MetS_{DLP}$ cohort (see Table 5.2), but not significantly different from those in the three-month $MetS_{non\text{-}DLP}$ cohort: the histogram of Figure 5.5C demonstrates that the majority of data points lies within the three-month $MetS_{non\text{-}DLP}$ range (mean ± standard deviation, i.e. 68%

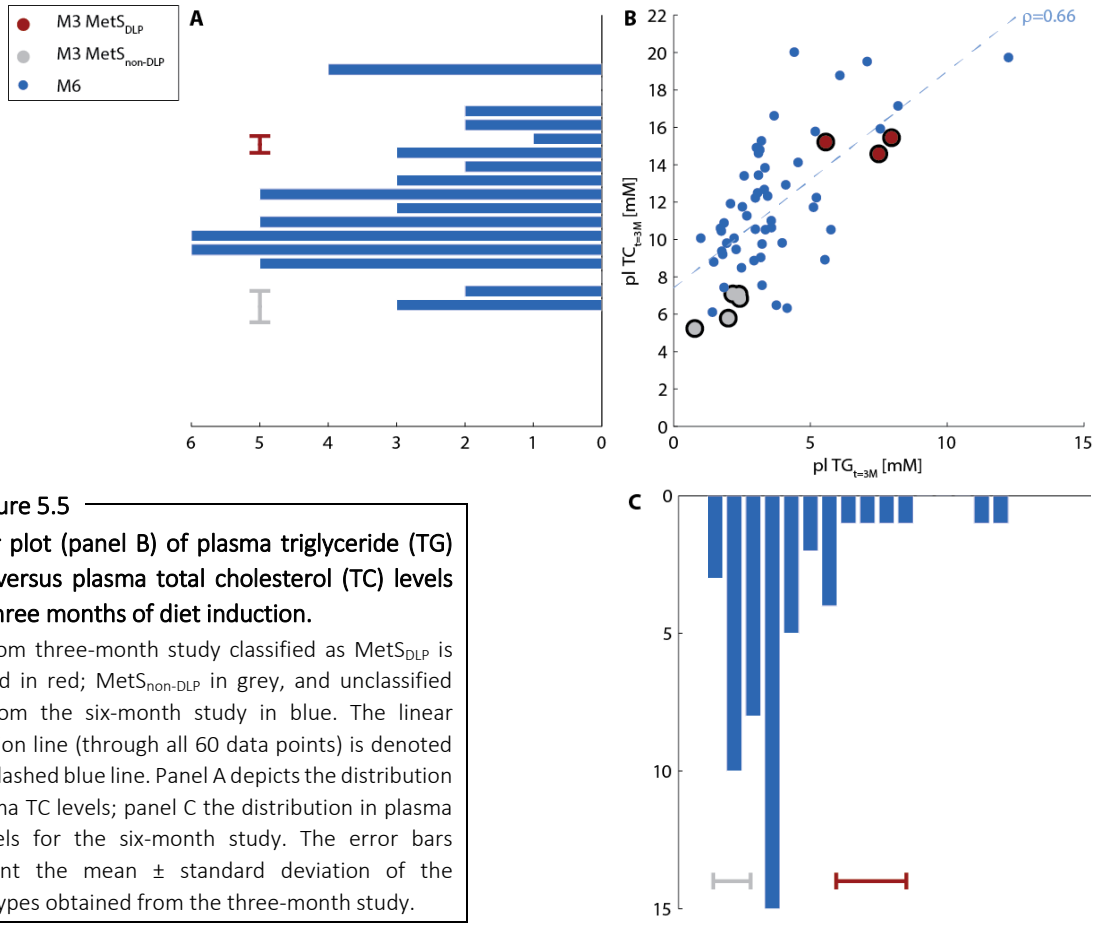

Figure 5.5

Scatter plot (panel B) of plasma triglyceride (TG) levels versus plasma total cholesterol (TC) levels after three months of diet induction.

Data from three-month study classified as $MetS_{DLP}$ is depicted in red; $MetS_{non\text{-}DLP}$ in grey, and unclassified data from the six-month study in blue. The linear regression line (through all 60 data points) is denoted by the dashed blue line. Panel A depicts the distribution in plasma TC levels; panel C the distribution in plasma TG levels for the six-month study. The error bars represent the mean ± standard deviation of the phenotypes obtained from the three-month study.

Table 5.2

Plasma triglyceride (TG) and total cholesterol (TC) levels after three months of dietary induction expressed as the mean ± standard deviation.

	plasma TG [mM]	plasma TC [mM]
$MetS_{DLP}$	7.0 ± 1.3 §§§	15.1 ± 0.4 §§§
$MetS_{non\text{-}DLP}$	1.9 ± 0.7 §§§	6.4 ± 0.8 §§§
M6 (pooled)	3.7 ± 2.2 *	11.9 ± 3.4 ###
M6-1	3.9 ± 2.1 ***,##	11.0 ± 3.6 #
M6-2	3.7 ± 3.1 ***	13.2 ± 3.7 ###
M6-3	3.6 ± 1.5 ***	12.1 ± 2.7 ###
M6-4	NA[1]	NA[1]
M6-5	NA[2]	NA[2]

Statistical significance levels obtained using a one-way ANOVA are depicted as:

§ P<0.05; §§ P<0.01; §§§ P<0.001 $MetS_{DLP}$ vs. $MetS_{non\text{-}DLP}$

* P<0.05; ** P<0.01; *** P<0.001 vs. $MetS_{DLP}$

# P<0.05; ## P<0.01; ### P<0.001 vs. $MetS_{non\text{-}DLP}$

[1] no data available; this cohort ends after ten weeks.

[2] no data available; this cohort ends after one month.

confidence interval) and a little above. On the other hand, plasma TC levels are significantly higher than those in the three-month $MetS_{non\text{-}DLP}$ group (see the histogram in Figure 5.5A) and characterised by a broader range, of which the majority lies in between the three-month $MetS_{DLP}$ and $MetS_{non\text{-}DLP}$ ranges.

In conclusion, the data from the six-month cohort cannot be classified using the previously made definitions in $MetS_{DLP}$ and $MetS_{non\text{-}DLP}$ since plasma TG is significantly different from $MetS_{DLP}$, and plasma TC is significantly different from $MetS_{non\text{-}DLP}$. However, from correlation and regression analyses (Figure 5.5B) it is evident that plasma TG and plasma TC are correlated (ρ=0.66, p=8.7e-9), although the R^2 of the linear regression line is just 0.44. Therefore we use a clustering approach to identify subgroups based on plasma TG and plasma TC levels after three months of diet induction.

5.5 Identification of subgroups in dyslipidemic status using a clustering approach

We combined both the three-month and six-month study data, yielding 60 data points describing plasma TG and plasma TC after three months of diet induction (data depicted in Figure 5.5B). These data were divided into subpopulations identified using a *k*-means clustering approach. [MacQueen, 1967] This method iteratively partitions the data by minimizing the squared Euclidean distance between cluster points and cluster centroid location. The clustering approach was performed using only plasma TG and TC values measured after three months of diet.

We performed the clustering procedure for two up to fifteen clusters. The initial centroid seeds were based on the centroid locations of the mean TG and mean TC in the three-month $MetS_{DLP}$ and $MetS_{non\text{-}DLP}$ populations. When identifying more than two clusters, the initial seed was complemented by random samples taken from the TG and TC data, assuming TG and TC to be normally distributed. For each number of clusters, the *k*-means clustering procedure was repeated 1,000 times. Figure 5.6 depicts the relationship between the obtained least squared Euclidean distance and the number of clusters used. Subdividing the data into at least two groups (as we already did with the $MetS_{DLP}$ and $MetS_{non\text{-}DLP}$ groups) reduced the squared Euclidean distance by 60%. Introducing increasingly more groups (n≥3) yielded a substantial decrease of the distance up to around four to five clusters. Although theoretically, the error

would become zero with 60 clusters (each point belonging to a single cluster), increasing the number of clusters above around 10 did not provide any significant improvement. To reduce the risk of overfitting, we, therefore, chose to work with up to seven clusters to analyse the obtained cluster topologies. Figure 5.7 depicts several acceptable obtained cluster topologies. When using up to four clusters (Figures 5.7A2-C4), the algorithm performs its separation mainly based on plasma TC levels. When starting to use five clusters or more (Figures 5.7A5-B5), we observe the effect of TG taken into account as well. The more clusters that are introduced, the more TG begins to play a role as well, which is probably due to the fact that the range in which the TC values lie is larger than for TG.

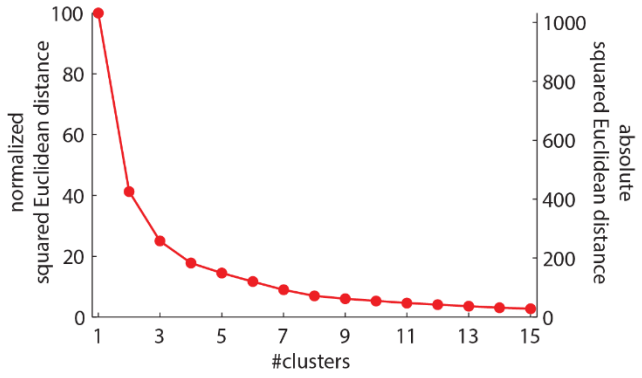

Figure 5.6
Convergence with increasing numbers of clusters being introduced.

However, using four clusters we notice a single outlier to be allocated to a single cluster (Figure 5.7B4) and this remains an issue for increasing numbers of clusters (Figures 5.7A5, A6, A7, B7, C7). This raises the question of how many subpopulations should be identified. As a pre-requisite, we used the earlier classified animals from the three-month cohort (depicted by the dots with black border). We imposed that the data points from the three-month $MetS_{DLP}$ group would remain together in one group, and *vice versa* for the three-month $MetS_{non\text{-}DLP}$ group. Therefore we chose to work with three subpopulations (see Figure 5.7A3): cluster 2 (in green) representing the lowest degree of dyslipidemia (DLP-1; previously referred to as $MetS_{non\text{-}DLP}$), cluster 1 (in orange) the highest degree of dyslipidemia (DLP-3; previously referred to as $MetS_{DLP}$) and cluster 3 (in blue) as intermediate range of dyslipidemia (DLP-2). The experimental time course data on body weight and plasma and liver metabolite pools corresponding to these subpopulations is categorically shown in Figures 5.11-5.14 in Appendix 5.8.2. These clusters are separated well and are significantly different (see Table 5.3) from each other in both plasma TG and plasma TC. We also assessed the quality of the clustering procedure using silhouette plots (see Figure 5.10 in Appendix 5.8.1), providing evidence that the data has been separated well into the corresponding clusters.

Table 5.3
Cluster characteristics (one-way ANOVA) at three months of diet induction corresponding to Figure 5.7A3.

			plasma triglycerides$_{t=3M}$ [mM]				plasma total cholesterol$_{t=3M}$ [mM]			
		n	mean	median	std	range	mean	median	std	range
DLP-1: low DLP	cluster 2	25	2.5$^{\alpha}$	2.2	1.1	0.8-5.5	8.4$^{\alpha}$	8.9	1.6	5.3-10.6
DLP-2: intermediate DLP	cluster 3	24	3.4$^{\beta}$	3.2	0.9	1.8-5.8	12.5$^{\beta}$	12.3	1.5	10.5-15.3
DLP-3: high DLP	cluster 1	11	6.9$^{\gamma}$	7.1	2.3	3.7-12.2	17.2$^{\gamma}$	16.6	2.0	14.6-20.0
			$^{\alpha}$ DLP-1 vs. DLP-2: p=0.0022				$^{\alpha}$ DLP-1 vs. DLP-2: p=3.1e-12			
			$^{\beta}$ DLP-2 vs. DLP-3: p=3.9e-7				$^{\beta}$ DLP-2 vs. DLP-3: p=9.1e-9			
			$^{\gamma}$ DLP-1 vs. DLP-3: p=4.3e-9				$^{\gamma}$ DLP-1 vs. DLP-3: p=9.9e-16			

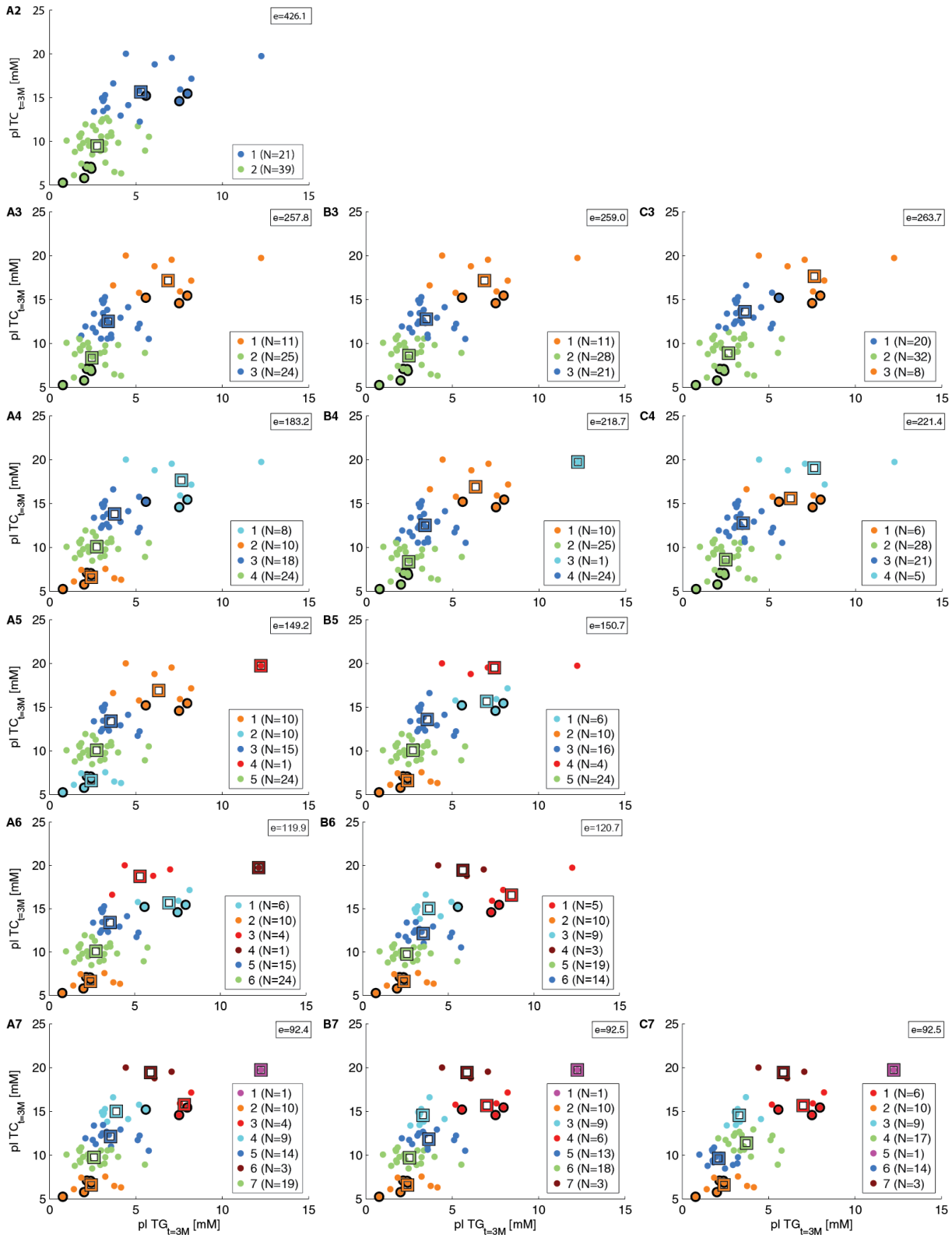

Figure 5.7

Clustering results of dyslipidemic status after three months of diet induction.

Panels A2-A7 describe the results for 2-7 clusters in total. When multiple model topologies were obtained that have a similar (absolute) sum of squared Euclidean distance (depicted as e in the legend), the corresponding results are depicted in panels B-C. Each dot (n=60) represents a single individual and is colour-coded for the cluster to which it was assigned. The previously identified mice from the three-month study are highlighted with a black border. Cluster centroid locations are depicted by the squares in corresponding colours.

5.6 Earlier detection of phenotypic outcome?

The data from the three-month study suggested that the plasma TG and plasma TC levels after two months of diet could be an early indicator for phenotypic outcome. Because of the limited population size, it had to be investigated carefully whether this early detection provides accurate predictions of dyslipidemia development.

First, we analysed the data from the second month after diet induction in a similar fashion as was done in section 5.4. From Table 5.4 and Figure 5.8 we infer that the plasma TG and TC data are correlated (ρ=0.52, p=2.8e-5) in time, but weaker (R^2 of the linear regression line is 0.27) than after three months.

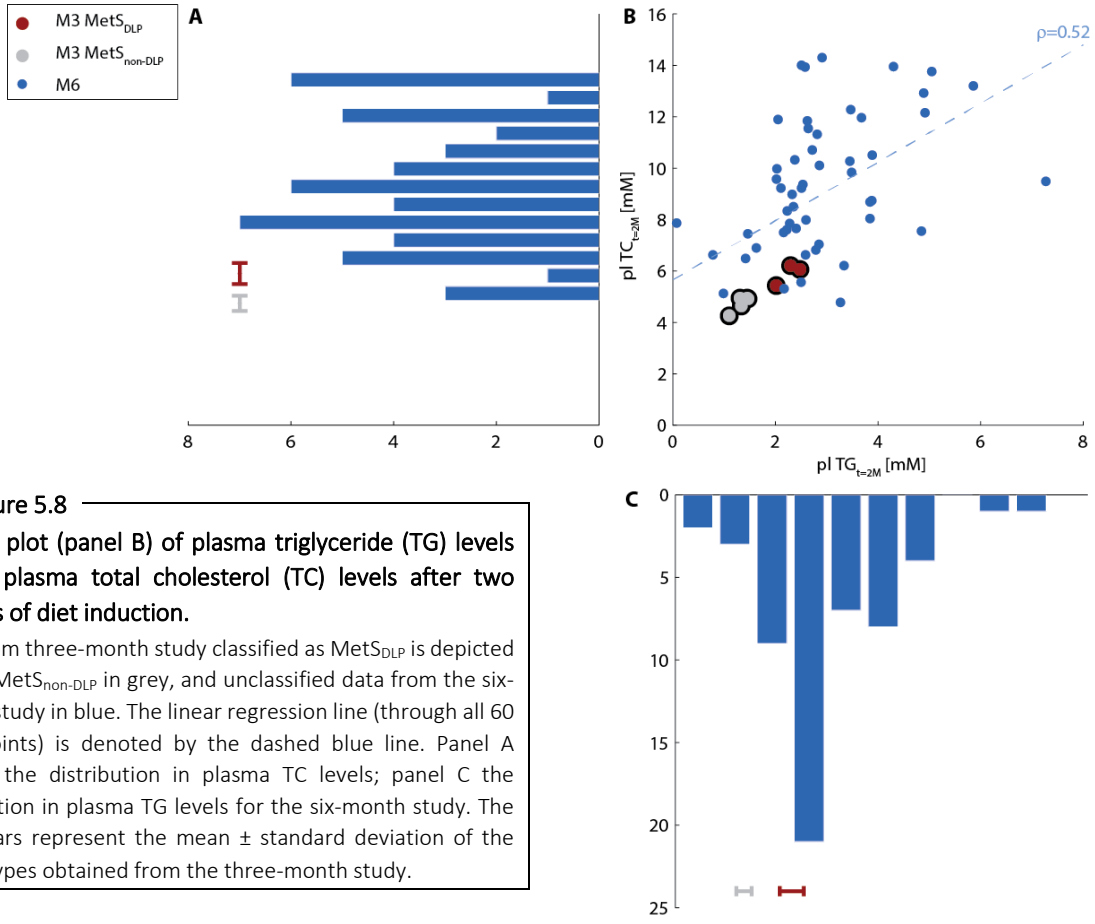

Figure 5.8

Scatter plot (panel B) of plasma triglyceride (TG) levels versus plasma total cholesterol (TC) levels after two months of diet induction.

Data from three-month study classified as $MetS_{DLP}$ is depicted in red; $MetS_{non\text{-}DLP}$ in grey, and unclassified data from the six-month study in blue. The linear regression line (through all 60 data points) is denoted by the dashed blue line. Panel A depicts the distribution in plasma TC levels; panel C the distribution in plasma TG levels for the six-month study. The error bars represent the mean ± standard deviation of the phenotypes obtained from the three-month study.

Table 5.4

Plasma triglyceride (TG) and total cholesterol (TC) levels after two months of dietary induction expressed as the mean ± standard deviation.

	plasma TG [mM]	plasma TC [mM]
$MetS_{DLP}$	2.3 ± 0.2 §§§	5.9 ± 0.4 §§
$MetS_{non\text{-}DLP}$	1.3 ± 0.1 §§§	4.7 ± 0.3 §§
M6 (pooled)	3.0 ± 1.2 ##	9.4 ± 2.6 *,###
M6-1	3.6 ± 1.3 ***	8.0 ± 2.3 ##
M6-2	NA[1]	NA[1]
M6-3	2.6 ± 1.0 *,##	10.5 ± 2.2 **,###
M6-4	2.5 ± 1.1 ###	9.6 ± 2.7 *,###
M6-5	NA[2]	NA[2]

Statistical significance levels obtained using a one-way ANOVA are depicted as:

§ P<0.05; §§ P<0.01; §§§ P<0.001 $MetS_{DLP}$ vs. $MetS_{non\text{-}DLP}$

* P<0.05; ** P<0.01; *** P<0.001 vs. $MetS_{DLP}$

# P<0.05; ## P<0.01; ### P<0.001 vs. $MetS_{non\text{-}DLP}$

[1] no data measured at eight weeks of dietary induction only at six or twelve weeks).

[2] no data available; this cohort ends after one month.

Next, we examined the trend in both plasma TG and plasma TC levels between two and three months of diet induction. Figure 5.9 displays that the three-month $MetS_{DLP}$ phenotype shows large increases in plasma TG (Figure 5.9A) and plasma TC (Figure 5.9B), whereas the change in the three-month $MetS_{non\text{-}DLP}$ phenotype is only minor. The pattern in the six-month cohort was not consistent and largely deviates among animals. Nevertheless, and more importantly, the newly defined phenotypic clusters do reveal a coherent pattern: both ΔTG and ΔTC increase with the degree of dyslipidemia.

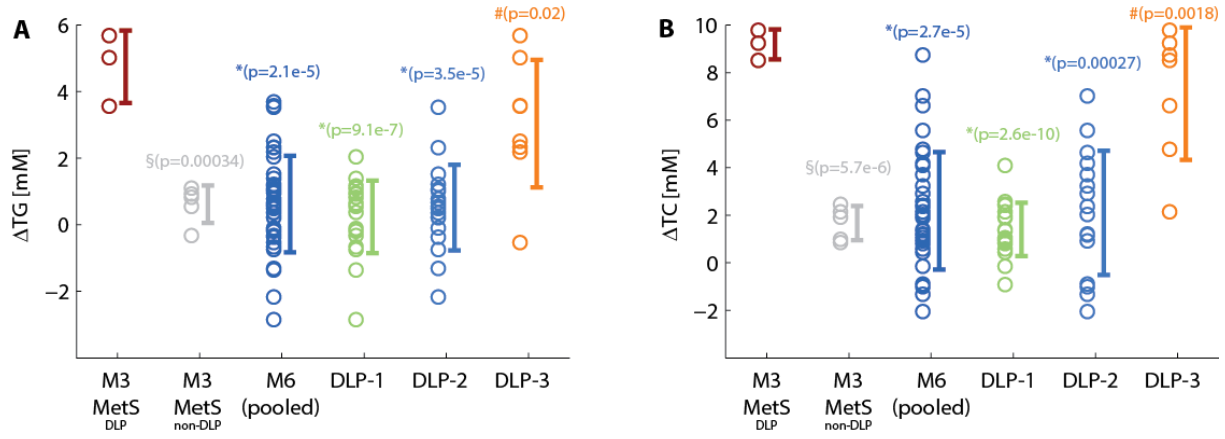

Figure 5.9

Change in plasma triglycerides (panel A) and plasma cholesterol (panel B) between three and two months of diet induction.

Individual data points are depicted with circles for the respective groups on the horizontal axis. The corresponding error bar represents the mean ± standard deviation for each group. It should be noted that not all data could be taken into account since only from two cohorts in the six-month study data of both the second and third month were available (see also Tables 5.2 and 5.4). Therefore, the M6 (pooled) group consists of 34 data points (but contains actually 52 animals); DLP-1 has 21 data points (25 animals); DLP-2 has eighteen data points (24 animals) and DLP-3 has eight data points (11 animals).

Statistical significance levels obtained using a one-way ANOVA are depicted as:

§ $MetS_{DLP}$ vs. $MetS_{non\text{-}DLP}$

* vs. $MetS_{DLP}$

vs. $MetS_{non\text{-}DLP}$

5.7 Discussion

The assessment of the long-term development of the Metabolic Syndrome in male E3L.CETP mice upon a high-fat, high-cholesterol diet using both a larger population and a longer timespan yielded a large dataset. In this chapter, we focused on the identification of phenotypes differing in degree of dyslipidemia development.

5.7.1 Heterogeneity in MetS development

We considered data from an experiment that uses the same set-up and design as described in chapter 4. Strikingly, we found that the variability increased with increasing population size, rather than providing a narrower confidence interval. [Cumming *et al.*, 2007] Phenotype development appears to be more disperse and heterogeneous than anticipated based on the initial study, where we found two clear-cut subpopulations based on the three-month plasma triglyceride and total cholesterol levels.

It is known that despite experimental standardization (same diet, same genetic background, animals obtained from the same breeding facility, etc.), differences between laboratories and lab technicians may affect reproducibility of animal experiments. [Richter *et al.*, 2009] Also, we have to acknowledge that although these mice may be genetically identical siblings, each of these animals is a unique, independent variable in our experiments.

These experiments were performed using the same protocol, except for the laboratory in which and lab technician by whom the experiments were performed. In addition, it appeared that the mice in the six-month cohort were roughly one month older at the start of the diet induction experiment than the mice in the three-month cohort. However, correcting for this one-month difference in timeline (data not shown), did not improve the comparison of the data. Therefore, we chose to adhere to the original timeline since the start of the diet induction as a basis for comparison of data among both cohorts.

To the best of our knowledge, we were not able to identify substantial causes of differences among both studies and therefore acknowledge that the variability with which this animal model develops MetS is larger than anticipated from the initial study. The longer timespan involved could possibly have induced effects of ageing, which might have implications on the metabolic endpoints of this longitudinal study. [Whitehead *et al.*, 2014]

Moreover, from the human perspective we known that the MetS population is largely heterogeneous and that MetS can present itself in many different phenotypic outcomes. Therefore we decided to identify different subpopulations specifying phenotypic outcome using this animal model of MetS development.

5.7.2 Identification of subpopulations based on plasma TG and TC after three months of feeding a high-fat, high-cholesterol diet

In the previous chapter, we identified two subpopulations in the three-month cohort: $MetS_{DLP}$ and $MetS_{non\text{-}DLP}$. Based on these findings, we initiated our clustering approach using plasma TG and plasma TC after three months of diet induction as the two entities based on which the subgroups were separated.

The simple *k*-means clustering procedure proved to be sufficient to classify our data. Since MetS is considered to be a multi-factorial disorder in which both lipid and glucose regulation are disturbed, we could possibly extend the clustering method to include also other measured entities such as plasma glucose and/or insulin levels, or e.g. body weight.

5.7.3 Taking the time-dependency of MetS development into account in the identification of subpopulations

The time course data for the newly introduced subpopulations (see Figures 5.11-5.14 in Appendix 5.8.2) shows a coherent separation among animals around the three months' time point, but this separation does not persist for up to six months. It would be interesting to see whether the overall separation could be improved by incorporating time course data into the clustering procedure. This would require more sophisticated machine learning techniques such as mixed-effect modelling approaches that have been used for the clustering of time course gene expression data. [Luan and Li, 2003; Schliep *et al.*, 2003]

5.7.4 Using a systems approach to identify subpopulations

Alternatively, we could use our systems approach to employ modelling of the six-month dataset using MINGLeD with ADAPT. Data processing would become a challenge here due to the disperse, heterogeneous data of the different cohorts. To benefit from the intermediate measurements of metabolic fluxes and hepatic lipid pool sizes, the data should be pooled carefully. Since we have seen that different animals may respond much differently than others, we should first test whether the measured fluxes and hepatic pools originate from cohorts that are overall similar and can, therefore, be considered in the estimation of the time course fluxes and hepatic pool sizes.

Simply pooling the data of the five individual cohorts may lead to observing patterns in the data that are probably due to artefacts. This can e.g. be seen in the plasma total cholesterol data. The shaded blue area in the right-hand side panel of Figure 5.3B represents the pooled data and indicates an oscillating pattern between three and six months. Since the data pre-processing for ADAPT involves both sampling and interpolation, this may yield splines that start oscillating to meet the individual mean data points although visually we would probably regard this pattern to be an artefact and would draw a plateauing line through the plasma total cholesterol data over the time course of six months. This large variability issue will, therefore, require careful assessment of data handling prior to the model fitting by ADAPT.

In [Paalvast *et al.*, manuscript in preparation] we show that it is feasible to employ our systems approach to separate responders from non-responders based on the modelled trajectories, rather than pre-selecting them based on the baseline plasma TG and plasma TC data as we did in Section 5.2. However, these baseline criteria for responders/non-responders do provide a "ground truth" with which the results of the *in silico* classification could be verified.

5.7.5 Conclusion

Male E3L.CETP mice develop Metabolic Syndrome after being fed with a high-fat, high-cholesterol diet for at least three months. The development of MetS symptoms mainly occurs in the first three months of the diet induction and stabilizes in the later months in a time window up to six months. The degree to which these animals develop dyslipidemia is highly heterogeneous. We have identified three different subpopulations that develop dyslipidemia to different degrees (relatively low, intermediate and relatively high) based on the three-month plasma triglyceride and plasma total cholesterol levels.

5.8 Appendix

5.8.1 Silhouette analysis

A method to graphically assess the clustering performance is provided by silhouette plots. [Rousseeuw, 1987] Silhouettes represent how well each object lies within its cluster and which objects are merely somewhere in between clusters. These silhouettes allow for evaluating the cluster performance and may assist in identifying an appropriate number of clusters for the examined data.

Figure 5.10 displays the silhouettes for the clustering results using two up to seven clusters. The silhouette plot consists of one bar for each object (data point) in the corresponding cluster. The silhouette value measures how well the object has been classified, i.e. how well the object is matched to the resulting clusters. A silhouette value close to one implies that the within-cluster-dissimilarity is much smaller than the smallest between-cluster-dissimilarity. When that is the case, we can say with confidence that the object has been assigned to the appropriate cluster. A silhouette value close to zero implies that it is unclear whether the object is correctly assigned to its cluster, or whether it should actually belong to another cluster. Silhouette values close to minus one indicate that the object actually lies closer to another cluster than the cluster to which it was assigned. Hence, these objects are labelled as being misclassified.

From Figure 5.10 we can appreciate that an increasing number of clusters being introduced, decreases the silhouette values per cluster. Little misclassified objects were obtained for the clustering results with up to seven clusters. The previously made decision of using three clusters (Figure 5.10B) is strengthened by its silhouette plot that shows little misclassified objects and relatively high silhouette values throughout the clusters.

5.8.2 Clustering results in terms of time course body weight and plasma and liver metabolites

Figures 5.11-5.14 show the average (Figures 5.11-5.12) and individual (Figures 5.13-5.14) data of the six-month diet induction study as clustered using plasma TG and plasma TC at the three months' time point in the identified dyslipidemic categories according to the lowest (DLP-1), intermediate (DLP-2), and the highest degree of dyslipidemia (DLP-3).

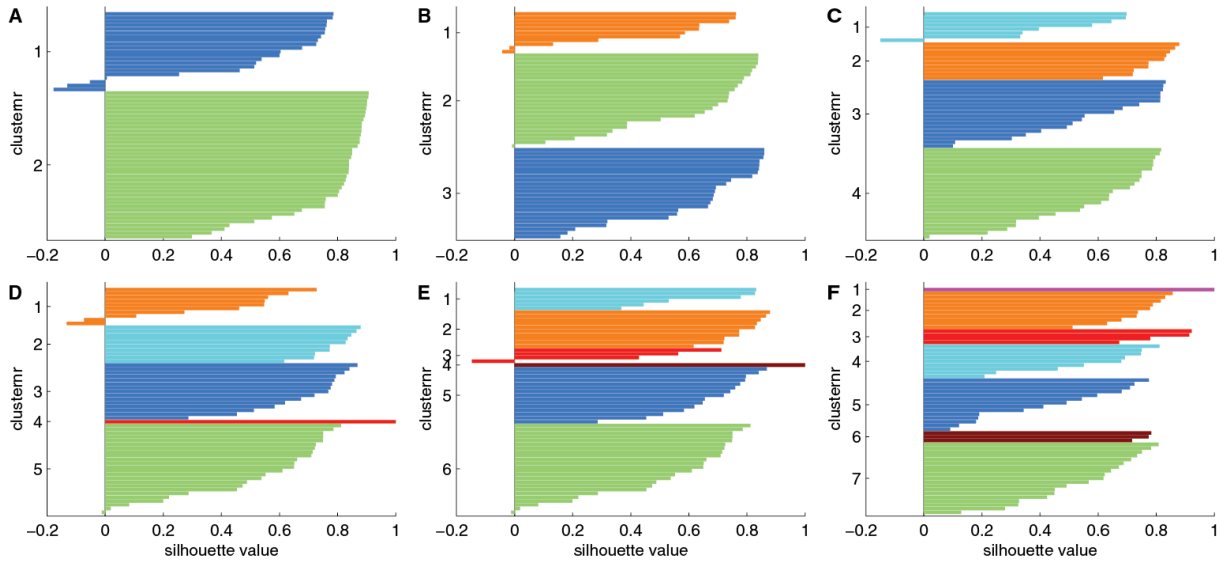

Figure 5.10

Silhouette plots for two (panel A) through seven (panel F) clusters.

These silhouette plots correspond to the cluster topologies depicted in Figures 5.7A2-A7.

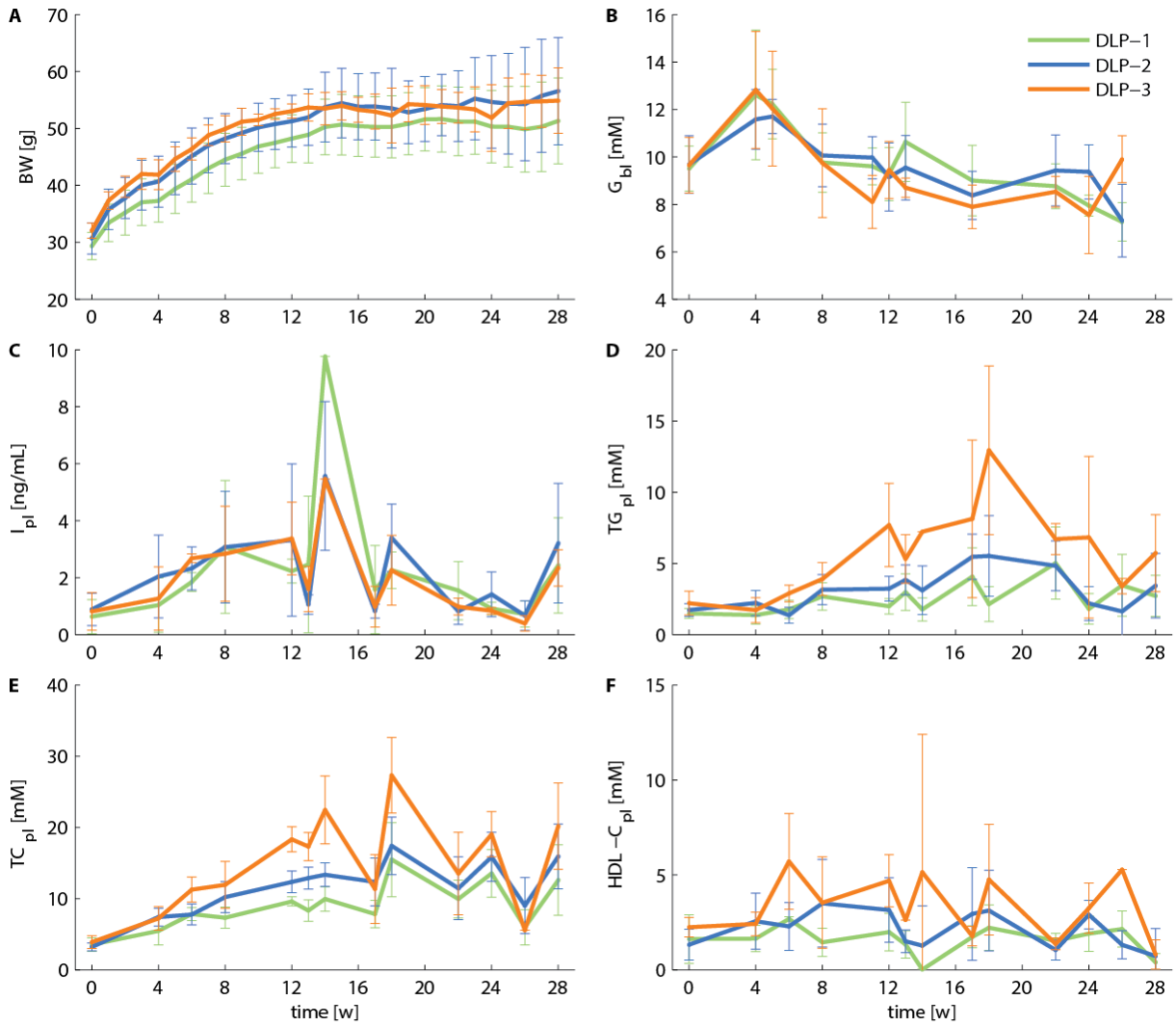

Figure 5.11

Average body weight and plasma metabolite pool data in the different dyslipidemic subpopulations.

DLP-1 corresponds with the lowest degree of dyslipidemia, DLP-2 with an intermediate degree of dyslipidemia, and DLP-3 with the highest degree of dyslipidemia.

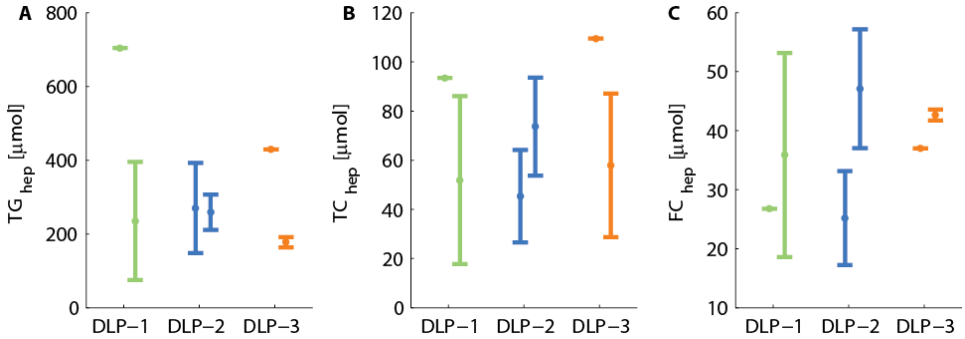

Figure 5.12

Average hepatic lipid pools (error bars: mean ± standard deviation) in the different dyslipidemic subpopulations.

The error bars on the left depict data obtained after thirteen weeks of diet induction; the right error bars after 28 weeks.

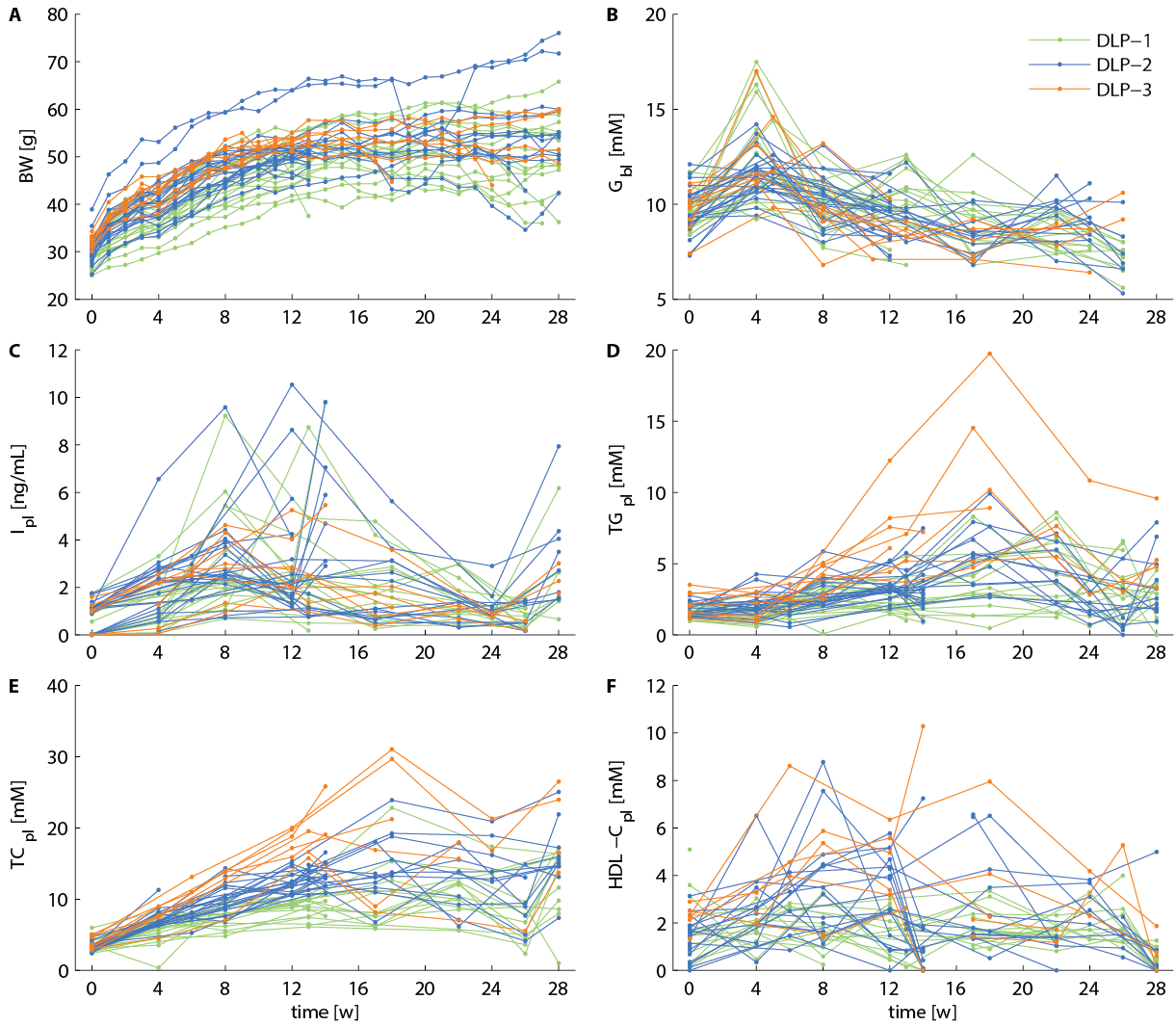

Figure 5.13

Individual body weight and plasma metabolite pools in the different dyslipidemic subpopulations.

DLP-1 corresponds with the lowest degree of dyslipidemia, DLP-2 with an intermediate degree of dyslipidemia, and DLP-3 with the highest degree of dyslipidemia.

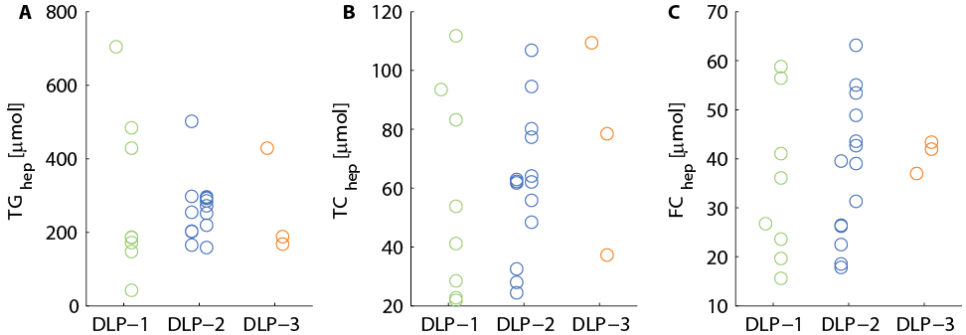

Figure 5.14

Individual hepatic lipid pools in the different dyslipidemic subpopulations.

The dots on the left for each subpopulation depict the data obtained after thirteen weeks of diet induction; the dots on the right after 28 weeks.

6

Computational modelling of energy balance in individuals with Metabolic Syndrome

This chapter is submitted as:

Rozendaal YJW, Wang Y, Hilbers PAJ, van Riel NAW. Computational modelling of energy balance in individuals with Metabolic Syndrome. *BMC Systems Biology*, 2018

A positive energy balance is considered to be the primary cause of the development of obesity-related diseases. Treatment often consists of a combination of reducing energy intake and increasing energy expenditure. Here we use an existing computational modelling framework describing the long-term development of Metabolic Syndrome (MetS) in mice with a human-like metabolic system. This model was used to analyse energy expenditure and energy balance in a large set of individual model realizations.

We developed and applied a strategy to select specific individual models for a detailed analysis of heterogeneity in energy metabolism. Models were stratified based on energy expenditure. A substantial surplus of energy was found to be present during MetS development, which explains the weight gain during MetS development. In the majority of the models, energy was mainly expended in the peripheral tissues, but also distinctly different subgroups were identified.

In silico perturbation of the system to induce increased peripheral energy expenditure implied changes in lipid metabolism, but not in carbohydrate metabolism. *In silico* analysis provided predictions for which individual models an increase of peripheral energy expenditure would be an effective treatment.

The computational analysis confirmed that the energy imbalance plays an important role in the development of obesity. Furthermore, the model is capable to predict whether an increase in peripheral energy expenditure – for instance by cold exposure to activate brown adipose tissue (BAT) – could resolve MetS symptoms.

6.1 Introduction

A positive energy balance is a major contributor to the development of obesity and its related disorders such as the Metabolic Syndrome (MetS). [Romieu *et al.*, 2017; Hill *et al.*, 2012; Hamilton *et al.*, 2007; Rodrigues *et al.*, 2016] Given the obesity-driven pathophysiology of MetS, the main driver for weight gain is considered to be the surplus of energy caused by excessive caloric intake (overnutrition) and/or combined with insufficient energy utilization, characterised by a sedentary lifestyle with little physical activity. [Pang *et al.*, 2014; Romieu *et al.*, 2017] Treatment of MetS is therefore often aimed at diminishing the surplus of energy in the system. This can be accomplished by making adjustments at both sides of the equation, but we are in particular interested in how increasing energy expenditure (EE) could contribute to the treatment of MetS.

Energy expenditure comprises multiple entities that consume energy, of which the most important ones include basal metabolic activity to maintain e.g. body temperature and skeletal muscle activity. The latter can easily be stimulated by increasing physical activity. However, brown adipose tissue (BAT) also plays an important role in thermogenesis and energy management. [Nedergaard and Cannon, 2010; Cannon and Nedergaard, 2004; Chechi *et al.*, 2014; Lidell *et al.*, 2014; Lee *et al.*, 2013] Recent studies have shown that activation of BAT has beneficial effects on weight loss, implying that this may be a promising therapeutic target against MetS. [Bartelt and Heeren, 2014; Broeders *et al.*, 2015; Hanssen *et al.*, 2015] Activated BAT combusts substantial amounts of triglycerides and glucose in the circulation. [Hanssen *et al.*, 2015; Khedoe *et al.*, 2015; Wang *et al.*, 2015; Berbée *et al.*, 2015; Schlein *et al.*, 2016] A clinically feasible way to activate BAT is by cold exposure. [Lichtenbelt *et al.*, 2014; Romu *et al.*, 2016] Most of these studies do show an increased energy expenditure but

allow for direct compensation by increased food intake. To aid our understanding, we demonstrate a method to study the effects of increased energy expenditure isolated from other possible compensatory mechanisms. Since the effectiveness of such treatments may also strongly depend on the differential response of patients, our method will also take this into consideration.

In chapter 4, we developed a computational modelling framework describing the progressive and heterogeneous development of MetS. [Rozendaal *et al.*, 2018b] This study yielded an extensive library of n=1,000 different model realizations. This ensemble of models was established by Monte Carlo sampling of experimental data assessed from a pre-clinical mouse model that describe onset and development of diet-induced MetS over a timespan of three months. This Monte Carlo sampling entails the generation of random samples of the data to account for experimental uncertainties. Subsequent model fitting yielded alternative parameterizations that describe the same phenotypic readout (in terms of plasma and liver biomarkers characteristic for MetS) but are established by different combinations of underlying model parameters and metabolic fluxes to match the sampled data to which this model realization was calibrated.

This collection of n=1,000 model realizations entails uniquely different parameter sets and different model outcomes. However, since the data to which each model instance has been calibrated was sampled from the same experimental data set, these different model realizations do describe the same overall observable phenotype. Each model realization yields a different model outcome, which is a result of quantification of uncertainty that was introduced by variability in data. So far, this collection of models was analysed on the population level. [Allen *et al.*, 2016] Here, we evaluate this virtual patient cohort using an individualized perspective using so-called virtual patients. [Kansal and Trimmer, 2005; Zazzu *et al.*, 2013; Alkema *et al.*, 2006; Kononowicz *et al.*, 2015; de Graaf *et al.*, 2009] Virtual patients can be regarded as different sets of model simulations that are representative of the differences in real-life. These virtual patients can subsequently be used in virtual trials to delineate how different individuals may respond differently to perturbations to the system and hence how effective potential treatment interventions may be. [Viceconti *et al.*, 2016; Schork, 2015]

Whereas food intake was explicitly incorporated in the model, the energy balance had not been analysed. To identify differences between virtual patients in terms of energy handling, we first quantify the variation in energy expenditure and resulting energy balance and use this information for further stratification. Since the virtual patient cohort consists of n=1,000 different model realizations, we expect to find various combinations of metabolic fluxes underlying MetS.

Secondly, we analyse how robust the system is to changes in energy handling. Sensitivity and control of this type of metabolic systems are often assessed by applying perturbation experiments and is similar to methodologies often used in metabolic control analysis and flux balance analysis. [Moreno-Sánchez *et al.*, 2008; Orth *et al.*, 2010] Here we apply perturbations that induce increased peripheral energy expenditure – representing an increase in BAT activity. Energy is expended in the model by both the liver and the periphery. Peripheral tissues include metabolically active tissues such as skeletal muscle and adipose tissue. Hence, peripheral energy expenditure describes, amongst others, thermogenesis by BAT. [Nedergaard and Cannon, 2010; Lidell *et al.*, 2014; Din *et al.*, 2018] We therefore hypothesize that by simulating an increase in peripheral

energy expenditure, activation of BAT can be studied in an *in silico* setting. We expect this additional drainage of energy from the peripheral compartment to diminish the energy surplus in the system. We hypothesize this perturbation leads to a decrease in peripheral triglyceride pool and also result in improvement in plasma biomarkers.

6.2 Computational model of energy management in Metabolic Syndrome

The previously published computational model describing the metabolic system in both healthy and Metabolic Syndrome conditions (Model Integrating Glucose and Lipid Dynamics; MINGLeD; chapter 3) [Rozendaal *et al.*, 2018b] is schematically displayed in Figure 6.1. MINGLeD consists of four compartments (liver, intestine, plasma, and periphery) in which carbohydrate, lipid and cholesterol species are described. The peripheral compartment comprises the major metabolic tissues (except for the liver, intestine, and plasma) including adipose tissue and (skeletal) muscle.

MINGLeD describes energy handling with two components: energy intake (known from food intake data; depicted by the grey fluxes from the intestinal lumen in Figure 6.1) and energy expenditure (EE; predicted by the model). Energy expenditure is represented by respiration of acetyl-Coenzyme A (ACoA) in the liver (indicated by the blue arrow in Figure 6.1; EE_{hep}) and in the peripheral compartment (indicated by the red arrow in Figure 6.1; EE_{per}).

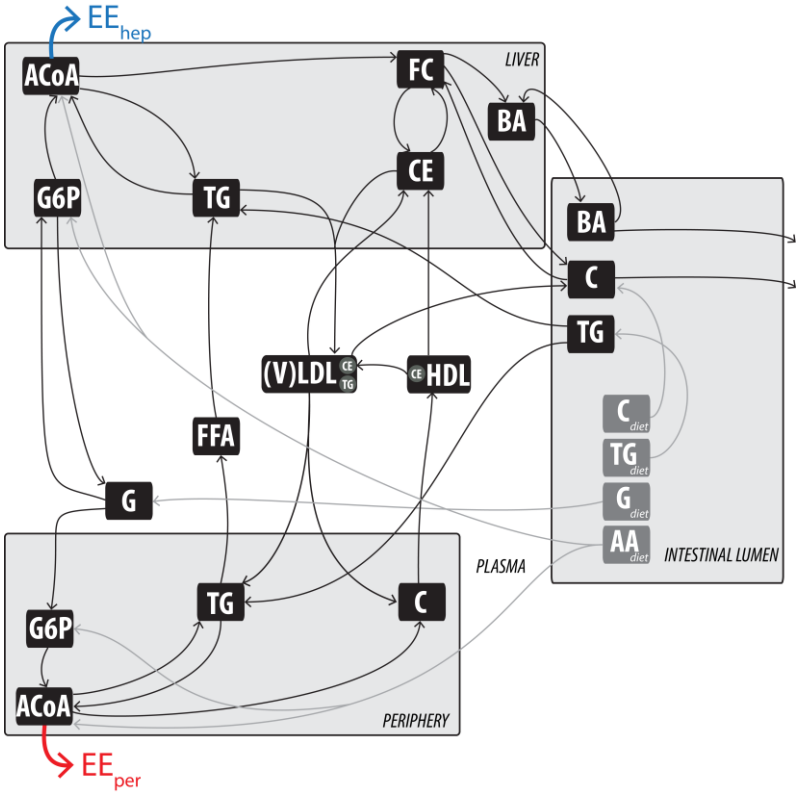

Figure 6.1

Schematic overview of energy expenditure in the computational model MINGLeD.

Energy expenditure takes place in both hepatic (indicated by the blue arrow) and peripheral (indicated by the red arrow) compartments.

In chapter 4, the model was calibrated to data derived from E3L.CETP mice that respond in a human-like manner [van den Hoek *et al.*, 2014; Westerterp *et al.*, 2006] to a high-fat diet supplemented with cholesterol, thereby inducing MetS. This data set [Rozendaal *et al.*, 2018b] comprises monthly samples of plasma metabolic pool sizes and body weight and compostion over the course of three months and was used for calibration of the model using maximum likelihood estimation. Here we specifically utilize the n=1,000 model realizations subset representing the onset and progression of dyslipidemic MetS. [Rozendaal *et al.*, 2018b] This phenotype presents itself with the development of obesity and glucose intolerance in combination with dyslipidemia (high levels of plasma total cholesterol and high levels of plasma triglycerides). The collection of model realizations comprises trajectories (model simulations over a timespan of three months) describing the metabolic pool sizes and fluxes in the plasma, liver, intestine, and periphery.

6.3 Stratification of energy expenditure

Prior to applying any constraints on energy handling, any individuals that did not comply with the calibration data – i.e. did not accurately describe the data on which the trajectories were constraint – or those with unrealistic (high) flux magnitudes were excluded. This yielded a collection of n=887, i.e. virtual individuals with physiologically correct MetS biomarkers.

However, the models should not only adequately describe biomarkers, but energy handling is also an important criterion for model selection. While energy intake is known from food intake, energy expenditure is not yet studied. Therefore, we first stratify the population to ensure physiologically plausible values of energy expenditure in the system. Figure 6.2A shows the distribution of trajectories of total energy expenditure (summation of hepatic and peripheral EE) over time. The timespan on the horizontal axis describes development from a healthy phenotype to MetS over a period of three months. The collection of trajectories contains models ranging from low to high energy expenditure, but in general, the EE remains relatively stable over time. Therefore, the mean, as shown in the histogram of Figure 6.2B, is sufficient to summarize these results.

We applied physiological constraints obtained via indirect calorimetry (see Table 6.3 in section 6.8.3). Metabolic cages were used to measure VO2 and VCO2 such that metabolic rate and energy expenditure can be quantified. [Even and Nadkarni, 2012; Ferrannini, 1988] The physiological constraints obtained from these experiments are depicted as the 99.7% confidence interval (green error bars in Figure 6.2A and green shaded area in Figure 6.2B). This demonstrates that the majority of the virtual population (76%; n=678) presented itself with a physiologically plausible energy expenditure. Models with extremely low EE and high EE are presumed to be artefacts of solving the inverse problem of fitting a model with many degrees of freedom to a limited amount of data.

For the following analyses, we limit ourselves to the subgroup of n=678 virtual individuals. With an average energy expenditure of 12 kcal/day (calculated by the model) and an average energy intake of 19 kcal/day (known from dietary composition and daily food intake), the resulting energy balance is a constant surplus of energy of around 7 kcal/day. This explains the weight gain and development of obesity over time.

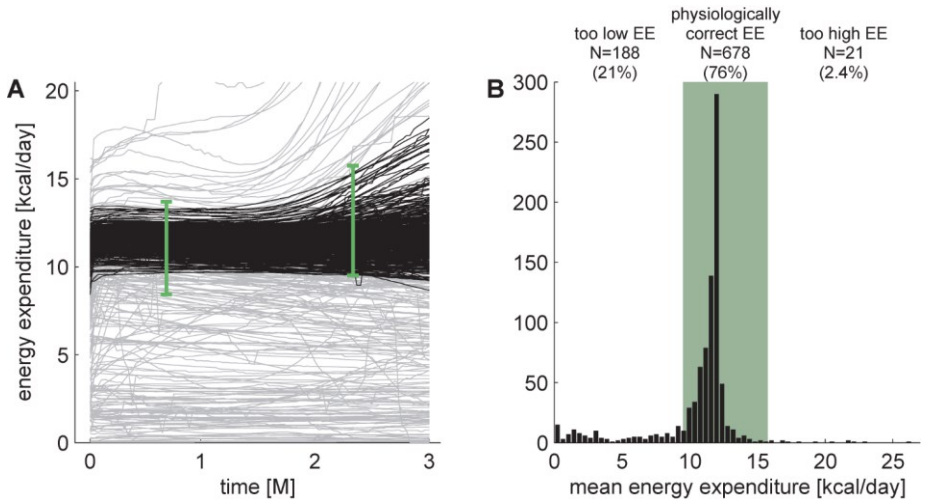

Figure 6.2

Energy expenditure predicted by MINGLeD as trajectories over time (A) and mean over time (B).

A: distribution of trajectories describing total energy expenditure. The trajectories that adhere to the physiological constraints (represented by the green error bars) are depicted in black; the unacceptable ones in grey. B: histogram of the mean energy expenditure. The physiologically acceptable range is depicted in green and derived from the following inclusion criteria:

- EE at t=3w within three-weeks confidence interval, i.e. [8.4 - 13.6 kcal/day];
- EE at t=10w within three-weeks confidence interval, i.e. [9.5 - 15.7 kcal/day];
- overall minimum EE above the lower bound of the 3w confidence interval, i.e. 8.4 kcal/day;
- overall maximum EE below 20 kcal/day.

6.4 Energy is mainly expended in the peripheral compartment

The next step in the stratification process comprises the breakdown of the contribution of different tissues to the total energy expenditure. The total energy expenditure consists of energy utilization in both liver (Figure 6.3A) and periphery (Figure 6.3B). We expected to find a significant contribution from the periphery, compared to the liver. The periphery is the largest compartment; both in volume and in number of cells. Since it also comprises muscle and BAT, we expect that the periphery utilizes much more energy than the liver, although the liver is also a metabolically active organ. However, we found a distribution with a strong bimodal profile. This bimodality indicates that energy can predominantly be utilized by just either of these tissues, but that energy can also be utilized by both compartments to the same extent.

Consequently, we divided the population into three different subgroups, each with its own characteristic contribution of hepatic and peripheral energy expenditure. Figure 6.3C shows the relative contribution of hepatic (blue) and peripheral (red) EE for each virtual individual at the three months' time point of MetS development. It reveals the existence of a continuous "spectrum" in the contribution of hepatic and peripheral energy expenditure. As suggested by Figure 6.3C, in a part of the population, the majority of energy is utilized in the periphery (on the l eft-hand side); another subgroup exists in which the majority of energy is utilized in the liver (on the right-hand side); and an intermediate group in which both peripheral and hepatic energy expenditure are significantly contributing to the total energy consumption. Therefore, the virtual individuals were separated into three different subgroups:

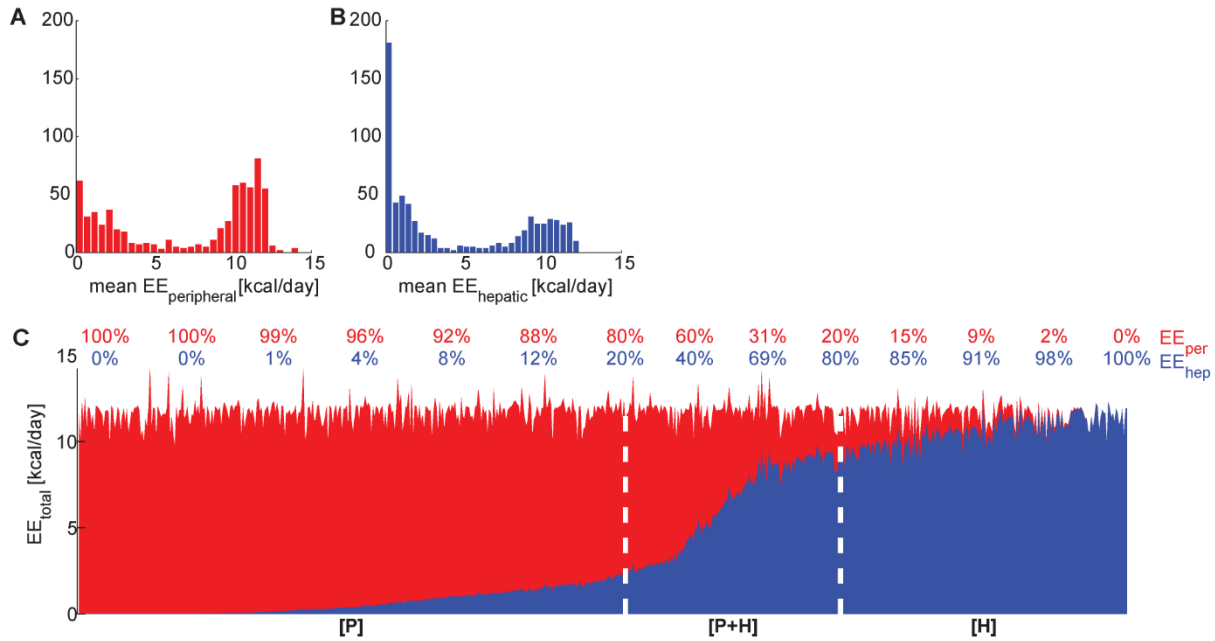

Figure 6.3

Peripheral (red) and hepatic (blue) contribution of energy expenditure.

Panels A and B include histograms of the mean energy expenditure. Panel C shows the relative contribution (numbers above graph) where each vertical line represents a single virtual individual. The white dashed lines indicate the division in subgroups [P], [P+H], and [H].

- [P]: predominantly peripheral energy expenditure (>80% originates from the peripheral compartment);
- [H]: predominantly hepatic energy expenditure (>80% originates from the hepatic compartment);
- [P+H]: intermediate subgroup in which both periphery and liver contribute significantly (>20% originates from the peripheral compartment and >20% originates from the liver).

Table 6.1 lists the characteristics for each of these subgroups and shows that these subgroups are clearly separated in their average peripheral and hepatic energy consumption. Figure 6.7 in Appendix 6.9 shows that although the predominant compartment of energy expenditure varies among these individuals, the same MetS phenotype in terms of biomarker profiles has been established, whereas the underlying metabolic fluxes may be different (see Figure 6.8 in Appendix 6.9).

Table 6.1

Division into subgroups characteristic for the peripheral and hepatic contribution to the total energy expenditure.

		relative contribution of peripheral EE [%]				relative contribution of hepatic EE [%]			
	n	mean	std	min	max	mean	std	min	max
[P]	354 (52%)	94	5.6	80	100	5.5	5.6	4.3e-7	20
[P+H]	139 (21%)	47	21	20	80	53	21	20	80
[H]	185 (27%)	8.5	6.5	2.6e-4	20	92	6.5	80	100

6.5 Further stratification based on substrate oxidation

The subsequent step of the stratification process involves further specification of the source of energy. Energy expenditure in MINGLeD is described by the respiration of ACoA. The ACoA pool originates from three different substrates: carbohydrate, lipid, and protein. ACoA is obtained from carbohydrate substrates via glycolysis of glucose-6-phosphate. ACoA from lipid substrate originates from the β-oxidation of triglycerides (TG). ACoA can also be derived from ketogenic protein uptake from the diet.

In Figure 6.4 the relative peripheral (A) and hepatic (B) energy utilization are shown, split into the relative contribution of carbohydrate, lipid, and protein oxidation. MINGLeD predicts a range of substrate ratios (carbohydrate:lipid:protein) to be possible and predicts that the majority of the virtual individuals utilize mainly carbohydrate substrates as an energy source while lipids are stored in the form of TG.

Literature has revealed that on a high-fat diet, mammals mainly utilize TG as energy source. [Bobbioni-Harsch *et al.*, 1997; Cooling and Blundell, 1998; Melzer, 2011; Thomas *et al.*, 1992] In our diet- induced MetS animal model, physiological data (see Table 6.3 in section 6.8.3) has placed this cut-off on at least 57% of energy to result from lipid substrates. Therefore, we imposed this as the criterion for the minimal contribution of fat oxidation, indicated by the dashed lines in Figure 6.4.

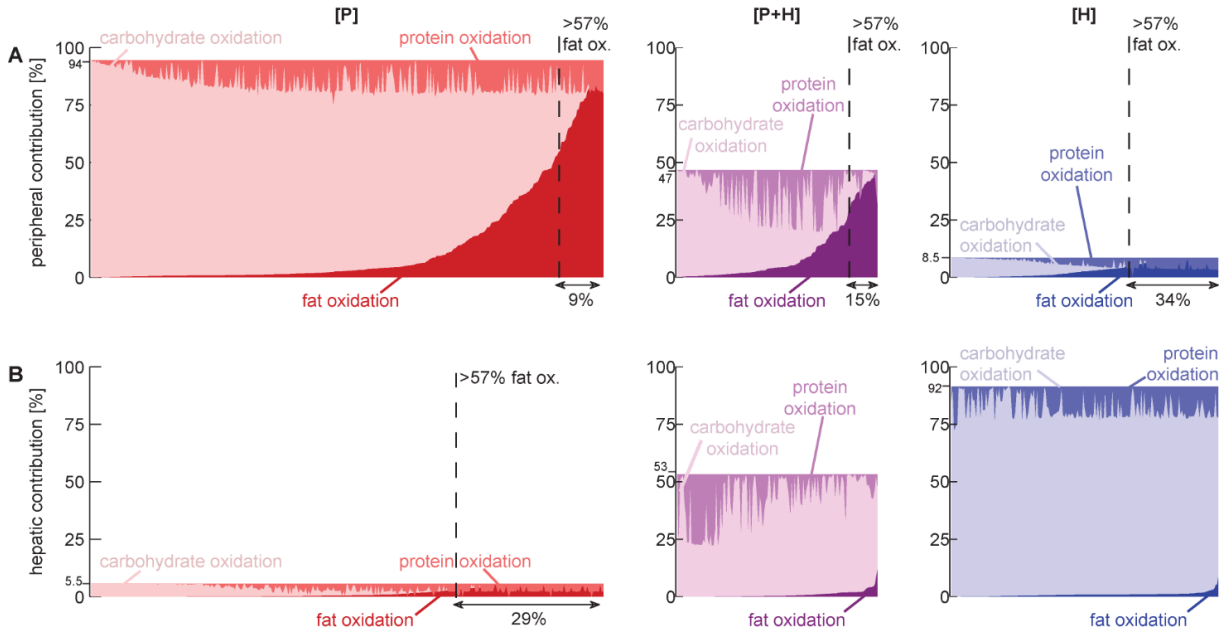

Figure 6.4

Contribution of carbohydrate and fat oxidation to the peripheral (A) and hepatic (B) energy expenditure.

In subgroup [P] (left-hand side panels), energy is predominantly utilized in the periphery (>80% originates from the peripheral compartment). In subgroup [H] (right-hand side panels), energy is predominantly utilized in the liver (>80% originates from the hepatic compartment). Subgroup [P+H] (panels in the centre) is an intermediate subgroup in which both periphery and liver contribute significantly (>20% originates from the peripheral compartment and >20% originates from the liver).

The dark coloured areas (bottom right) correspond with fat oxidation, the medium coloured areas (top left) indicate protein oxidation and the light areas (middle) specify carbohydrate oxidation. The dashed line bounds of the acceptable physiological range on the lipid oxidation ratio (at least 57% originates from lipid substrates). The fraction of individuals that adheres to this constraint is depicted below each graph.

Table 6.2 lists the overall statistics of the substrate oxidation for peripheral and hepatic energy expenditure for each subgroup separately. In the predominantly peripheral subgroup [P], overall, 75% of peripheral energy originates from carbohydrate sources, 15% from fat oxidation and 10% from protein substrates. Although most of these numbers are not close to our 57% fat-threshold, a subset of this group does adhere to this criterion (highlighted in grey in Table 6.2).

Note that in the predominantly hepatic subgroup [H], only acceptable solutions regarding the relative contribution of fat oxidation were found for the peripheral energy consumption, but that the contribution of the periphery to the total energy expenditure is very low (<10%).

To conclude, our stratification process resulted in a reduced population of n=32 virtual individuals. This is a representative subgroup as the selected individuals 1) have an accurate description of plasma and liver biomarkers (the characteristic MetS phenotype); 2) have a physiologically correct EE; 3) predominantly utilize energy in the periphery; and 4) of which energy originates for at least 57% from lipid substrates.

This stratification and selection process reduced the virtual population of interest from several hundred to a few dozen virtual individuals. Since each virtual individual in the selected subgroup is described by a different parameter set, we decided to analyse each model in more detail to understand how differences in model parameters affect the behaviour of the metabolic system. For this analysis, the subgroup of n=32 virtual individuals was sufficiently large to represent the variability within the population and to interpret results on an individual basis.

Table 6.2

Relative contribution of substrate oxidation to peripheral and hepatic energy expenditure.

The relative contribution of substrate oxidation is depicted as the mean ± standard deviation, and the minimum and maximum bounds are denoted between brackets. The number of virtual individuals adhering to the physiological bound of at least 57% fat oxidation is highlighted in grey.

	peripheral energy expenditure				hepatic energy expenditure			
	carbohydrate oxidation [%]	fat oxidation [%]		protein oxidation [%]	carbohydrate oxidation [%]	fat oxidation [%]		protein oxidation [%]
[P]	75.1 ± 21.8 [5.1 - 100]	15.4 ± 24.1 [7.3e-10 - 95]	≥57%: n=32 (9%)	9.6 ± 5.4 [6.7e-9 - 20]	32.6 ± 26.7 [1.8e-8 - 100]	33.5 ± 29.4 [0.049 - 100]	≥57%: n=103 (29%)	33.9 ± 28.3 [3.1e-11 - 100]
[P+H]	58.1 ± 29.4 [0.59 - 99]	23.4 ± 28.8 [5.1e-6 - 99]	≥57%: n=21 (15%)	18.5 ± 19.6 [8e-6 - 58]	80.8 ± 20.7 [33 - 100]	1.8 ± 2.9 [0.017 - 23]	≥57%: n=0	17.3 ± 19.6 [1e-7 - 58]
[H]	29.2 ± 20.5 [0.0015 - 93]	40.5 ± 36.1 [7.7e-11 - 100]	≥57%: n=63 (34%)	9.6 ± 5.8 [4e-12 - 90]	89.4 ± 5.7 [74 - 99]	1.0 ± 1.0 [0.012 - 9.7]	≥57%: n=0	9.6 ± 5.8 [5.3e-12 - 21]

6.6 *In silico* perturbation experiment to study the robustness of energy homeostasis

Subsequently, we employed MINGLeD to simulate an increase in peripheral energy expenditure. To induce an increase in peripheral energy expenditure, we perturbed each of the n=32 selected models (that adhered to physiological constraints in terms of EE and substrate oxidation) by multiplication of the peripheral ACoA flux with different activation factors as shown in Figure 6.5A. This factor was iteratively increased from 1 to 25 as explained in detail in section 6.8.4. For each factor, the steady-state of the model system was re-calculated while the nutritional intake was kept constant at the original values for macronutrient intake. Since each virtual individual is described by a different parameter set, the different individuals can be expected to respond differently to perturbation in energy balance.

Figure 6.5A demonstrates the effects of perturbation in energy expenditure (results are colour-coded for each model) versus the activation factor on the horizontal axis. Whereas these models respond differently to the perturbation, the majority shows a strong increase in total

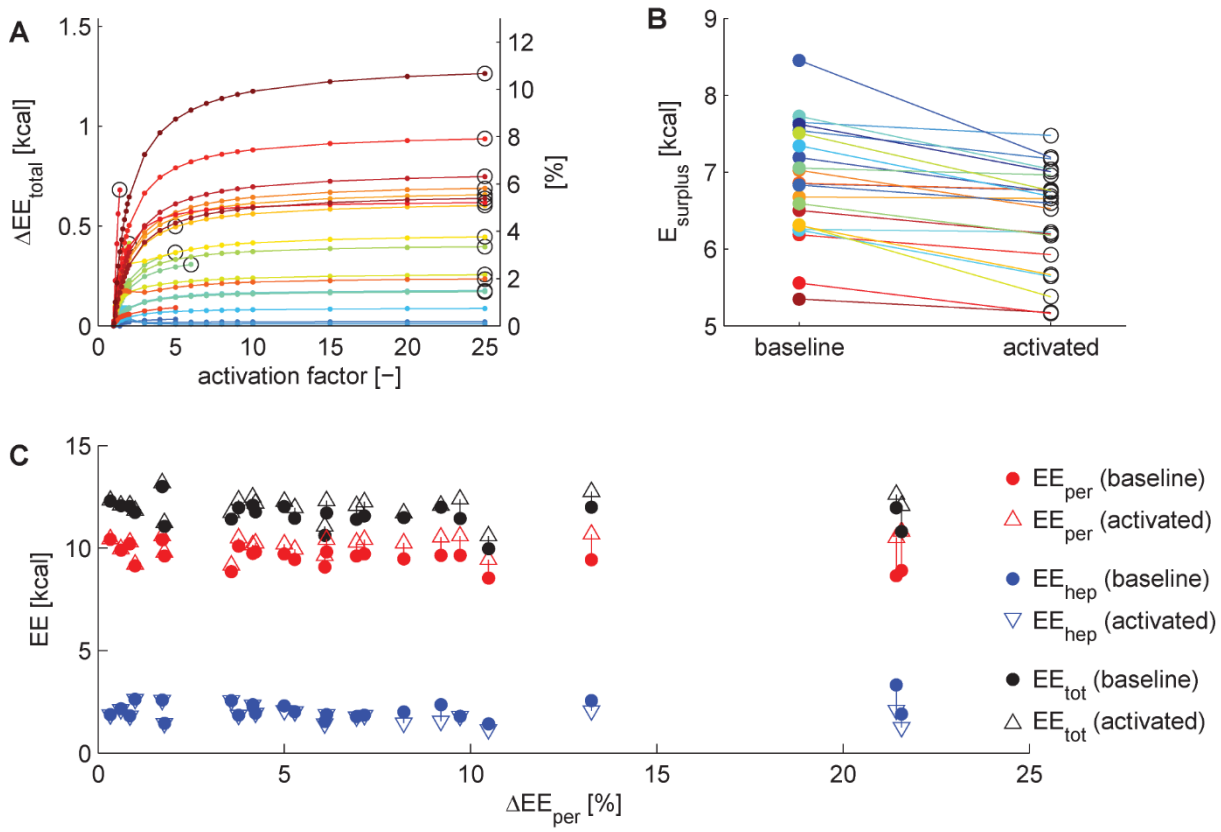

Figure 6.5

***In silico* activation of peripheral energy expenditure leads to an increase of total EE.**

Panel A shows the absolute (left vertical axis) and relative (right vertical axis) change in total EE upon increasing activation factor. Each line depicts a different virtual individual where data are colour-coded according to the maximally achieved increase in peripheral energy expenditure.

For each virtual individual, the highest activation result (if yielding at least a 0.1% increase in total EE) was used for further analysis and indicated by the black circle.

Panel B displays the resulting decrease of the energy surplus in the system. Results are colour-coded based on panel A. Panel C presents the shift in peripheral (red), hepatic (blue) and total (black) EE from baseline (represented with dots) to *in silico* activation (represented with upward facing triangles for increasing values and downward triangles for decreasing values) versus the relative increase in peripheral EE (on the horizontal axis).

energy expenditure upon increasing values of the activation factor and saturating towards a plateau. However, the level of the plateau is different throughout our population. This means that in some individuals, the peripheral energy expenditure can be activated to a much larger extent than for others. For further analysis, we selected the activation factor that achieved highest increase in EE (indicated by the black circle), but yielding at least an increase of 0.1% in total energy expenditure – as an increase in total energy expenditure should be substantial in order to induce propagation of effects throughout the system. This showed that the perturbation was successfully applied in 23 virtual individuals.

The maximally achieved increase in EE is different for each individual and for some the effects of the perturbation are much higher than for others (Figure 6.5A). For some models, application of larger activation factors led to depletion of the peripheral ACoA pool, preventing a further increase in the externally applied perturbation (these are the solutions that do not span the entire horizontal axis).

The perturbation yielded a decrease of the energy surplus (Figure 6.5B) of up to 2 kcal, but not sufficient to create an energy deficit. Under the condition of fixed food intake, increase in peripheral EE (Figure 6.5C in red) is paralleled by a decrease in hepatic EE (Figure 6.5C in blue). This decrease in hepatic EE is more profound when the increase in peripheral energy expenditure is higher (towards the right on the horizontal axis) – but the total EE (Figure 6.5C in black) does increase upon increased peripheral EE.

Figure 6.6 shows the resulting relative change in metabolite pool sizes (A) and metabolic fluxes (B) upon the highest achieved increase in total EE. Using heatmaps, we depicted these results for the n=23 different individualized models with from left to right increasing relative change of peripheral EE. Decreasing pool sizes and fluxes are shown in red and increases in blue. Perturbation induced a drastic increase in peripheral ACoA respiration (top row in Figure 6.6B), obviously depleting large quantities of the peripheral ACoA pool. Results reveal direct changes in peripheral lipid and lipoprotein metabolism, but also propagation into the plasma, liver, and intestine. Circulating lipoprotein levels decrease with increased peripheral energy expenditure (whilst dietary intake was kept the same). Remarkably, the perturbation did not imply any changes in the carbohydrate metabolic system.

6.7 Discussion

We successfully studied energy handling in Metabolic Syndrome development. Our perturbation experiments have shown that an additional drain of peripheral energy expenditure successfully decreases lipid and lipoprotein pools in the periphery, but also lipid contents in the surrounding tissues. This thereby provided insight into how a change in energy handling could be beneficial in the treatment of MetS.

The growing incidence rates of obesity and related diseases in combination with the heterogeneity in phenotypic presentation and metabolic manifestations ask for a more patient-specific approach towards treatment. [Lynes and Tseng, 2018; Neeland *et al.*, 2018] Hereto we should first gain insight into which patient subgroups can be identified. Recently we have demonstrated

the differential response to high-fat, high-cholesterol feeding, which induces two different MetS phenotypes. [Rozendaal *et al.*, 2018b] These findings are in line with the expected phenotypic heterogeneity in metabolic component combinations [Agyemang *et al.*, 2012; Lee *et al.*, 2008], but also

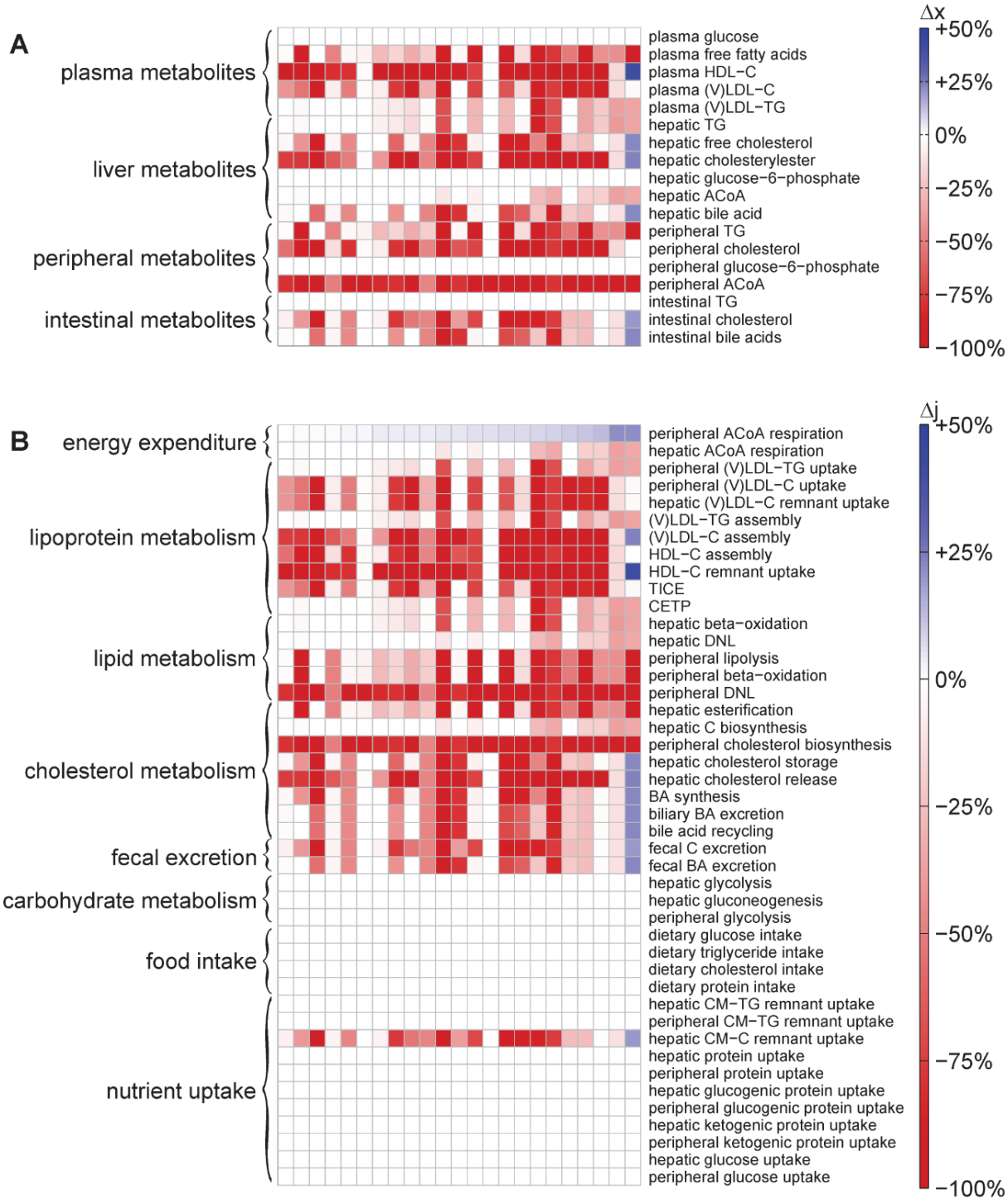

Figure 6.6

Increased peripheral energy expenditure affects metabolite pools (A) and metabolic fluxes (B) throughout the system.

The impact of the activation is depicted as relative change using a heatmap for n=23 virtual individuals (from left to right: increasing relative change of peripheral energy expenditure). The changes are colour-coded such that decreases are shown in red and increases in blue, and according to intensity: a darker colour indicates a stronger change in metabolite concentration than a lighter colour. White indicates a 0% change.

the heterogeneity within the same phenotypic presentation – and energy handling – may be large. Whereas most conventional studies make predictions based on the population level, we, therefore, took a step further and evaluated virtual patient subgroups. This follows the path towards evaluating individual, patient-specific data and enabling predictions in an individualized framework by classifying patients into a corresponding subgroup. [Kononowicz *et al.*, 2015]

6.7.1 Stratification tool

We have shown the feasibility of (virtual) patient stratification. Relevant individuals were first filtered out based on physiological constraints. This approach parallels with many *in vivo* experimental set-ups as a reduction of the population is applied to retain only those individuals expressing the desired features, but also yielding a manageable amount of data. This is a crucial step in the "era of precision medicine" [Valdes *et al.*, 2016] towards identifying a framework to classify patients in corresponding subgroups and often used in virtual (and clinical) trials. [Lindon and Nicholson, 2014; Fryburg *et al.*, 2011]

6.7.2 Virtual trial of BAT activation

Our perturbation experiment can also be regarded as a virtual trial. For this, we even took one step further and provided simulations on an individual level. For instance, we can demonstrate that enhanced peripheral energy expenditure can be used as an *in silico* proxy to study the effects of BAT activation. Firstly, the imposed perturbation is in the same order of magnitude as achieved in clinical practice with exposure to cold (despite possibly extra energy intake). In our virtual individuals, large differences have been observed to what extent the energy expenditure could be increased. However, (pre)clinical studies report that cold exposure (CEX) induces a similarly large range of average increase of energy expenditure compared to thermo-neutral conditions ranging from only a few percent to several dozen percent increase. [Lichtenbelt *et al.*, 2014; Yoneshiro *et al.*, 2013; Ouellet *et al.*, 2012] These results strongly depend on the conditions of the experiment: degree (mild versus strong, i.e. how cold) and the duration of the period of cold exposure.

Secondly, the imposed flux changes are in line with clinical observations showing that BAT can be activated by cold exposure [Lichtenbelt *et al.*, 2014; Romu *et al.*, 2016; Lee *et al.*, 2011; Nedergaard *et al.*, 2007; Saito *et al.*, 2009; Seale and Lazar, 2009] and that it possesses anti-obesogenic properties. [Yoneshiro *et al.*, 2013] We found a reduction of (circulating) lipid and cholesterol levels after simulating short and acute CEX. Radioactive tracer experiments confirmed direct changes in TG uptake fluxes after one-day of CEX but did not report changes in plasma markers. [Bartelt *et al.*, 2011; Khedoe *et al.*, 2015]

This difference could be explained by differences in experimental conditions: the *in silico* study induced a quite extreme activation compared to one-day CEX treatment. If CEX would have induced an activation as strong as in the *in silico* case, supposedly changes in plasma metabolite pools would have been observed as well.

Literature indicates that BAT also possesses the ability to improve glucose handling. This is in contrast to our results as the carbohydrate system remains unaffected upon increased peripheral EE. This difference may be explained by considering the model's stoichiometry, and more specifically, the direction of the fluxes in the model. MINGLeD was designed to describe

the most important elements and processes in lipid, cholesterol, and carbohydrate metabolism. Thorough model testing using different scenarios and/or metabolic conditions (such as in this study the *in silico* activation of peripheral EE) indicates how MINGLeD can be extended and improved. The observation that the glucose system remains unaffected upon increased peripheral EE is an indication to further investigate the relationship between glucose and ACoA, which is currently implemented as a one-way interaction (glucose-6-phosphate can only be donated to ACoA).

6.7.3 Opportunity for other activation schemes of BAT

Experimental studies have shown that BAT activation can induce weight loss. [Bartelt and Heeren, 2014; Broeders *et al.*, 2015; Hanssen *et al.*, 2015] Our perturbation experiment has shown that increased peripheral energy expenditure is able to induce a decrease of the energy surplus in the system. To yield a negative energy balance, we would recommend longer and/or more frequent periods of CEX treatment to induce a sustained and/or prolonged BAT activation. Experimental studies with intermittent CEX schemes have shown to be feasible to do this. [Ravussin *et al.*, 2014; Wang *et al.*, 2015; Yoo *et al.*, 2014] Recent studies have also shown the potential to chronically activate BAT using a pharmacological intervention with the thermogenic β3-adrenergic receptor agonist CL316,243. [Bartelt *et al.*, 2017; Berbée *et al.*, 2015] Dietary supplementation of the short-chain fatty acid butyrate has also shown promising results in both animals [Li *et al.*, 2018] and in humans [Bouter *et al.*, 2018; Fluitman *et al.*, 2018] to reduce both appetite and active BAT through the gut-brain axis. [Li *et al.*, 2018]

6.7.4 Computational energy metabolism models

Most computational models describing energy metabolism are specifically developed for the human metabolic system, and hardly any for murine energy metabolism. [Guo and Hall, 2011] Whereas specific metabolic pathways may be different between mouse and human [Hall, 2012], much can be learned from mouse computational models. Our computational model (Figure 6.1) was designed to be a generic representation for both murine and human energy metabolism. Since no human data is available as of yet, our work using the murine model calibration provides a step towards translation of *in silico* models developed using genetically modified mice towards the human energy management in metabolic diseases.

6.7.5 Conclusions

The computational analysis of energy handling and energy expenditure for stratification and perturbation experiments confirmed that the energy imbalance plays an important role in the development of obesity and its related diseases. Furthermore, increasing peripheral energy expenditure has a positive effect on lipid metabolism in Metabolic Syndrome.

6.8 Methods

6.8.1 Stratification of energy handling in an *in silico* model

We employ our previously developed computational model MINGLeD (Model Integrating Glucose and Lipid Dynamics) describing the metabolic system from a healthy state towards the development of Metabolic Syndrome. [Rozendaal *et al.*, 2018b] MINGLeD was utilized in combination with ADAPT (Analysis of Dynamic Adaptations in Parameter Trajectories) [Tiemann *et al.*, 2013, 2011; van Riel *et al.*, 2013] to achieve a model library describing various phenotypes. Here we analyse the n=1,000 model simulations for the dyslipidemic Metabolic Syndrome phenotype. These model simulations describe MetS development over a timescale of three months, with a discretization of 90 days. Based on this large set of *in silico* data, we performed data reduction by applying physiological constraints to obtain a manageable amount of physiologically-correct data.

Physiological data on the energy expenditure was obtained using metabolic cages (see also section 6.8.3). In the experimental study of [Rozendaal *et al.*, 2018b], the animals were subjected to indirect calorimetry after three and ten weeks of diet induction. This information was used to select those virtual individuals of which the energy expenditure lies within a physiologically correct range, defined using both the three-week (8.4-13.6 kcal/day) and the ten-week (9.5-15.7 kcal/day) 99.7% confidence interval (see Table 6.3).

Moreover, this physiological data was also utilized to define a threshold for the relative contribution of fat oxidation to energy expenditure. As criterion we used that for mice on a high-fat diet at least 57% of the energy should originate from lipid substrates. This cut-off value is based on the lower bound of the 99.7% confidence interval for fat oxidation (see Table 6.3) obtained by indirect calorimetry after ten weeks of MetS induction (since this resembles the fully developed phenotype the closest). The virtual individuals we selected for further analysis predominantly utilize energy in the periphery (subgroup [P]), with approximately 75% of energy from carbohydrate, 15% from fat, and ~10% from protein substrate oxidation, resulting in a cohort of n=32 individuals that was used for further analysis.

6.8.2 Converting energy expenditure into energy units

Traditionally, all fluxes in MINGLeD are expressed in µmol/day. To recalculate the energy expenditure fluxes in MINGLeD into energy units, we made use of the energy content of TG particles. Hereto, we first recalculated the ACoA respiratory fluxes into the equivalent of TG particles assuming that 1 mole of TG is equivalent to 21.4 moles of ACoA:

$$EE\left[\frac{\mu mol\ TG}{day}\right] = EE\left[\frac{\mu mol\ ACoA}{day}\right] \cdot \frac{1}{21.4} \tag{6.1}$$

Then these fluxes were converted from molar units to grams per day by assuming that the molar mass of TG is 853 u:

$$EE\left[\frac{g\ TG}{day}\right] = EE\left[\frac{\mu mol\ TG}{day}\right] \cdot 853 \cdot 10^{-6}\left[\frac{g}{\mu mol}\right] \tag{6.2}$$

We then can calculate how much energy is equivalent to this flux assuming that 1 gram of fat contains 9 kilocalories:

$$EE\left[\frac{kcal}{day}\right] = EE\left[\frac{g\ TG}{day}\right] \cdot 9\left[\frac{kcal}{g}\right] \tag{6.3}$$

Hence, the energy expenditure fluxes can easily be converted from molar units (6.1) into energy content (6.3) using:

$$EE\left[\frac{kcal}{day}\right] = EE\left[\frac{\mu mol\ ACoA}{day}\right] \cdot \frac{1}{21.4} \cdot 853 \cdot 10^{-6} \cdot 9 \tag{6.4}$$

6.8.3 Physiological ranges provided by *in vivo* assessment of energy expenditure

To measure energy expenditure in the *in vivo* situation, male E3L.CETP mice on a high-fat, high-cholesterol diet (the same individuals as were the subject in chapter 4 [Rozendaal *et al.*, 2018b]) underwent indirect calorimetry using metabolic cages [Even and Nadkarni, 2012] after three and ten weeks of diet induction respectively. Mice were housed individually in these metabolic cages for four days. The first day was used to let the mice get used to the new environment. The animals were non-invasively, fully computer operated monitored during these four days. Afterwards, the animals were put back into their normal cages.

O_2 and CO_2 concentrations were measured every ten minutes to calculate the energy expenditure. [Ferrannini, 1988] Different substrates yield different consumption rates. We can infer the relative contribution of substrate utilization from the measured changes in oxygen and carbon dioxide:

$$\begin{aligned} EE_{total} &= EE_{glucose} + EE_{fat} + EE_{protein} \\ EE_{glucose} &= VO_2 \cdot f_{glucose} \cdot RED_{glucose} \\ EE_{fat} &= VO_2 \cdot f_{fat} \cdot RED_{fat} \\ EE_{protein} &= VO_2 \cdot f_{protein} \cdot RED_{protein} \end{aligned} \tag{6.5}$$

where VO_2 represents consumed oxygen (L O_2/day), RED_x is the respiratory energy density (in kcal/L O_2) of substrate x, and f_x is the relative contribution to the total oxygen consumption by oxidation of substrate x. Based on the respiratory quotient (RQ):

$$RQ = \frac{VCO_2}{VO_2} = f_{glucose} \cdot RQ_{glucose} + f_{fat} \cdot RQ_{fat} + f_{protein} \cdot RQ_{protein} \tag{6.6}$$

assuming $RQ_{glucose} = 1$, $RQ_{fat} = 0.71$, $RQ_{protein} = 0.835$ [Livesey and Elia, 1988], the relative contribution of the respiratory energy density parameters should adhere to:

$$f_{glucose} + f_{fat} + f_{protein} = 1 \tag{6.7}$$

Assuming that body mass of protein is constant, the rate of protein oxidation should equal the rate of protein intake. Hence, protein oxidation will be a consistent factor γ of the total energy expenditure:

$$EE_{protein} = \gamma \cdot \left(EE_{glucose} + EE_{fat} + EE_{protein}\right) \tag{6.8}$$

Substitution with (6.5) and some rearranging yields:

$$f_{protein} = \frac{\frac{\gamma}{1-\gamma} \cdot \left(f_{glucose} \cdot RED_{glucose} + f_{fat} \cdot RED_{fat}\right)}{RED_{protein}} \tag{6.9}$$

which can be simplified using substitution with α and β by:

$$\begin{aligned} \alpha &= \frac{\gamma}{1-\gamma} \cdot \frac{RED_{glucose}}{RED_{protein}} \\ \beta &= \frac{\gamma}{1-\gamma} \cdot \frac{RED_{fat}}{RED_{protein}} \end{aligned} \tag{6.10}$$

and yields:

$$f_{protein} = \alpha \cdot f_{glucose} + \beta \cdot f_{fat} \quad (6.11)$$

Therefore the relative contribution of the other substrates is determined by:

$$f_{glucose} = \frac{RQ - \frac{(RQ_{fat} + \beta \cdot RQ_{protein})}{1+\beta}}{RQ_{glucose} + \alpha \cdot RQ_{protein} - \frac{(1+\alpha)(RQ_{fat} + \beta \cdot RQ_{protein})}{1+\beta}} \quad (6.12)$$

$$f_{fat} = \frac{1 - f_{glucose} \cdot (1+\alpha)}{1+\alpha}$$

assuming that $\gamma = 0.2$, $RED_{protein} = 4.17$, $RED_{fat} = 4.66$, and $RED_{glucose} = 5.02$. [Livesey and Elia, 1988]

The statistics of the obtained calculations for the energy expenditure for the different substrates are depicted in Table 6.3.

Table 6.3

Total energy expenditure assessed using indirect calorimetry.

Data are depicted as the mean ± standard deviation, and as 99.7% confidence interval (between brackets).

	EE [kcal/day]	fat oxidation [%]	carbohydrate oxidation [%]	protein oxidation [%]
MetS-3w	11.1 ± 0.87	57.6 ± 2.8	22.4 ± 2.8	20.0 ± 2.6e-4
	[8.4 - 13.6]	[49.3 - 65.9]	[14.1 - 30.7]	[20.0 - 20.0]
MetS-10w	12.6 ± 1.04	63.2 ± 2.0	16.8 ± 2.0	20.0 ± 1.3e-4
	[9.5 - 15.7]	[57.4 - 69.1]	[10.9 - 22.6]	[20.0 - 20.0]

6.8.4 *In silico* perturbation experiment inducing enhanced peripheral energy expenditure

Since we aim to study the effects of short-term BAT activation through cold exposure, we chose to perform our *in silico* simulation using the one-day snapshot obtained in the fully developed phenotype, i.e. after three months of MetS induction. This timescale is also consistent with the time window in which an *in vivo* cold exposure intervention would be applied.

The perturbation experiment involved applying an external perturbation such that an *in silico* increase in peripheral energy expenditure was achieved. Since the peripheral compartment comprises all metabolically active tissues apart from the liver, plasma, and intestinal lumen, we assumed that the respiration of peripheral acetyl-Coenzyme A (represented by the red arrow in Figure 6.1) can be used as a proxy for BAT activation.

An increase in peripheral ACoA respiratory flux was induced by multiplication of the flux equation with activation factor f_{act}:

$$j^{ACoA}_{resp,per} = k_{resp,per} \cdot ACoA_{per} \cdot f_{act} \quad (6.13)$$

However, since it is not *a priori* known how high this activation factor should be, and this factor may differ among different virtual individuals, we applied a variety of activation factors that ranged different scales (1+1e-10, 1+1e-8, 1+1e-6, 1+1e-4, 1+1e-3, 1+1e-2, 1.1:0.1:1.9, 2:9 10:5:25) to the system. The system was re-simulated to steady state with these perturbations applied, yielding the results presented in Figures 6.5 and 6.6.

6.9 Appendix: Subgroups in energy expenditure

We identified three subgroups based on where the majority of energy is utilized: predominantly peripheral [P], predominantly hepatic [H], and both peripheral and hepatic energy expenditure [P+H]. Here we examined the metabolic fluxes and pool sizes corresponding to these different classes. Regardless of where the majority of energy is utilized, the resulting MetS phenotype in terms of plasma and liver biomarkers (top three rows in Figure 6.7) is equivalent. However, this phenotype can develop with different combinations of underlying metabolic fluxes (see Figure 6.8).

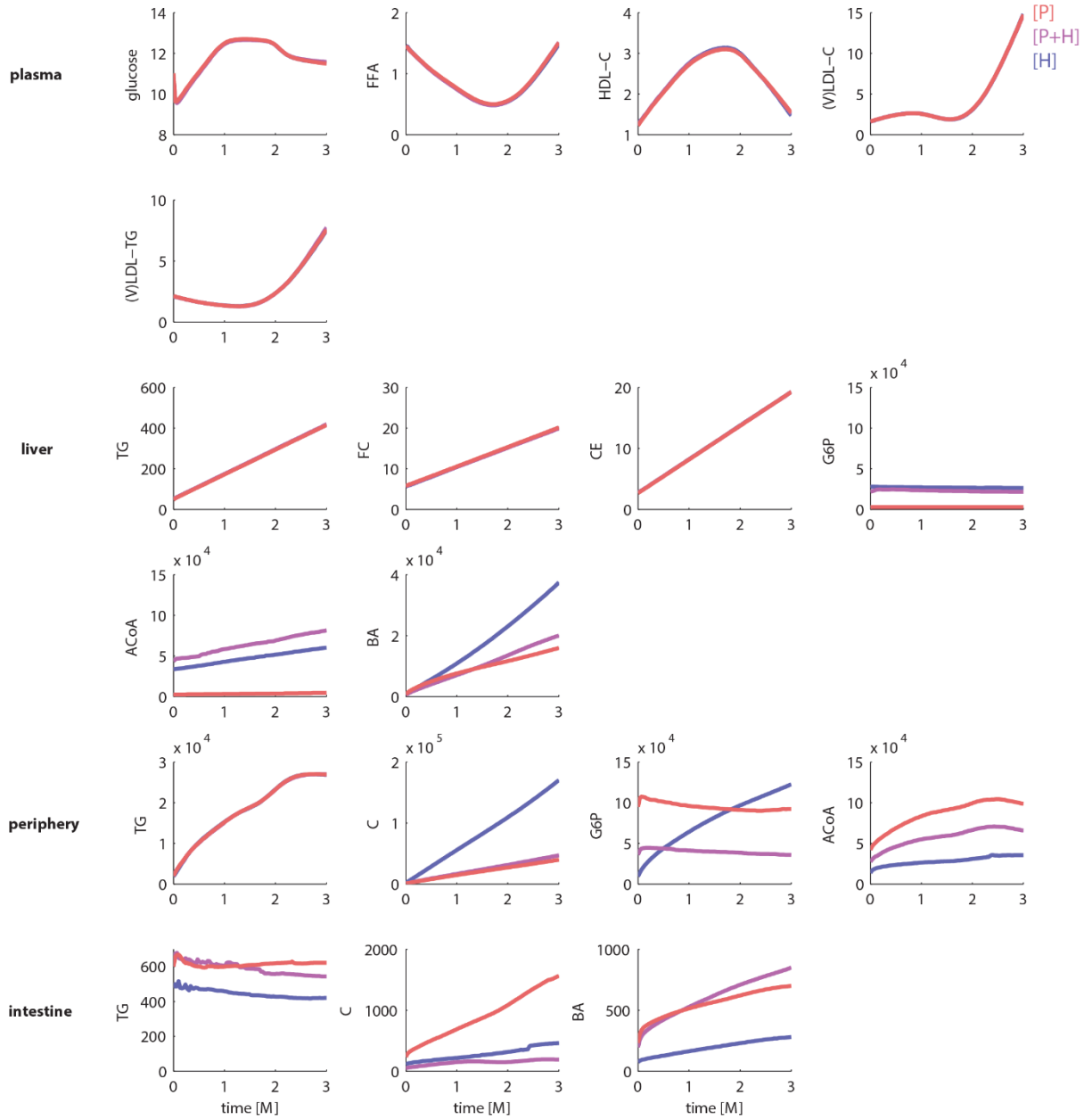

Figure 6.7

Metabolite pool sizes depend on where the majority of energy is utilized.

The mean pool sizes in individuals with predominantly peripheral energy expenditure [P] are depicted in red; mean pool sizes in individuals with predominantly hepatic energy expenditure [H] in blue; and mean pool sizes of individuals with both peripheral and hepatic energy expenditure [P+H] in purple. All pool sizes of plasma metabolites are expressed as concentration in mM; all other pool sizes are expressed in µmol.

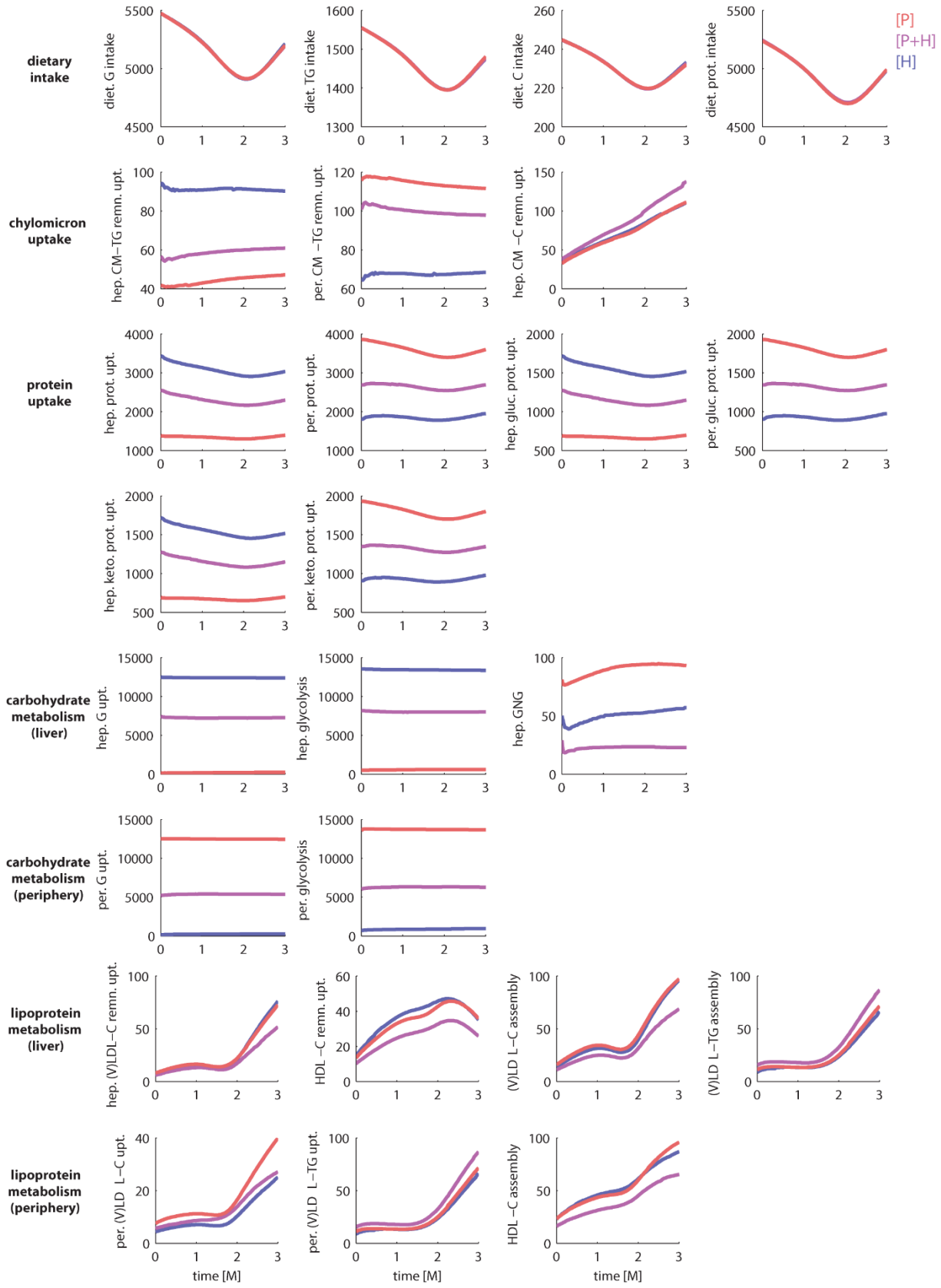
dietary intake
diet. G intake
diet. TG intake
diet. C intake
diet. prot. intake
[P]
[P+H]
[H]
chylomicron uptake
hep. CM−TG remn. upt.
per. CM −TG remn. upt.
hep. CM −C remn. upt.
protein uptake
hep. prot. upt.
per. prot. upt.
hep. gluc. prot. upt.
per. gluc. prot. upt.
hep. keto. prot. upt.
per. keto. prot. upt.
carbohydrate metabolism (liver)
hep. G upt.
hep. glycolysis
hep. GNG
carbohydrate metabolism (periphery)
per. G upt.
per. glycolysis
lipoprotein metabolism (liver)
hep. (V)LDL−C remn. upt.
HDL −C remn. upt.
(V)LD L−C assembly
(V)LD L−TG assembly
lipoprotein metabolism (periphery)
per. (V)LD L−C upt.
per. (V)LD L−TG upt.
HDL −C assembly
time [M]
time [M]
time [M]

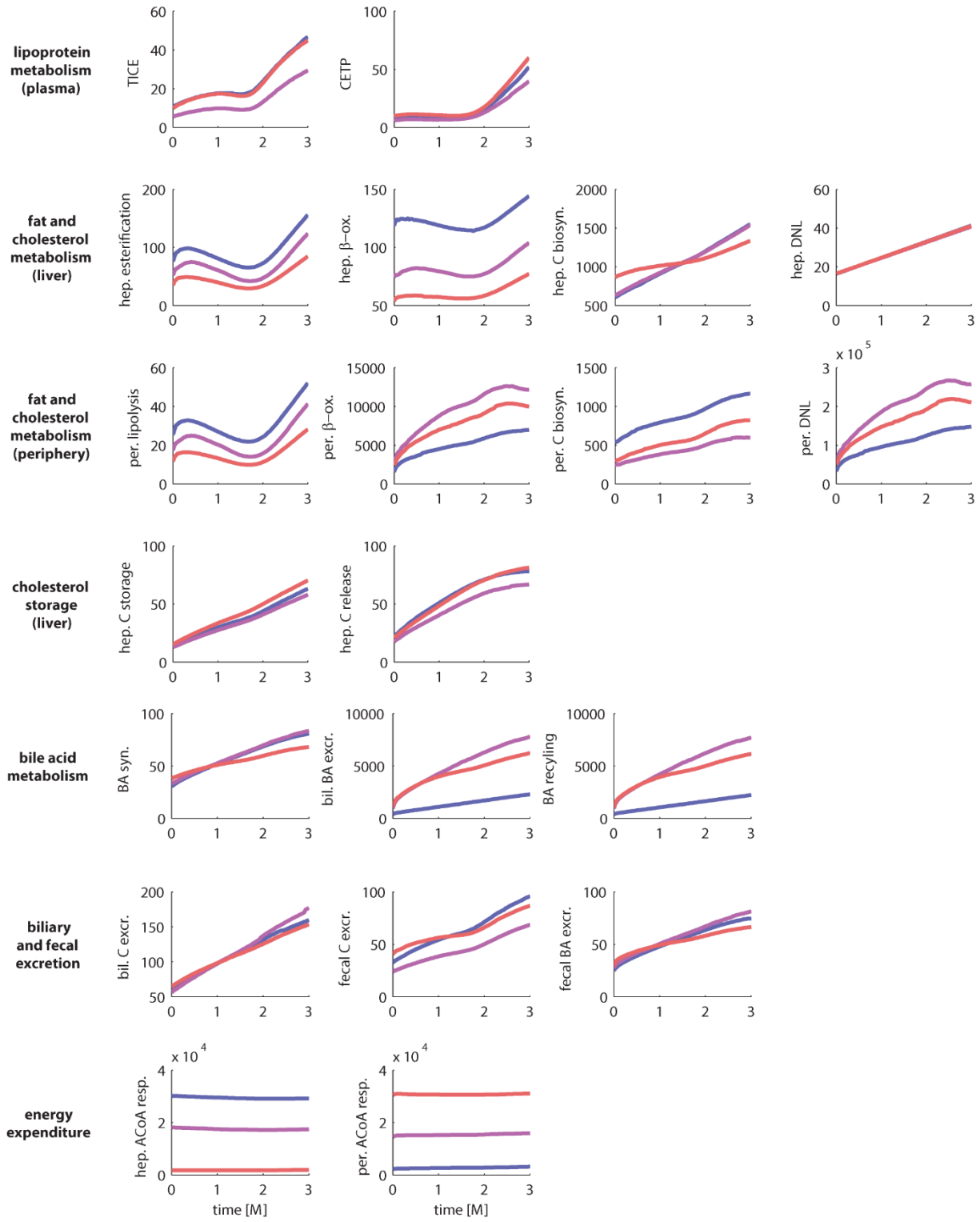

Figure 6.8

Metabolic fluxes depend on where the majority of energy is consumed.

The mean fluxes in individuals with predominantly peripheral energy expenditure [P] are depicted in red; mean fluxes in individuals with predominantly hepatic energy expenditure [H] in blue; and mean fluxes of individuals with both peripheral and hepatic energy expenditure [P+H] in purple. All fluxes are expressed in µmol/day.

7

Summarizing discussion and future perspectives

7.1 Summary of contributions

Metabolic Syndrome is gaining increasing attention in both biomedical and clinical research. Research has, however, often focused on singular pillars (symptoms or comorbidities) of MetS such as insulin resistance [Romeo *et al.*, 2012], atherosclerosis [Barbalho *et al.*, 2015; González-Navarro *et al.*, 2008], or very specific co-occurring side effects such as periodontal health [Hatipoglu *et al.*, 2015], sleeping disorders [Vgontzas *et al.*, 2005], and neurological disorders. [Farooqui *et al.*, 2012] We used a comprehensive and systematic approach overarching the traditional borders of medicine to allow for an integrative and interdisciplinary study of MetS.

Thanks to the innovative set-up of the *in vivo* experiments in RESOLVE – with its longitudinal design, frequent measurements at intermediate time points, and follow-up for a long period of time – we were able to extract much more information than with just a cross-sectional or prospective set-up. We acquired a very rich and fruitful dataset (chapter 4) that allowed for studying disease onset and progression in individuals, as well as across the population, in a mouse model.

The heterogeneity in this population could be quantified by classification of distinctly different MetS phenotypes based on dyslipidemic status (low-grade dyslipidemia versus strong dyslipidemia). These distinct phenotypes were found to be reproducible in an independent and larger cohort (chapter 5). This follow-up study also revealed an additional group spanning the continuum between mild to moderate dyslipidemia, and indicates an even more heterogeneous and less coherent population than expected from chapter 4. These preclinical studies underline that MetS is not simply caused by overeating and an inactive lifestyle, but that its origin involves many more intricate underlying mechanisms in the onset and development of MetS.

We focused our modelling on the data describing the development of the distinct subgroups as identified in chapter 4. A fundamental problem in the analysis of such data using conventional statistical methods would be the lack of reproducibility and wide sample-to-sample variation in statistical outcome. [Goodman, 2001; Halsey *et al.*, 2015; Nuzzo, 2014] Our systems biology approach does take this variability into account: the data is supplied as constraints to the model. The physiology-based mechanistic model MINGLeD encapsulates both carbohydrate, lipid, and cholesterol regulation (chapter 3), it also allowed for the integration of these different research domains into one coherent framework. Moreover, ADAPT made the model parameters dynamic and time-dependent (chapter 2), providing a methodology to describe the continuous, longitudinal development of MetS in terms of modelled trajectories by quantitatively linking the (discrete data) samples in time. The sampling procedure that is essential in the ADAPT methodology drastically scaled up the number of individuals from the few animals in the *in vivo* cohort, to a much larger *in silico* population. This approach nicely demonstrates the implementation of the "3R principle" (i.e. replacement, reduction, and refinement) of animal research using *in silico* methods. [Lang *et al.*, 2018] Compared to conventional statistical methods, our computational approach requires a lot fewer animals (*reduction*) by utilizing the obtained data in a more intelligent way. The boundaries within we performed Monte Carlo sampling were constraint by the *in vivo* data. We did not only look at

the mean of the *in vivo* population, but by feeding the sampled data to the model (*refinement*), we yielded a large set of *in silico* trajectories, i.e. virtual individuals, that represent different phenotypic presentations (*replacement*) within a reasonable, physiological range (estimated from the *in vivo* data).

The resulting *in silico* predicted trajectories show parallels with the concept of "parameters becoming dynamic phenotypes". [Rajasingh *et al.*, 2008; Wang *et al.*, 2012] Furthermore, these predictions provide a deeper understanding of the complex underlying pathophysiology associated with the development of distinct phenotypic representations. Differences in dietary cholesterol uptake and hepatic turnover were elucidated as potential drivers for the emergence of these different MetS phenotypes. This underlines that the multi-factorial nature of MetS is much more complex than just originating from overfeeding and an inactive lifestyle. However, the imbalance in energy handling does indeed play an important role as well. The case study outlined in chapter 6 has shown that our modelling framework can be used for stratification purposes to gain insight into the heterogeneity of the population as well as that it can facilitate the implementation and execution of *in silico* trials. We have demonstrated that inducing an increase of peripheral energy expenditure – a representative entity for BAT activation by e.g. cold exposure – is effective in the treatment of MetS.

In conclusion, we have developed a novel modelling framework that describes the metabolic derailments during the onset and development of MetS. It also provides insight into phenotypic differentiation and allows for studying treatment interventions aimed at ameliorating, and possibly reversal of the metabolic derailments in MetS. Systems biology and computational modelling have been essential to gain a deeper and integrative understanding of the complex and multi-factorial nature of MetS.

7.2 Study limitations

Thus far, we have applied our model to and with data obtained from a transgenic murine population that possesses human-like metabolic properties. However, throughout this study, we have kept our focus on being able to translate this modelling methodology also to the human MetS population. Several issues concerning this translational challenge are discussed below.

7.2.1 Implications and translational challenges of E3L.CETP as a disease model for human Metabolic Syndrome

Animals, and in particular mice, have been used as experimental *in vivo* models in (bio)medical research and preclinical studies for over a century. Mice respond strikingly similar to humans and can (genetically) be manipulated to mimic a wide spectrum of human diseases and conditions. Furthermore, disease pathophysiology in mice has shown to be similar to that in humans. [Kõks *et al.*, 2016] Genetically engineered mouse models (GEMMs) are therefore considered relevant models for studying human diseases since specific mouse genes can be replaced by their human counterpart. This yields a so-called "humanised" mouse that produces the human version of the modified protein. [European Commission, 2010; Vandamme, 2014]

Other advantages of using animal models over human subjects in preclinical studies include the implementation of standardization procedures and the set-up in controlled testing facilities. Thereby yielding an environment in which variability due to external factors can be reduced. Variability is also restraint by inbreeding to yield genetically identical strains. Another practical benefit is the accelerated lifespan in comparison to humans – one mouse year is equivalent to roughly 30 human years according to The Jackson Laboratory (JAX) [Flurkey *et al.*, 2007] – which makes it an ideal candidate to study slowly progressing diseases, such as MetS. [Perlman, 2016; Vandamme, 2014]

Preclinical models to study human diseases

The abundance of (preclinical) animal models has created a considerable knowledge base regarding metabolic diseases. [Softic *et al.*, 2017] However, extrapolation and the translational scope of many of these models remain challenging. We therefore specifically selected an animal model that possesses many human-like metabolic properties. The E3L.CETP mouse is currently the best available transgenic animal model to induce and study the co-occurrence of MetS symptoms and comorbidities. [van den Hoek *et al.*, 2014] The metabolic system of the E3L.CETP mouse was designed to mimic human lipoprotein metabolism. As explained in detail in section 4.10.1, E3L.CETP mice have a defective triglyceride-rich lipoprotein (TRL) clearance to mimic the lower clearance of TRL in humans compared to mice. In addition, the (V)LDL:HDL ratio in E3L.CETP mice is similar to that in humans. The transfer of cholesteryl esters and triglycerides between LDL and HDL (facilitated by CETP) does not naturally occur in mice but is introduced in the E3L.CETP mouse through genetic modification to include the human CETP gene. [Rensen and Havekes, 2006; Westerterp *et al.*, 2006] Therefore, it can be concluded that the lipid and lipoprotein metabolism of E3L.CETP mice is representative for that in humans.

Although it may be debatable whether glucose biology is species-specific, it has been shown that reduced insulin sensitivity occurs naturally upon obesity development in mice. [Toye *et al.*, 2005; Wang and Liao, 2012] The latter can easily be induced by feeding mice a high-fat, Western-type diet. No additional genetic alterations in the glucose domain are thus required to mimic the (defective) glucose handling in obese humans.

Animal model of complete clinical Metabolic Syndrome?

The E3L.CETP mouse has indeed demonstrated to be a good disease model for MetS. The data presented in this thesis show the development of the majority of the characteristic phenomena in terms of both symptoms (obesity, hyperglycemia, dyslipidemia) and comorbidities (insulin resistance, fatty liver). It is noteworthy as well as remarkable that this preclinical animal model was specifically designed to describe MetS symptoms, but also appears to be suitable to study clinical endpoints within the same timeframe. This shows that MetS is not just a precursor stage towards possibly certain metabolic diseases, but that this risk is indeed drastically increased since we found both insulin resistance and hepatic lipid accumulation in the majority of animals at the end of the experimental studies.

However, this *in vivo* disease model does not include one clinical hallmark of MetS: hypertension. This criterion was assessed neither in this thesis nor in other E3L.CETP studies, although murine models of hypertension do exist. [Johns *et al.*, 1996; Lerman *et al.*, 2005; Monassier *et al.*, 2006] In that sense, MetS may be incompletely represented, but hypertension is a phenomenon

that does not fit within the scope of our current modelling framework as that is merely focused on the metabolic derailments of MetS.

Heterogeneity

Another important MetS characteristic is its heterogeneous presentation. This was initially one of the main reasons to pursue a model describing the human MetS complexity, but being set-up and calibrated with data derived from a dedicated animal model. Variability in phenotypic presentation is a phenomenon that is, allegedly, less profound in animal models than in the human population (due to standardization, controlled environment, etc.). Both E3L and E3L.CETP strains are known for their non-uniform response to Western-type diets. [Paalvast *et al.*, 2017]

We have partially unravelled this heterogeneity by classification of distinct MetS phenotypes. This subdivision could be related to differences in dietary cholesterol uptake and hepatic turnover. However, the exact precipitating factor(s) underlying phenotypic variation has(have) not fully been identified yet. Part of the observed heterogeneity may be attributed to inter-individual differences in food intake, but it is unclear which other factors may also contribute to this. Note that the heterogeneity cannot solely be attributed to the transgenes introduced in E3L.CETP as heterogeneity is also observed in its background strain C57BL/6J. [Burcelin *et al.*, 2002; Peyot *et al.*, 2010] The microbiome and gut barrier dysfunction have recently also been found to be predisposing factors in this heterogeneous presentation. [Chakrabarti *et al.*, 2017; Festi *et al.*, 2014; Lee *et al.*, 2017; Nieuwdorp *et al.*, 2014]

In conclusion, the E3L.CETP mouse model comprises the majority of phenotypic MetS outcomes and therefore matches our objective. The heterogeneity, however, underlines the importance of stratification into coherent subpopulations prior to data and model analysis.

Robustness, reproducibility, and frailty

An inherent next trait involves the reproducibility and robustness of the selected disease model on the long-term. This topic was briefly touched upon in chapter 5, where we observed drop-outs indicated by sudden trends of rapid weight loss in several animals. It appears that the health span is limited as these animals develop (age-related?) abnormalities with time [Drechsler *et al.*, 2016], but also various tumours. Ageing and frailty [Whitehead *et al.*, 2014] may have important implications for the outcome of such long-term experiments.

Moreover, another important aspect remains the consistency and coherence of the metabolic response to the high-fat, high-cholesterol diet. The phenomenon of responders and non-responders appears to play an important role in this. Both in the data presented in this thesis and in other studies regarding the E3L.CETP strain, a substantial number (20-30%) of animals does not develop the full metabolic complexity of MetS. Many of these non-responders suffer from a severe inflammatory hepatic condition, which may severely impair liver function. [Tarasco *et al.*, 2018] The underlying pathophysiology remains unclear, but it might be related to the genetic intervention, as baseline (i.e. prior to the HFD+C diet) liver abnormalities have been observed in several individuals. Hence, it is critical to identify and separate the respective animals by making use of both clinical chemistry and histological analysis to retrospectively confirm the animals' classification. Nevertheless, our conclusion remains that male E3L.CETP

mice fed a high-fat, high-cholesterol diet yield a representative *in vivo* disease model with relevance for human MetS.

7.2.2 Implications for MINGLeD as a disease model for human Metabolic Syndrome

Next, we discuss how representative the developed computational modelling framework – based on murine data – is for the human MetS population and what potential hurdles could be encountered in the application of the model to the human population.

Throughout the development of both the computational model and its framework, we have kept our focus primarily on the relevance in the human population. Hence, the topology of MINGLeD is specifically designed to describe the human metabolic system and does not require any adjustments for when implemented with human data. It can, however, be extended with additional regulations – such as hormonal regulation, e.g. effects of insulin (resistance) – or metabolites, provided that the current model topology is insufficient to describe a specific dataset and/or specific research question. However, it does require a large amount of data to be collected longitudinally.

Translation of murine model results to the human situation

Since *in vivo* data describing human-like MetS development was used to construct the model, its results provide valuable insights into the pathophysiology involved in MetS onset, development, and progression. Although exact values cannot be extrapolated (e.g. thresholds for hyperglycemia are different among mouse and human), we assume that the trend and dynamics of processes involved can be generalized towards human MetS pathophysiology.

This raises the question of how these model results can objectively and quantitatively be interpreted. Distributions of time-dependent trajectory solutions have been generated for each phenotypic subgroup. Analysis of time-series data quickly becomes complicated when considering multiple entities, e.g. a subset of metabolite and/or flux trajectories. Thus far, we limited the interpretation to visual comparisons, but this will not suffice when more phenotypic subgroups would become involved – as is expected when applying the model with human data. Conventional statistical methods to compare time-series data are limited, but a more elegant and objective approach to interpret the modelled trajectory distributions could involve techniques for continuous model evaluation, such as Profile Likelihood Analysis (PLA). [Nguyen *et al.*, 2017; Raue *et al.*, 2009] Future application of this type of models does require a sophisticated analysis approach to enable systematic interpretation of the predicted data within the context of the modelled network.

ADAPT is a very powerful tool to incorporate uncertainty in experimental data in an ODE model. Since the model is data-driven in that sense, this uncertainty propagates into the model predictions. The result of this is reflected by the width of the trajectory distributions. Although the data did span the entire plasma compartment of the model, tissue compartments may be underrepresented in that context. This is also reflected by the wider trajectory distributions for species and fluxes in the tissues that have not been constraint by data (possibly an indication of overmodelling or underfitting). It can, therefore, be a challenge to estimate model parameters and to quantify the uncertainty of the model predictions.

Another important contribution of ADAPT is that it provides (possibly unintuitive but) testable predictions, such as the differences in pathophysiology underlying the different MetS phenotypes as observed in chapter 4. However, these predictions still need to be verified.

Modifications for application of modelling framework to the human situation

Application of the modelling framework to human data requires some minor modifications. Tissue and distribution volumes are considerably larger in human versus mouse. This can easily be taken into account, as estimates for body fat and blood volume are well-known. [Friesen, 2014; Janmahasatian *et al.*, 2005; Lemmens *et al.*, 2006]

Timescales may appear more challenging, but the time axis is provided by the input data. Therefore, time is an entity that is independent of the model results. No changes have to be made to the modelling framework. To extrapolate longitudinal modelling results from murine to human timescales, several studies have provided suggestions for this. [Demetrius, 2006; Dutta and Sengupta, 2016] An issue that is related to this, involves the less clear demarcated time window of disease development in human patients. No true "healthy" t=0 point of onset has been identified in MetS patients, as they are usually diagnosed when already metabolically altered and are located somewhere along the disease progression curve.

Furthermore, specification and logging of food intake for the human situation will not be trivial. Although controlled and standardized meals are often used in e.g. postprandial tests [Rozendaal *et al.*, 2018a; Zeevi *et al.*, 2015], it is practically unrealistic to maintain such an artificial diet for a prolonged period of time. Although day-to-day nutrition may deviate, overall dietary patterns can be logged and will, in general, average out over the scope of months to years. To gain a model that is more realistic in terms of lifestyle, dietary interventions in terms of caloric restriction and/or macronutrient restriction can easily be implemented. Especially the effect of dietary composition in terms of carbohydrate:fat ratio has been the focus of many diets in order to lose weight. [Abete *et al.*, 2010; Eaton and Konner, 1985; Iacovides and Meiring, 2018] Physical activity levels, however, have not yet been taken into account as constraints to the model.

Longitudinal data collection

The real bottleneck in the application of the modelling framework to the human MetS population lies elsewhere. The model can only perform effectively and predict sensible results if provided with sufficient longitudinal data. For humans, however, long-term data collection is challenging. ADAPT has been shown to require large amounts of data on many metabolic species and at many time intervals. Intermediate monitoring of plasma metabolites and macroscopic markers (body weight, fat percentage) can be achieved relatively easily at e.g. intervals for general check-ups in the clinic or at the general practitioner. The main challenge will be to obtain tissue-specific data, let alone time-series tissue data. It is questionable whether plasma data alone would be a sufficient read-out of intra-tissue metabolic status. Biopsies are invasive, but possibly one could make use of imaging modalities such as proton magnetic resonance spectroscopy to noninvasively measure ectopic fat and thereby obtaining an estimate of hepatic lipid composition and content. [Dall'Ara *et al.*, 2016; Johnson *et al.*, 2008; Nissen *et al.*, 2016] In addition, nonradioactive, stable isotopes can be employed as metabolic tracers for flux measurements. [Adiels *et al.*, 2005; Kim *et al.*, 2016] Preferably these measurements should also be performed at multiple points in time, as it has been shown that only t=0 and t=end is insufficient

to thoroughly describe the longitudinal dynamics. ADAPT is designed to only infer complex dynamics when necessary to describe longitudinal trends. Since ADAPT minimizes unnecessary changes in parameters over time, it will inherently predict a simple linear trajectory when only two points in time are provided – whereas from a biological point of view this might be unlikely. [Scott, 2007] Keeping in mind the much longer timescales in human compared to our *in vivo* MetS model, disease progression will also be affected by ageing [Figueira *et al.*, 2016; Mooney *et al.*, 2016] and frailty [von Zglinicki *et al.*, 2016] as the prevalence of the different components of MetS has been shown to increase with age. [Bellantuono *et al.*, 2018]

We should also take into account the use of medication that affects metabolic regulation. For example, statins and metformin are both used very often in clinical practice to, respectively, lower cholesterol and glucose levels. When such treatment is effective, the plasma read-out would result in an indication of lower concentrations of these metabolic species. However, it should somehow be taken into account in the modelling framework that this change was pharmaceutically induced, and is not caused by disease progression (or rather amelioration) in the underlying network. In a previous study (and chapter 2) using human data, we have shown that ADAPT is capable to distinguish between disease progression and treatment effects. [Nyman *et al.*, 2016]

7.3 Future perspectives

The developed modelling framework provides a solid basis for further research of MetS pathophysiology as well as as a potential tool for patient stratification. We recognize that this work is ongoing and discuss several possible directions in which this work can be extended and applied.

7.3.1 Extending the modelling framework: more phenotypic subgroups and multiple treatment interventions

The first direct extension of the modelling framework lies in the integration of more data. Chapter 5 has provided an extensive dataset that captures a longer period of time. With these data, we can extend our model and assess the longitudinal dynamics more thoroughly. Moreover, this study also indicated an additional dyslipidemic MetS subgroup that spans the continuum between mild and moderate dyslipidemia, and fills the gap between the more extreme phenotypes that we have analysed thus far.

Extension of in silico database: phenotypic subgroups

Chapter 6 has shown the applicability of our modelling framework to study the effects of therapeutic interventions. Although the simulated treatment effect of short-term cold exposure revealed to be insufficient to result in a full reversal of energy balance, it did ameliorate the metabolic derailments associated with MetS. We expect that exposure to cold for a longer period of time would eventually induce reversal of the energy balance.

Still, it is questionable whether MetS is fully reversible. However, several studies have shown that the metabolic system is flexible in the genesis, but also in treatment towards reversal of metabolic diseases associated with obesity. [Aucouturier *et al.*, 2011; Galgani *et al.*, 2008; Goodpaster and

Sparks, 2017; Tareen *et al.*, 2018] This is an interesting future application of the model. Hereto other treatment strategies aimed at slowing down, and – best-case scenario – reversal and prevention of the metabolic derailments of MetS have been explored in the context of RESOLVE. These *in vivo* studies have provided data obtained from our specific animal model (male E3L.CETP on a high-fat, high-cholesterol diet) that should fit nicely into this framework using the substantial *in silico* database describing MetS development (chapter 4). Especially if this database would be extended with virtual individuals generated using the data from chapter 5, this would yield an extensive database comprising a large range of MetS phenotypes. When applying the modelling framework to simulate treatment interventions, we would suggest to first select a proper (subset of) baseline phenotypic model(s) from the *in silico* population to ensure alignment with the *in vivo* measured (baseline) data. Next, the model can be used to simulate a treatment intervention, and *in silico* predictions can then be compared to *in vivo* observations. This methodology allows differentiation between disease developmental effects and treatment effects, whereas if the model would be fitted to *in vivo* treatment data, this separation cannot be made.

Therapeutic interventions in E3L.CETP

Therapeutic interventions such as dietary interventions (e.g. caloric restriction or modification of the carbohydrate:fat ratio) can easily be implemented in the model since food intake in terms of macronutrients is specified as input fluxes to the system. Also other sophisticated dietary approaches, such as butyrate supplementation, are suggested for the treatment of obesity-related disorders. Butyrate is a short-chain fatty acid of which oral treatment has been associated with beneficial metabolic effects both in (E3L.CETP) mice [Li *et al.*, 2018] and in humans. [Bouter *et al.*, 2018] The underlying mechanism of the effects of butyrate intake remain unclear but it seems to be associated with BAT activation. This makes butyrate supplementation an ideal case study for our modelling framework.

Another type of dietary intervention involves tetrahydrolipstatin (THL). THL is a lipase inhibitor that has been shown to reduce weight gain and improve glycemic control by reducing dietary fat lipolysis and subsequent absorption from the intestinal lumen; both in mice [Hassanein *et al.*, 2015] and in humans. [Aldekhail *et al.*, 2015] THL treatment data has recently become available for male E3L.CETP mice fed an HFD+C diet (unpublished data), making it an excellent case study for our modelling framework.

A more invasive approach that is often performed in morbidly obese patients involves bariatric surgery. The Roux-en-Y gastric bypass (RYGB) has been shown to improve comorbidities such as diabetes and hypertension and lowers the risk of obesity-related cancers both in mice [Frohman *et al.*, 2018] and in humans. [Camastra *et al.*, 2013; Jørgensen *et al.*, 2012] RYGB not only reduces stomach size, it also involves rerouting of the intestinal tract. Immediate improvements in glucose metabolism, prior to weight loss are observed, but the mechanism behind this remains unclear. Observations of RYGB applied to E3L.CETP mice have recently become available (unpublished data), making it an interesting case study for our modelling framework.

7.3.2 Towards precision and personalized medicine

Throughout the design and development of our modelling framework, the clinical relevance has been the primary focus. However, the road towards a population-based, let alone a patient-specific, MetS model remains long.

Population-based MetS model

As discussed above, some minor modifications of the modelling framework will be required. The most important first step towards the application of the framework for the human MetS population involves the acquisition of a time-course calibration dataset, and subsequent time-course validation dataset. The heterogeneous clinical presentation requires a large population of MetS patients to be followed for a long period of time. Data acquisition should be performed both extensively and carefully to yield a population-based model for the most common MetS phenotypes that arise from the patient population. Previous studies have shown that also in the human population, distinct subgroups can be identified that differ in MetS severity. [Poon *et al.*, 2014]

Patient-specific MetS model

The population-based model can then be refined and applied with different scopes. It can be used to identify the phenotypic classification of a specific patient (i.e. to which MetS subgroup he/she belongs) and to estimate the phase and severity of MetS (i.e. at which point in the progression timeline the patient is located). Eventually, it may be useful as a decision support tool to predict the efficacy of different treatment interventions aiming at the reversal of MetS. A prognosis can then be made by outlining different clinical outcomes as a result of different combinations of treatment strategies and/or lifestyles. The modelling framework can be used as a tool to provide insight into which individuals are (more) at risk of the development of comorbidities.

We have developed a novel modelling framework that is not exclusive for MetS but can be employed to study the longitudinal behaviour of other slowly progressing diseases. The ultimate goal of this work is in line with the long advocated scope of the “P4 paradigm” – *predictive*, *preventive*, *personalized*, and *participatory* – of systems medicine. [Hood *et al.*, 2012] Personalized and precision medicine and healthcare are essential for refining patient-specific treatment as well as in the prevention of complex disorders, both with a metabolic, but also with an oncogenic pathophysiological origin. [Shin *et al.*, 2017; Yanovski and Yanovski, 2018; Schork, 2015]

Bibliography

Abate N, Chandalia M. Ethnic differences in the Metabolic Syndrome. In: Atlas of atherosclerosis and Metabolic Syndrome. Springer New York; ISBN: 978-1-4419-5839-6, 2011, 195–206 doi.org/10.1007/978-1-4419-5839-6_9

Abete I, Astrup A, Martínez JA, Thorsdottir I, Zulet MA. Obesity and the metabolic syndrome: role of different dietary macronutrient distribution patterns and specific nutritional components on weight loss and maintenance. *Nutr. Rev.*, 2010, 68(4):214–231 doi.org/10.1111/j.1753-4887.2010.00280.x

Adiels M, Olofsson SO, Taskinen MR, Borén J. Overproduction of very low-density lipoproteins is the hallmark of the dyslipidemia in the Metabolic Syndrome. *Arterioscler. Thromb. Vasc. Biol.*, 2008, 28(7):1225–1236 doi.org/10.1161/ATVBAHA.107.160192

Adiels M, Packard C, Caslake MJ, Stewart P, Soro A, Westerbacka J, Wennberg B, Olofsson SO, Taskinen MR, Borén J. A new combined multicompartmental model for apolipoprotein B-100 and triglyceride metabolism in VLDL subfractions. *J. Lipid Res.*, 2005, 46(1):58–67 doi.org/10.1194/jlr.M400108-JLR200

Agyemang C, van Valkengoed IG, van den Born BJ, Bhopal R, Stronks K. Heterogeneity in sex differences in the metabolic syndrome in Dutch white, Surinamese African and South Asian populations. *Diabet. Med.*, 2012, 29(9):1159–1164 doi.org/10.1111/j.1464-5491.2012.03616.x

Ajmera I, Swat M, Laibe C, Novère NL, Chelliah V. The impact of mathematical modeling on the understanding of diabetes and related complications. *CPT Pharmacomet. Syst. Pharmacol.*, 2013, 2:e54 doi.org/10.1038/psp.2013.30

Alberti KGMM, Eckel RH, Grundy SM, Zimmet PZ, Cleeman JI, Donato KA, Fruchart JC, James WPT, Loria CM, Smith SC. Harmonizing the metabolic syndrome: a joint interim statement of the International Diabetes Federation Task Force on Epidemiology and Prevention; National Heart, Lung, and Blood Institute; American Heart Association; World Heart Federation; International Atherosclerosis Society; and International Association for the Study of Obesity. *Circulation*, 2009, 120(16):1640–1645 doi.org/10.1161/CIRCULATIONAHA.109.192644

Alberti KG, Zimmet PZ. Definition, diagnosis and classification of diabetes mellitus and its complications. Part 1: diagnosis and classification of diabetes mellitus provisional report of a WHO consultation. *Diabet. Med.*, 1998, 15(7):539–553 doi.org/10.1002/(SICI)1096-9136(199807)15:7<539::AID-DIA668>3.0.CO;2-S

Aldekhail NM, Logue J, McLoone P, Morrison DS. Effect of orlistat on glycaemic control in overweight and obese patients with type 2 diabetes mellitus: a systematic review and meta-analysis of randomized controlled trials. *Obes. Rev.*, 2015, 16(12):1071–1080 doi.org/10.1111/obr.12318

Alkema W, Rullmann T, van Elsas A. Target validation in silico: does the virtual patient cure the pharma pipeline? *Expert Opin. Ther. Targets*, 2006, 10(5):635–638 doi.org/10.1517/14728222.10.5.635

Allen RJ, Rieger TR, Musante CJ. Efficient Generation and Selection of Virtual Populations in Quantitative Systems Pharmacology Models. *CPT Pharmacomet. Syst. Pharmacol.*, 2016, 5(3):140–146 doi.org/10.1002/psp4.12063

Apovian CM, Garvey WT, Ryan DH. Challenging obesity: Patient, provider, and expert perspectives on the roles of available and emerging nonsurgical therapies. *Obes. Silver Spring Md*, 2015, 23 Suppl 2:S1–S26 doi.org/10.1002/oby.21140

Aronoff S, Rosenblatt S, Braithwaite S, Egan JW, Mathisen AL, Schneider RL. Pioglitazone hydrochloride monotherapy improves glycemic control in the treatment of patients with type 2 diabetes: a 6-month randomized placebo-controlled dose-response study. The Pioglitazone 001 Study Group. *Diabetes Care*, 2000, 23(11):1605–1611 doi.org/10.2337/diacare.23.11.1605

Atkinson AJ, Lalonde RL. Introduction of quantitative methods in pharmacology and clinical pharmacology: a historical overview. *Clin. Pharmacol. Ther.*, 2007, 82(1):3–6 doi.org/10.1038/sj.clpt.6100248

Aucouturier J, Duché P, Timmons BW. Metabolic flexibility and obesity in children and youth. *Obes. Rev.*, 2011, 12(5):e44–e53 doi.org/10.1111/j.1467-789X.2010.00812.x

Auvinen HE, Wang Y, Princen H, Romijn JA, Havekes LM, Smit JWA, Meijer OC, Biermasz NR, Rensen PCN, Pereira AM. Both transient and continuous corticosterone excess inhibit atherosclerotic plaque formation in APOE*3-leiden.CETP mice. *PloS One*, 2013, 8(5):e63882 doi.org/10.1371/journal.pone.0063882

Bagust A, Beale S. Deteriorating beta-cell function in type 2 diabetes: a long-term model. *QJM*, 2003, 96(4):281–288 doi.org/10.1093/qjmed/hcg040

Balkau B, Charles MA. Comment on the provisional report from the WHO consultation. European Group for the Study of Insulin Resistance (EGIR). *Diabet. Med.*, 1999, 16(5):442–443 doi.org/10.1046/j.1464-5491.1999.00059.x

Barbalho SM, Bechara MD, Quesada K, Gabaldi MR, Goulart R de A, Tofano RJ, Gasparini RG, Barbalho SM, Bechara MD, Quesada K, Gabaldi MR, Goulart R de A, Tofano RJ, Gasparini RG. Metabolic syndrome, atherosclerosis and inflammation: an inseparable triad? *J. Vasc. Bras.*, 2015, 14(4):319–327 doi.org/10.1590/1677-5449.04315

Bartelt A, Bruns OT, Reimer R, Hohenberg H, Ittrich H, Peldschus K, Kaul MG, Tromsdorf UI, Weller H, Waurisch C, Eychmüller A, Gordts PLSM, Rinninger F, Bruegelmann K, Freund B, Nielsen P, Merkel M, Heeren J. Brown adipose tissue activity controls triglyceride clearance. *Nat. Med.*, 2011, 17(2):200–205 doi.org/10.1038/nm.2297

Bartelt A, Heeren J. Adipose tissue browning and metabolic health. *Nat. Rev. Endocrinol.*, 2014, 10(1):24–36 doi.org/10.1038/nrendo.2013.204

Bartelt A, John C, Schaltenberg N, Berbée JFP, Worthmann A, Cherradi ML, Schlein C, Piepenburg J, Boon MR, Rinninger F, Heine M, Toedter K, Niemeier A, Nilsson SK, Fischer M, Wijers SL, Lichtenbelt W van M, Scheja L, Rensen PCN, Heeren J. Thermogenic adipocytes promote HDL turnover and reverse cholesterol transport. *Nat. Commun.*, 2017, 8:15010 doi.org/10.1038/ncomms15010

Bartolomucci A, Cabassi A, Govoni P, Ceresini G, Cero C, Berra D, Dadomo H, Franceschini P, Dell'Omo G, Parmigiani S, Palanza P. Metabolic consequences and vulnerability to diet-induced obesity in male mice under chronic social stress. *PLoS ONE*, 2009, 4(1) doi.org/10.1371/journal.pone.0004331

Bassi N, Karagodin I, Wang S, Vassallo P, Priyanath A, Massaro E, Stone NJ. Lifestyle modification for metabolic syndrome: a systematic review. *Am. J. Med.*, 2014, 127(12):1242.e1–10 doi.org/10.1016/j.amjmed.2014.06.035

Batsis JA, Romero-Corral A, Collazo-Clavell M, Sarr MG, Somers VK, Lopez-Jimenez F. Effect of bariatric surgery on the Metabolic Syndrome: A population-based, long-term controlled study. *Mayo Clin. Proc.*, 2008, 83(8):897–907 doi.org/10.4065/83.8.897

Bellantuono I, DeCabo R, Ehninger D, Fernandes A, Howlett SE, Müller R, Potter P, Tchkonia T, Trendelenburg AU, Luis J, Vandenbroucke RE, van Os R, van Riel NAW. Find drugs that delay many diseases of old age. *Nature*, 2018, 554:293–295 doi.org/doi: 10.1038/d41586-018-01668-0

Beltrán-Sánchez H, Harhay MO, Harhay MM, McElligott S. Prevalence and trends of metabolic syndrome in the adult U.S. population, 1999-2010. *J. Am. Coll. Cardiol.*, 2013, 62(8):697–703 doi.org/10.1016/j.jacc.2013.05.064

Berbée JFP, Boon MR, Khedoe PPSJ, Bartelt A, Schlein C, Worthmann A, Kooijman S, Hoeke G, Mol IM, John C, Jung C, Vazirpanah N, Brouwers LPJ, Gordts PLSM, Esko JD, Hiemstra PS, Havekes LM, Scheja L, Heeren J, Rensen PCN. Brown fat activation reduces hypercholesterolaemia and protects from atherosclerosis development. *Nat. Commun.*, 2015, 6:6356 doi.org/10.1038/ncomms7356

Bergman RN, Ider YZ, Bowden CR, Cobelli C. Quantitative estimation of insulin sensitivity. *Am. J. Physiol.*, 1979, 236(6):E667-677 doi.org/10.1152/ajpendo.1979.236.6.E667

Bligh EG, Dyer WJ. A rapid method of total lipid extraction and purification. *Can. J. Biochem. Physiol.*, 1959, 37(8):911–917 doi.org/10.1139/o59-099

Bobbioni-Harsch E, Habicht F, Lehmann T, James RW, Rohner-Jeanrenaud F, Golay A. Energy expenditure and substrates oxidative patterns, after glucose, fat or mixed load in normal weight subjects. *Eur. J. Clin. Nutr.*, 1997, 51(6):370–374 doi.org/10.1038/sj.ejcn.1600413

Bonomini F, Rodella LF, Rezzani R. Metabolic syndrome, aging and involvement of oxidative stress. *Aging Dis.*, 2015, 6(2):109–120 doi.org/10.14336/AD.2014.0305

Bosner MS, Lange LG, Stenson WF, Ostlund RE. Percent cholesterol absorption in normal women and men quantified with dual stable isotopic tracers and negative ion mass spectrometry. *J. Lipid Res.*, 1999, 40(2):302-308 jlr.org/content/40/2/302.full

Bouter K, Bakker GJ, Levin E, Hartstra AV, Kootte RS, Udayappan SD, Katiraei S, Bahler L, Gilijamse PW, Tremaroli V, Stahlman M, Holleman F, van Riel NAW, Verberne HJ, Romijn JA, Dallinga-Thie GM, Serlie MJ, Ackermans MT, Kemper EM, Willems van Dijk K, Backhed F, Groen AK, Nieuwdorp M. Differential metabolic effects of oral butyrate treatment in lean versus metabolic syndrome subjects. *Clin. Transl. Gastroenterol.*, 2018, 9(5):155 doi.org/10.1038/s41424-018-0025-4

Brodland GW. How computational models can help unlock biological systems. *Semin. Cell Dev. Biol.*, 2015, 47–48:62–73 doi.org/10.1016/j.semcdb.2015.07.001

Broeders EPM, Nascimento EBM, Havekes B, Brans B, Roumans KHM, Tailleux A, Schaart G, Kouach M, Charton J, Deprez B, Bouvy ND, Mottaghy F, Staels B, van Marken Lichtenbelt WD, Schrauwen P. The bile acid chenodeoxycholic acid increases human brown adipose tissue activity. *Cell Metab.*, 2015, 22(3):418–426 doi.org/10.1016/j.cmet.2015.07.002

Brunk E, Sahoo S, Zielinski DC, Altunkaya A, Dräger A, Mih N, Gatto F, Nilsson A, Preciat Gonzalez GA, Aurich MK, Prlić A, Sastry A, Danielsdottir AD, Heinken A, Noronha A, Rose PW, Burley SK, Fleming RMT, Nielsen J, Thiele I, Palsson BO. Recon3D enables a three-dimensional view of gene variation in human metabolism. *Nat. Biotechnol.*, 2018, 36(3):272–281 doi.org/10.1038/nbt.4072

Burcelin R, Crivelli V, Dacosta A, Roy-Tirelli A, Thorens B. Heterogeneous metabolic adaptation of C57BL/6J mice to high-fat diet. *Am. J. Physiol. Endocrinol. Metab.*, 2002, 282(4):E834-842 doi.org/10.1152/ajpendo.00332.2001

Camastra S, Muscelli E, Gastaldelli A, Holst JJ, Astiarraga B, Baldi S, Nannipieri M, Ciociaro D, Anselmino M, Mari A, Ferrannini E. Long-term effects of bariatric surgery on meal disposal and β-cell function in diabetic and nondiabetic patients. *Diabetes*, 2013, 62(11):3709–3717 doi.org/10.2337/db13-0321

Cameron AJ, Shaw JE, Zimmet PZ. The metabolic syndrome: prevalence in worldwide populations. *Endocrinol. Metab. Clin. North Am.*, 2004, 33(2):351–375 doi.org/10.1016/j.ecl.2004.03.005

Cannon B, Nedergaard J. Brown adipose tissue: function and physiological significance. *Physiol. Rev.*, 2004, 84(1):277–359 doi.org/10.1152/physrev.00015.2003

Cazzo E, Gestic MA, Utrini MP, Machado RR, Geloneze B, Pareja JC, Chaim EA. Impact of Roux-en-Y gastric bypass on Metabolic Syndrome and insulin resistance parameters. *Diabetes Technol. Ther.*, 2014, 16(4):262–265 doi.org/10.1089/dia.2013.0249

Cedersund G, Roll J. Systems biology: model based evaluation and comparison of potential explanations for given biological data. *FEBS J.*, 2009, 276(4):903–922 doi.org/10.1111/j.1742-4658.2008.06845.x

Chakrabarti A, Membrez M, Morin-Rivron D, Siddharth J, Chou CJ, Henry H, Bruce S, Metairon S, Raymond F, Betrisey B, Loyer C, Parkinson SJ, Masoodi M. Transcriptomics-driven lipidomics (TDL) identifies the microbiome-regulated targets of ileal lipid metabolism. *Npj Syst. Biol. Appl.*, 2017, 3(1):33 doi.org/10.1038/s41540-017-0033-0

Chalhoub E, Hanson RW, Belovich JM. A computer model of gluconeogenesis and lipid metabolism in the perfused liver. *Am. J. Physiol. Endocrinol. Metab.*, 2007a, 293(6):E1676-1686 doi.org/10.1152/ajpendo.00161.2007

Chalhoub E, Xie L, Balasubramanian V, Kim J, Belovich J. A distributed model of carbohydrate transport and metabolism in the liver during rest and high-intensity exercise. *Ann. Biomed. Eng.*, 2007b, 35(3):474–491 doi.org/10.1007/s10439-006-9217-2

Charbonnel BH, Matthews DR, Schernthaner G, Hanefeld M, Brunetti P, QUARTET Study Group. A long-term comparison of pioglitazone and gliclazide in patients with Type 2 diabetes mellitus: a randomized, double-blind, parallel-group comparison trial. *Diabet. Med.*, 2005, 22(4):399–405 doi.org/10.1111/j.1464-5491.2004.01426.x

Chechi K, Nedergaard J, Richard D. Brown adipose tissue as an anti-obesity tissue in humans. *Obes. Rev.*, 2014, 15(2):92–106 doi.org/10.1111/obr.12116

Chelliah V, Laibe C, Le Novère N. BioModels Database: a repository of mathematical models of biological processes. *Methods Mol. Biol.*, 2013, 1021:189–199 doi.org/10.1007/978-1-62703-450-0_10

Cobelli C, Dalla Man C, Toffolo G, Basu R, Vella A, Rizza R. The oral minimal model method. *Diabetes*, 2014, 63(4):1203–1213 doi.org/10.2337/db13-1198

Coleman T, Li Y. An interior trust region approach for nonlinear minimization subject to bounds. *SIAM J. Optim.*, 1996, 6(2):418–445 doi.org/10.1137/0806023

Çölmekçi C. The insulin signalling pathway in skeletal muscle: in silico and in vitro (PhD thesis). 144 pages, Eindhoven University of Technology; ISBN: 978-90-386-3838-6, 2015 repository.tue.nl/793112

Cook SF, Bies RR. Disease progression modeling: Key concepts and recent developments. *Curr. Pharmacol. Rep.*, 2016, 2(5):221–230 doi.org/10.1007/s40495-016-0066-x

Cooling J, Blundell J. Differences in energy expenditure and substrate oxidation between habitual high fat and low fat consumers (phenotypes). *Int. J. Obes. Relat. Metab. Disord.*, 1998, 22(7):612-618 nature.com/articles/0800635

Crabbe JC, Wahlsten D, Dudek BC. Genetics of mouse behavior: interactions with laboratory environment. *Science*, 1999, 284(5420):1670–1672 doi.org/10.1126/science.284.5420.1670

Craven P, Wahba G. Smoothing noisy data with spline functions. *Numer. Math.*, 1978, 31(4):377–403 doi.org/10.1007/BF01404567

Cumming G, Fidler F, Vaux DL. Error bars in experimental biology. *J. Cell Biol.*, 2007, 177(1):7–11 doi.org/10.1083/jcb.200611141

Dalla Man C, Camilleri M, Cobelli C. A system model of oral glucose absorption: validation on gold standard data. *IEEE Trans. Biomed. Eng.*, 2006, 53(12 Pt 1):2472–2478 doi.org/10.1109/TBME.2006.883792

Dalla Man C, Rizza RA, Cobelli C. Meal simulation model of the glucose-insulin system. *IEEE Trans. Biomed. Eng.*, 2007, 54(10):1740–1749 doi.org/10.1109/TBME.2007.893506

Dall'Ara E, Boudiffa M, Taylor C, Schug D, Fiegle E, Kennerley AJ, Damianou C, Tozer GM, Kiessling F, Müller R. Longitudinal imaging of the ageing mouse. *Mech. Ageing Dev.*, 2016, 160:93–116 doi.org/10.1016/j.mad.2016.08.001

van Dam AD, Nahon KJ, Kooijman S, van den Berg SM, Kanhai AA, Kikuchi T, Heemskerk MM, van Harmelen V, Lombès M, van den Hoek AM, de Winther MPJ, Lutgens E, Guigas B, Rensen PCN, Boon MR. Salsalate activates brown adipose tissue in mice. *Diabetes*, 2015, 64(5):1544–1554 doi.org/10.2337/db14-1125

Dayneka NL, Garg V, Jusko WJ. Comparison of four basic models of indirect pharmacodynamic responses. *J. Pharmacokinet. Biopharm.*, 1993, 21(4):457–478 doi.org/10.1007/BF01061691

DeBoer MD. Ethnicity, obesity and the metabolic syndrome: implications on assessing risk and targeting intervention. *Expert Rev. Endocrinol. Metab.*, 2011, 6(2):279–289 doi.org/10.1586/eem.11.17

DeFronzo RA. Pharmacologic therapy for type 2 diabetes mellitus. *Ann. Intern. Med.*, 1999, 131(4):281–303 doi.org/10.7326/0003-4819-131-4-199908170-00008

DeFronzo RA, Tobin JD, Andres R. Glucose clamp technique: a method for quantifying insulin secretion and resistance. *Am. J. Physiol.*, 1979, 237(3):E214-223 doi.org/10.1152/ajpendo.1979.237.3.E214

Delsing DJM, Offerman EH, van Duyvenvoorde W, van der Boom H, de Wit ECM, Gijbels MJJ, van der Laarse A, Jukema JW, Havekes LM, Princen HMG. Acyl-CoA:cholesterol acyltransferase inhibitor avasimibe reduces atherosclerosis in addition to its cholesterol-lowering effect in APOE*3-Leiden mice. *Circulation*, 2001, 103(13):1778–1786 doi.org/10.1161/01.CIR.103.13.1778

Demetrius L. Aging in mouse and human systems: a comparative study. *Ann. N. Y. Acad. Sci.*, 2006, 1067:66–82 doi.org/10.1196/annals.1354.010

Denis GV, Obin MS. "Metabolically healthy obesity": origins and implications. *Mol. Aspects Med.*, 2013, 34(1):59–70 doi.org/10.1016/j.mam.2012.10.004

Desilva PE. Système International (SI) units for plasma, serum, or blood concentrations. *Diabetes Care*, 2007, 30(3):769 doi.org/10.2337/diab.46.12.2128

Desroches S, Lamarche B. The evolving definitions and increasing prevalence of the metabolic syndrome. *Appl. Physiol. Nutr. Metab.*, 2007, 32(1):23–32 doi.org/10.1139/h06-095

van Diepen A. Analysis of the effect of type and temporal resolution of fluxes on model performance using ADAPT (BSc thesis). Eindhoven University of Technology, 2014

Din MU, Saari T, Raiko J, Kudomi N, Maurer SF, Lahesmaa M, Fromme T, Amri EZ, Klingenspor M, Solin O, Nuutila P, Virtanen KA. Postprandial oxidative metabolism of human brown fat indicates thermogenesis. *Cell Metab.*, 2018, 28(2):207-216.e3 doi.org/10.1016/j.cmet.2018.05.020

Dominguez LJ, Barbagallo M. The biology of the metabolic syndrome and aging. *Curr. Opin. Clin. Nutr. Metab. Care*, 2016, 19(1):5–11 doi.org/10.1097/MCO.0000000000000243

Drechsler S, Lynch MA, Novella S, González-Navarro H, Hecimovic S, Barini E, Tucci V, Castro RE, Vandenbroucke RE, Osuchowski M, Potter PK. With mouse age comes wisdom: A review and suggestions of relevant mouse models for age-related conditions. *Mech. Ageing Dev.*, 2016, 160:54–68 doi.org/10.1016/j.mad.2016.07.005

Dumas ME, Kinross J, Nicholson JK. Metabolic phenotyping and systems biology approaches to understanding metabolic syndrome and fatty liver disease. *Gastroenterology*, 2014, 146(1):46–62 doi.org/10.1053/j.gastro.2013.11.001

Dunn WB, Broadhurst DI, Atherton HJ, Goodacre R, Griffin JL. Systems level studies of mammalian metabolomes: the roles of mass spectrometry and nuclear magnetic resonance spectroscopy. *Chem. Soc. Rev.*, 2011, 40(1):387–426 doi.org/10.1039/b906712b

Dutta S, Sengupta P. Men and mice: Relating their ages. *Life Sci.*, 2016, 152:244–248 doi.org/10.1016/j.lfs.2015.10.025

Eaton SB, Konner M. Paleolithic nutrition. A consideration of its nature and current implications. *N. Engl. J. Med.*, 1985, 312(5):283–289 doi.org/10.1056/NEJM198501313120505

Eckel N, Li Y, Kuxhaus O, Stefan N, Hu FB, Schulze MB. Transition from metabolic healthy to unhealthy phenotypes and association with cardiovascular disease risk across BMI categories in 90 257 women (the Nurses' Health Study): 30 year follow-up from a prospective cohort study. *Lancet Diabetes Endocrinol.*, 2018, 6(9):714–724 doi.org/10.1016/S2213-8587(18)30137-2

Einhorn D, Reaven GM, Cobin RH, Ford E, Ganda OP, Handelsman Y, Hellman R, Jellinger PS, Kendall D, Krauss RM, Neufeld ND, Petak SM, Rodbard HW, Seibel JA, Smith DA, Wilson PWF. American College of Endocrinology position statement on the insulin resistance syndrome. *Endocr. Pract.*, 2003, 9(3):237–252 doi.org/10.4158/EP.9.S2.5

Enrique Caballero A. Long-term studies of treatments for type 2 diabetes. *Postgrad. Med.*, 2017, 129(3):352–365 doi.org/10.1080/00325481.2017.1265417

European Commission. Of mice and men – Are mice relevant models for human disease? Outcomes of the European Commission workshop "Are mice relevant models for human disease?" held in London, UK, 21 May 2010. 10 pages, 2010 ec.europa.eu/research/health/pdf/summary-report-25082010_en.pdf

Even PC, Nadkarni NA. Indirect calorimetry in laboratory mice and rats: principles, practical considerations, interpretation and perspectives. *Am. J. Physiol. Regul. Integr. Comp. Physiol.*, 2012, 303(5):R459-476 doi.org/10.1152/ajpregu.00137.2012

Expert Panel on Detection, Evaluation, and Treatment of High Blood Cholesterol in Adults. Executive summary of the third report of the National Cholesterol Education Program (NCEP) Expert Panel on detection, evaluation, and treatment of high blood cholesterol in adults (Adult Treatment Panel III). *JAMA*, 2001, 285(19):2486–2497 doi.org/10.1001/jama.285.19.2486

Farooqui AA, Farooqui T, Panza F, Frisardi V. Metabolic syndrome as a risk factor for neurological disorders. *Cell. Mol. Life Sci.*, 2012, 69(5):741–762 doi.org/10.1007/s00018-011-0840-1

Ferrannini E. The theoretical bases of indirect calorimetry: a review. *Metabolism.*, 1988, 37(3):287–301 doi.org/10.1016/0026-0495(88)90110-2

Festi D, Schiumerini R, Eusebi LH, Marasco G, Taddia M, Colecchia A. Gut microbiota and metabolic syndrome. *World J. Gastroenterol.*, 2014, 20(43):16079–16094 doi.org/10.3748/wjg.v20.i43.16079

Figueira I, Fernandes A, Mladenovic Djordjevic A, Lopez-Contreras A, Henriques CM, Selman C, Ferreiro E, Gonos ES, Trejo JL, Misra J, Rasmussen LJ, Xapelli S, Ellam T, Bellantuono I. Interventions for age-related diseases: Shifting the paradigm. *Mech. Ageing Dev.*, 2016, 160:69–92 doi.org/10.1016/j.mad.2016.09.009

Finkelstein EA, Khavjou OA, Thompson H, Trogdon JG, Pan L, Sherry B, Dietz W. Obesity and severe obesity forecasts through 2030. *Am. J. Prev. Med.*, 2012, 42(6):563–570 doi.org/10.1016/j.amepre.2011.10.026

Fluitman KS, Wijdeveld M, Nieuwdorp M, IJzerman RG. Potential of butyrate to influence food intake in mice and men. *Gut*, 2018, 67(7):1203–1204 doi.org/10.1136/gutjnl-2017-315543

Flurkey K, Currer JM, Harrison DE. The Mouse in Aging Research (Chapter 20). In: The Mouse in Biomedical Research (2nd Edition). Academic Press; ISBN: 978-0-12-369454-6, Burlington, MA, 2007, 637–672 doi.org/10.1016/B978-012369454-6/50074-1

Font-Burgada J, Sun B, Karin M. Obesity and cancer: The oil that feeds the flame. *Cell Metab.*, 2016, 23(1):48–62 doi.org/10.1016/j.cmet.2015.12.015

Fonteijn HM, Clarkson MJ, Modat M, Barnes J, Lehmann M, Ourselin S, Fox NC, Alexander DC. An event-based disease progression model and its application to familial Alzheimer's disease. *Inf. Process. Med. Imaging*, 2011, 22:748–759 doi.org/10.1007/978-3-642-22092-0_61

Friesen JHP. Lean-scaled weight can be used to estimate blood volume for obese patients. *Can. J. Anaesth.*, 2014, 61(11):1059–1060 doi.org/10.1007/s12630-014-0218-6

Frisard M, Ravussin E. Energy metabolism and oxidative stress: impact on the metabolic syndrome and the aging process. *Endocrine*, 2006, 29(1):27–32 doi.org/10.1385/ENDO:29:1:27

Frohman HA, Rychahou PG, Li J, Gan T, Evers BM. Development of murine bariatric surgery models: lessons learned. *J. Surg. Res.*, 2018, 229:302–310 doi.org/10.1016/j.jss.2018.04.022

Fryburg DA, Song DH, de Graaf D. Early patient stratification is critical to enable effective and personalised drug discovery and development. *Drug Discov. World*, 2011, 12(3):47-56 ddw-online.com/personalised-medicine/p149258-early-patient-stratification-is-critical-to-enable-effective-and-personalised-drug-discovery-and-development.html

Gábor A, Banga JR. Robust and efficient parameter estimation in dynamic models of biological systems. *BMC Syst. Biol.*, 2015, 9:74 doi.org/10.1186/s12918-015-0219-2

Galgani JE, Moro C, Ravussin E. Metabolic flexibility and insulin resistance. *Am. J. Physiol. Endocrinol. Metab.*, 2008, 295(5):E1009–E1017 doi.org/10.1152/ajpendo.90558.2008

Gao Z, Yin J, Zhang J, Ward RE, Martin RJ, Lefevre M, Cefalu WT, Ye J. Butyrate improves insulin sensitivity and increases energy expenditure in mice. *Diabetes*, 2009, 58(7):1509–1517 doi.org/10.2337/db08-1637

Ghosal S, Nunley A, Mahbod P, Lewis AG, Smith EP, Tong J, D'Alessio DA, Herman JP. Mouse handling limits the impact of stress on metabolic endpoints. *Physiol. Behav.*, 2015, 150:31–37 doi.org/10.1016/j.physbeh.2015.06.021

Goldstone AP, Beales PL. Genetic obesity syndromes. *Front. Horm. Res.*, 2008, 36:37–60 doi.org/10.1159/0000115336

González-Navarro H, Vinué Á, Vila-Caballer M, Fortuño A, Beloqui O, Zalba G, Burks D, Díez J, Andrés V. Molecular mechanisms of atherosclerosis in Metabolic Syndrome: Role of reduced IRS2-dependent signaling. *Arterioscler. Thromb. Vasc. Biol.*, 2008, 28(12):2187–2194 doi.org/10.1161/ATVBAHA.108.175299

Goodman SN. Of P-values and Bayes: a modest proposal. *Epidemiol. Camb. Mass*, 2001, 12(3):295–297 doi.org/10.1097/00001648-200105000-00006

Goodpaster BH, Sparks LM. Metabolic flexibility in health and disease. *Cell Metab.*, 2017, 25(5):1027–1036 doi.org/10.1016/j.cmet.2017.04.015

Goossens GH, Blaak EE. Adipose tissue dysfunction and impaired metabolic health in human obesity: a matter of oxygen? *Front. Endocrinol.*, 2015, 6:55 doi.org/10.3389/fendo.2015.00055

de Graaf AA, Freidig AP, De Roos B, Jamshidi N, Heinemann M, Rullmann JAC, Hall KD, Adiels M, van Ommen B. Nutritional systems biology modeling: from molecular mechanisms to physiology. *PLoS Comput. Biol.*, 2009, 5(11):e1000554 doi.org/10.1371/journal.pcbi.1000554

Grave RD, Calugi S, Centis E, Marzocchi R, Ghoch ME, Marchesini G. Lifestyle modification in the management of the metabolic syndrome: achievements and challenges. *Diabetes Metab. Syndr. Obes.*, 2010, 3:373–385 doi.org/10.2147/DMSOTT.S13860

Grundy SM, Brewer HB, Cleeman JI, Smith SC, Lenfant C. Definition of Metabolic Syndrome report of the National Heart, Lung, and Blood Institute/American Heart Association Conference on scientific issues related to definition. *Circulation*, 2004, 109(3):433–438 doi.org/10.1161/01.CIR.0000111245.75752.C6

Guldberg CM, Waage P. Studier i affiniteten. *Forhandelinger Vidensk. Christ.*, 1864, 35

Guo J, Hall KD. Predicting changes of body weight, body fat, energy expenditure and metabolic fuel selection in C57BL/6 mice. *PLOS ONE*, 2011, 6(1):e15961 doi.org/10.1371/journal.pone.0015961

Ha J, Satin LS, Sherman AS. A mathematical model of the pathogenesis, prevention, and reversal of type 2 diabetes. *Endocrinology*, 2016, 157(2):624–635 doi.org/10.1210/en.2015-1564

de Haan W, de Vries-van der Weij J, van der Hoorn JWA, Gautier T, van der Hoogt CC, Westerterp M, Romijn JA, Jukema JW, Havekes LM, Princen HMG, Rensen PCN. Torcetrapib does not reduce atherosclerosis beyond atorvastatin and induces more proinflammatory lesions than atorvastatin. *Circulation*, 2008, 117(19):2515–2522 doi.org/10.1161/CIRCULATIONAHA.107.761965

Hall KD. Metabolism of mice and men: mathematical modeling of body weight dynamics. *Curr. Opin. Clin. Nutr. Metab. Care*, 2012, 15(5):418–423 doi.org/10.1097/MCO.0b013e3283561150

Hallgreen CE. The interplay between glucose and fat metabolism: a biosimulation approach (PhD thesis). 141 pages, Technical University of Denmark, Copenhagen, 2009 orbit.dtu.dk/fedora/objects/orbit:81855/datastreams/file_4260839/content

Halsey LG, Curran-Everett D, Vowler SL, Drummond GB. The fickle P value generates irreproducible results. *Nat. Methods*, 2015, 12(3):179–185 doi.org/10.1038/nmeth.3288

Hamilton MT, Hamilton DG, Zderic TW. Role of low energy expenditure and sitting in obesity, metabolic syndrome, type 2 diabetes, and cardiovascular disease. *Diabetes*, 2007, 56(11):2655–2667 doi.org/10.2337/db07-0882

Han TS, Lean ME. A clinical perspective of obesity, metabolic syndrome and cardiovascular disease. *JRSM Cardiovasc. Dis.*, 2016, 25(5) doi.org/10.1177/2048004016633371

Hanssen MJW, Hoeks J, Brans B, van der Lans AAJJ, Schaart G, van den Driessche JJ, Jörgensen JA, Boekschoten MV, Hesselink MKC, Havekes B, Kersten S, Mottaghy FM, van Marken Lichtenbelt WD, Schrauwen P. Short-term cold acclimation improves insulin sensitivity in patients with type 2 diabetes mellitus. *Nat. Med.*, 2015, 21(8):863–865 doi.org/10.1038/nm.3891

Hassanein NMA, Elwy AHM, Tabl GA, Al-Mallah THY. Therapeutic potential of orlistat-bupropion treatment on high fat diet-induced lipotoxicity. *Toxicol. Environ. Health Sci.*, 2015, 7(5):262–271 doi.org/10.1007/s13530-015-0247-8

Hatipoglu H, Yaylak F, Gungor Y. A brief review on the periodontal health in metabolic syndrome patients. *Diabetes Metab. Syndr.*, 2015, 9(2):124–126 doi.org/10.1016/j.dsx.2015.02.007

Hijmans BS, Tiemann CA, Grefhorst A, Boesjes M, van Dijk TH, Tietge UJF, Kuipers F, van Riel NAW, Groen AK, Oosterveer MH. A systems biology approach reveals the physiological origin of hepatic steatosis induced by liver X receptor activation. *FASEB J.*, 2015, 29(4):1153–1164 doi.org/10.1096/fj.14-254656

Hill JO, Wyatt HR, Peters JC. Energy balance and obesity. *Circulation*, 2012, 126(1):126–132 doi.org/10.1161/CIRCULATIONAHA.111.087213

Hindmarsh AC, Brown PN, Grant KE, Lee SL, Serban R, Shumaker DE, Woodward CS. SUNDIALS: Suite of Nonlinear and Differential/Algebraic Equation Solvers. *ACM Trans Math Softw*, 2005, 31(3):363–396 doi.org/10.1145/1089014.1089020

van den Hoek AM, van der Hoorn JWA, Maas AC, van den Hoogen RM, van Nieuwkoop A, Droog S, Offerman EH, Pieterman EJ, Havekes LM, Princen HMG. APOE*3Leiden.CETP transgenic mice as model for pharmaceutical treatment of the metabolic

syndrome. *Diabetes Obes. Metab.*, 2014, 16(6):537–544 doi.org/10.1111/dom.12252

Hood L, Balling R, Auffray C. Revolutionizing medicine in the 21st century through systems approaches. *Biotechnol. J.*, 2012, 7(8):992–1001 doi.org/10.1002/biot.201100306

van der Hoogt CC, de Haan W, Westerterp M, Hoekstra M, Dallinga-Thie GM, Romijn JA, Princen HMG, Jukema JW, Havekes LM, Rensen PCN. Fenofibrate increases HDL-cholesterol by reducing cholesteryl ester transfer protein expression. *J. Lipid Res.*, 2007, 48(8):1763–1771 doi.org/10.1194/jlr.M700108-JLR200

van der Hoorn JWA, de Haan W, Berbée JFP, Havekes LM, Jukema JW, Rensen PCN, Princen HMG. Niacin increases HDL by reducing hepatic expression and plasma levels of cholesteryl ester transfer protein in APOE*3Leiden.CETP mice. *Arterioscler. Thromb. Vasc. Biol.*, 2008, 28(11):2016–2022 doi.org/10.1161/ATVBAHA.108.171363

van der Hoorn JWA, Jukema JW, Havekes LM, Lundholm E, Camejo G, Rensen PCN, Princen HMG. The dual PPARalpha/gamma agonist tesaglitazar blocks progression of pre-existing atherosclerosis in APOE*3Leiden.CETP transgenic mice. *Br. J. Pharmacol.*, 2009, 156(7):1067–1075 doi.org/10.1111/j.1476-5381.2008.00109.x

van der Hoorn JWA, Kleemann R, Havekes LM, Kooistra T, Princen HMG, Jukema JW. Olmesartan and pravastatin additively reduce development of atherosclerosis in APOE*3Leiden transgenic mice. *J. Hypertens.*, 2007, 25(12):2454–2462 doi.org/10.1097/HJH.0b013e3282ef79f7

Iacovides S, Meiring RM. The effect of a ketogenic diet versus a high-carbohydrate, low-fat diet on sleep, cognition, thyroid function, and cardiovascular health independent of weight loss: study protocol for a randomized controlled trial. *Trials*, 2018, 19 doi.org/10.1186/s13063-018-2462-5

International Diabetes Federation. The IDF consensus worldwide definition of the metabolic syndrome. 2006 idf.org/e-library/consensus-statements/60-idfconsensus-worldwide-definitionof-the-metabolic-syndrome.html

Inzucchi SE. Oral antihyperglycemic therapy for type 2 diabetes: scientific review. *JAMA*, 2002, 287(3):360–372 doi.org/10.1001/jama.287.3.360

Janmahasatian S, Duffull SB, Ash S, Ward LC, Byrne NM, Green B. Quantification of lean bodyweight. *Clin. Pharmacokinet.*, 2005, 44(10):1051–1065 doi.org/10.2165/00003088-200544100-00004

Jelic K, Hallgreen CE, Colding-Jørgensen M. A model of NEFA dynamics with focus on the postprandial state. *Ann. Biomed. Eng.*, 2009, 37(9):1897–1909 doi.org/10.1007/s10439-009-9738-6

Jiang XC, Agellon LB, Walsh A, Breslow JL, Tall A. Dietary cholesterol increases transcription of the human cholesteryl ester transfer protein gene in transgenic mice. Dependence on natural flanking sequences. *J. Clin. Invest.*, 1992, 90(4):1290–1295 doi.org/10.1172/JCI115993

Johns C, Gavras I, Handy DE, Salomao A, Gavras H. Models of experimental hypertension in mice. *Hypertension*, 1996, 28(6):1064–1069 doi.org/10.1161/01.HYP.28.6.1064

Johnson KA, Goody RS. The original Michaelis constant: Translation of the 1913 Michaelis-Menten paper. *Biochemistry*, 2011, 50(39):8264–8269 doi.org/10.1021/bi201284u

Johnson NA, Walton DW, Sachinwalla T, Thompson CH, Smith K, Ruell PA, Stannard SR, George J. Noninvasive assessment of hepatic lipid composition: Advancing understanding and management of fatty liver disorders. *Hepatology*, 2008, 47(5):1513–1523 doi.org/10.1002/hep.22220

Jørgensen NB, Jacobsen SH, Dirksen C, Bojsen-Møller KN, Naver L, Hvolris L, Clausen TR, Wulff BS, Worm D, Lindqvist Hansen D, Madsbad S, Holst JJ. Acute and long-term effects of Roux-en-Y gastric bypass on glucose metabolism in subjects with type 2 diabetes and normal glucose tolerance. *Am. J. Physiol. Endocrinol. Metab.*, 2012, 303(1):E122-131 doi.org/10.1152/ajpendo.00073.2012

Kansal AR, Trimmer J. Application of predictive biosimulation within pharmaceutical clinical development: examples of significance for translational medicine and clinical trial design. *IEE Proc. Syst. Biol.*, 2005, 152(4):214–220 doi.org/10.1049/ip-syb:20050043

Karas RH, Kashyap ML, Knopp RH, Keller LH, Bajorunas DR, Davidson MH. Long-term safety and efficacy of a combination of niacin extended release and simvastatin in patients with dyslipidemia: the OCEANS study. *Am. J. Cardiovasc. Drugs*, 2008, 8(2):69–81 doi.org/10.2165/00129784-200808020-00001

Karns R, Succop P, Zhang G, Sun G, Indugula SR, Havas-Augustin D, Novokmet N, Durakovic Z, Milanovic SM, Missoni S, Vuletic S, Chakraborty R, Rudan P, Deka R. Modeling metabolic syndrome through structural equations of metabolic traits, comorbid diseases, and GWAS variants. *Obes. Silver Spring Md*, 2013, 21(12):E745-754 doi.org/10.1002/oby.20445

Kassi E, Pervanidou P, Kaltsas G, Chrousos G. Metabolic syndrome: definitions and controversies. *BMC Med.*, 2011, 9(1):48 doi.org/10.1186/1741-7015-9-48

Kataria I, Chadha R, Pathak R. Dietary and lifestyle modification in metabolic syndrome: a review of randomized control trials in different population groups. *Rev. Health Care*, 2013, 4(4):209–230 doi.org/10.7175/rhc.v4i4.667

Kaur J. A comprehensive review on Metabolic Syndrome. *Cardiol. Res. Pract.*, 2014, 2014 doi.org/10.1155/2014/943162

Kesäniemi YA, Miettinen TA. Cholesterol absorption efficiency regulates plasma cholesterol level in the Finnish population. *Eur. J. Clin. Invest.*, 1987, 17(5):391–395 doi.org/10.1111/j.1365-2362.1987.tb01132.x

Khedoe PPSJ, Hoeke G, Kooijman S, Dijk W, Buijs JT, Kersten S, Havekes LM, Hiemstra PS, Berbée JFP, Boon MR, Rensen PCN. Brown adipose tissue takes up plasma triglycerides mostly after lipolysis. *J. Lipid Res.*, 2015, 56(1):51–59 doi.org/10.1194/jlr.M052746

Khoo MCK, Oliveira FMGS, Cheng L. Understanding the metabolic syndrome: a modeling perspective. *IEEE Rev. Biomed. Eng.*, 2013, 6:143–155 doi.org/10.1109/RBME.2012.2232651

Kim J, Saidel GM, Cabrera ME. Multi-scale computational model of fuel homeostasis during exercise: effect of hormonal control. *Ann. Biomed. Eng.*, 2007, 35(1):69–90 doi.org/10.1007/s10439-006-9201-x

Kim IY, Suh SH, Lee IK, Wolfe RR. Applications of stable, nonradioactive isotope tracers in in vivo human metabolic research. *Exp. Mol. Med.*, 2016, 48(1):e203 doi.org/10.1038/emm.2015.97

Kleemann R, Princen HMG, Emeis JJ, Jukema JW, Fontijn RD, Horrevoets AJG, Kooistra T, Havekes LM. Rosuvastatin reduces atherosclerosis development beyond and independent of its plasma cholesterol-lowering effect in APOE*3-Leiden transgenic mice: evidence for antiinflammatory effects of rosuvastatin. *Circulation*, 2003, 108(11):1368–1374 doi.org/10.1161/01.CIR.0000086460.55494.AF

Kõks S, Dogan S, Tuna BG, González-Navarro H, Potter P, Vandenbroucke RE. Mouse models of ageing and their relevance to disease. *Mech. Ageing Dev.*, 2016, 160:41–53 doi.org/10.1016/j.mad.2016.10.001

Kolovou GD, Anagnostopoulou KK, Cokkinos DV. Pathophysiology of dyslipidaemia in the metabolic syndrome. *Postgrad. Med. J.*, 2005, 81(956):358–366 doi.org/10.1136/pgmj.2004.025601

Kolovou GD, Anagnostopoulou KK, Salpea KD, Mikhailidis DP. The prevalence of metabolic syndrome in various populations. *Am. J. Med. Sci.*, 2007, 333(6):362–371 doi.org/10.1097/MAJ.0b013e318065c3a1

König M, Bulik S, Holzhütter HG. Quantifying the contribution of the liver to glucose homeostasis: a detailed kinetic model of human hepatic glucose metabolism. *PLoS Comput. Biol.*, 2012, 8(6):e1002577 doi.org/10.1371/journal.pcbi.1002577

Kononowicz AA, Zary N, Edelbring S, Corral J, Hege I. Virtual patients - what are we talking about? A framework to classify the meanings of the term in healthcare education. *BMC Med. Educ.*, 2015, 15 doi.org/10.1186/s12909-015-0296-3

Kooistra T, Verschuren L, de Vries-van der Weij J, Koenig W, Toet K, Princen HMG, Kleemann R. Fenofibrate reduces atherogenesis in APOE*3Leiden mice: evidence for multiple antiatherogenic effects besides lowering plasma cholesterol. *Arterioscler. Thromb. Vasc. Biol.*, 2006, 26(10):2322–2330 doi.org/10.1161/01.ATV.0000238348.05028.14

Kühnast S, van der Tuin SJL, van der Hoorn JWA, van Klinken JB, Simic B, Pieterman E, Havekes LM, Landmesser U, Lüscher TF, Willems van Dijk K, Rensen PCN, Jukema JW, Princen HMG. Anacetrapib reduces progression of atherosclerosis, mainly by reducing non-HDL-cholesterol, improves lesion stability and adds to the beneficial effects of atorvastatin. *Eur. Heart J.*, 2015, 36(1):39–48 doi.org/10.1093/eurheartj/ehu319

Lang A, Volkamer A, Behm L, Röblitz S, Ehrig R, Schneider M, Geris L, Wichard J, Buttgereit F. In silico methods – Computational alternatives to animal testing. *ALTEX*, 2018, 35(1):126–128 doi.org/10.14573/altex.1712031

Lee CMY, Huxley RR, Woodward M, Zimmet P, Shaw J, Cho NH, Kim HR, Viali S, Tominaga M, Vistisen D, Borch-Johnsen K, Colagiuri S. The metabolic syndrome identifies a heterogeneous group of metabolic component combinations in the Asia-Pacific region. *Diabetes Res. Clin. Pract.*, 2008, 81(3):377–380 doi.org/10.1016/j.diabres.2008.05.011

Lee JC, Lee HY, Kim TK, Kim MS, Park YM, Kim J, Park K, Kweon MN, Kim SH, Bae JW, Hur KY, Lee MS. Obesogenic diet-induced gut barrier dysfunction and pathobiont expansion aggravate experimental colitis. *PloS One*, 2017, 12(11):e0187515 doi.org/10.1371/journal.pone.0187515

Lee P, Swarbrick MM, Ho KKY. Brown adipose tissue in adult humans: a metabolic renaissance. *Endocr. Rev.*, 2013, 34(3):413–438 doi.org/10.1210/er.2012-1081

Lee P, Zhao JT, Swarbrick MM, Gracie G, Bova R, Greenfield JR, Freund J, Ho KKY. High prevalence of brown adipose tissue in adult humans. *J. Clin. Endocrinol. Metab.*, 2011, 96(8):2450–2455 doi.org/10.1210/jc.2011-0487

Leiden Metabolic Research Services. APOE*3-Leiden.CETP mouse: Translational model for Cardiovascular and Metabolic Diseases. 2016 lprs.nl/wp-content/uploads/2016/01/Leiden-Metabolic-Research-Services-Flyer.pdf

Lemmens HJM, Bernstein DP, Brodsky JB. Estimating blood volume in obese and morbidly obese patients. *Obes. Surg.*, 2006, 16(6):773–776 doi.org/10.1381/096089206777346673

Lerman LO, Chade AR, Sica V, Napoli C. Animal models of hypertension: An overview. *J. Lab. Clin. Med.*, 2005, 146(3):160–173 doi.org/10.1016/j.lab.2005.05.005

Li Z, Wang Y, van der Sluis RJ, van der Hoorn JWA, Princen HMG, van Eck M, van Berkel TJC, Rensen PCN, Hoekstra M. Niacin reduces plasma CETP levels by diminishing liver macrophage content in CETP transgenic mice. *Biochem. Pharmacol.*, 2012, 84(6):821–829 doi.org/10.1016/j.bcp.2012.06.020

Li Z, Yi CX, Katiraei S, Kooijman S, Zhou E, Chung CK, Gao Y, van den Heuvel JK, Meijer OC, Berbée JFP, Heijink M, Giera M, Willems van Dijk K, Groen AK, Rensen PCN, Wang Y. Butyrate reduces appetite and activates brown adipose tissue via the gut-brain neural circuit. *Gut*, 2018, 67(7):1269–1279 doi.org/10.1136/gutjnl-2017-314050

Liang W, Menke AL, Driessen A, Koek GH, Lindeman JH, Stoop R, Havekes LM, Kleemann R, van den Hoek AM. Establishment of a general NAFLD scoring system for rodent models and comparison to human liver pathology. *PloS One*, 2014, 9(12):e115922 doi.org/10.1371/journal.pone.0115922

Lichtenbelt W van M, Kingma B, van der Lans A, Schellen L. Cold exposure--an approach to increasing energy expenditure in humans. *Trends Endocrinol. Metab.*, 2014, 25(4):165–167 doi.org/10.1016/j.tem.2014.01.001

Lidell ME, Betz MJ, Enerbäck S. Brown adipose tissue and its therapeutic potential. *J. Intern. Med.*, 2014, 276(4):364–377 doi.org/10.1111/joim.12255

Lindon JC, Nicholson JK. The emergent role of metabolic phenotyping in dynamic patient stratification. *Expert Opin. Drug Metab. Toxicol.*, 2014, 10(7):915–919 doi.org/10.1517/17425255.2014.922954

Livesey G, Elia M. Estimation of energy expenditure, net carbohydrate utilization, and net fat oxidation and synthesis by indirect calorimetry: evaluation of errors with special reference to the detailed composition of fuels. *Am. J. Clin. Nutr.*, 1988, 47(4):608–628 doi.org/10.1093/ajcn/47.4.608

Loos RJF, Bouchard C. Obesity--is it a genetic disorder? *J. Intern. Med.*, 2003, 254(5):401–425 doi.org/10.1046/j.1365-2796.2003.01242.x

Lu J, Hübner K, Nanjee MN, Brinton EA, Mazer NA. An in-silico model of lipoprotein metabolism and kinetics for the evaluation of targets and biomarkers in the reverse cholesterol transport pathway. *PLoS Comput Biol*, 2014, 10(3):e1003509 doi.org/10.1371/journal.pcbi.1003509

Luan Y, Li H. Clustering of time-course gene expression data using a mixed-effects model with B-splines. *Bioinformatics*, 2003, 19(4):474–482 doi.org/10.1093/bioinformatics/btg014

Lusis AJ, Attie AD, Reue K. Metabolic syndrome: from epidemiology to systems biology. *Nat. Rev. Genet.*, 2008, 9(11):819–830 doi.org/10.1038/nrg2468

Lutz TA, Woods SC. Overview of animal models of obesity. *Curr. Protoc. Pharmacol.*, 2012, CHAPTER:Unit5.61 doi.org/10.1002/0471141755.ph0561s58

Lynes MD, Tseng YH. Deciphering adipose tissue heterogeneity. *Ann. N. Y. Acad. Sci.*, 2018, 1411(1):5–20 doi.org/10.1111/nyas.13398

van den Maagdenberg AM, Hofker MH, Krimpenfort PJ, de Bruijn I, van Vlijmen B, van der Boom H, Havekes LM, Frants RR. Transgenic mice carrying the apolipoprotein E3-Leiden gene exhibit hyperlipoproteinemia. *J. Biol. Chem.*, 1993, 268(14):10540-10545 jbc.org/content/268/14/10540

Maas AH, Rozendaal YJW, van Pul C, Hilbers PAJ, Cottaar WJ, Haak HR, van Riel NAW. A physiology-based model describing heterogeneity in glucose metabolism: The core of the Eindhoven Diabetes Education Simulator (E-DES). *J. Diabetes Sci. Technol.*, 2015, 9(2):282–292 doi.org/10.1177/1932296814562607

MacQueen J. Some methods for classification and analysis of multivariate observations. *Proc. Fifth Berkeley Symp. Math. Stat. Probab.*, 1967, 1:281-297 projecteuclid.org/euclid.bsmsp/1200512992

Matfin G. Developing therapies for the metabolic syndrome: challenges, opportunities, and… the unknown. *Ther. Adv. Endocrinol. Metab.*, 2010, 1(2):89–94 doi.org/10.1177/2042018810375812

Matsuda M, DeFronzo RA. Insulin sensitivity indices obtained from oral glucose tolerance testing: comparison with the euglycemic insulin clamp. *Diabetes Care*, 1999, 22(9):1462–1470 doi.org/10.2337/diacare.22.9.1462

Matthaei S, Stumvoll M, Kellerer M, Häring HU. Pathophysiology and pharmacological treatment of insulin resistance. *Endocr. Rev.*, 2000, 21(6):585–618 doi.org/10.1210/edrv.21.6.0413

Mc Auley MT, Mooney KM. Computationally modeling lipid metabolism and aging: A mini-review. *Comput. Struct. Biotechnol. J.*, 2014, 13:38–46 doi.org/10.1016/j.csbj.2014.11.006

Mc Auley MT, Wilkinson DJ, Jones JJL, Kirkwood TBL. A whole-body mathematical model of cholesterol metabolism and its age-associated dysregulation. *BMC Syst. Biol.*, 2012, 6:130 doi.org/10.1186/1752-0509-6-130

Melzer K. Carbohydrate and fat utilization during rest and physical activity. *ESPEN Eur. EJournal Clin. Nutr. Metab.*, 2011, 6(2):e45–e52 doi.org/10.1016/j.eclnm.2011.01.005

Mendizábal Y, Llorens S, Nava E. Hypertension in metabolic syndrome: vascular pathophysiology. *Int. J. Hypertens.*, 2013, 2013:230868 doi.org/10.1155/2013/230868

Michaelis L, Menten ML. Die Kinetik der Invertinwirkung. *Biochem. Z.*, 1913, 49:333–369

Micheloni A, Orsi G, De Maria C, Vozzi G. ADMET: ADipocyte METabolism mathematical model. *Comput. Methods Biomech. Biomed. Engin.*, 2014, 18(13):1386–1391 doi.org/10.1080/10255842.2014.908855

Monassier L, Combe R, Fertak LE. Mouse models of hypertension. *Drug Discov. Today Dis. Models*, 2006, 3(3):273–281 doi.org/10.1016/j.ddmod.2006.10.008

Mooney KM, Morgan AE, Mc Auley MT. Aging and computational systems biology. *Wiley Interdiscip. Rev. Syst. Biol. Med.*, 2016, 8(2):123–139 doi.org/10.1002/wsbm.1328

Moore JX. Metabolic Syndrome prevalence by race/ethnicity and sex in the United States, national health and nutrition examination Survey, 1988–2012. *Prev. Chronic. Dis.*, 2017, 14 doi.org/10.5888/pcd14.160287

Moreira GC, Cipullo JP, Ciorlia LAS, Cesarino CB, Vilela-Martin JF. Prevalence of Metabolic Syndrome: Association with risk factors and cardiovascular complications in an urban population. *PLoS ONE*, 2014, 9(9) doi.org/10.1371/journal.pone.0105056

Moreno-Sánchez R, Saavedra E, Rodríguez-Enríquez S, Olín-Sandoval V. Metabolic Control Analysis: A tool for designing strategies to manipulate metabolic pathways. *J. Biomed. Biotechnol.*, 2008, 2008 doi.org/10.1155/2008/597913

Mukherjee J, Baranwal A, Schade KN. Classification of Therapeutic and Experimental Drugs for Brown Adipose Tissue Activation: Potential Treatment Strategies for Diabetes and Obesity. *Curr. Diabetes Rev.*, 2016, 12(4):414–428 doi.org/10.2174/1573399812666160517115450

Muzio F, Mondazzi L, Sommariva D, Branchi A. Long-term effects of low-calorie diet on the Metabolic Syndrome in oObese nondiabetic patients. *Diabetes Care*, 2005, 28(6):1485–1486 doi.org/10.2337/diacare.28.6.1485

Nassour I, Almandoz JP, Adams-Huet B, Kukreja S, Puzziferri N. Metabolic syndrome remission after Roux-en-Y gastric bypass or sleeve gastrectomy. *Diabetes Metab. Syndr. Obes. Targets Ther.*, 2017, 10:393–402 doi.org/10.2147/DMSO.S142731

Nathan DM, Turgeon H, Regan S. Relationship between glycated haemoglobin levels and mean glucose levels over time. *Diabetologia*, 2007, 50(11):2239–2244 doi.org/10.1007/s00125-007-0803-0

NCD Risk Factor Collaboration. Worldwide trends in body-mass index, underweight, overweight, and obesity from 1975 to 2016: a pooled analysis of 2416 population-based measurement studies in 128·9 million children, adolescents, and adults. *Lancet Lond. Engl.*, 2017, 390(10113):2627–2642 doi.org/10.1016/S0140-6736(17)32129-3

Nedergaard J, Bengtsson T, Cannon B. Unexpected evidence for active brown adipose tissue in adult humans. *Am. J. Physiol. Endocrinol. Metab.*, 2007, 293(2):E444-452 doi.org/10.1152/ajpendo.00691.2006

Nedergaard J, Cannon B. The changed metabolic world with human brown adipose tissue: therapeutic visions. *Cell Metab.*, 2010, 11(4):268–272 doi.org/10.1016/j.cmet.2010.03.007

Neeland IJ, Poirier P, Després JP. Cardiovascular and metabolic heterogeneity of obesity: Clinical challenges and implications for management. *Circulation*, 2018, 137(13):1391–1406 doi.org/10.1161/CIRCULATIONAHA.117.029617

Neels JG, Olefsky JM. Inflamed fat: what starts the fire? *J. Clin. Invest.*, 2006, 116(1):33–35 doi.org/10.1172/JCI27280

Ness-Abramof R, Apovian CM. Drug-induced weight gain. *Timely Top Med Cardiovasc Dis*, 2005, 9:E31 doi.org/10.1358/dot.2005.41.8.893630

Nguyen THT, Mouksassi MS, Holford N, Al-Huniti N, Freedman I, Hooker AC, John J, Karlsson MO, Mould DR, Ruixo JJP, Plan EL, Savic R, van Hasselt JGC, Weber B, Zhou C, Comets E, Mentré F. Model Evaluation of Continuous Data Pharmacometric Models: Metrics and Graphics. *CPT Pharmacomet. Syst. Pharmacol.*, 2017, 6(2):87–109 doi.org/10.1002/psp4.12161

Nieuwdorp M, Gilijamse PW, Pai N, Kaplan LM. Role of the microbiome in energy regulation and metabolism. *Gastroenterology*, 2014, 146(6):1525–1533 doi.org/10.1053/j.gastro.2014.02.008

Nissen A, Fonvig CE, Chabanova E, Bøjsøe C, Trier C, Pedersen O, Hansen T, Thomsen HS, Holm J -C. 1H-MRS measured ectopic fat in liver and muscle is associated with the metabolic syndrome in Danish girls but not in boys with overweight and obesity. *Obes. Sci. Pract.*, 2016, 2(4):376–384 doi.org/10.1002/osp4.61

Nunn AV, Bell JD, Guy GW. Lifestyle-induced metabolic inflexibility and accelerated ageing syndrome: insulin resistance, friend or foe? *Nutr. Metab.*, 2009, 6:16 doi.org/10.1186/1743-7075-6-16

Nuzzo R. Scientific method: statistical errors. *Nature*, 2014, 506(7487):150–152 doi.org/10.1038/506150a

Nyman E, Brännmark C, Palmér R, Brugård J, Nyström FH, Strålfors P, Cedersund G. A hierarchical whole-body modeling approach elucidates the link between in vitro insulin signaling and in vivo glucose homeostasis. *J. Biol. Chem.*, 2011, 286(29):26028–26041 doi.org/10.1074/jbc.M110.188987

Nyman E, Rozendaal YJW, Helmlinger G, Hamrén B, Kjellsson MC, Strålfors P, van Riel NAW, Gennemark P, Cedersund G. Requirements for multi-level systems pharmacology models to reach end-usage: the case of type 2 diabetes. *Interface Focus*, 2016, 6(2):20150075 doi.org/10.1098/rsfs.2015.0075

Olefsky JM. Treatment of insulin resistance with peroxisome proliferator-activated receptor gamma agonists. *J. Clin. Invest.*, 2000, 106(4):467–472 doi.org/10.1172/JCI10843

Orešič M, Vidal-Puig A. A systems biology approach to study metabolic syndrome. 1st ed., Springer International Publishing; ISBN: 978-3-319-01007-6, Switzerland, 2014 springer.com/biomed/book/978-3-319-01007-6

Orsi G, De Maria C, Guzzardi M, Vozzi F, Vozzi G. HEMETβ: improvement of hepatocyte metabolism mathematical model. *Comput. Methods Biomech. Biomed. Engin.*, 2011, 14(10):837–851 doi.org/10.1080/10255842.2010.497145

Orth JD, Thiele I, Palsson BØ. What is flux balance analysis? *Nat. Biotechnol.*, 2010, 28(3):245–248 doi.org/10.1038/nbt.1614

Ouellet V, Labbé SM, Blondin DP, Phoenix S, Guérin B, Haman F, Turcotte EE, Richard D, Carpentier AC. Brown adipose tissue oxidative metabolism contributes to energy expenditure during acute cold exposure in humans. *J. Clin. Invest.*, 2012, 122(2):545–552 doi.org/10.1172/JCI60433

Paalvast Y, Gerding A, Wang Y, Bloks VW, van Dijk TH, Havinga R, Willems van Dijk K, Rensen PCN, Bakker BM, Kuivenhoven JA, Groen AK. Male APOE*3-Leiden.CETP mice on high-fat high-cholesterol diet exhibit a biphasic dyslipidemic response, mimicking the changes in plasma lipids observed through life in men. *Physiol. Rep.*, 2017, 5(19):e13376 doi.org/10.14814/phy2.13376

Paalvast Y, Kuivenhoven JA, Groen AK. Evaluating computational models of cholesterol metabolism. *Biochim. Biophys. Acta*, 2015, 1851(10):1360–1376 doi.org/10.1016/j.bbalip.2015.05.008

Paalvast Y, Rozendaal YJW, Wang Y, Gerding A, Rensen PCN, Willems van Dijk K, Kuivenhoven JA, Bakker BM, van Riel NAW, Groen AK. Triglyceride absorption drives phenotype heterogeneity in APOE*3Leiden.CETP-mice on high-fat high-cholesterol diet. manuscript in preparation

Palumbo P, Ditlevsen S, Bertuzzi A, De Gaetano A. Mathematical modeling of the glucose–insulin system: A review. *Math. Biosci.*, 2013, 244(2):69–81 doi.org/10.1016/j.mbs.2013.05.006

Pang G, Xie J, Chen Q, Hu Z. Energy intake, metabolic homeostasis, and human health. *Food Sci. Hum. Wellness*, 2014, 3(3):89–103 doi.org/10.1016/j.fshw.2015.01.001

Parikh RM, Mohan V. Changing definitions of metabolic syndrome. *Indian J. Endocrinol. Metab.*, 2012, 16(1):7–12 doi.org/10.4103/2230-8210.91175

van de Pas NCA, Woutersen RA, van Ommen B, Rietjens IMCM, de Graaf AA. A physiologically based in silico kinetic model predicting plasma cholesterol concentrations in humans. *J. Lipid Res.*, 2012, 53(12):2734–2746 doi.org/10.1194/jlr.M031930

Perlman RL. Mouse models of human disease. *Evol. Med. Public Health*, 2016, 2016(1):170–176 doi.org/10.1093/emph/eow014

Peyot ML, Pepin E, Lamontagne J, Latour MG, Zarrouki B, Lussier R, Pineda M, Jetton TL, Murthy Madiraju SR, Joly E, Prentki M. Beta-cell failure in diet-induced obese mice stratified according to body weight gain: secretory dysfunction and altered islet lipid metabolism without steatosis or reduced beta-cell mass. *Diabetes*, 2010, 59(9):2178–2187 doi.org/10.2337/db09-1452

Poon VTW, Kuk JL, Ardern CI. Trajectories of Metabolic Syndrome development in young adults. *PLoS ONE*, 2014, 9(11) doi.org/10.1371/journal.pone.0111647

Rajasingh H, Gjuvsland AB, Våge DI, Omholt SW. When parameters in dynamic models become phenotypes: a case study on flesh pigmentation in the chinook salmon (Oncorhynchus tshawytscha). *Genetics*, 2008, 179(2):1113–1118 doi.org/10.1534/genetics.108.087064

Rask-Madsen C, Kahn CR. Tissue-specific insulin signaling, metabolic syndrome, and cardiovascular disease. *Arterioscler. Thromb. Vasc. Biol.*, 2012, 32(9):2052–2059 doi.org/10.1161/ATVBAHA.111.241919

Rasouli N, Kern PA, Reece A, Elbein SC. Effects of pioglitazone and metformin on β-cell function in nondiabetic subjects at high risk for type 2 diabetes. *Am. J. Physiol. Endocrinol. Metab.*, 2007, 292(1):E359–E365 doi.org/10.1152/ajpendo.00221.2006

Raue A, Kreutz C, Maiwald T, Bachmann J, Schilling M, Klingmüller U, Timmer J. Structural and practical identifiability analysis of partially observed dynamical models by exploiting the profile likelihood. *Bioinformatics*, 2009, 25(15):1923–1929 doi.org/10.1093/bioinformatics/btp358

Ravussin Y, Xiao C, Gavrilova O, Reitman ML. Effect of intermittent cold exposure on brown fat activation, obesity, and energy homeostasis in mice. *PloS One*, 2014, 9(1):e85876 doi.org/10.1371/journal.pone.0085876

Reaven GM. Role of insulin resistance in human disease (syndrome X): an expanded definition. *Annu. Rev. Med.*, 1993, 44:121–131 doi.org/10.1146/annurev.me.44.020193.001005

Redinger RN. The pathophysiology of obesity and its clinical manifestations. *Gastroenterol. Hepatol.*, 2007, 3(11):856-863 ncbi.nlm.nih.gov/pmc/articles/PMC3104148/

Rensen PCN, Havekes LM. Cholesteryl ester transfer protein inhibition: effect on reverse cholesterol transport? *Arterioscler. Thromb. Vasc. Biol.*, 2006, 26(4):681–684 doi.org/10.1161/01.ATV.0000214979.24518.95

Richter SH, Garner JP, Würbel H. Environmental standardization: cure or cause of poor reproducibility in animal experiments? *Nat. Methods*, 2009, 6(4):257–261 doi.org/10.1038/nmeth.1312

van Riel NAW. Dynamic modelling and analysis of biochemical networks: mechanism-based models and model-based experiments. *Brief. Bioinform.*, 2006, 7(4):364–374 doi.org/10.1093/bib/bbl040

van Riel NAW, Tiemann CA, Vanlier J, Hilbers PAJ. Applications of analysis of dynamic adaptations in parameter trajectories. *Interface Focus*, 2013, 3(2):20120084 doi.org/10.1098/rsfs.2012.0084

Roberts CK, Hevener AL, Barnard RJ. Metabolic Syndrome and insulin resistance: Underlying causes and modification by exercise training. *Compr. Physiol.*, 2013, 3(1):1–58 doi.org/10.1002/cphy.c110062

Rodrigues CQD, Santos JAP, Quinto BMR, Marrocos MSM, Teixeira AA, Rodrigues CJO, Batista MC. Impact of metabolic syndrome on resting energy expenditure in patients with chronic kidney disease. *Clin. Nutr. ESPEN*, 2016, 15:107–113 doi.org/10.1016/j.clnesp.2016.07.001

Romeo GR, Lee J, Shoelson SE. Metabolic syndrome, insulin resistance, and roles of inflammation--mechanisms and therapeutic targets. *Arterioscler. Thromb. Vasc. Biol.*, 2012, 32(8):1771–1776 doi.org/10.1161/ATVBAHA.111.241869

Romieu I, Dossus L, Barquera S, Blottière HM, Franks PW, Gunter M, Hwalla N, Hursting SD, Leitzmann M, Margetts B, Nishida C, Potischman N, Seidell J, Stepien M, Wang Y, Westerterp K, Winichagoon P, Wiseman M, Willett WC. Energy balance and obesity: what are the main drivers? *Cancer Causes Control*, 2017, 28(3):247–258 doi.org/10.1007/s10552-017-0869-z

Romu T, Vavruch C, Dahlqvist-Leinhard O, Tallberg J, Dahlström N, Persson A, Heglind M, Lidell ME, Enerbäck S, Borga M, Nystrom FH. A randomized trial of cold-exposure on energy expenditure and supraclavicular brown adipose tissue volume in humans. *Metabolism.*, 2016, 65(6):926–934 doi.org/10.1016/j.metabol.2016.03.012

Rousseeuw PJ. Silhouettes: A graphical aid to the interpretation and validation of cluster analysis. *J. Comput. Appl. Math.*, 1987, 20(Supplement C):53–65 doi.org/10.1016/0377-0427(87)90125-7

Roy A, Parker RS. Dynamic modeling of free fatty acid, glucose, and insulin: an extended "minimal model." *Diabetes Technol. Ther.*, 2006, 8(6):617–626 doi.org/10.1089/dia.2006.8.617

Rozendaal YJW, Maas AH, van Pul C, Cottaar WJ, Haak HR, Hilbers PAJ, van Riel NAW. Model-based analysis of postprandial glycemic response dynamics for different types of food. *Clin. Nutr. Exp.*, 2018a, 19:32–45 doi.org/10.1016/j.yclnex.2018.01.003

Rozendaal YJW, Wang Y, Paalvast Y, Tambyrajah LL, Li Z, Willems van Dijk K, Rensen PCN, Kuivenhoven JA, Groen AK, Hilbers PAJ, van Riel NAW. In vivo and in silico dynamics of the development of Metabolic Syndrome. *PLoS Comput. Biol.*, 2018b, 14(6):e1006145 doi.org/10.1371/journal.pcbi.1006145

Saito M, Okamatsu-Ogura Y, Matsushita M, Watanabe K, Yoneshiro T, Nio-Kobayashi J, Iwanaga T, Miyagawa M, Kameya T, Nakada K, Kawai Y, Tsujisaki M. High incidence of metabolically active brown adipose tissue in healthy adult humans: effects of cold exposure and adiposity. *Diabetes*, 2009, 58(7):1526–1531 doi.org/10.2337/db09-0530

Salinari S, Bertuzzi A, Mingrone G. Intestinal transit of a glucose bolus and incretin kinetics: a mathematical model with application to the oral glucose tolerance test. *Am. J. Physiol. Endocrinol. Metab.*, 2011, 300(6):E955-965 doi.org/10.1152/ajpendo.00451.2010

Samtani MN, Raghavan N, Shi Y, Novak G, Farnum M, Lobanov V, Schultz T, Yang E, DiBernardo A, Narayan VA. Disease progression model in subjects with mild cognitive impairment from the Alzheimer's disease neuroimaging initiative: CSF biomarkers predict population subtypes. *Br. J. Clin. Pharmacol.*, 2013, 75(1):146–161 doi.org/10.1111/j.1365-2125.2012.04308.x

Sarkar J, Dwivedi G, Chen Q, Sheu IE, Paich M, Chelini CM, D'Alessandro PM, Burns SP. A long-term mechanistic computational model of physiological factors driving the onset of type 2 diabetes in an individual. *PLOS ONE*, 2018, 13(2):e0192472 doi.org/10.1371/journal.pone.0192472

Sauer U, Heinemann M, Zamboni N. Getting Closer to the Whole Picture. *Science*, 2007, 316(5824):550–551 doi.org/10.1126/science.1142502

Schernthaner G, Matthews DR, Charbonnel B, Hanefeld M, Brunetti P, QUARTET Study Group. Efficacy and safety of pioglitazone versus metformin in patients with type 2 diabetes mellitus: a double-blind, randomized trial. *J. Clin. Endocrinol. Metab.*, 2004, 89(12):6068–6076 doi.org/10.1210/jc.2003-030861

Schlein C, Talukdar S, Heine M, Fischer AW, Krott LM, Nilsson SK, Brenner MB, Heeren J, Scheja L. FGF21 Lowers Plasma Triglycerides by Accelerating Lipoprotein Catabolism in White and Brown Adipose Tissues. *Cell Metab.*, 2016, 23(3):441–453 doi.org/10.1016/j.cmet.2016.01.006

Schliep A, Schönhuth A, Steinhoff C. Using hidden Markov models to analyze gene expression time course data. *Bioinformatics*, 2003, 19(suppl_1):i255–i263 doi.org/10.1093/bioinformatics/btg1036

Schork NJ. Personalized medicine: Time for one-person trials. *Nature*, 2015, 520(7549):609–611 doi.org/10.1038/520609a

Scott AC. Nonlinear Biology. In: The Nonlinear Universe. The Frontiers Collection, Springer, Berlin, Heidelberg; ISBN: 978-3-540-34152-9, 2007, 181–276 doi.org/10.1007/978-3-540-34153-6_7

Seale P, Lazar MA. Brown fat in humans: Turning up the heat on obesity. *Diabetes*, 2009, 58(7):1482–1484 doi.org/10.2337/db09-0622

Sheiner LB, Rosenberg B, Marathe VV. Estimation of population characteristics of pharmacokinetic parameters from routine clinical data. *J. Pharmacokinet. Biopharm.*, 1977, 5(5):445-479 ncbi.nlm.nih.gov/pubmed/925881

Sheiner LB, Rosenberg B, Melmon KL. Modelling of individual pharmacokinetics for computer-aided drug dosage. *Comput. Biomed. Res.*, 1972, 5(5):411-459 ncbi.nlm.nih.gov/pubmed/4634367

Shin SH, Bode AM, Dong Z. Precision medicine: the foundation of future cancer therapeutics. *NPJ Precis. Oncol.*, 2017, 1(1):12 doi.org/10.1038/s41698-017-0016-z

Sips FLP, Nyman E, Adiels M, Hilbers PAJ, Strålfors P, van Riel NAW, Cedersund G. Model-based quantification of the systemic interplay between glucose and fatty acids in the postprandial state. *PloS One*, 2015, 10(9):e0135665 doi.org/10.1371/journal.pone.0135665

Snel RCQ. Implications of the Roux-en-Y gastric bypass on glucose homeostasis and type 2 diabetes (MSc thesis). Eindhoven University of Technology, 2015 repository.tue.nl/794488

Softic S, Gupta MK, Wang GX, Fujisaka S, O'Neill BT, Rao TN, Willoughby J, Harbison C, Fitzgerald K, Ilkayeva O, Newgard CB, Cohen DE, Kahn CR. Divergent effects of glucose and fructose on hepatic lipogenesis and insulin signaling. *J. Clin. Invest.*, 2017, 127(11):4059–4074 doi.org/10.1172/JCI94585

Song Q, Wang S, Zafari AM. Genetics of Metabolic Syndrome. *Hosp. Physician*, 2006, 42(10):51-61 turner-white.com/memberfile.php?PubCode=hp_oct06_genetic.pdf

van Stee MF, de Graaf AA, Groen AK. Actions of metformin and statins on lipid and glucose metabolism and possible benefit of combination therapy. *Cardiovasc. Diabetol.*, 2018, 17(1):94 doi.org/10.1186/s12933-018-0738-4

Strimbu K, Tavel JA. What are biomarkers? *Curr. Opin. HIV AIDS*, 2010, 5(6):463–466 doi.org/10.1097/COH.0b013e32833ed177

Swainston N *et al.* Recon 2.2: from reconstruction to model of human metabolism. *Metabolomics*, 2016, 12 doi.org/10.1007/s11306-016-1051-4

Symonds ME, Sebert SP, Hyatt MA, Budge H. Nutritional programming of the metabolic syndrome. *Nat. Rev. Endocrinol.*, 2009, 5(11):604–610 doi.org/10.1038/nrendo.2009.195

Tarasco E, Pellegrini G, Whiting L, Lutz TA. Phenotypical heterogeneity in responder (R) and non-responder (NR) male APOE*3Leiden.CETP mice. *Am. J. Physiol. Gastrointest. Liver Physiol.*, 2018, 315(4):G602–G617 doi.org/10.1152/ajpgi.00081.2018

Tareen SHK, Kutmon M, Adriaens ME, Mariman ECM, de Kok TM, Arts ICW, Evelo CT. Exploring the cellular network of metabolic flexibility in the adipose tissue. *Genes Nutr.*, 2018, 13(1):17 doi.org/10.1186/s12263-018-0609-3

Thiele I *et al.* A community-driven global reconstruction of human metabolism. *Nat. Biotechnol.*, 2013, 31(5):419–425 doi.org/10.1038/nbt.2488

Thomas CD, Peters JC, Reed GW, Abumrad NN, Sun M, Hill JO. Nutrient balance and energy expenditure during ad libitum feeding of high-fat and high-carbohydrate diets in humans. *Am. J. Clin. Nutr.*, 1992, 55(5):934–942 doi.org/10.1093/ajcn/55.5.934

Tiemann CA, Vanlier J, Hilbers PAJ, van Riel NAW. Parameter adaptations during phenotype transitions in progressive diseases. *BMC Syst. Biol.*, 2011, 5(26):174 doi.org/10.1186/1752-0509-5-174

Tiemann CA, Vanlier J, Oosterveer MH, Groen AK, Hilbers PAJ, van Riel NAW. Parameter trajectory analysis to identify treatment effects of pharmacological interventions. *PLoS Comput. Biol.*, 2013, 9(8):e1003166 doi.org/10.1371/journal.pcbi.1003166

Tillin T, Forouhi NG. Metabolic Syndrome and ethnicity (Chapter 2). In: The Metabolic Syndrome. Wiley-Blackwell; ISBN: 978-1-4443-4731-9, 2011, 19–44 doi.org/10.1002/9781444347319.ch2

Toghaw P, Matone A, Lenbury Y, De Gaetano A. Bariatric surgery and T2DM improvement mechanisms: a mathematical model. *Theor. Biol. Med. Model.*, 2012, 9:16 doi.org/10.1186/1742-4682-9-16

Topp B, Promislow K, deVries G, Miura RM, Finegood DT. A model of beta-cell mass, insulin, and glucose kinetics: pathways to diabetes. *J. Theor. Biol.*, 2000, 206(4):605–619 doi.org/10.1006/jtbi.2000.2150

Toye AA, Lippiat JD, Proks P, Shimomura K, Bentley L, Hugill A, Mijat V, Goldsworthy M, Moir L, Haynes A, Quarterman J, Freeman HC, Ashcroft FM, Cox RD. A genetic and physiological study of impaired glucose homeostasis control in C57BL/6J mice. *Diabetologia*, 2005, 48(4):675–686 doi.org/10.1007/s00125-005-1680-z

van der Tuin S, Wang Y, Tjeerdema N, Bieghs V, Rensen SS, Fu J, Wolfs MG, Hofker MH, Shiri-Sverdlov R, Smit JWA, Havekes LM, Willems van Dijk K, Rensen PCN. Plasma cholesteryl ester transfer protein: a biomarker for hepatic macrophages. *Ned. Tijdschr. Voor Diabetol.*, 2013, 11(4):195–195 doi.org/10.1007/s12467-013-0153-0

Turnbaugh PJ, Ridaura VK, Faith JJ, Rey FE, Knight R, Gordon JI. The effect of diet on the human gut microbiome: a metagenomic analysis in humanized gnotobiotic mice. *Sci. Transl. Med.*, 2009, 1(6):6ra14 doi.org/10.1126/scitranslmed.3000322

Valdes G, Luna JM, Eaton E, Ii CBS, Ungar LH, Solberg TD. MediBoost: a patient stratification tool for interpretable decision making in the era of precision medicine. *Sci. Rep.*, 2016, 6:37854 doi.org/10.1038/srep37854

Vandamme TF. Use of rodents as models of human diseases. *J. Pharm. Bioallied Sci.*, 2014, 6(1):2–9 doi.org/10.4103/0975-7406.124301

Vanita P, Jhansi K. Metabolic Syndrome in endocrine system. *J. Diabetes Metab.*, 2011, 2(9) doi.org/10.4172/2155-6156.1000163

Vanlier J, Tiemann CA, Hilbers PAJ, van Riel NAW. An integrated strategy for prediction uncertainty analysis. *Bioinforma. Oxf. Engl.*, 2012, 28(8):1130–1135 doi.org/10.1093/bioinformatics/bts088

Vanlier J, Tiemann CA, Hilbers PAJ, van Riel NAW. Parameter uncertainty in biochemical models described by ordinary differential equations. *Math. Biosci.*, 2013, 246(2):305–314 doi.org/10.1016/j.mbs.2013.03.006

Vgontzas AN, Bixler EO, Chrousos GP. Sleep apnea is a manifestation of the metabolic syndrome. *Sleep Med. Rev.*, 2005, 9(3):211–224 doi.org/10.1016/j.smrv.2005.01.006

Viceconti M, Henney A, Morley-Fletcher E. In silico clinical trials: how computer simulation will transform the biomedical industry. *Int. J.*

Clin. Trials, 2016, 3(2):37–46 doi.org/10.18203/2349-3259.ijct20161408

Virtue S, Vidal-Puig A. Adipose tissue expandability, lipotoxicity and the Metabolic Syndrome--an allostatic perspective. *Biochim. Biophys. Acta*, 2010, 1801(3):338–349 doi.org/10.1016/j.bbalip.2009.12.006

van Vliet-Ostaptchouk JV *et al.* The prevalence of metabolic syndrome and metabolically healthy obesity in Europe: a collaborative analysis of ten large cohort studies. *BMC Endocr. Disord.*, 2014, 14:9 doi.org/10.1186/1472-6823-14-9

Voit EO, Martens HA, Omholt SW. 150 Years of the mass action law. *PLoS Comput. Biol.*, 2015, 11(1) doi.org/10.1371/journal.pcbi.1004012

Wahlsten D, Metten P, Phillips TJ, Boehm SL, Burkhart-Kasch S, Dorow J, Doerksen S, Downing C, Fogarty J, Rodd-Henricks K, Hen R, McKinnon CS, Merrill CM, Nolte C, Schalomon M, Schlumbohm JP, Sibert JR, Wenger CD, Dudek BC, Crabbe JC. Different data from different labs: lessons from studies of gene-environment interaction. *J. Neurobiol.*, 2003, 54(1):283–311 doi.org/10.1002/neu.10173

Wallace TM, Levy JC, Matthews DR. Use and abuse of HOMA modeling. *Diabetes Care*, 2004, 27(6):1487–1495 doi.org/10.2337/diacare.27.6.1487

Wang Y, Berbée JFP, Stroes ES, Smit JWA, Havekes LM, Romijn JA, Rensen PCN. CETP expression reverses the reconstituted HDL-induced increase in VLDL. *J. Lipid Res.*, 2011, 52(8):1533–1541 doi.org/10.1194/jlr.M016659

Wang Y, Gjuvsland AB, Vik JO, Smith NP, Hunter PJ, Omholt SW. Parameters in dynamic models of complex traits are containers of missing heritability. *PLoS Comput. Biol.*, 2012, 8(4):e1002459 doi.org/10.1371/journal.pcbi.1002459

Wang CY, Liao JK. A mouse model of diet-induced obesity and insulin resistance. *Methods Mol. Biol.*, 2012, 821:421–433 doi.org/10.1007/978-1-61779-430-8_27

Wang TY, Liu C, Wang A, Sun Q. Intermittent cold exposure improves glucose homeostasis associated with brown and white adipose tissues in mice. *Life Sci.*, 2015, 139:153–159 doi.org/10.1016/j.lfs.2015.07.030

Wang Y, Parlevliet ET, Geerling JJ, van der Tuin SJL, Zhang H, Bieghs V, Jawad AHM, Shiri-Sverdlov R, Bot I, de Jager SCA, Havekes LM, Romijn JA, Willems van Dijk K, Rensen PCN. Exendin-4 decreases liver inflammation and atherosclerosis development simultaneously by reducing macrophage infiltration. *Br. J. Pharmacol.*, 2014a, 171(3):723–734 doi.org/10.1111/bph.12490

Wang X, Sontag D, Wang F. Unsupervised learning of disease progression models. *Proc. 20th ACM SIGKDD Int. Conf. Knowl. Discov. Data Min.*, 2014b,:85–94 doi.org/10.1145/2623330.2623754

Weinberg EJ, Schoen FJ, Mofrad MRK. A computational model of aging and calcification in the aortic heart valve. *PLoS ONE*, 2009, 4(6) doi.org/10.1371/journal.pone.0005960

Westerterp M, van der Hoogt CC, de Haan W, Offerman EH, Dallinga-Thie GM, Jukema JW, Havekes LM, Rensen PCN. Cholesteryl ester transfer protein decreases high-density lipoprotein and severely aggravates atherosclerosis in APOE*3-Leiden mice. *Arterioscler. Thromb. Vasc. Biol.*, 2006, 26(11):2552–2559 doi.org/10.1161/01.ATV.0000243925.65265.3c

Whitehead JC, Hildebrand BA, Sun M, Rockwood MR, Rose RA, Rockwood K, Howlett SE. A clinical frailty index in aging mice: comparisons with frailty index data in humans. *J. Gerontol. A. Biol. Sci. Med. Sci.*, 2014, 69(6):621–632 doi.org/10.1093/gerona/glt136

de Winter W, DeJongh J, Post T, Ploeger B, Urquhart R, Moules I, Eckland D, Danhof M. A mechanism-based disease progression model for comparison of long-term effects of pioglitazone, metformin and gliclazide on disease processes underlying Type 2 Diabetes Mellitus. *J. Pharmacokinet. Pharmacodyn.*, 2006, 33(3):313–343 doi.org/10.1007/s10928-006-9008-2

Wittgrove AC, Clark GW, Tremblay LJ. Laparoscopic gastric bypass, Roux-en-Y: preliminary report of five cases. *Obes. Surg.*, 1994, 4(4):353–357 doi.org/10.1381/096089294765558331

World Health Organization. Global status report on noncommunicable diseases 2014. 79–94 pages, ISBN: 978-92-4-156485-4, 2014 who.int/nmh/publications/ncd-status-report-2014/en/

World Health Organization. Fact sheet N°311: Obesity and overweight. 2016 who.int/mediacentre/factsheets/fs311/en/

Xu K, Morgan KT, Todd Gehris A, Elston TC, Gomez SM. A whole-body model for glycogen regulation reveals a critical role for substrate cycling in maintaining blood glucose homeostasis. *PLoS Comput Biol*, 2011, 7(12):e1002272 doi.org/10.1371/journal.pcbi.1002272

Yanai H, Tomono Y, Ito K, Furutani N, Yoshida H, Tada N. The underlying mechanisms for development of hypertension in the metabolic syndrome. *Nutr. J.*, 2008, 7:10 doi.org/10.1186/1475-2891-7-10

Yanovski SZ, Yanovski JA. Toward precision approaches for the prevention and treatment of obesity. *JAMA*, 2018, 319(3):223–224 doi.org/10.1001/jama.2017.20051

Yen TT, Stienmetz J, Simpson PJ. Blood volume of obese (ob-ob) and diabetic (db-db) mice. *Proc. Soc. Exp. Biol. Med.*, 1970, 133(1):307–308 doi.org/10.3181/00379727-133-34462

Yoneshiro T, Aita S, Matsushita M, Kayahara T, Kameya T, Kawai Y, Iwanaga T, Saito M. Recruited brown adipose tissue as an antiobesity agent in humans. *J. Clin. Invest.*, 2013, 123(8):3404–3408 doi.org/10.1172/JCI67803

Yoo HS, Qiao L, Bosco C, Leong LH, Lytle N, Feng GS, Chi NW, Shao J. Intermittent cold exposure enhances fat accumulation in mice. *PloS One*, 2014, 9(5):e96432 doi.org/10.1371/journal.pone.0096432

Zadelaar S, Kleemann R, Verschuren L, de Vries-van der Weij J, van der Hoorn J, Princen HM, Kooistra T. Mouse models for atherosclerosis and pharmaceutical modifiers. *Arterioscler. Thromb. Vasc. Biol.*, 2007, 27(8):1706–1721 doi.org/10.1161/ATVBAHA.107.142570

Zazzu V, Regierer B, Kühn A, Sudbrak R, Lehrach H. IT future of medicine: from molecular analysis to clinical diagnosis and improved treatment. *New Biotechnol.*, 2013, 30(4):362–365 doi.org/10.1016/j.nbt.2012.11.002

Zeevi D, Korem T, Zmora N, Israeli D, Rothschild D, Weinberger A, Ben-Yacov O, Lador D, Avnit-Sagi T, Lotan-Pompan M, Suez J, Mahdi JA, Matot E, Malka G, Kosower N, Rein M, Zilberman-Schapira G, Dohnalová L, Pevsner-Fischer M, Bikovsky R, Halpern Z, Elinav E, Segal E. Personalized nutrition by prediction of glycemic responses. *Cell*, 2015, 163(5):1079–1094 doi.org/10.1016/j.cell.2015.11.001

von Zglinicki T, Varela-Nieto I, Brites D, Karagianni N, Ortolano S, Georgopoulos S, Cardoso AL, Novella S, Lepperdinger G, Trendelenburg AU, van Os R. Frailty in mouse ageing: A conceptual approach. *Mech. Ageing Dev.*, 2016, 160:34–40 doi.org/10.1016/j.mad.2016.07.004

Ethical paragraph

The Metabolic Syndrome (MetS) is defined as a cluster of multiple metabolic abnormalities including obesity, insulin resistance, dyslipidemia, and hypertension. These abnormalities are well-documented risk factors for cardiovascular diseases and type 2 diabetes. The obesity pandemic and MetS prevalence are increasing steadily; not only in the Western societies but also in developing countries. This is cause for a global concern and has a strong societal impact since current pharmacological strategies remain inadequate and insufficient in dealing with the growing rate of MetS. Lifestyle modulation (including diet adjustment) still remains the fundamental approach to combat MetS. Personalized approaches are limited since the mechanisms underlying the pathophysiology of MetS remain unclear.

The experiments and methodologies described in this thesis contribute to reducing this gap in understanding by systematically studying the onset and longitudinal development of the co-occurrence of MetS symptoms (obesity, hyperglycemia, dyslipidemia) and comorbidities (insulin resistance, liver lipid accumulation) by using computational modelling techniques integrated with data obtained from a transgenic, diet-induced MetS mouse model. This animal model has been indispensable in the construction of the computational modelling framework described in this thesis.

The majority of medical breakthroughs have involved preclinical studies performed on animals. Although considerable efforts are being made in the design of appropriate alternatives, animal models do remain valuable tools for gaining a deeper understanding of pathophysiology and etiology of complex and multi-factorial diseases such as MetS. Nevertheless, the use of animals remains controversial. Well-informed choices should be made in experimental design, set-up, and conduct. The research described in this thesis was therefore designed and performed conforming to the 3R principle:

- ***Replacement*** of animal experiments with non-animal experiments when possible. MetS is a complex and multi-factorial disease and many different tissues and metabolites are involved. Therefore, *in vitro* techniques and video or film modalities are not sufficiently suitable to study the integrated effects of diet-induced MetS development. Computational modelling techniques are able to generate large amounts of *in silico* data but do require *in vivo* obtained data for model calibration.
- ***Reduction*** of the number of animals used was possible by the sampling of *in vivo* obtained data to generate large amounts of *in silico* data for which only a few mice were sacrificed. To keep this number of mice as little as possible, standardisation was applied. Mice were housed in identical cages with constant temperature and ventilation. Furthermore, all actions were performed by the same, experienced personnel.
- ***Refinement*** of experiments was realized to minimize animal distress and discomfort. The severity of painful and distressing procedures was decreased by using proper methods of anaesthesia. All *in vivo* experiments described in this thesis were performed in accordance with the regulations of Dutch law on animal welfare. The experimental procedures regarding the *in vivo* data described in chapters 4 and 6 have been approved by the Animal Ethics Committee of the Leiden University Medical Centre, The Netherlands. The

experimental procedures regarding the *in vivo* study described in chapter 5 have been approved by the Ethics Committees for Animal Experiments of the University of Groningen, The Netherlands.

In this thesis, we have demonstrated that *in silico* computational methods allow for a more intelligent and more resourceful use of a smaller number of animals. The study outcome was maximized by generating large amounts of *in silico* data. Moreover, all *in vivo* and *in silico* generated data have been made publically available.

Summary

Systems biology of Metabolic Syndrome development and treatment

The worldwide increase in overweight and obesity co-occurs with the development of various other abnormalities. This drastically increases the risk of the development of diabetes and cardiovascular diseases. The cluster of comorbidities associated with obesity development is referred to as the Metabolic Syndrome (MetS). It is characterized by alterations in both carbohydrate (glucose intolerance) and lipid (high cholesterol, high triglycerides) metabolism that develop over long timescales. Due to its progressive, complex, and multi-factorial nature, its presentation is highly heterogeneous, i.e. many different phenotypes can be classified under the terminology of MetS. Therefore, we propose the use of a systems biology approach to study the longitudinal development of MetS in both *in vivo* and *in silico* settings. This approach involves three main methodologies:

- A computational technique to predict dynamic adaptations during long-term disease development. Hereto we made use of ADAPT (Analysis of Dynamic Adaptations in Parameter Trajectories), which describes the long-term timespan using time-dependent model parameters. Its data-driven approach enables integration of longitudinal biomarker data to describe phenotype transition over time.
- A dedicated mathematical model consisting of a system of coupled nonlinear ordinary differential equations that describes carbohydrate and lipid metabolism in a systemic, whole-body perspective: MINGLeD (Model Integrating Glucose and Lipid Dynamics). Its steady state represents a single metabolic snapshot and is applicable under both healthy and (different) diseased conditions.
- *In vivo* data from a preclinical animal model with human-like lipid handling. Male APOE*3-Leiden.CETP mice were fed a high-fat, high-cholesterol diet for three months to induce symptoms (obesity, glucose intolerance, dyslipidemia) and comorbidities (insulin resistance, hepatic steatosis) characteristic for MetS. This data was integrated into MINGLeD by employing ADAPT and yielded a large set of predictions of the longitudinal dynamics of MetS onset and development in thousands of virtual individuals. This revealed the emergence of two distinct MetS phenotypes that differ in severity of dyslipidemia. Flux trajectory analysis revealed increased hepatic lipid fluxes in those with dyslipidemia, whereas the dietary cholesterol uptake from the intestinal lumen is decreased in the non-dyslipidemic MetS phenotypes.

The heterogeneity and variability in phenotypic presentation of MetS were further explored in an *in vivo* study involving a larger population followed up to six months. This showed that although the degree to which these animals develop dyslipidemia is highly heterogeneous, three different subpopulations could be identified based on the three-month plasma triglyceride and total cholesterol levels: those with a low, mild to moderate, and high degree of dyslipidemia. The first and third group comprise the groups previously identified based on the three-month experiment.

Subsequently, we shifted our focus from the developmental aspects of MetS towards possible therapeutic interventions. Obesity is considered to be the central hallmark of MetS, indicating an inherent energy imbalance (surplus). The virtual population of dyslipidemic MetS was first stratified in terms of biologically plausible measures of energy expenditure prior to performing *in silico* perturbation experiments on the peripheral energy expenditure to study the robustness and sensitivity of the system. Enhanced peripheral energy expenditure led to a direct decrease of cholesterol and lipid fluxes and pool sizes, indicating its potential to improve MetS related symptoms. To translate these findings into an experimental study, we considered the contribution of Brown Adipose Tissue (BAT) in energy homeostasis. BAT can be activated for a short period of time by cold exposure and can contribute to reduce the metabolic derailments associated with MetS.

We have shown that our comprehensive systems biology approach by combining *in silico* studies with *in vivo* data yielded new insights into the development of various MetS phenotypes. Although this thesis was limited to preclinical datasets, our methodology can be applied to the human situation. We have shown that our generic modelling methodology is able to stratify the large heterogeneity in MetS presentation and that it can make predictions on sub-population level. These virtual populations could also be created for the human case, which can be used to facilitate stratification and contribute to a more personalized approach. Eventually, this is expected to provide possibilities for early diagnosis of patients, simulate scenarios for disease progression, and to support decision making of therapeutic interventions to refrain from further development of MetS.

Samenvatting

Systeembiologie van de ontwikkeling en behandeling van Metabool Syndroom

De wereldwijde toename aan zwaarlijvigheid en obesitas gaat gepaard met de ontwikkeling van allerlei andere afwijkingen. Ook is de kans op de ontwikkeling van diabetes en hart- en vaatziekten sterk verhoogd. Het tegelijkertijd voorkomen van deze afwijkingen en indicatoren zijn geclusterd onder de term "Metabool Syndroom" (MetS). Karakteristiek voor deze aandoening zijn de verstoringen in zowel koolhydraat- (glucose-intolerantie) als vetstofwisseling (hoog cholesterol- en triglyceridegehalte), welke zich langzaam ontwikkelen over de tijd. De klinische presentatie van MetS is zeer heterogeen, mede vanwege haar progressieve, complexe, en multi-factoriële aard. Dit betekent dat meerdere verschillende fenotypes geschaard kunnen worden onder de definitie van MetS. We hebben daarom besloten om gebruik te maken van een systeembiologische aanpak om de longitudinale, geleidelijke ontwikkeling van MetS te bestuderen in zowel een *in vivo* als een *in silico* omgeving. Deze methodologie bestaat uit drie hoofdcomponenten:

- Een simulatiemethode welke de dynamische veranderingen tijdens ziekteontwikkeling kan beschrijven. Hiervoor is gebruik gemaakt van de rekenmethode "ADAPT" (Analysis of Dynamic Adaptations in Parameter Trajectories; een methode om dynamische adaptaties in parametertrajectorieën te analyseren). Deze methode beschrijft de lange termijn tijdspanne door middel van tijdafhankelijke modelparameters. De data-gedreven aanpak maakt het mogelijk om longitudinale biomarker data te integreren in een model voor een beschrijving van de transitie van het ene fenotype naar het andere fenotype over de tijd.
- Een rekenkundig model op basis van differentiaalvergelijkingen welke de koolhydraat- en vetstofwisseling beschrijft op weefselniveau. Dit model wordt "MINGLeD" (Model Integrating Glucose and Lipid Dynamics; een integraal model van glucose en lipide dynamiek) genoemd. De steady state van dit model geeft een momentopname van de stofwisseling weer, en is toepasbaar voor zowel een gezonde stofwisseling, als voor diverse afwijkingen in de stofwisseling.
- *In vivo* data verkregen uit een preklinisch proefdiermodel met een vetstofwisseling vergelijkbaar met die van ons. Hiervoor zijn mannelijke APOE*3-Leiden.CETP transgene muizen gevoed met een vet- en cholesterolrijk dieet gedurende drie maanden. Dit induceerde de karakteristieke symptomen (obesitas, glucose intolerantie, dyslipidemie) en comorbiditeiten (insuline resistentie, leververvetting) van MetS. De integratie van deze data in MINGLeD door middel van de ADAPT methodologie leverde een grote verzameling van voorspellingen op die de longitudinale dynamiek in MetS ontwikkeling beschrijft in duizenden virtuele individuen. Dit liet een duidelijke tweedeling in ziekteontwikkeling zien: we hebben onderscheid gemaakt tussen twee verschillende MetS fenotypes op basis van de ernst van dyslipidemie. Analyse van de uitwisseling- en omzettingsfluxen van de metabolieten toonde aan waarin deze fenotypes van elkaar verschillen. Het sterk dyslipidemische fenotype is gekarakteriseerd door verhoogde activiteit in de lever, terwijl

juist de opname van cholesterol uit het dieet door de darmen verlaagd is in het licht dyslipidemische fenotype.

De gevonden heterogeniteit en variabiliteit in de ontwikkeling van verschillende fenotypes is hierna verder onderzocht. Hiervoor is een *in vivo* studie opgezet welke een grotere hoeveelheid proefdieren omvatte en welke voor een periode tot en met zes maanden bestudeerd is. Hoewel de gradatie van dyslipidemie erg heterogeen blijkt te zijn, hebben we deze wel kunnen opdelen in drie klassen op basis van de bloedwaarden van het triglyceride- en totaal cholesterolgehalte gemeten na drie maanden dieetinterventie. Deze subgroepen zijn vervolgens geclassificeerd als licht, gematigd, en sterk dyslipidemisch – waarbij de eerste en laatste groep overeenkomen met deze geïdentificeerd op basis van het drie-maanden experiment.

Hierna hebben we ons gericht op de toepassing van deze ontwikkelde modellen in onderzoek naar passende therapeutische behandelingen. Obesitas is een belangrijke graadmeter in de ontwikkeling van MetS. Het overschot aan energie dat hieraan ten grondslag ligt, duidt aan dat de energiehuishouding niet in evenwicht is. Om hier meer inzicht in te krijgen, hebben we naar de energiehuishouding in onze virtuele MetS populatie gekeken. Deze populatie is eerst gestratificeerd op basis van biologisch plausibele waardes van energieverbruik. Hierna hebben we een *in silico* verstoring opgelegd in het perifere energieverbruik om de robuustheid en gevoeligheid van het systeem te bestuderen. Verhoging van het perifere energieverbruik leidde tot een directe verlaging van cholesterol- en vetgehalte. Deze toepassing geeft de mogelijkheid weer in de behandeling van de symptomen gerelateerd aan MetS. En deze uitkomsten kunnen mogelijk gerelateerd worden aan de bijdrage van bruin vet (Brown Adipose Tissue; BAT) aan de energiehuishouding. Eerdere studies hebben aangetoond dat bruin vet geactiveerd kan worden voor een korte periode door blootstelling aan kou, en dat dit kan bijdragen aan het verminderen van de ernst van MetS.

Onze systeembiologische aanpak waarin *in silico* experimenten geïntegreerd zijn met *in vivo* gemeten data, heeft nieuwe inzichten opgeleverd in de ontwikkeling van diverse ziektebeelden welke onder MetS vallen. Hoewel deze thesis gelimiteerd is tot preklinische datasets, kan de generieke modelleringsmethodologie ook toegepast worden voor de mens. We hebben aangetoond dat onze methodologie in staat is om de heterogene presentatie van de MetS populatie te stratificeren. Ook kan deze methode voorspellingen maken op sub-populatie niveau. Zulke virtuele populaties kunnen ook gemaakt worden voor de mens, welke patiëntstratificatie faciliteren en kunnen bijdragen aan een patiënt-specifiekere behandeling. De verwachting is dat dit soort werk deuren zal openen richting eerdere diagnostiek van patiënten, en dat het scenario's kan simuleren als voorspelling van ziekteontwikkeling en mogelijke uitkomsten bij diverse behandelmethodes.

List of publications

Publications related to this thesis

2018 **Rozendaal YJW**, Wang Y, Hilbers PAJ, van Riel NAW. Computational modelling of energy balance in individuals with Metabolic Syndrome. *BMC Syst. Biol.* (submitted)

2018 **Rozendaal YJW**, Wang Y, Paalvast Y, Tambyrajah L, Li Z, Willems van Dijk K, Rensen PCN, Kuivenhoven JA, Groen AK, Hilbers PAJ, van Riel NAW. *In vivo* and *in silico* dynamics of the development of Metabolic Syndrome. *PLoS Comput. Biol.*, 14(6):e1006145 doi.org/10.1371/journal.pcbi.1006145

2016 Nyman E, **Rozendaal YJW**, Helmlinger G, Hamrén B, Kjellsson MC, Strålfors P, van Riel NAW, Gennemark P, Cedersund G. Requirements for multi-level systems pharmacology models to reach end-usage: the case of type 2 diabetes. *Interface Focus*, 6(2):20150075 doi.org/10.1098/rsfs.2015.0075

Other publications

2018 **Rozendaal YJW**, Maas AH, van Pul C Cottaar WJ, Haak HR, Hilbers PAJ, van Riel NAW. Model-based analysis of postprandial glycemic response dynamics for different types of food. *Clin. Nutr. Exp.*, 19:32-45 doi.org/10.1016/j.yclnex.2018.01.003

2016 **Rozendaal YJW**, van Luijtelaar G, Ossenblok PPW. Spatiotemporal mapping of interictal epileptiform discharges in human absence epilepsy: A MEG study *Epilepsy Res.*, 119:67-76 doi.org/10.1016/j.eplepsyres.2015.11.013

2015 Maas AH, **Rozendaal YJW**, van Pul C, Hilbers PAJ, Cottaar WJ, Haak HR, van Riel NAW. A physiology-based model describing heterogeneity in glucose metabolism: The core of the Eindhoven Diabetes Education Simulator (E-DES). *J. Diabetes Sci. Technol.*, 9(2):282-292 doi.org/10.1177/1932296814562607

In preparation

2018 Paalvast Y, **Rozendaal YJW**, Wang Y, Gerding A, Rensen PCN, Willems van Dijk K, Kuivenhoven JA, Bakker BM, van Riel NAW, Groen AK. Triglyceride absorption drives phenotype heterogeneity in APOE*3-Leiden.CETP-mice on high-fat high-cholesterol diet. *Manuscript in preparation*

Press releases

June 25th 2018 TU/e news page "New computational tool reveals subtypes of metabolic syndrome in mice" tue.nl/en/university/news-and-press/news/new-computational-tool-reveals-subtypes-of-metabolic-syndrome-in-mice/

June 25th 2018 "Nieuw model voor metabool syndroom leidt tot vondst van twee ziektevarianten" tue.nl/universiteit/nieuws-en-pers/nieuws/nieuw-model-voor-metabool-syndroom-leidt-tot-vondst-van-twee-ziektevarianten/

June 7th 2018 EurekAlert! "New computational tool predict progression of metabolic syndrome in mice" eurekalert.org/pub_releases/2018-06/p-nct053118.php

Conference contributions, awards, and nominations

2017 **Rozendaal YJW**, Paalvast Y, Wang Y, Hilbers PAJ, Groen AK, van Riel NAW. The effects of different *in silico* treatment strategies and therapeutic interventions on Metabolic Syndrome
☐ poster presentation @ Dutch Bioinformatics & Systems Biology Conference (BioSB), Lunteren

2016 **Rozendaal YJW**, Paalvast Y, Wang Y, Hilbers PAJ, Groen AK, van Riel NAW. *In silico* BAT activation in a glucose-lipid model of the Metabolic Syndrome
☐ poster presentation @ Conference of the European Association of Systems Medicine (EASyM), Berlin
🏆 *awarded with best poster price*

2016 Paalvast Y, **Rozendaal YJW**, Wang Y, Willems van Dijk K, Rensen PCN, Kuivenhoven JA, van Riel NAW, Groen AK. Dynamic metabolic modelling indicates that heterogeneity in plasma triglyceride and body weight development in "humanized" APOE*3-Leiden.CETP mice is in part explained by differences in intestinal triglyceride absorption
☐ poster presentation @ Conference of the European Association of Systems Medicine (EASyM), Berlin

2016 **Rozendaal YJW**. Computational modelling of the development and progression of Metabolic Syndrome in E3L.CETP mice and the effect of interventions
☐ poster presentation @ RESOLVE 3rd annual meeting, Hamburg

2016 **Rozendaal YJW**, Wang Y, Paalvast Y, Groen AK, Hilbers PAJ, van Riel NAW. Modelling the glucose and lipid system during health and disease reveals differences in the underlying pathways
☐ poster presentation @ Dutch Bioinformatics & Systems Biology Conference (BioSB), Lunteren
🏆 *nominated for best poster award*

2016 **Rozendaal YJW**, Wang Y, Paalvast Y, Groen AK, Hilbers PAJ, van Riel NAW. Modelling the glucose and lipid system during health and diseases
☐ oral & poster presentation @ Biomedical Engineering Research Day

2015 Sips FLP, Snel RCQ, **Rozendaal YJW**, Hilbers PAJ, van Riel NAW. *In silico* investigation of the changes in postprandial bile acid concentrations after metabolic surgery
☐ poster presentation @ Dutch Bioinformatics & Systems Biology Conference (BioSB), Lunteren

2015 **Rozendaal YJW**, Wang Y, Willems van Dijk K, Rensen PCN, Groen AK, Hilbers PAJ, van Riel NAW. Dynamic modelling of the development of Metabolic Syndrome through longitudinal data integration using ADAPT
☐ poster presentation @ Biomedical Engineering Research Day, Eindhoven

2015 **Rozendaal YJW**, Paalvast Y. – ADAPT tutorial in the Lorentz Center Training Course "Data Integration in the Life Sciences"
☐ giving a hands-on tutorial and workshop @ Lorentz Center, Leiden

2015 Paalvast Y, **Rozendaal YJW**, Wang Y, Willems van Dijk K, Kuivenhoven JA, Rensen PCN, van Riel NAW, Groen AK Use of dynamic metabolic modelling to study heterogeneity in development of metabolic syndrome in "humanized" APOE*3-Leiden.CETP mice on a high-fat diet
☐ poster presentation @ International Atherosclerosis Society (ISA), Amsterdam

2014 **Rozendaal YJW**, Wang Y, Willems van Dijk K, Rensen PCA, Groen AK, Hilbers PAJ, van Riel NAW. Dynamical modelling of the onset and progression of the metabolic syndrome through longitudinal data integration using ADAPT
☐ oral and poster presentation @ Systems Biology Symposium (SB@NL), Maastricht

2014 **Rozendaal YJW**, Tiemann CA, Hilbers PAJ, van Riel NAW. A knowledge- and data-driven approach to integrate transcriptomic and metabolomic time-course data and application in biomedical systems biology

☐ poster presentation @ Dutch Bioinformatics & Systems Biology Conference (BioSB), Lunteren

2014 **Rozendaal YJW**, Wang Y. The effects of additional dietary cholesterol intake on glucose metabolism in obese APOE*3-Leiden.CETP mice fed on a high-fat diet: Predicted from a mathematical model

☐ oral presentation @ RESOLVE 1st annual meeting, Heraklion

2014 **Rozendaal YJW**, Hilbers PAJ, van Riel NAW. Computational modelling approaches to study disease progression in type 2 diabetes

☐ poster presentation @ Biomedical Engineering Research Day, Eindhoven

🏆 *nominated for best poster award*

2014 Maas AH, **Rozendaal YJW**, van Pul C, Cottaar EJE, Hilbers PAJ, Haak HR, van Riel. NAW Incorporating the intake of meals in the Eindhoven Diabetes Education Simulator (E-DES)

☐ poster presentation @ Conference on Advanced Technologies & Treatments for Diabetes (ATTD), Vienna

2013 **Rozendaal YJW**. A mechanism-based disease progression model to analyse long-term treatment effects on disease processes underlying type 2 diabetes

☐ oral presentation & co-organized this workshop @ Eindhoven Metabolic Syndrome Workshop: "The interplay of fat and carbohydrate metabolism with application in Metabolic Syndrome and type 2 diabetes", Eindhoven

2013 **Rozendaal YJW**, Maas AH, van Pul C, Cottaar EJE, Haak HR, Hilbers PAJ, van Riel NAW. Understanding glycemic control in everyday life: The importance of accurate quantification of postprandial response profiles for different types of food

☐ poster presentation @ Systems Biology Symposium (SB@NL), Egmond aan Zee

2013 Maas AH, **Rozendaal YJW**, van Pul C, Cottaar EJE, Hilbers PAJ, van Riel NAW, Haak HR. Incorporating different food products and composite meals in the Eindhoven Diabetes Education Simulator

☐ poster presentation @ Annual Dutch Diabetes Research Meeting (ADDRM), Oosterbeek

2013 **Rozendaal YJW**, Maas AH, van Pul C, van Riel NAW, Haak HR. Voedselspecificatie binnen een educatieve diabetes simulator

☐ poster presentation @ MMC Wetenschapsavond, Veldhoven

🏆 *nominated for best poster award*

2013 **Rozendaal YJW**, Maas AH, van Pul C, Haak HR, van Riel NAW. – Food specification within an educational diabetes simulator

☐ poster presentation @ Biomedical Engineering Research Day, Eindhoven

Dankwoord

Na vijf jaar, 134 pagina's, en ruim 50.000 woorden is het dan eindelijk zover: de laatste pagina's van het proefschrift zijn in zicht! De promotie is nu écht "bijna af"!

Wie mij tijdens de eerste jaren van het VWO had verteld dat ik een technische studie zou gaan doen, had ik voor gek verklaard. En wie mij tijdens mijn Master had verteld dat ik ook zo gek zou zijn, om uiteindelijk tien jaar vol te maken aan de TU/e, tja... Daar waar sommige gebouwen op de campus een totale make-over kregen, is W-hoog (behalve haar naam) vrijwel onveranderd gebleven. Ikzelf daarentegen heb heel wat kennis en kunde vergaard in die periode. Voor beiden geldt: dezelfde building blocks, maar met een nieuwe naam en titel aan het einde van de rit!

Ondanks dat promoveren veel van je zelfstandigheid en eigen doorzettingsvermogen vraagt, heb ik deze weg zeker niet alleen bewandeld. Daarom wil ik graag een aantal mensen in het bijzonder bedanken omdat ze het mogelijk hebben gemaakt om de kans om te promoveren na te jagen én deze hebben helpen te realiseren.

Natal, het heeft je heel wat overtuigingskracht nodig gehad voor ik inging op jouw aanbod om te promoveren. Ik wil je bedanken voor al je support door de jaren heen. Jouw positieve mindset en altijd aanwezige enthousiasme voor het doen van gedegen wetenschappelijk onderzoek met behulp van systeembiologie en modellering zijn belangrijke eigenschappen waar ik veel van heb mogen leren. Zeker in de perioden dat ik besluiteloos was, geen richting kon (of wilde) innemen, en niet inzag hoe dit werk ooit zou gaan convergeren naar een consistent manuscript, was jouw kritische en constructieve input onmisbaar. Heel erg bedankt daarvoor!

Peter, nog voor ik het voor mezelf doorhad, wist jij al zo'n beetje halverwege mijn afstuderen, dat ik – ook al ontkende ik dat op dat moment hardgrondig – tóch verder zou gaan in het opzetten en uitvoeren van onderzoek binnen een academische setting. Bedankt voor de prettige samenwerkingen, zowel in het onderwijs als bij het bespreken van onderzoeksresultaten. Je hebt me hierbij erg geholpen om te leren uitzoomen en door minder "ja, maar" te zeggen, en tot concrete, maar gedegen conclusies te komen. Heel erg bedankt hiervoor!

Daarnaast wil ik graag prof.dr. Barbara Bakker, prof.dr.ir. Ilja Arts, prof.dr.ir. Uzay Kaymak, prof.dr. Bert Groen, en prof.dr.ir. Cees Oomens bedanken voor lezen van dit proefschrift en het plaatsnemen in de promotiecommissie.

Ik realiseer me dat ik erg bevoorrecht ben dat ik heb deel mogen nemen in RESOLVE. Hereto I would like to express my gratitude to all RESOLVE colleagues. Thanks to the highly interdisciplinary team, I think we were able to provide valuable research efforts in the field of

Metabolic Syndrome. I really enjoyed the collaboration between all these different research fields and felt very supported by this research team!

Bert, als spreekwoordelijke vader van RESOLVE heb je een belangrijke rol gehad in het tot stand komen van dit proefschrift. Jouw rijkdom aan kennis van het stofwisselingssysteem heeft mij altijd weten te fascineren, maar is ook onmisbaar geweest in het opbouwen van het model, en in de interpretatie van alle data. Jouw eindeloze geduld en ontelbare revisies hebben uiteindelijk geleid tot een aantal mooie papers!

Yanan, throughout RESOLVE I have really enjoyed the many opportunities that we had to work together extensively. Your expertise and heaps of biological knowledge have been indispensable. Thanks to your never ending enthusiasm and empathy, I really enjoyed working together! You were always very eager to learn from our complex mathematical models and to really understand them. On the other hand, you were always willing to explain any experimental details and help to interpret the (also complex) raw experimental data. In the end, I think we have published very nice work together and I wish you all the best with your little family and academic career!

Yared, de vele trip(je)s van en naar Groningen (cq. Eindhoven) hebben hun vruchten af geworpen: jouw enorme biologische kennis en interpretatie van signaalcascades hebben me enorm geholpen bij het ontwikkelen van een consistent en sterk wiskundig model, maar wat ook direct toepasbaar is met de experimentele data van de hoofdstukken 4 en 5. Bedankt voor de prettige samenwerking en ik wens je veel succes met de afronding van jouw proefschrift!

Naast de RESOLVE partners zijn mijn directe collega's aan de TU/e minstens zo belangrijk geweest. Een promotietraject kan erg eenzaam zijn, en dan is het heel prettig als je samen je frustraties kunt delen en mijlpalen kunt vieren. I would like to thank everyone who is or at some point in time was a member of the CBio group. Special thanks goes to Fianne, Anne, Zandra, Rik, Huili, and Ceylan for the many enjoyable PhD dinners and nice cups of tea!

Naast het doen van onderzoek, heb ik ook een aantal studenten mogen begeleiden bij OGO projecten, minor projecten, bachelor eindprojecten, master projecten, en afstudeerprojecten. In het bijzonder: Anouk, Twan, Roderick, Zihan, and Pascal – thank you all for your help and insightful discussions with data analysis and/or implementation of the computational framework.

Hoewel het wellicht ietwat onconventioneel (en ambitieus) is om nog voor het einde van het schrijven van je proefschrift te beginnen aan een nieuwe baan in een nieuw onderzoeksveld, ben ik erg dankbaar dat ik deze kans mogen krijgen binnen de Precision & Decentralized Diagnostics groep bij Philips. Uiteindelijk heeft dit mij juist geholpen om het proefschrift af te ronden en om het promotieonderzoek in perspectief te kunnen stellen. Ik kijk er naar uit om de systematische en modelleringsaanpakken die ik mij tijdens mijn promotie eigen gemaakt heb, toe te passen in het oncologische onderzoeksveld!

Een promotieonderzoek vindt ook niet uitsluitend plaats op de universiteit. Ik heb ervaren dat morele support minstens zo belangrijk is als inhoudelijke support. Hiervoor ben ik mijn lieve

ouders en schoonouders immens dankbaar dat ze altijd klaar staan met een luisterend oor en mij geholpen hebben om mijn soms ietwat technische mijmeringen en issues in perspectief te stellen. Zowel bij het vieren van mijlpalen, als het kunnen rekenen op aandacht wanneer je het even niet ziet zitten – dankjewel dat jullie er altijd voor mij zijn!

En bovenstaande geldt ook dubbel en dwars voor mijn lieve broer. Hans, jij hebt een hele belangrijke rol gehad in het afronden van dit proefschrift. Jouw inzichten in hoe ik dit juist procesmatig, maar ook communicatief sterk aan kon pakken, hebben me geholpen om de struikelblokken minder abstract en meer behapbaar te maken. Indirect heb ik dus mijn proefschrift af weten te maken tijdens de vrijdagavonden in het zwembad en bij het omploegen van onze tuinen ;) Heel erg bedankt dat je ook tijdens mijn verdediging aan mijn zij wilt staan als paranimf!

En *saving the best for last:* mijn grootste dank gaat uit naar Dennis. Jouw onuitputtelijke vrolijkheid, enthousiasme, oneindige geduld, en liefde maken van iedere dag een feestje; ik kan me geen beter maatje wensen! Met jou altijd aan mijn zij, en zelfs nu als paranimf tijdens mijn verdediging; samen kunnen wij alles aan! Bedankt voor alles *senpai*!!

Yvonne Wesseling-Rozendaal
Luyksgestel, 8 november 2018

Curriculum Vitae

Yvonne Rozendaal was born on July 18th, 1990 in Eindhoven, The Netherlands. She grew up in Valkenswaard and graduated from pre-university at Were Di in Valkenswaard in 2008. In the same year, she started with her Bachelor in Biomedical Engineering at the Eindhoven University of Technology and graduated in 2011. She continued with the Master's program in Biomedical Engineering at the same university.

During this Master's program, Yvonne carried out a research internship at the Academic Centre of Epileptology, Kempenhaeghe (Heeze, The Netherlands) under the supervision of dr. Pauly Ossenblok. During this internship, she performed spatiotemporal mapping of interictal epileptiform discharges in human absence epilepsy using magnetoencephalography. Her Master's thesis was carried out in the Computational Biology group (prof.dr. Peter Hilbers and prof.dr.ir. Natal van Riel) in collaboration with the Máxima Medical Centre Eindhoven (dr.ir. Anne Maas and dr. Harm Haak). This thesis described the development of an educational simulation tool for diabetes patients and healthcare providers. The main focus was on model development, analysis, improvement, and the implementation of food specification for this diabetes simulator.

After obtaining her Master's degree in 2013, she had the opportunity to continue her research on metabolic diseases during a PhD study in collaboration with the FP7-European Research programme RESOLVE. The results of this PhD project are described in this thesis.

As of July 2018, she is employed as Computational Biology Scientist at the Precision & Decentralized Diagnostics department at Philips Research.